

UNIVERSITE DE NANTES

**ECOLE DOCTORALE**  
**Sciences pour l'ingénieur**

Année 2008

# **Etude de l'oxydation de matériaux carbonés**

**THESE DE DOCTORAT**

Discipline : Sciences pour l'ingénieur  
Spécialité : Génie des Procédés

*Présentée  
et soutenue publiquement par*

**Thangavelu JAYABALAN**

*Le 6 Mai 2008, à l'Ecole des Mines de Nantes  
devant le jury ci-dessous*

Rapporteurs	G. FURDIN C. VIX	<i>Professeur</i> <i>Directrice de Recherche</i>	Université Henri Poincare de Nancy 1 ICSI Mulhouse
Examinateurs	J. LEGRAND J. N. ROUZAUD	<i>Professeur</i> <i>Directeur de Recherche</i>	Université de Nantes Ecole Normale Supérieure de Paris
	A. THOREL V. HEQUET	<i>Maitre de Recherche (HDR)</i> <i>Maitre-assistante</i>	Ecole des Mines de Paris Ecole des Mines de Nantes
	P. PRE P. LE CLOIREC	<i>Maitre-assistante</i> <i>Professeur</i>	Ecole des Mines de Nantes Ecole Nationale Supérieure De chimie de Rennes.

*Directeur de thèse : Pierre LE CLOIREC, Professeur*

Laboratoires : Ecole des Mines de Nantes  
GEPEA UMR CNRS 6144  
4, rue Alfred Kastler, La Chantrerie, BP 20722, 44307 Nantes Cedex 3

N° ED 0367-338





## **REMERCIEMENTS**

Je tiens à exprimer toute ma reconnaissance au Professeur Pierre LE CLOIREC, directeur scientifique à l'Ecole Nationale Supérieure de Chimie de Rennes pour m'avoir permis de préparer mon doctorat dans les meilleures conditions. Je tiens à le remercier tout particulièrement pour ses efforts et pour le soutien qu'il m'a témoigné tout au long de cette étude placée sous sa direction.

Je tiens également à exprimer tous mes sincères remerciements à Madame Pascaline PRE et Madame Valérie HEQUET pour avoir co-encadré cette thèse. Je tiens encore à leur exprimer ma profonde gratitude pour son aide et tous leurs précieux conseils.

Je suis très honoré de la présence au titre de rapporteurs de Monsieur Guy FURDIN, Professeur (Université de Henri Poincaré de Nancy 1), et de Madame Catherine VIX, Directrice de Recherche au CNRS (ICSI Mulhouse). Je remercie aussi Monsieur Alain THOREL, Maître de Recherche (Ecole des Mines de Paris), Monsieur Jack LEGRAND, Professeur (Université de Nantes), Monsieur Jean Noël ROUZAUD, Directeur de Recherche (Ecole Normale Supérieure de Paris), d'avoir accepté de participer à ce jury.

Je suis aussi très reconnaissant à Monsieur Jean Noël ROUZAUD, pour avoir réalisé gracieusement les analyses des images obtenues par MET. Ainsi qu'à Monsieur Guy FURDIN, pour m'avoir fourni les échantillons de charbon actif. Je remercie aussi toutes les équipes du DSEE : professeurs, techniciens, doctorants et les stagiaires.

Je tiens enfin à exprimer toute ma gratitude à ma famille dont le soutien a été essentiel tout au long de mes études, et tout particulièrement au cours de ce travail.



## **TABLE OF CONTENTS**

<b>PRÉAMBULE.....</b>	<b>XII</b>
<b>CHAPTER 1.....</b>	<b>I</b>
<b>GENERAL INTRODUCTION.....</b>	<b>I</b>
<b>CHAPTER 2.....</b>	<b>5</b>
<b>LITERATURE REVIEW.....</b>	<b>5</b>
<b><u>1 ACTIVATED CARBON .....</u></b>	<b><u>5</u></b>
<u><i>1.1.1 Definition.....</i></u>	<u><i>5</i></u>
<u><i>1.1.2 Raw materials.....</i></u>	<u><i>5</i></u>
<u><i>1.1.3 Production methods.....</i></u>	<u><i>7</i></u>
<u><i>1.1.3.1 Physical activation method.....</i></u>	<u><i>8</i></u>
<u><i>1.1.3.2 Chemical activation.....</i></u>	<u><i>9</i></u>
<u><i>1.1.4 Characteristics of activated carbons.....</i></u>	<u><i>9</i></u>
<u><i>1.1.4.1 Physical structure of activated carbons.....</i></u>	<u><i>10</i></u>
<u><i>1.1.4.2 Chemical properties of activated carbons.....</i></u>	<u><i>14</i></u>
<b><u>2 IGNITION OF ACTIVATED CARBONS.....</u></b>	<b><u>20</u></b>
<u><i>2.1.1 Accidents occurring in practice.....</i></u>	<u><i>20</i></u>
<u><i>2.1.2 Organic chemicals (VOC) AND SOLVENTS present in gas phase or adsorbed .....</i></u>	<u><i>24</i></u>
<u><i>2.1.3 Influence of impregnation of activated carbon.....</i></u>	<u><i>26</i></u>
<u><i>2.1.4 Introduction of air into solvent loaded carbon bed adsorption system.....</i></u>	<u><i>27</i></u>
<u><i>2.1.5 Influence of air/oxygen on the reactivity of activated carbons.....</i></u>	<u><i>28</i></u>
<u><i>2.1.6 Influence of moisture.....</i></u>	<u><i>28</i></u>
<u><i>2.1.7 Influence of carbon type.....</i></u>	<u><i>30</i></u>
<b><u>3 MECHANISMS OF OXIDATION AND IGNITION.....</u></b>	<b><u>30</u></b>
<u><i>3.1.1 Air oxidation studies.....</i></u>	<u><i>31</i></u>
<u><i>3.1.1.1 Oxygen consumption.....</i></u>	<u><i>32</i></u>
<u><i>3.1.1.2 Reaction mechanisms and oxidation products .....</i></u>	<u><i>33</i></u>
<u><i>3.1.2 Mechanism of oxidation and ignition reactions with VOC's .....</i></u>	<u><i>36</i></u>
<u><i>3.1.2.1 VOC oxidation mechanisms.....</i></u>	<u><i>37</i></u>
<b><u>4 EXPERIMENTAL METHODS ADOPTED TO STUDY OXIDATION PROPERTIES OF ACTIVATED CARBONS.....</u></b>	<b><u>39</u></b>
<b><u>5 CONCLUSION.....</u></b>	<b><u>42</u></b>
<b><u>6 REFERENCES.....</u></b>	<b><u>44</u></b>
<b>CHAPTER 3 .....</b>	<b>50</b>

<b>MATERIALS AND EXPERIMENTAL METHODS .....</b>	<b>50</b>
<b>7 INVENTORY .....</b>	<b>51</b>
<i>7.1.1 Activated carbon samples.....</i>	<i>51</i>
<i>7.1.1.1 Physically activated carbons .....</i>	<i>51</i>
<i>7.1.1.2 Chemically activated carbons.....</i>	<i>52</i>
<i>7.1.1.3 Carbonized samples.....</i>	<i>52</i>
<b>8 OXIDATION PROPERTIES AND REACTIVITY STUDIES.....</b>	<b>54</b>
<i>8.1.1 TG-DSC analysis.....</i>	<i>54</i>
<i>8.1.2 Apparatus SETERAM ATG-DSC- 111.....</i>	<i>55</i>
<i>8.1.2.1 Thermogravimeter (TG).....</i>	<i>56</i>
<i>8.1.2.2 Differential Scanning Calorimeter (DSC).....</i>	<i>56</i>
<i>8.1.3 Experimental procedures.....</i>	<i>58</i>
<i>8.1.3.1 Sample preparation.....</i>	<i>58</i>
<i>8.1.3.2 Temperature programmation.....</i>	<i>58</i>
<i>8.1.4 Tg-dsc thermograms.....</i>	<i>60</i>
<i>8.1.5 kinetic parameters from DSC and TG curves.....</i>	<i>62</i>
<i>8.1.5.1 Oxidation kinetics from the DSC curves .....</i>	<i>62</i>
<i>8.1.5.2 Combustion kinetics from the TG-curves.....</i>	<i>63</i>
<i>8.1.6 Operating conditions .....</i>	<i>64</i>
<b>9 CHARACTERIZATION OF POROUS PROPERTIES OF CARBONS.....</b>	<b>64</b>
<i>9.1.1 Nitrogen adsorption analysis.....</i>	<i>65</i>
<i>9.1.1.1 Isotherm models.....</i>	<i>65</i>
<i>9.1.1.2 Evaluation approaches.....</i>	<i>68</i>
<i>9.1.1.3 DFT method .....</i>	<i>72</i>
<i>9.1.1.4 Experimental aspects characterization by nitrogen adsorption technique.....</i>	<i>73</i>
<i>9.1.1.5 Advantages and limitations of nitrogen gas adsorption.....</i>	<i>74</i>
<i>9.1.2 Mercury porosimetry .....</i>	<i>74</i>
<i>9.1.2.1 Density and total pore volume determinations .....</i>	<i>75</i>
<i>9.1.2.2 Experimental aspects of characterization by mercury porosimetry technique.....</i>	<i>76</i>
<i>9.1.2.3 Advantages and limitations of mercury porosimetry.....</i>	<i>77</i>
<i>9.1.3 Comparison of nitrogen adsorption and mercury porosimetry techniques.....</i>	<i>78</i>
<i>9.1.4 Chemical composition analysis.....</i>	<i>78</i>
<i>9.1.4.1 Boehm's method.....</i>	<i>78</i>
<i>9.1.4.2 Elementary analysis.....</i>	<i>80</i>
<i>9.1.4.3 Determination of ash content.....</i>	<i>80</i>
<i>9.1.5 Structural characterization.....</i>	<i>81</i>
<i>9.1.5.1 High Resolution Transmission Electron Microscopy (HRTEM).....</i>	<i>81</i>
<i>9.1.5.2 Scanning Electron Microscopy (SEM).....</i>	<i>86</i>
<b>10 CONCLUSIONS.....</b>	<b>88</b>
<b>11 REFERENCES.....</b>	<b>89</b>

<b>CHAPTER 4.....</b>	<b>92</b>
<b>RESULTS AND DISCUSSIONS.....</b>	<b>92</b>
<b><u>12 CHARACTERIZATION OF ACTIVATED CARBONS .....</u></b>	<b><u>92</u></b>
<i><u>12.1.1 Chemical composition.....</u></i>	<i><u>92</u></i>
<i><u>12.1.1.1 Carbon content .....</u></i>	<i><u>94</u></i>
<i><u>12.1.1.2 Oxygen and hydrogen content .....</u></i>	<i><u>94</u></i>
<i><u>12.1.1.3 Nitrogen content .....</u></i>	<i><u>95</u></i>
<i><u>12.1.2 Boehm's method.....</u></i>	<i><u>96</u></i>
<i><u>12.1.3 Ash and Mineral content .....</u></i>	<i><u>97</u></i>
<i><u>12.1.3.1 Ash content.....</u></i>	<i><u>97</u></i>
<i><u>12.1.3.2 Mineral analysis.....</u></i>	<i><u>97</u></i>
<i><u>12.1.4 Porosity.....</u></i>	<i><u>99</u></i>
<i><u>12.1.4.1 Analysis of nitrogen adsorption data.....</u></i>	<i><u>99</u></i>
<i><u>12.1.4.2 Specific surface area.....</u></i>	<i><u>100</u></i>
<i><u>12.1.4.3 Pore size distribution.....</u></i>	<i><u>101</u></i>
<i><u>12.1.4.4 Porous volumes.....</u></i>	<i><u>102</u></i>
<i><u>12.1.5 Structural properties.....</u></i>	<i><u>105</u></i>
<i><u>12.1.5.1 SEM images.....</u></i>	<i><u>105</u></i>
<i><u>12.1.5.2 HRTEM image analysis.....</u></i>	<i><u>107</u></i>
<i><u>12.1.6 Comparison of micropore dimensions.....</u></i>	<i><u>112</u></i>
<i><u>12.1.7 Conclusions.....</u></i>	<i><u>114</u></i>
<b><u>13 REACTIVITY STUDIES .....</u></b>	<b><u>115</u></b>
<i><u>13.1.1 Oxidation at low temperatures .....</u></i>	<i><u>115</u></i>
<i><u>13.1.1.1 Point of Initial Oxidation (PIO).....</u></i>	<i><u>115</u></i>
<i><u>13.1.1.2 DSC curve analysis.....</u></i>	<i><u>118</u></i>
<i><u>13.1.1.3 TG-curves.....</u></i>	<i><u>120</u></i>
<i><u>13.1.1.4 Oxidation kinetics .....</u></i>	<i><u>122</u></i>
<i><u>13.1.2 ignition studies .....</u></i>	<i><u>125</u></i>
<i><u>13.1.2.1 Spontaneous ignition temperature (SIT).....</u></i>	<i><u>125</u></i>
<i><u>13.1.2.2 Combustion kinetics .....</u></i>	<i><u>127</u></i>
<i><u>13.1.3 Conclusions.....</u></i>	<i><u>130</u></i>
<b><u>14 INFLUENCE OF THE ACTIVATED CARBON PROPERTIES ON THEIR REACTIVITY .....</u></b>	<b><u>131</u></b>
<i><u>14.1.1 influence of the surface oxygenated groups.....</u></i>	<i><u>131</u></i>
<i><u>14.1.1.1 Oxygen and hydrogen content.....</u></i>	<i><u>131</u></i>
<i><u>14.1.1.2 Nitrogen content .....</u></i>	<i><u>135</u></i>
<i><u>14.1.2 Effect of mineral matter .....</u></i>	<i><u>136</u></i>
<i><u>14.1.3 Influence of Impregnation.....</u></i>	<i><u>137</u></i>
<i><u>14.1.4 Effect of textural and structural properties.....</u></i>	<i><u>138</u></i>
<i><u>14.1.4.1 Influence of textural properties.....</u></i>	<i><u>138</u></i>
<i><u>14.1.4.2 Influence of quantitative structural properties.....</u></i>	<i><u>139</u></i>

<b>15 INFLUENCE OF THE OPERATING CONDITIONS .....</b>	<b>140</b>
<i>15.1.1 Influence of Oxygen concentration in the ambient gas.....</i>	<i>140</i>
<i>15.1.1.1 Effect on PIO.....</i>	<i>141</i>
<i>15.1.1.2 Effect on SIT.....</i>	<i>142</i>
<i>15.1.2 Influence of flow rate.....</i>	<i>143</i>
<i>15.1.3 Influence of heating rate.....</i>	<i>145</i>
<i>15.1.4 Influence of adsorbed VOC's .....</i>	<i>146</i>
<i>15.1.4.1 Nature of VOC's.....</i>	<i>146</i>
<b>16 STATISTICAL ANALYSIS.....</b>	<b>149</b>
<i>16.1.1 Multiple Linear Regression (MLR).....</i>	<i>149</i>
<i>16.1.1.1 Residuals .....</i>	<i>150</i>
<i>16.1.1.2 Sum of square terms.....</i>	<i>150</i>
<i>16.1.1.3 Assessment of MLR predictive ability.....</i>	<i>150</i>
<i>16.1.1.4 Hypothesis testing.....</i>	<i>152</i>
<i>16.1.1.5 Multicollinearity .....</i>	<i>153</i>
<i>16.1.1.6 Analysis of Residuals.....</i>	<i>154</i>
<i>16.1.1.7 Stepwise Multiple Linear Regression.....</i>	<i>155</i>
<b>17 CONCLUSION.....</b>	<b>159</b>
<b>18 REFERENCES.....</b>	<b>161</b>
<b>CONCLUSIONS AND PERSPECTIVES</b>	
.....	165
<b>RESUMÉ EN FRANÇAIS.....</b>	<b>168</b>
<i>Utilisation : .....</i>	<i>180</i>
Oxydation des charbons actifs – risques d'inflammation.....	180
<i>Inflammation.....</i>	<i>181</i>
<i>Transport : .....</i>	<i>181</i>
<i>Stockage.....</i>	<i>181</i>
<i>Lits adsorbants en service.....</i>	<i>181</i>
<i>Caractérisation expérimentale de la réactivité des charbons actifs : .....</i>	<i>182</i>
<i>Analyseur élémentaire CHNS-O:.....</i>	<i>202</i>
<i>Propriétés physiques.....</i>	<i>205</i>
<i>Propriétés chimiques.....</i>	<i>206</i>
Résultats du TPD : .....	224
<i>Résultat de l'analyse élémentaire : .....</i>	<i>224</i>
<i>Influence sur les paramètres caractéristiques : .....</i>	<i>225</i>
<b>CONCLUSION.....</b>	<b>226</b>
<b>APPENDIX.....</b>	<b>238</b>
<b>APPENDIX-A.....</b>	<b>239</b>

<u>APPENDIX-B.....</u>	<u>241</u>
<u>3. PHYSICALLY ACTIVATED METAL IMPREGNATED CARBONS.....</u>	<u>243</u>
<u>APPENDIX-C.....</u>	<u>244</u>
<u>1. CHEMICALLY ACTIVATED CARBONS.....</u>	<u>245</u>
<u>2. PHYSICALLY ACTIVATED CARBONS.....</u>	<u>246</u>
<u>3. PHYSICALLY ACTIVATED METAL IMPREGNATED CARBONS.....</u>	<u>247</u>
<u>APPENDIX-D.....</u>	<u>247</u>
<u>APPENDIX-F.....</u>	<u>254</u>
<u>APPENDIX-G SEM MICROGRAPHS OF ACTIVATED CARBON SAMPLES.....</u>	<u>255</u>
<u>APPENDIX-H.....</u>	<u>257</u>

## LIST OF TABLES

## LIST OF FIGURES

FIGURE 1 - 1: SCHEMATIC REPRESENTATION OF THE PLAN OF THIS RESEARCH WORK.....3

---

## Préambule

---

Cette étude a fait l'objet d'un certain nombre de publications et de communications dont la liste est indiquée ci dessous :

### Publications

1. T. **Jayabalan**, P. Pré, V. Héquet and P. Le Cloirec: Statistical quantification of the influence of chemical composition and porosity on the oxidation and ignition of activated carbons. ADSORPTION, Article dans presse.

### En préparation

1. T. **Jayabalan**, P. Pré, V. Héquet, J.N. Rouzaud and P. Le Cloirec: Analysis of structural properties of activated carbons by HRTEM study and their influence on the oxidation and ignition characteristics. Article soumis à FUEL.

### Communications internationales

1. T. **Jayabalan**, P. Pré, V. Héquet and P. Le Cloirec : *Influence of material properties on the oxidation and ignition characteristics of activated carbons*. FOA9: 9th International Symposium on Fundamentals Of Adsorption, SICILY-ITALY, 20-25 Mai 2007.
2. T. **Jayabalan**, P. Pré, V. Héquet, P. Le Cloirec and J.N. Rouzaud: Material properties influencing the reactivity of activated carbons: thermal analysis, HRTEM study and statistical modelling. CARBON-2007, SEATTLE-USA, 15-20, Juillet 2007.
3. T. **Jayabalan**, P. Pré, V. Héquet, J.N Rouzaud and P. Le Cloirec: Analysis of structural properties of activated carbons by HRTEM study and their influence on the oxidation and ignition characteristics. Carbon for Energy Storage and Environment Protection. CESEP-2007, Krakow, POLAND, September 2-6, 2007.



---

# **Chapter 1**

---

## **GENERAL INTRODUCTION**

---

Activated carbons are carbonaceous materials used widely in heterogeneous catalysis, filtration of hazardous industrial effluents, and personal protection equipment within contaminated atmospheres. They are commonly used for the removal of Volatile Organic Compounds (VOC) and odours. The VOC's have dangerous effects on the human health, ecosystem and on the global warming of the planet. The French regulations define VOC's as the organic compounds excluding methane which has vapour pressure of about 10 Pa or more with a temperature of 293.15 K. The sources of VOC's emissions include industrial processes involving solvents (basic and fine chemicals, degreasing of metals, use of CFC's, paint production, glues and adhesives) and other industries include (oil refineries, production of alcoholic beverages and livestock production).

Stricter environmental policies and commitments have ensured lower emission standards and greater efficiency in the removal of air pollutants. The major outcome is the extensive use of pollution abatement techniques involving activated carbon materials particularly in the removal of VOC's. But the utilization, stockage and transportation of activated carbons present serious inflammation risks. The utilization risk signifies the use of activated carbon beds for adsorption of VOC's, odours and for solvent recoveries. The adsorption is an exothermic phenomenon with the gas solid transfer taking place with the liberation of heat. The gas phase does not possess the same thermal inertia like that of the fluid phase in water treatment applications. Even waste management facilities involving tanks which extensively use activated carbons for accumulating, storing and treating hazardous and non-hazardous liquid wastes that contain VOC's ( e.g. spent solvents, used oil, process waters or sludge) are vulnerable to oxidation and ignition risks. Hence the air treatment systems charged with VOC has greater probability of oxidation and ignition risks.

The stockage and transportation risks are associated with the activated carbons with or without organic compounds adsorbed in them. External heating, exothermic chemical reactions and adsorption may rise the carbon temperature well above ambient thus making the

understanding of its properties at elevated temperatures of great operational and safety significance.

From this point of view, the main objectives of the thesis is to study the major material properties and operating conditions influencing the reactivity of activated carbons at elevated temperatures in the presence of air and VOC's. Also the main objectives are to derive quantitative statistical correlations relating the oxidation and ignition parameters with the material properties, finally to assess the ignition risks of the activated carbons. This requires an in depth study of the textural, structural and the chemical properties of the activated carbons followed by their oxidation and ignition mechanisms. The major novelty of this work is approach of deriving statistical correlations quantifying the influence of the important properties of the activated carbons on their oxidation and ignition reactivity does not exist in the previous works.

The research study is presented as three main chapters to accomplish the objectives of this thesis, given in the form of flow sheet in Figure1-1. The first chapter consists of a literature review about the activated carbon materials particularly the method of manufacture along with the important physical and chemical properties. It also includes a review of different industrial accidents in France and around the world associated with the activated carbons in order to identify the various factors responsible for the thermal incidents. The review part concerns the mechanisms of oxidation and ignition in activated carbons is studied in detail with an account of the experimental methods necessary for characterizing their reactivity. Hence the first chapter gives a global review on the material, principal factors responsible for the thermal incidents and the mechanism of oxidation and ignition.

The second chapter principally deals with the materials and experimental procedures. The various characterization techniques to measure the material properties as well as the thermal characteristics are taken up. The material properties include textural, structural and chemical composition. The thermal characteristics comprises of the measurement of parameters characterizing oxidation and ignition of activated carbons.

Finally, the last chapter deals with the analysis of the results of the different characterization techniques followed by establishing correlations between the reactivity parameters and the material properties. This is done by first analysing the qualitative trends followed by quantitative correlations using statistical tools giving physical significance. The statistical

correlations established relate the important material properties of activated carbons with the reactivity parameters assessing the safety of the activated carbons.

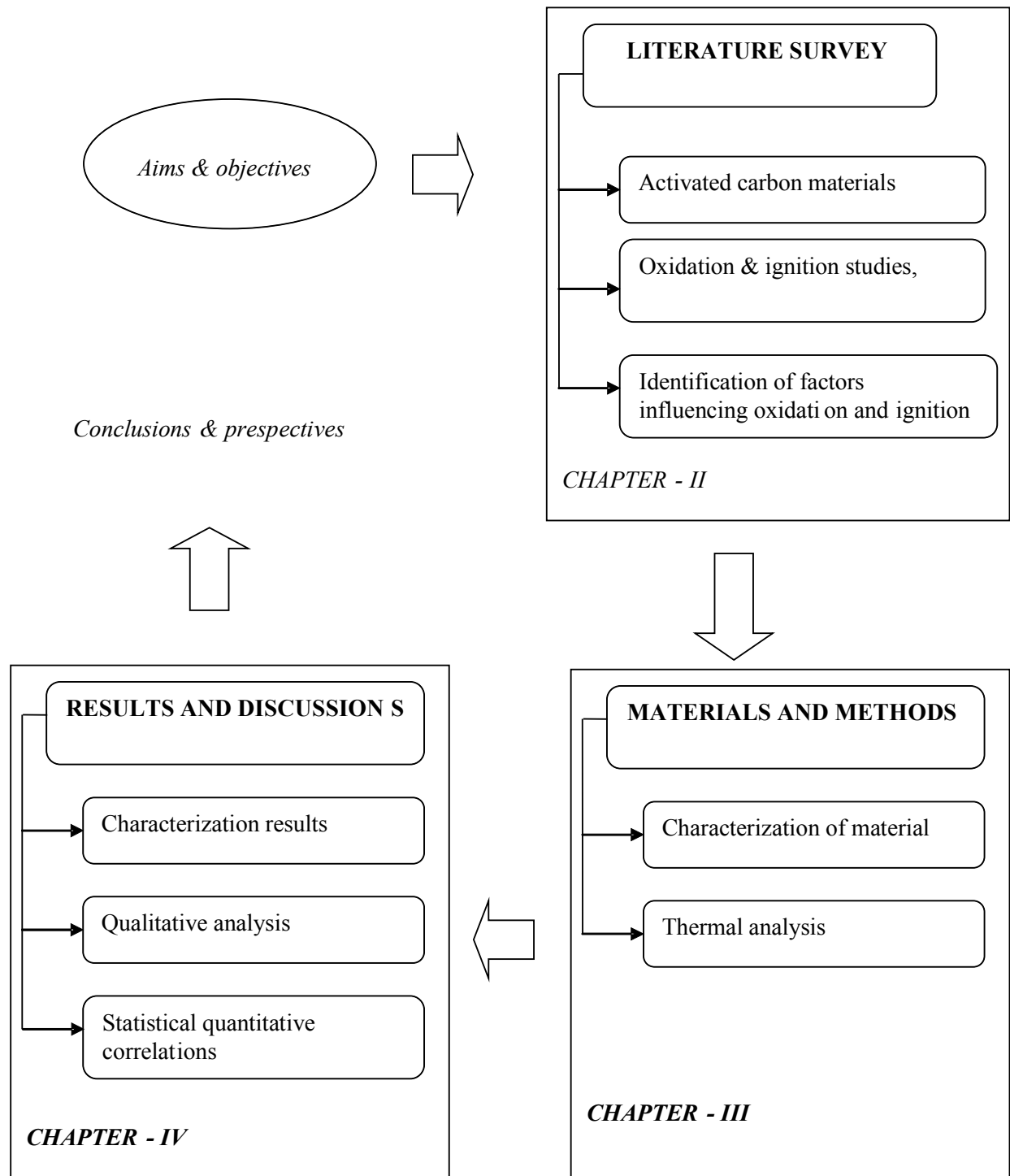


**Figure1- :** Schematic representation of the plan of this research work.



---

## **Chapter 2**

---

### **LITERATURE REVIEW**

---

## **2. LITERATURE REVIEW**

The main objective of the literature survey is to undertake a brief study about activated carbons in order to better know their characteristics and to understand the oxidation and ignition problems related to them. The different circumstances and properties leading to the oxidation and ignition of activated carbons will be discussed.

This chapter is composed of 4 main sections. The first section gives a description about the activated carbons: raw materials used for their manufacture, production methods and their characteristics giving emphasis on the textural, structural and chemical properties particularly that of the surface oxygenated functional groups. The second and third part give an account of the fire accidents associated with activated carbons, citing details about the nature and circumstances leading to it. This is then followed by a review on the mechanisms of oxidation and ignition of activated carbons in the presence of VOC's and air. The final section of this chapter deals with the experimental studies associated with testing and quantifying the oxidation and ignition parameters of activated carbons.

## **1 ACTIVATED CARBON**

### **1.1.1 DEFINITION**

The term activated carbon in its broadest sense includes a wide range of disordered carbon based materials prepared to exhibit a high degree of porosity and an extended intraparticulate surface area [Bansal *et al.*, 1988]. Activated carbons consist of strongly modified graphite like structure which is much more disordered than graphite. The porous structure and chemical nature of an activated carbon is a function of the raw materials used in its preparation and the activation method employed.

### **1.1.2 RAW MATERIALS**

The differences found between the activated carbons are mainly due to the variability in the source of the raw materials, which differ deeply in their chemical composition and

## ***Chapter 2: Literature Review***

---

texture. The textural property here refers to the surface properties quantifying the porosity characteristics like the specific surface area, pore volume and pore width. Any cheap substance with high carbon and low ash contents are mostly used as the raw material [Bansal *et al.*, 1988]. The raw materials for the production of activated carbon include a number of carbonaceous materials like apricot stones, wood, peat, brown coal, bituminous coal, lignite, coconut shells, almond shells, petroleum residues and pulp mill residues [Balci, 1992].

The desired property of the activated carbons to be obtained and their end applications dictate the selection of the raw materials. Higher density (around 1.4 Kg. L<sup>-1</sup>) and sufficient volatile matter (approximately 60 %) of the raw material give higher mechanical strength with larger micropore volume and prevents activated carbons from crumbling during use. For example coconut shell, fruit pits and nut shells produce hard granular carbons with large micropore volume particularly suited for gas phase applications like adsorption of VOC's [Bansal *et al.*, 1988].

Carbons produced from wood are noted for their greater variability in pore size with a larger percentage of mesopores and macropores and they are normally suitable for adsorption of large molecular species. Coal based activated carbons, depending on the type and rank of coal used, contain pore structures somewhere between coconut shell and wood. Nowadays lignite, peat and coke are frequently used sources of activated carbon due to their availability and attractive price.

Younger fossil materials like peat and materials from vegetable sources like coconut shell, apricot stones and almond shells can be activated easily giving high quality products with higher surface area and adsorption characteristics [Martin, 1981 ; Holden, 1982]. Fixed carbon contents (carbon content found after removing the volatile matter) of some raw materials are given in Table 2-1. High carbon content materials like anthracite have a carbon content as high as 90 %, whilst wood based materials have carbon content as low as 40 %.

Material	(%) Carbon content
Soft wood	40
Hard wood	40
Coconut shell	40
Lignite	60
Bituminous coal	75
Anthracite	90

**Table 2 - :** Fixed carbon contents of raw materials employed in activated carbon manufacture [Holden, 1982].

### 1.1.3 PRODUCTION METHODS

Activated carbon can be prepared by one of the following two methods:

1. by allowing the previously carbonized product to react with suitable activating agent like steam or carbon dioxide and the procedure is known as ‘physical activation’,
2. by carbonizing the precursor with the addition of activating agent’s mainly organic acids and other chemical agents which influence the course of carbonization. The method is generally known as ‘chemical activation’. The two methods are shown by a schematic representation in Figure 2-1.

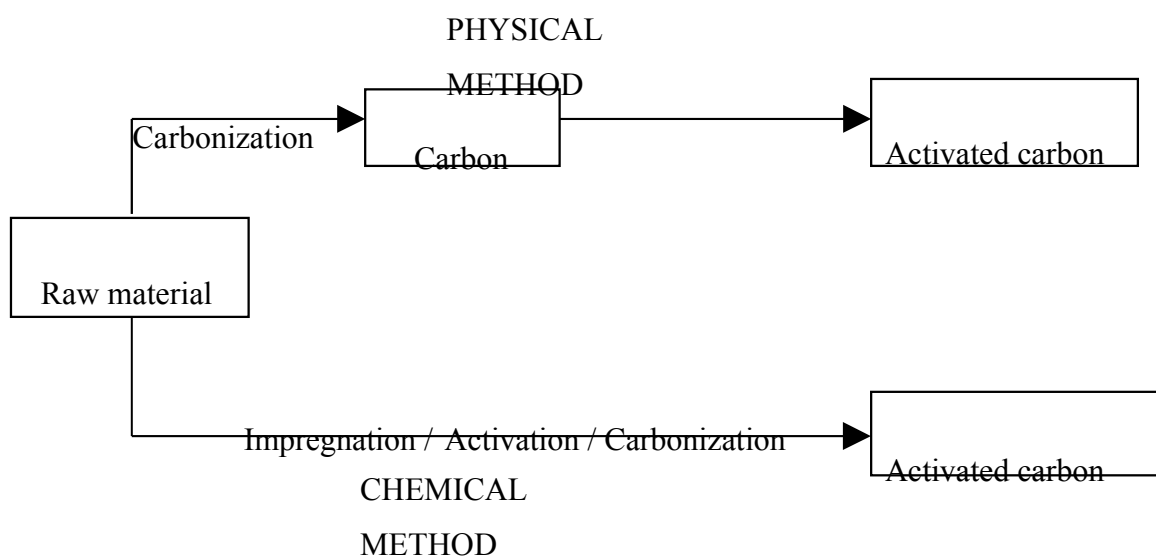


**Figure 2 - :** Method of production of Activated Carbon [Le Cloirec, 2003].

### ***1.1.3.1 PHYSICAL ACTIVATION METHOD***

Physical activation method is a two step process consisting of the carbonization of the raw material followed by activation of the carbonized product.

#### ***1.1.3.1.1 Carbonization***

The carbonization process results in the reduction of the volatile content and the subsequent increase of the fixed carbon content of the raw material. During the carbonization phase most of the non-carbon elements, i.e. hydrogen, oxygen, carbon di oxide and water vapour are removed in the gaseous form by pyrolytic decomposition. The precursor is semi-carbonized between 500 - 800 °C under the presence of the pyrolysis gas. All the polycyclic aromatic structures were supposed to be planar and stacked by 2 or 3 to form Basic Structural Units (BSU) with similar dimensions. The free atoms of elementary carbon are grouped into organized formation [Lu, 2006], but the mutual arrangement is almost random, so that free interstices remain between them and form pores. As a result of deposition of tarry substances, the interstices can be filled or at least blocked by disorganized carbon.

#### ***1.1.3.1.2 Physical activation of the carbonized product***

The activation step is generally conducted at temperatures between 800 °C and 1100 °C. The most common activating agents are steam and CO<sub>2</sub>. Basically the oxygen atom present in the activating agent burns away the more reactive portion of the carbon skeleton to form carbon monoxide. In the case of steam activation the active oxygen formation mechanism is explained by the reaction sequences represented in equation 2.1. A steam molecule is first decomposed into a hydrogen atom and a hydroxyl radical (OH<sup>·</sup>), both chemisorbed rapidly on edge carbon sites. This step is followed by the hydrogen atom transfer from the hydroxyl radical to hydrogen [Long and Sykes, 1948].



The oxygen atom reacts with an atom of carbon from the solid matrix to form gaseous carbon monoxide. The hydrogen atom of the chemisorbed hydroxyl radical joins the hydrogen atom on the adjacent carbon site and leaves as a hydrogen molecule (H<sub>2</sub>) [Walker et al., 1959].

## ***Chapter 2: Literature Review***

---

Reactions with carbon can be directly expressed as:



The activation process enables to enlarge the volume and the diameters of the pores. The activation also removes the disorganized carbon by exposing the aromatic sheets to the oxidation of activating agents and leads to the development of the microporous structure.

### ***1.1.3.2 CHEMICAL ACTIVATION***

In the chemical activation method, the starting material is impregnated with activated agent (aqueous solution) followed by pyrolysis and washing. Chemical activation is used almost exclusively for carbons produced from materials of recently fossilized lignocellulosic materials. Chemical activation consists of heating the raw material with a dehydrating chemical agent. During chemical activation, the reaction takes place at a temperature range of 450-700°C. The activation agent influences the pyrolytic process and restricts the formation of tar to minimum. The temperature needed for the pyrolysis is being lower than that needed for physical activation; development of the porous structure is promoted.

The most widely used chemical agents employed for carbon activation are phosphoric acid, sulphuric acid and potassium sulphide [Bansal *et al.*, 1988]. Apart from these hydroxides of an alkali metal, magnesium and calcium chloride are also used in the chemical activation. These agents are strong dehydrating agents, resulting in the aromatization of the carbon skeleton, and the creation of a porous structure. One advantage of using phosphoric acid in chemical activation is that it can be removed easily from the activated carbon by rinsing with pure boiling water.

### ***1.1.4 CHARACTERISTICS OF ACTIVATED CARBONS***

The aim of the following section is to describe the different characteristics of activated carbons, related to the structure, the texture and the chemical composition.

### **1.1.4.1 PHYSICAL STRUCTURE OF ACTIVATED CARBONS**

Activated carbons have a complex physical structure, which is derived from the structure of graphite. Using X-ray diffraction techniques the structural studies of Franklin [1951] on carbonized materials showed two distinct well-defined classes namely the non-graphitizing and the graphitizing carbons.

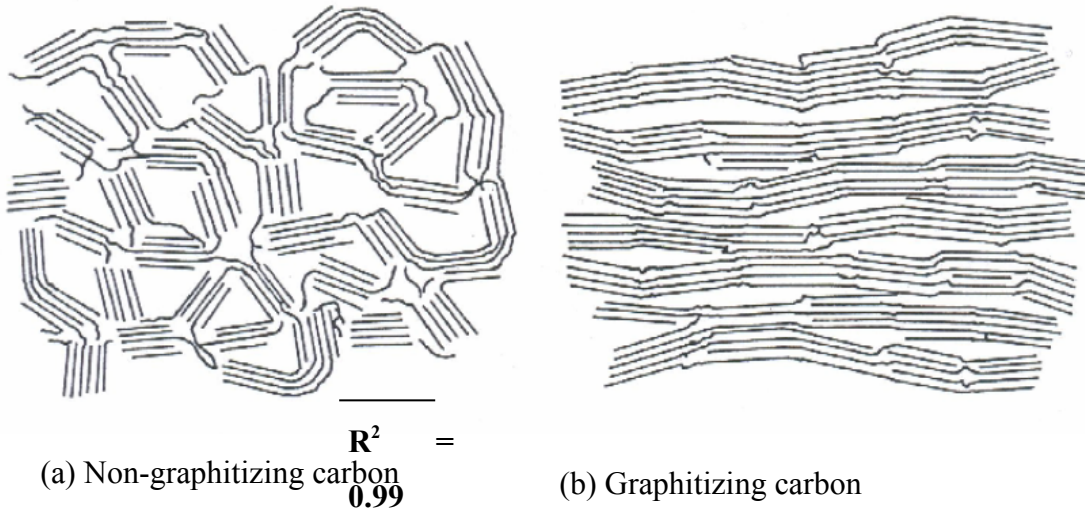


**Figure 2 - :** Schematic representation of (a) Non graphitizing and (b) Graphitizing structure of activated carbon [Franklin, 1951].

One of the closest and most famous microstructural models of carbon material, which is now considered is the classical one proposed by Franklin [1951]. The Franklin model assumes that the microstructure of carbon material consisted either of short fragments of graphite cross-linked by bridging groups or of a twisted network of carbon polyaromatic planar layers.

The structures of carbon materials are very complex and present characteristic structural features at different length scales; these are changing during the carbonization and graphitization process. All the carbonaceous materials contain the same elemental bricks or basic structural units (BSU). These exhibit diverse three-dimensional arrangements at different scales, according to the occurrence of the various microscopic bodies. The latter depend on the chemical composition and the amount of carbonization or graphitization process. An external modification of the chemical compositions may even deeply modify the three-dimensional arrangements of BSU [Oberlin, 1989]. The BSU consist of 2 to 4 planar polyaromatic molecules piling up parallel to each other. The number of layers in a stack, its

## ***Chapter 2: Literature Review***

---

size and arrangement in space are function primarily of the chemical properties of the starting materials and the carbonization process (rate of heat treatment, final temperature, pressure).

The non-graphitizing carbons contain structural units that are oriented randomly and the cross-links are sufficiently strong to prevent a more parallel arrangement. The graphitizing carbons are prepared from substances containing more hydrogen and less oxygen. The structural units in a graphitizing carbon are approximately parallel to each other, and the links between the adjacent units are assumed to be weak. The transformation of such a structure into crystallite graphite on heating (3000 °C) would be relatively simple, forming a softer and less porous mass.

The graphitic crystal structure is composed of fused hexagons held approximately 0.335 nm apart by van der Waal's forces. However, the structure of activated carbon differs strongly from that of graphite. During carbonization process, several aromatic nuclei with no triperiodic order with only 2D organization at a local (nm) scale with more or less stacked polyaromatic structures are formed. From X-ray spectrograph, these structures have been interpreted as "microcrystallites" consisting of stacks of fused hexagonal rings of carbon atoms. Structurally, activated carbons can therefore be considered as a rigid interlinked cluster of units, each of them comprising a stack of polyaromatic graphene planes. The microcrystallites are connected to each other by interaction of functional groups terminating the graphene planes. The diameter of the planes forming the microcrystallites, as well as the stacking height, were estimated at 0.5 nm – 5 nm indicating that each microcrystallite consists of 5 -15 layers of graphite planes [Wolff, 1959].

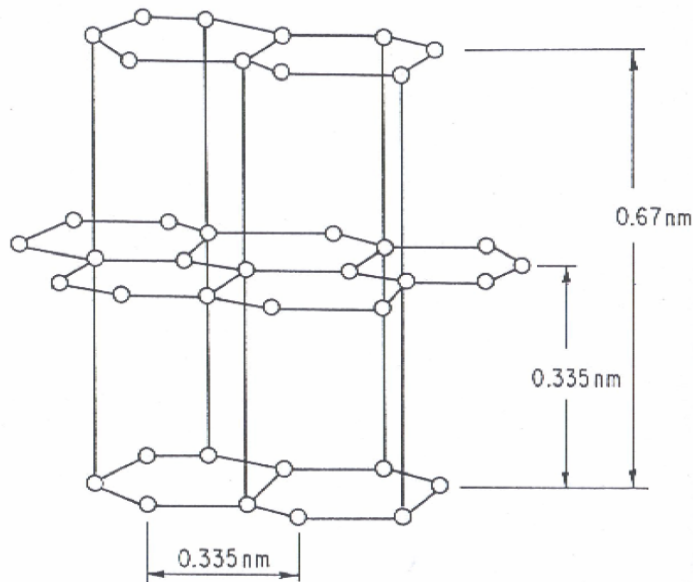


**Figure 2 - :** Carbon atoms arrangements in graphite crystal [Lu, 2006].

Therefore the structure of activated carbons consists of aromatic sheets and strips often bent. Many structural defects are bonded together to create a three dimensional network and the spaces between them constitute the porosity. They resemble a mixture of wood shavings or crumpled paper with variable gaps of molecular dimensions, termed as the micropores [Oberlin, 1984]. The characteristics of the disordered structure depend on the nature of the precursor and on its treatment. During the pyrolysis of the precursor, volatiles and inorganics are removed with the residual carbon consisting of stacks of flat aromatic sheets cross-linked in a quasi random manner. The irregular arrangement leaves free interstitial spaces that are either blocked or partly filled with tar and surface functional groups.

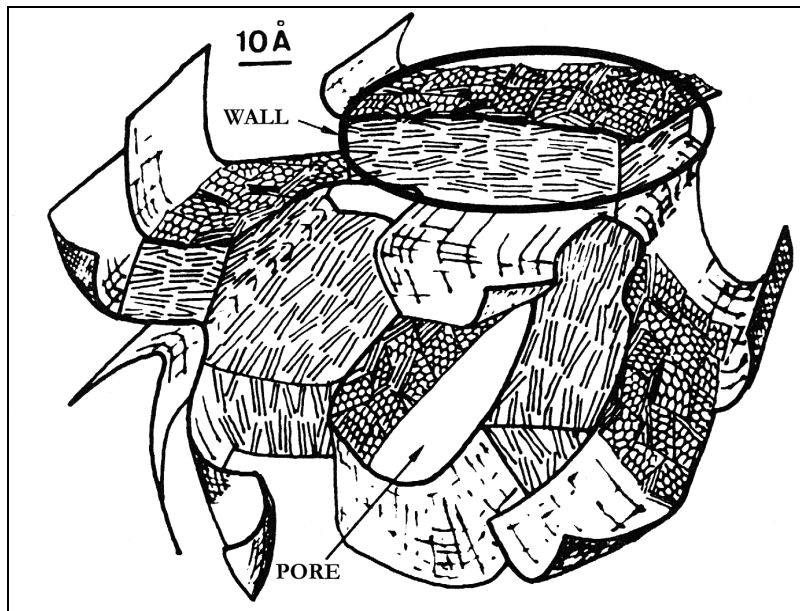


**Figure 2 - :** Schematic representation of microstructure of activated carbons [Oberlin *et al.*, 1989].

#### **1.1.4.1.1 Pore structure of activated carbon**

The structure of activated carbon micropores is often assumed to be slit shaped, though there are many assumptions found in literature like cylindrical and circular pores. The pore size depends on the width and represents the distance between the walls of a slit shaped pore or the radius of a cylindrical pore [Bansal *et al.*, 1988]. The carbonaceous materials possess a range of pore sizes, which according to IUPAC (International Union of Pure and Applied Chemistry) are classified into three groups:

1. Micropore: width less than 2 nm;
2. Mesopore: width between 2 nm and 50 nm;
3. Macropore: width greater than 50 nm.

Pores with an effective diameter larger than about 50 nm are classified as *macropores*. Their volume in the activated carbon is generally in the range  $0.2 - 0.5 \text{ cm}^3 \text{ g}^{-1}$  and their surface area represents  $0.5$  to  $2 \text{ m}^2 \text{ g}^{-1}$ . Transitional pores or mesopores are those in which capillary condensation of gases can take place. This phenomenon usually produces the hysteresis loop on the adsorption isotherm. The effective diameters of transitional pores are in the range of 2 nm to 50 nm. Their specific surface area is generally around 5 % of the total surface area of

## ***Chapter 2: Literature Review***

---

the activated carbon. Pores with an effective diameter less than about 2 nm are called *micropores*. The volume of micropores is generally around 0.15 to 0.50 cm<sup>3</sup> g<sup>-1</sup> and their specific surface area usually amounts to over 90 % of the total specific surface area [Gregg and Sing, 1982; Rodriguez Reinoso, 1998]. Each of these three groups of pores has its specific function in the process of adsorption on activated carbon. Depending on the target application, the volume fractions of the transitional pores and of the micropores can be adjusted by employing specific production procedures.

### ***1.1.4.2 CHEMICAL PROPERTIES OF ACTIVATED CARBONS***

The adsorption capacities of activated carbons are not only determined by their textural and structural characteristics, but are also strongly influenced by their chemical composition. Activated carbons are characterized by a certain degree of surface chemical heterogeneity, which is related to the presence of heteroatoms such as oxygen, nitrogen, hydrogen and phosphorous. The contents of these elements vary depending upon the nature of the organic precursor, the method of activation and degree of carbonization.

#### ***1.1.4.2.1 Oxygen containing functional groups***

The oxygen content of the activated carbon ranges between 1 to 30 % by weight and has been shown to vary considerably with the activation temperatures. The amount of oxygen decreases with an increase in the activation temperature. Actually, at the edge of the basal planes of carbon atoms in the graphitic structure, the bonding in the plane is terminated by unsaturated carbon atoms. These are normally associated with high concentrations of unpaired electrons and therefore play a significant role in oxygen chemisorption [Reinoso, 1998]. In crystallite graphite, the edge area is small compared to the basal plane and the graphitic structure does not exhibit significant chemisorption. However with nanometre sized units, activated carbons have much more disordered structures and edge area, which result in the larger propensity for oxygen chemisorption. Apart from these, there are deformities and discontinuities in the activated carbons that aid in the chemisorption of oxygen.

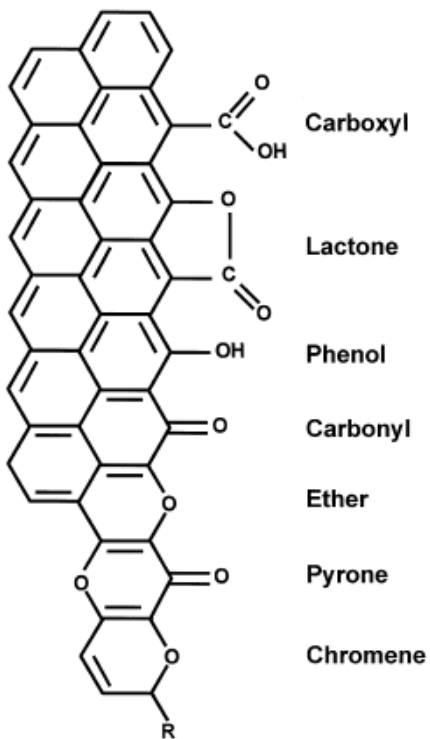


**Figure 2 - :** Surface oxygenated groups present in activated carbons [Boehm, 1994].

Carbon-oxygen surface groups are not only formed by reaction with oxygen in air but also from reaction with many other oxidizing gases like ozone, nitrous oxide, nitric oxide, carbon di oxide and oxidizing solutions like nitric acid, sodium hypochlorite, hydrogen peroxide, etc [Puri, 1970]. The nature and the amount of oxygen surface complexes of a given carbon are affected by its surface area, particle size, ash content as well as the degree of carbonization. Carboxyl, lactone, carbonyl, phenol, ether, pyrone and chromene are the important oxygen containing functional groups found in the activated carbons, (Figure 2-5). These heteroatoms determine the acidity/basicity of the activated carbons.

#### **1.1.4.2.2 Acidic surface groups**

Oxygen containing functional groups such as carboxyl, lactone or lactols, anhydrides and phenolic groups are postulated as the sources of surface acidity. Actually, more oxygen is bound to the surface of the carbons for the creation of the acidic surfaces than the basic ones. Activated carbons can acquire acidic character when exposed to oxygen between 473 – 973 K or to oxidants like air, water vapour, nitric acid, mixture of nitric acid and sulphuric acids and H<sub>2</sub>O<sub>2</sub> [Puri, 1970].

### ***1.1.4.2.3 Basic surfaces***

Carbons can acquire a basic character by heating at high temperature (973 K) in an inert atmosphere and followed by subsequent exposure to air below 473 K [Puri and Bansal, 1966]. Heat treatment will create unsaturated surfaces as a result of thermal desorption of acidic functional groups in the form of CO<sub>2</sub> and these surfaces are prone to oxygen re-adsorption when the sample is exposed to air. Another method to create basic carbon surfaces involves heat treatment in an ammonia atmosphere. Treatment with ammonia at 673-1173 K effectively removes acidic oxygen-containing functional groups and introduces basic nitrogen containing functional groups.

Whilst acidic properties of activated carbons samples are well known and explained, the basic properties of the activated carbon surface are not well understood. Gartein and Weiss, 1957 described the basic properties of activated carbons to chromene like and pyrone type structures as shown in Figure 2-5. But it has not been clearly established that oxide structures are responsible for the basic character exhibited by some carbon surfaces [Boehm, 1994]. Leon *et al.*, [1992] studied the surface basicity of two series carbons and provided direct evidence that oxygen free carbon sites (C<sub>π</sub>) can adsorb protons from solution. The C<sub>π</sub> sites are located in π-electron rich regions on the basal plane i.e. away from the edges. Therefore basic sites are Lewis type basic sites associated with the carbon structure itself [Boehm, 2002].

### ***1.1.4.2.4 Identification of the surface oxygenated groups***

The surface functional groups namely the acidic and basic groups can be identified using different techniques like

1. *Chemical titrations,*
2. *Temperature programmed desorption,*
3. *Infra red spectroscopy,*
4. *X-ray photoelectron spectroscopy,*

A short description of the few methods widely used in literature is given below.

#### ***1.1.4.2.4.1 Chemical titration***

The identification of the surface oxygenated groups was extensively studied by Boehm, [1994]. The method employed is based on the neutralisations and titrations of the acidic and basic groups. Various alkali solutions are used for the neutralisation of the different acidic groups.

## ***Chapter 2: Literature Review***

---

GROUP 1 - The strongly acidic groups neutralised by the  $\text{NaHCO}_3$  are the carboxyl groups.

GROUP 2 - The groups neutralised by the  $\text{Na}_2\text{CO}_3$  and not by the  $\text{NaHCO}_3$  belong to the lactones.

GROUP 3 -The groups neutralised by  $\text{NaOH}$  but not by  $\text{Na}_2\text{CO}_3$  were postulated as phenols.

GROUP 4 - The groups reacting with  $\text{NaOC}_2\text{H}_5$  and not with  $\text{NaOH}$  are suggested to be carbonyl.

<b>Base</b>	<b>Formula</b>	<b>Neutralization groups</b>
Sodium bi-carbonate	$\text{NaHCO}_3$	G1
Sodium carbonate	$\text{Na}_2\text{CO}_3$	G1 and G2
Sodium hydroxide	$\text{NaOH}$	G1,G2 and G3
Sodium ethoxide	$\text{NaOC}_2\text{H}_5$	G1 and G4

**Table 2 - :** Classification of the surface acidic groups of activated carbon [Boehm, 1994]

Free carboxylic groups are strong acidic groups and their concentration can be determined by the adsorption neutralisation with  $\text{NaHCO}_3$  and re-titrating with a solution of  $\text{HCl}$  in the presence of phenolphthalein as an indicator. These groups liberate acetic acid from acetate and carbon di-oxide from sodium bicarbonate. The lactones are less acidic groups when compared to the carboxylic group. They are neutralized by alkalis and hydrolysed by the mineral acids. The groups neutralised by the sodium carbonate and not by sodium bi-carbonate are designated as the lactones. The lactone ring in the phenolphthalein solution is opened only by the sodium bi carbonate appearance of purple colour and not by the solution of sodium carbonate. These phenol groups are neutralised by the sodium hydroxide solution. These groups give acid resistant methoxy groups when treated with phenolic reagents, dinitrofluorobenzene and p-nitrobenzoylchloride.

Finally the carbonyl groups are the ones which are not neutralised by the sodium hydroxide but by the sodium ethoxide solution. Pairs of carbonyl groups can be rearranged at the periphery of the graphene layers with system of conjugated double bonds to form quinone structures. These groups can be confirmed by the chemical reactions with various carbonyl reagents like hydroxylamine, semicarbazide or dinitrophenylhydrazine.

### **1.1.4.2.4.2 Temperature programmed desorption**

The other method widely used is the Temperature Programmed Desorption (TPD). The surface oxygenated groups of carbon materials decompose upon heating in an inert atmosphere by releasing CO<sub>2</sub> and CO at different temperatures. The temperature programmed desorption method uses the difference in the thermal stability of the surface oxygenated groups. The temperature assigned during the desorption products depends on the texture of the material, the heating rate and the experimental system used. Table 2-3 gives the temperature range for the decomposition of the different surface groups of AC's; thus CO<sub>2</sub> is liberated from the carboxylic acids groups at a lower temperature than from lactone groups. Anhydrides are decomposed into CO<sub>2</sub> and CO at higher temperature, whereas phenols, ethers and carbonyls liberate only CO. The products of desorption are compared with the temperature ranges and the surface oxygenated groups can be identified. The different products of desorption along with their temperature can be found in the Table 2-3.

<b>Surface groups</b>	<b>Desorption products</b>	<b>Desorption temperature (°C)</b>
Carboxylic groups	CO <sub>2</sub>	100 - 400
Anhydrides	CO , CO <sub>2</sub>	400 - 630
Lactones	CO <sub>2</sub>	200 - 650
Phenol	CO	600 - 700
Carbonyl	CO	700 - 1000
Ethers	CO	700
Quinone	CO	700 - 100

**Table 2 - :** Temperature ranges for the decomposition of the surface groups of activated carbons [Figueiredo *et al.*, 1999].

### **1.1.4.2.4.3 IR spectroscopy**

Direct information on the presence of surface functional groups can be obtained from IR studies. However, carbon materials often present difficulties in IR studies, because of their unique physicochemical properties (such as difficulties in sample preparation, poor transmission and uneven light scattering) [Mattson and Mark, 1971]. Some success has been reported with attenuated total reflection (ATR) - Fourier Transform IR (FTIR). ATR-FTIR spectroscopy is a versatile and powerful technique for infrared sampling that requires minimal or no sample preparation for rapid analysis. Also, ATR is ideal for those materials that are strong absorbers of infrared light, such as activated carbon. When light travels across the boundary between two materials, the change in refractive index between the two materials causes reflection of some of the light. The proportion of reflected light is a function of the angle of incidence at which the light encounters the boundary.

IR spectra of activated carbons indicate the possible presence of oxygen containing groups, such as carboxylic, quinone, ether, phenolic, and lactone, C=C of aromatic rings, and nitrogen containing groups like pyridine, nitrile, cyclic amide [Selitti *et al.*, 1990, Mangun *et al.*, 2001]. However, in general, the interpretation of the spectra is complicated by the fact that each group originates several bands at different wave numbers; therefore each band may include contributions from various groups. Furthermore, IR does not provide quantitative information about the presence of individual functional groups on the activated carbon surface. It should also be noted that because of the very limited depth of penetration of the internal reflectance evanescent wave, the internal surface of an activated carbon is largely not accessible to IR spectroscopic techniques [Mattson and Mark, 1971].

### **1.1.4.2.4.4 X-ray photoelectron spectroscopy**

XPS is based on the photoelectric effect outlined by Einstein in 1905, where the concept of photons impinging a surface was used to describe the resulting ejection of electrons from that surface. The XPS technique is highly surface specific due to the short range of the photoelectrons that are excited from the solid. The energies of the photoelectrons leaving the sample, which is determined using a Concentric Hemispherical Analyser (CHA), give a spectrum with a series of photoelectron peaks. The binding energies of the peaks are characteristic of each element.

XPS is not sensitive to hydrogen or helium, but can detect all other elements. XPS is a non-destructive (or weak) surface technique that provides the information of the few uppermost

layers of the material. XPS can provide valuable information from the C1s region for carbon materials. Substantial changes in the nature of the carbon due to changes in surface chemistry such as oxidation can be identified through an examination of the C1s core region [Procter and Sherwood, 1982]. In the C1s core region, surface oxides were identified as –C–O groups, –C=O groups, and carboxylic acid or ester groupings, which correspond to chemical shifts of 1.6, 3.0 and 4.5eV (in C1s), respectively [Procter and Sherwood 1982]. XPS is the most successful method for studying nitrogen-containing functionalities in solid materials.

Characterization of the oxygen-containing surface functionalities on activated carbons is complicated, partly because of the complexity of the functionalities on the carbon surface, and partly because of the incomplete understanding of their behaviour. Currently, the total basic surface functionalities are measured as a single value because the nature of basic functionalities is not well known. Besides the above techniques, other commonly used methods include thermal desorption spectroscopy and electrokinetic measurements [Boehm, 1994]. Recently, Inverse gas chromatography has emerged as a new method for detecting oxygen surface functionalities [Donnet *et al.*, 2002]. Surface imaging techniques, such as SEM and STM, are also starting to be used in probing the activated carbon surface functionalities [Zielke *et al.*, 1996].

## **2 IGNITION OF ACTIVATED CARBONS**

Activated carbons are prone to oxidation and ignition reactions, which cause extensive damage to equipment and property, thus make the understanding of the oxidation and ignition properties of great operational and safety significance. A survey of various incidents of fires and thermal runaways associated with activated carbons explaining the circumstances and factors leading to ignition will be discussed.

### **2.1.1 ACCIDENTS OCCURRING IN PRACTICE**

A wide range of databases and literature sources give an account of thermal hazards and ignition accidents associated with activated carbons. Some of the major incidents are listed in the Table 2-4

## Chapter 2: Literature Review

Date	1962 – 1963
Location	United Kingdom
Description	Fire outbreaks occurred in consignments of chemically activated carbon. A total of six fires were reported during this period. The carbon was packed in multiwalled paper bags and the quantities were between 4-14 tons. Fires were discovered 3 – 4 weeks after stowing.
Source	[Bowes and Cameron, 1971].
Date	1972
Location	Scott Graphics, South Hadley, Massachusetts, USA.
Description	An unprecedented increase in the adsorber outlet temperature within 10 minutes after the restart of the activated carbon filter unit treating acetones. The same type of accident also occurred in this unit in 1972 and 1976 with ash found in the interior of the adsorbers confirming the combustion reactions.
Source	[Chapman and Field, 1979].
Date	1979
Location	SCM, Organic chemistry division, Jacksonville, USA.
Description	Many fire incidents in the activated carbon beds were reported due to the presence of turpentine.
Source	[Harrel <i>et al.</i> , 1979].
Date	1980
Location	Capture, treatment and distribution of water, Moerdjik Noord-Brabant, Netherlands.
Description	A reservoir tank containing water/hydrocarbon mixture (heavy fuel, xylene, toluene...) was overloaded in capacity which caused an explosion of the activated carbon in the sealing used for adsorption of the organic vapours. In order to avoid boil over of the reservoir contents and the spread to adjacent reservoirs, a massive cooling operation was carried out
Source	Ministry of Environment and Regional Planning [DPPR/SEI/BARPI, ARIA database, 1999].
Date	1995
Location	Powell Duffryn Terminals, Savannah, Georgia, USA.
Description	During the night, in the absence of workers, there was an explosion in the turpentine storage tank connected to the activated carbon beds. The explosion also caused damage to other storage tanks at the proximity emitting toxic

## ***Chapter 2: Literature Review***

---

	H <sub>2</sub> S gas that necessitated the evacuation of about 2000 people living in proximities. 11 people were injured and the river flowing adjacent to the facility was contaminated.
Source	[EPA 550-R-98-003, 1998].
Date	1996
Location	Fabrication of automobile equipment's, Audincourt (25), France.
Description	The industry manufactures automobile parts, a fire was declared on the activated carbon filter kept in the oven. The purpose was to test the filter for treating fumes at a higher temperature using forced ventilation.
Source	Ministry of Environment and Regional Planning [DPPR/SEI/BARPI, ARIA database, 1999].
Date	1996
Location	Chemical industry, Pardies (64), France.
Description	In the workshop of a chemical industry handling nitro compounds, an explosion occurred in a 9 m <sup>3</sup> cylinder containing activated carbons. No impact on the environment or loss of life was reported.
Source	Ministry of Environment and Regional Planning [DPPR/SEI/BARPI, ARIA database, 1999].
Date	1998
Location	Agrochemical industry, Limas (69), France.
Description	There was fire in a carbon unit of 4 m <sup>3</sup> used for adsorbing solvents and odours. There was no major damage or loss to life.
Source	Ministry of Environment and Regional Planning [DPPR/SEI/BARPI, ARIA database, 1999].
Date	1998
Location	Storage facility, South eastern chemical company, South Carolina - United States
Description	A fixed roof tank storing a mixture of thinners and lacquers (containing acetone, methyleethyl ketone and toluene) vented to a carbon canister exploded.
Source	[Kerr , 1998].

## ***Chapter 2: Literature Review***

---

Date	2001
Location	Halifax, Nova Scotia, Canada
Description	Container vessel Kitano reported a fire on the foredeck, which departed from New York to Halifax in Canada. The fire was reported in 2 containers which had activated carbon pellets impregnated with potassium hydroxide (caustic potash) whereas the rest of the containers remained unaffected.
Source	Marine Investigation Report, M01M0017 Transportation Safety board of Canada, 2001.
Date	2003
Location	Chemical industry, Vierzon, France (18).
Description	In an industry specializing in the manufacture of chemicals, fire was reported in stocks of activated carbon packed in polyethylene bags. The fire started in one of the bags and propagated to all the other bags situated nearby. The cause of the fire was not known, the economic loss of the fire was about 7000 euros with approximately 7 tons of activated carbon destroyed.
Source	[ARIA database].
Date	2004
Location	Feurs, France (42).
Description	A thermal runaway was observed in the site to treat metal wastes and battery recycling. The thermal runaway started was observed in a container with 8.7 tons of activated carbon treating fumes. The unit was newly installed and the activated carbon used was impregnated with sulphur. The unit was flooded with water to put off the fire and people were evacuated from the vicinity of the incident.
Source	[ARIA database].
Date	2005
Location	Industry producing lead, tin and zinc, Fouquierier – Lens, France (62).
Description	The stoppage of the ventilation system for maintenance used for the cleaning of the coke residues caused a rise in the temperature of a hopper with an activated carbon filter. The ignition of the activated carbon filter took place when the trap was opened to access it leaving the entry of air into the system causing rapid thermal runaway leading to ignition.
Source	[ARIA database].
Date	2006
Location	Site for incineration of household refuse, Guerville, France (78).

## ***Chapter 2: Literature Review***

---

Description	A fire was declared in the site for the incineration of household refuse. The fire started from a filter of dimension 20 – 25 m <sup>3</sup> containing 500 kg of activated charcoal used for treating the fumes. The origin of the fire was confirmed to be the ignition of the activated charcoal. There was no loss of life but fire-fighters were hospitalized for exposure to substantial quantities of CO.
Source	[ARIA database].

**Table 2 - :** Accidents of fires and thermal runaways associated with activated carbons.

From Table 2-4, we find that majority of the incidents with activated carbon have occurred on units used for organic chemical treatment or during the storage of activated carbon materials saturated or not with the organic chemicals. The table also indicates the diverse sector of activities involving the risk of thermal hazard with activated carbons in storage, transportation and shipping, chemical manufacturing, waste treatment and recycling units. There are numerous risk factors identified as a result of the accidents as well as extensive experimental studies. They include VOC's and organic solvents, introduction of air into the carbon bed system, the velocity of gas used, humidity in the carbon bed, impregnates and type of carbon used. These risk factors are taken up in the following section

### **2.1.2 ORGANIC CHEMICALS (VOC) AND SOLVENTS PRESENT IN GAS PHASE OR ADSORBED**

Activated carbons are extensively used for air purification and industrial gas treatment. The applications concern with the VOC removal, odour control, solvent extraction units and vehicle filters [van der Merwe and Bandosz, 2005]. Literature provides a large amount of studies dealing with thermal hazards associated with organic chemical treatment and particularly with volatile organic compounds (VOC).

The first reported accident involving combustion of an activated carbon bed dates back to the 40's. The adsorber ignition occurred during the treatment of cyclohexane by coconut based activated carbon [Wildman, 1988]. Even ignition cases in granular activated carbons were observed at an experimental scale in our laboratory while treating methyl ethyl ketone and hexane diluted in air at concentration levels equals to 150 g.m<sup>-3</sup> and 250 g.m<sup>-3</sup> [Delage, 2000]. Many carbon fires have been reported in the regenerable fixed bed carbon adsorbers (regenerated on site) which are large, multicomponent systems used to treat continuous gas

## ***Chapter 2: Literature Review***

---

streams with flows ranging several 1000 l/min. These systems are used both for pollution control and organic solvent recovery [Naujokas, 1985]. Thermal hazards are also found in carbon canisters which are a simplified type of activated carbon adsorption system normally used in facilities which store or process liquids containing volatile organic compounds.

Extensive experimental and theoretical studies were carried out by Delage, [2000] in our laboratory on the warming of the activated carbon beds during the adsorption of volatile organic compounds. The experiments were carried out using an adsorption column packed with activated carbons equipped with thermocouples. The experimental concentration and temperature profiles occurring inside the carbon bed was studied for various operating conditions. Also the oxidation and ignition temperatures were measured for the activated carbons saturated with VOC's using differential scanning calorimetry technique. Some of the important results of this work were the heat liberated during the adsorption is sufficient to start the oxidation reactions in the filter. The oxidation temperature depended on the nature of the COV and the adsorbent. Some VOC's like the ketone had lower oxidation temperature, and were identified to be more vulnerable to oxidation reactions when adsorbed in activated carbon.

A series of experiments were conducted by Naujokas [1985] to evaluate the activated carbon combustion during the adsorption of various industrial organic compounds in carbon beds. The experimental set-up consisted of a flow system with an adiabatic bed of 5 cm diameter and 100 cm long column having thermocouples positioned along the centerline at 5 cm intervals. The oxidation behaviour of about 22 organic compounds was studied and one of the aims of the study was to identify the more reactive organic compounds. The activated carbons were saturated with the various organic compounds under an inert atmosphere and then the carrier gas was switched to air. The heat generated by the oxidation reaction, the position and time required for the generation of the hot spots were measured. From that study it was shown that aldehydes and ketones exhibited high oxidation rates compared to aliphatic and aromatic solvents. Esters, acrylic monomer and tetrahydrofuran had the lowest reactivity.

Johnson and Woods, [1971] studied the flammability of activated carbon beds used in air purification systems like manned space vehicles, submarines and closed environmental systems. The flash point studies of the hydrocarbons adsorbed on charcoal was carried out by the authors using Pensky Martens closed cup apparatus. The flash point of a flammable liquid is the lowest temperature at which it can form an ignitable mixture in air. The hydrocarbon

## ***Chapter 2: Literature Review***

---

loading limit had to be around 30 % to have significant flashing indicating that loading limit of the hydrocarbon on the activated charcoal had an important impact on the flammability. Also experiments were conducted for the measurement of the spontaneous ignition temperature of the activated carbons using the ASTM D2155-66 method. The procedure included the introduction of the sample into a heated flask and records the evidence of ignition or non-ignition. Analysis of activated coconut and coal based charcoals used for air purification in submarines showed that hydrocarbons were mostly adsorbed onto these materials. The flammability hazard was observed only for the charcoals nearly saturated with hydrocarbons. The most important hazard was the lethal concentration build up due to the release of large amounts of CO and CO<sub>2</sub> produced by the oxidation of the carbon material in the presence of the hydrocarbons due to the utilization in closed environments in purification systems for space vehicles and submarines.

The carbon bed system activity is greatly enhanced by higher molecular weight or bifunctional solvents such as cyclohexanone or diacetone alcohol [Zerbonia *et al.*, 2001]. The adsorbed phase even at low gas phase concentrations of these solvents can create hot spots. The action of these solvents also depend on other factors like the characteristics of the activated carbon, system used and efficiency of the instrumentation used for monitoring. Takeuchi *et al.*, [1990] and Henning *et al.*, [1989] studied the oxidation of cyclohexanone and ketones. The investigators found that the adsorption of cyclohexanes and ketones were highly reactive and were largely responsible for the carbon bed ignition. The other important finding was that the adsorption temperature should not exceed 30 °C for methyl ethyl ketone and cyclohexane because surface reactions with these ketones increase exponentially above this temperature. The detailed reaction mechanisms of these compounds are dealt in detail in section 2.3.2.

Table 2-4 shows accidents like Scott graphics (USA) treating acetones, explosion in the storage facility in South Carolina involving thinners and lacquers (essentially containing acetone, methyl ethyl ketone and toluene) demonstrates the potential fire hazard caused by the adsorption of the organic solvents.

### **2.1.3 INFLUENCE OF IMPREGNATION OF ACTIVATED CARBON**

Carbons are usually impregnated to capture high vapour pressure toxic gases. The impregnates in the activated carbons may be responsible for their increase in the reactivity

## ***Chapter 2: Literature Review***

---

with oxygen. The impregnates may vary from metals like copper, chromium, molybdenum, zinc to chemicals such as  $K_2CO_3$  and  $ZnCl_2$ . The impregnate is selected based on the specific species to be adsorbed [Fortier *et al.*, 2004]. The type of impregnation, composition and the process of impregnation may also create or modify acidic or basic functional groups [Suzin *et al.*, 1998], thus providing numerous adsorption sites leading to high adsorption performances and at the same time causing hot spots and bed fires.

The impregnation can lead to the lowering of the self heating temperature and as a result, fire can occur during the bulk shipping of these activated carbons. The classical example is the fire reported in the containers of Kitano vessel loaded with activated carbon pellets impregnated with potassium hydroxide found (Table 2- 4). The increased reactivity found in these materials is due to the catalytic activity of the impregnates which oxidize easily producing high local temperature and oxidation of the carbon material [Suzin *et al.*, 1998].

### **2.1.4 INTRODUCTION OF AIR INTO SOLVENT LOADED CARBON BED ADSORPTION SYSTEM**

The air flow into the carbon adsorption systems or to activated carbons saturated with organics accelerates the oxidation and ignition reactions and helps to sustain the existing combustion reactions and hot spots.

Smisek and Cerney [1970], studied the characteristics of carbon fires that had occurred in regenerable fixed carbon beds used for the recovery of ketones, aldehydes or similar compounds. They found that the bed fires frequently occurred in carbon beds shut down for a few days due to production schedules and mechanical failures. The bed fires occurred when the adsorption cycle was restarted (i.e. air/vapour stream reintroduced into the system). The investigators attribute these fires to the spontaneous oxidation of carbon. When an insufficiently dried and cooled carbon bed adsorber is shut off air can be withdrawn into the carbon bed through the imperfectly sealed walls of the carbon adsorber vessel. Since the heat generated by this oxidation is removed slowly, localized areas in the carbon bed may be heated to the carbon's self ignition temperature. Self ignition is also aided by the oxidation of incompletely desorbed solvent residues (e.g., the oxidation of acetone to acetic acid). If the hot spots exist when the adsorber is restarted, the sudden increase or exposure to air/oxygen starts the fire.

This type of accidents is commonly found in carbon adsorbers with the typical example of the ignition of activated carbon filter in the industrial site in Lens (France) manufacturing lead, tin and zinc shown in Table 2-4. The fire was caused by the entry of air into the activated

## ***Chapter 2: Literature Review***

---

carbon filter system when the trap was opened for maintenance without proper precautions like inerting the system. This gives the scale of risk due to the introduction of air in the carbon bed adsorber system.

Naujokas [1985], studied the velocity of air bleed on the carbon bed combustion saturated with methyl ethyl ketone. Hot spots were observed for an air bleed velocity of 0.2 cm/sec whereas it was absent for 0.35 cm/sec. The higher velocity increased the convective heat transfer rate when compared to the heat generation rate. Hence lower air bleed velocities favoured the hot spots in activated carbon beds saturated with organics.

### **2.1.5 INFLUENCE OF AIR/OXYGEN ON THE REACTIVITY OF ACTIVATED CARBONS**

Above a certain temperature limit, activated carbons undergo oxidation reactions with air. Bowes and Cameron, [1971] reported that a newly manufactured chemically activated carbon undergoes appreciable exothermic reactions upon initial exposure to air at ambient temperatures. According to this author, these exothermic reactions, which are due to rapid adsorption of oxygen and moisture, are largely completed in a period of few minutes to few hours. The rate of the oxidation reaction thus decreases with the ageing of the carbons.

The influence of the oxygen concentration in air and the effect of varying pressures on the spontaneous ignition behaviour of the activated carbons were studied by Miyake *et al.*, [2005]. The ignition behaviour of the activated carbons was studied using high pressure differential scanning calorimeter in pressures varying from 1-5 MPa and for the concentration of oxygen ranging from 10 – 50 % of oxygen. The spontaneous ignition temperature was measured from the adiabatic self heating curve where the sample loaded in quartz cell is heated up to a desired set temperature in N<sub>2</sub> gas and then it is switched off to O<sub>2</sub>/N<sub>2</sub> atmosphere. A change in the sample temperature to the set value is adjudged as ignited. The results showed that the increase in the concentration and pressure of the oxygen decreased the ignition temperature and the onset temperature could be predicted with the oxygen concentration.

### **2.1.6 INFLUENCE OF MOISTURE**

The effect of moisture content of the activated carbons on the oxidation reactivity can be found in literature under two categories. The first one is the moisture content of the surrounding the gas and second one is the inherent moisture content of the carbon during the reactivity with VOC's and air. The inherent moisture content of the material and the moisture

## ***Chapter 2: Literature Review***

---

content of the surrounding gas play a promoting or an inhibiting role in the low temperature oxidation process. The moisture content in the activated carbons takes part in the mass transfer of the oxygen into the interior of the pores. Excess amount of moisture forms a film on the carbon particles and condense in pore channels blocking the oxygen diffusion to the reaction sites in the interior of the pores. The order of magnitude of diffusion of oxygen in water film is about 4 times lower than that in air.

Some authors have reported the existence of critical moisture content present in materials like coal which have an important impact on the oxidation at low temperatures below 100 °C [Wang *et al.*, 2003; Clemens and Matheson, 1996]. The oxygen consumption reaches a maximum value at critical moisture content and this rate may be reduced for some coals when the moisture content reaches above or below the critical value. The critical moisture content is said to vary from one type of coal to another. The critical moisture content may reflect particular oxidation conditions when the reactive sites in the coal pores are fully accessible to O<sub>2</sub> and H<sub>2</sub>O thus optimally enhancing the oxidation process. The formation of unstable intermediates like the peroxides and hydroperoxides during the oxidation process is facilitated by the molecules of H<sub>2</sub>O.

Naujokas [1985] and Delage *et al.*, [2003], studied the effect of moisture content on the hot spot formation in carbon beds used for adsorption of organic compounds and solvent recovery systems. The steam generated beds normally has significant amount of water after the desorption cycle. In addition there may be condensed water either inside the pores or on the outside of the carbon particles. Both the adsorbed and condensed water may be manipulated in an attempt to minimise spontaneous bed combustion by controlling oxidation reactions and providing a sink. Hot spots have been generated both for the dry carbon beds and carbon beds at 60 % relative humidity, but the system containing water vapour required several hours longer for the hot spot to develop.

Hence we can conclude from most of the accidents reported and from the literature studies that the heat accumulation of the exothermic oxidation of the adsorbed chemicals is the major cause for oxidation and ignition hazards of activated carbons. Apart from these, the physical adsorption of air and chemical oxidation with oxygen under usual atmospheric conditions are also responsible for the oxidation and ignition reactions. Activated carbons with oxygen may undergo oxidation and self heating followed by ignition at relatively low temperatures without the action of any other chemicals.

### **2.1.7 INFLUENCE OF CARBON TYPE**

The oxidation and ignition characteristic is function of the carbon type and condition of preparation. Chemically activated carbons are liable to easy oxidation and ignition reactions than the physically activated ones [Bowes and Cameron, 1971; Jones, 1998]. The main reason is attributed to the presence of volatile matter in the carbons which is not removed owing to the low temperatures experienced during activation.

In some cases, ash content in the activated carbons has an effect on their reactivity. The presence of ash content particularly the mineral matter present in some cases increases the reactivity of the activated carbons [Zerbonia *et al.*, 2001]. For applications in carbon canisters where the tank vent stream contains reactive organics, selection of activated carbons with high ignition temperature and low ash content may help avoid carbon bed fires. Ash contents can be lowered by washing the carbon with acid during the manufacturing process [Cameron and MacDowal, 1971].

## **3 MECHANISMS OF OXIDATION AND IGNITION**

After understanding about the various factors influencing the oxidation and ignition reactivity of activated carbons from literature, the following section explains the mechanisms of oxidation and ignition of activated carbons.

Based on studies on the self heating of charcoal [Johnson and Woods, 1971] and activated carbon [Bowes and Cameron, 1971] it has been admitted for a long time that self heating is principally a consequence of carbon oxidation. This oxidation is relatively slow and is different from the rapid adsorption of oxygen by freshly prepared carbons exposed to oxygen. The oxidation of the organic compounds also initiates a temperature rise, which accelerates the reaction rate, when the temperature is high enough; the carbon itself starts to be oxidized and contributes to further temperature increases. Hot spots are first developed in the carbon bed. Ignition occurs when sufficient oxygen is adsorbed in the form of oxygen complexes. The hot spots expand, causing the carbon to oxidize rapidly with the liberation of CO<sub>2</sub> and CO.

So the mechanisms of oxidation and ignition will be dealt in two parts namely, in the presence of air at low temperatures which is commonly called as the low temperature oxidation process and in cases leading to ignition and secondly due to the presence of organic chemicals.

### **3.1.1 AIR OXIDATION STUDIES**

The process of low temperature oxidation is a complex phenomenon that occurs from ambient conditions of temperature to an upper limit of around 300 °C. Among the carbonaceous materials, the low temperature oxidation is well explained in coal. There are numerous literature and experimental studies available for the low temperature oxidation process for coal, but very little is known about the mechanisms in activated carbons.

Literature sources [Wang *et al.*, 2003] commonly depict the oxidation and ignition of porous carbonaceous material like coal in oxygen with a sequence of steps and can be seen in figure 2- 6 :

1. The transport of oxygen from the surroundings to the surface of the carbon material. The transfer of oxygen here takes place from the bulk to the film surrounding the particle by convective mass transfer and then by the process of diffusion into the film.
2. It is then followed by the diffusion step where the oxygen penetrates into the pores of the activated carbons.
3. Then the interaction of oxygen with the surface oxygenated groups, impregnates takes place with the formation of intermediate complexes, emission of heat and gaseous products.
4. The final step is the continuation of the rapid oxidation and decomposition reactions leading to ignition of the material.

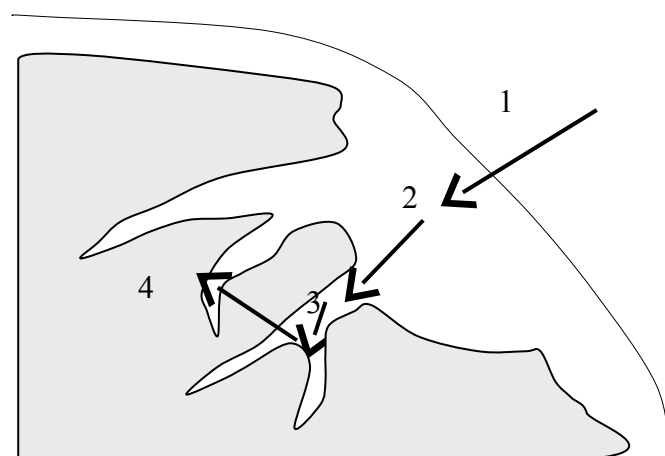


**Figure 2 - :** Schematic representation of the phenomena of mass and heat transfers [Giraudet, 2003].

### 3.1.1.1 OXYGEN CONSUMPTION

The primary step of the oxidation process is the consumption of oxygen. The consumed oxygen is then converted to oxidation products. The oxygen may be physically or chemically adsorbed on the surface of the activated carbons. The physical adsorption is similar to that of the process of condensation, here the oxygen molecules are bonded to the surface by the weak forces of attraction and they can easily be removed from the surface. The physical adsorption results in the single or the multilayer of adsorbed molecules and the heat of adsorption are of the same order of the heat of vaporisation.

On the contrary, the chemisorption process is surface specific and the forces involved are much stronger. Only particular sites at the internal surfaces of the pores can attract the oxygen molecules and hold them by the valence forces occurring between the atoms in molecules [Hayward *et al.*, 1964]. Chemisorption occurs in these active sites which are limited to the monolayer of the molecules and the heat of chemisorption is relatively higher than the heat of physisorption. Microcrystalline carbons like activated carbons have more disordered structures and edge area, which results in the large propensity for oxygen chemisorption. The end of the basal planes contains unsaturated carbon atoms, which form the sites for the attachment of heteroatom and thus play a significant role in chemisorption. The rate of uptake of oxygen at ambient temperature is very slow and can be analysed by measuring the rate of weight gain with time [Itay *et al.*, 1989].

Different reaction regimes may dominate the oxygen consumption depending upon the mass transfer process and the physical and chemical properties. These regimes include external diffusion, internal diffusion and chemical reactions. All the external mass transport of oxygen can be the rate limiting step if a water film is found on the particle surface.

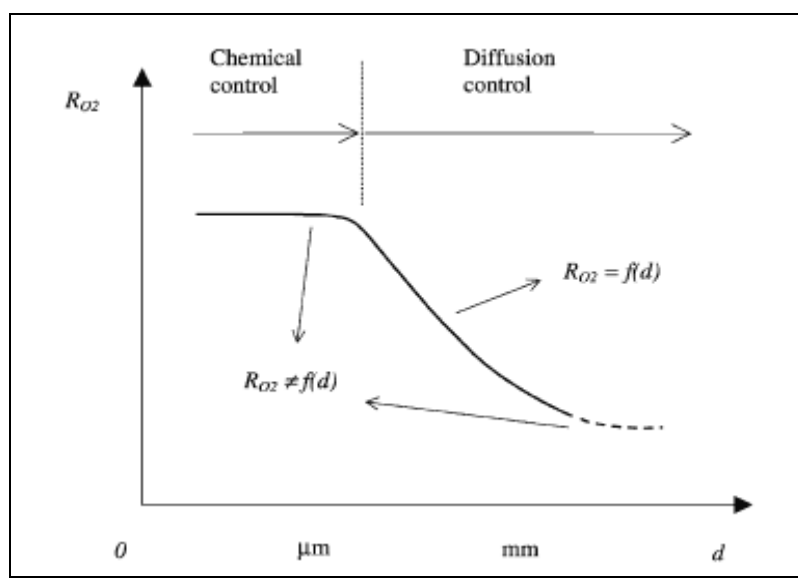


**Figure 2 - :** A typical trend illustrating the effect of particle size on the rate of oxygen consumption [Wang *et al.*, 2003].

The reaction regimes imposed by the particle size are shown in Figure 2-7. For large particles, the rate of oxidation is controlled by oxygen diffusion in the pores. When the particle size is very small, the reaction rate is mainly chemically controlled, as the oxygen diffuses deeply into the coal pores building up a gas concentration equal to that in the bulk phase. Hence the reaction regime is characterized by the apparent independence of the rate of oxygen consumption with the particle size.

### **3.1.1.2 REACTION MECHANISMS AND OXIDATION PRODUCTS**

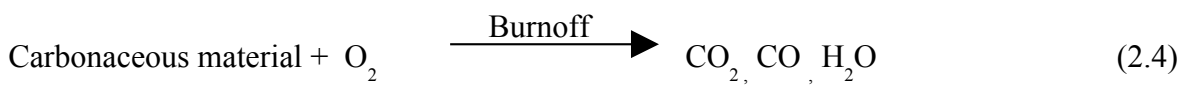
The main products of the oxidation of carbonaceous materials are the oxides of carbon and water. Extensive reaction mechanisms were proposed by different authors for the oxidation process with air. These mechanisms were based on the products evolved and the conditions of temperature and pressure.

Oxidation reactions have been extensively studied for carbonaceous materials like coal, and extended to other materials also. They are broadly grouped into two main parallel reactions namely: the direct burn off reaction and the sorption reaction.

#### **1. Direct burn-off reaction**

The direct burn-off reaction has been widely found in literature, but no direct evidence is quoted to confirm the mechanism. Wang *et al.*, [2003] did support the mechanism of direct burn-off reaction on the basis of some experimental evidence conducted by comparing the production rates of carbon oxides from the oxidation process and the subsequent desorption experiment using an isothermal flow reactor.

It was concluded that the presence of oxygen not only starts the chemisorption reaction but also results in the occurrence of the direct burn-off reaction that can produce carbon oxides. The reaction suggested resembles to that of the direct combustion (pre-ignition) reactions of solid fuels, which takes place at temperatures as high as 300 °C. But still a concrete conclusion or mechanism has not yet been reached. The direct burn off reaction is shown in equation 2.4

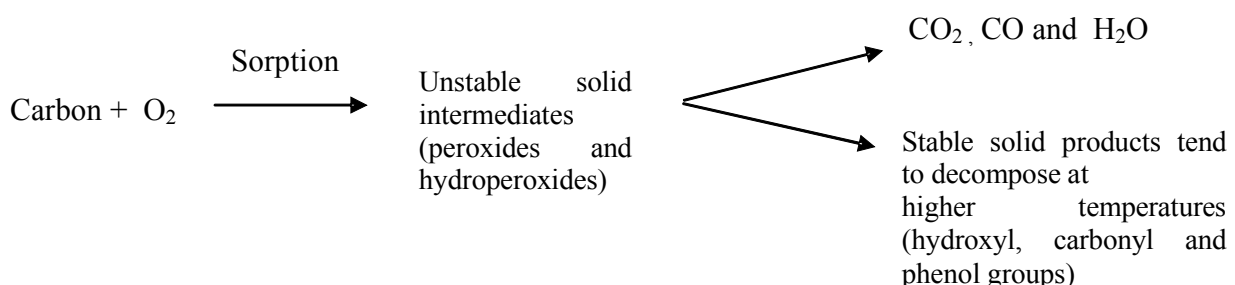


### **2. Sorption reactions**

The following steps were found to take place during the sorption sequence namely the

The chemisorption of oxygen takes place in the pores of the carbonaceous materials to form unstable carbon complexes. The unstable intermediates may be peroxides and hydroperoxides.

The decomposition of the unstable oxygenated complexes takes place with the liberation of oxides of carbon and water or the formation of stable solid complexes containing hydroxyl (OH), carboxyl (-COOH) or phenol groups. These stable complexes are degraded at high temperature. There is certain amount of exothermic heat given out during the decomposition of these unstable complexes.



#### ***3.1.1.2.1 Detailed reaction steps in chemisorption sequence***

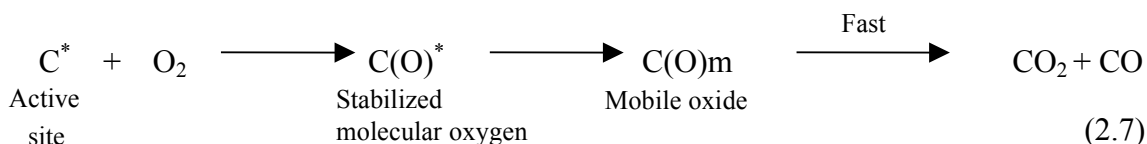
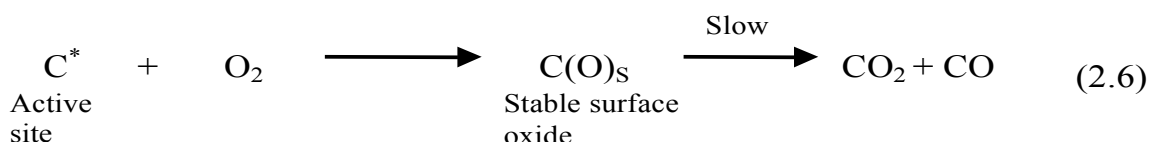
The chemisorption sequence starts with the formation of intermediate complexes like peroxides due to the coupling of the oxygen molecule with a free carbon centre. These intermediate complexes are highly unstable species and decompose into other products in a short period of time. These species can be detected by techniques like titrations, although the results are always a point of discussion for their ambiguity. The peroxides formed are converted into hydroperoxides (-O-O-H) with the removal of hydrogen atom from the aliphatic or the aromatic structure [Kudynska and Buckmaster, 1996]. This step is confirmed by the dissociation energy of about 377 kJ/mol obtained which is similar to the energy of cleavage of the C-H bond [Nelson, 1989].

## ***Chapter 2: Literature Review***

---

The formation of hydroperoxides is followed by the radical displacement to form hydroxyl (OH) and ether groups (C-O-C) [Liotta *et al.*, 1983]. The carboxyl and the aldehyde, may be produced from the thermal decomposition of the hydroxyl species [Clemens *et al.*, 1991] or by the thermolysis of hydroperoxides [Gethner *et al.*, 1985]. On the whole there are three main functional groups, the –OH (hydroxyl), carbonyl (C=O) and the carboxyl (COOH) and these are believed to be formed from the peroxides (-O-O-). Several researchers have proposed different mechanisms for the evolution of the oxidation products namely CO<sub>2</sub>, CO and H<sub>2</sub>O from the decomposition of the solid oxygenated complexes. Some suggested that the carbon oxides were directly formed from the hydroperoxides at low temperature by the process of thermolysis.

The mechanism involving oxygen chemisorption leading to ignition in cellulosic materials with the help of active sites was explained by Bradbury and Shafizader, [1980]. Two reaction mechanisms similar to the sorption sequence were proposed by the authors found in equation 2.6 and equation 2.7.



According to the authors, the cellulosic materials undergo direct oxidation at low temperatures and the reactions are very slow. The first process described in eq.(2.6) represents the formation of a stable surface oxide by chemisorption at an active site and subsequent slow desorption to give CO<sub>2</sub> and CO. It may require up to 1000 °C for the completion of the desorption reaction takes place in inert gas condition. The second process eq. (2.7) represents a short lived mobile oxide via a stabilized molecular oxygen reaction which is responsible for the majority of the carbon oxide gases formed during combustion. When the oxygen gas was replaced by air in the experiments, rates of chemisorption were reduced by a factor of 5 and ignition temperatures were raised by about 100 °C.

## ***Chapter 2: Literature Review***

Apart from the formation of the surface oxygenated complexes by the interaction with oxygen in air, some of the surface groups are already present in the material. These groups may interact directly with oxygen to give oxidation products which is the case commonly found in freshly prepared chemically activated carbons [Cameron and Macdowall, 1972]. The existence of a large number of reaction pathways and mechanisms indicate the complexity of the oxidation process of activated carbons.

### **3.1.2 MECHANISM OF OXIDATION AND IGNITION REACTIONS WITH VOC's**

The oxidation and ignition of the activated carbon in the presence of VOC takes place more rapidly than the interaction with oxygen. The reactivity depends on the nature of the activated carbon and the type of the VOC. The heat liberated during the adsorption reactions is high and is greater than  $200 \text{ kJ.mol}^{-1}$  and can exceed up to  $1000 \text{ kJ.mol}^{-1}$ . Such high values of exothermic heat make the activated carbons susceptible for ignition reactions.

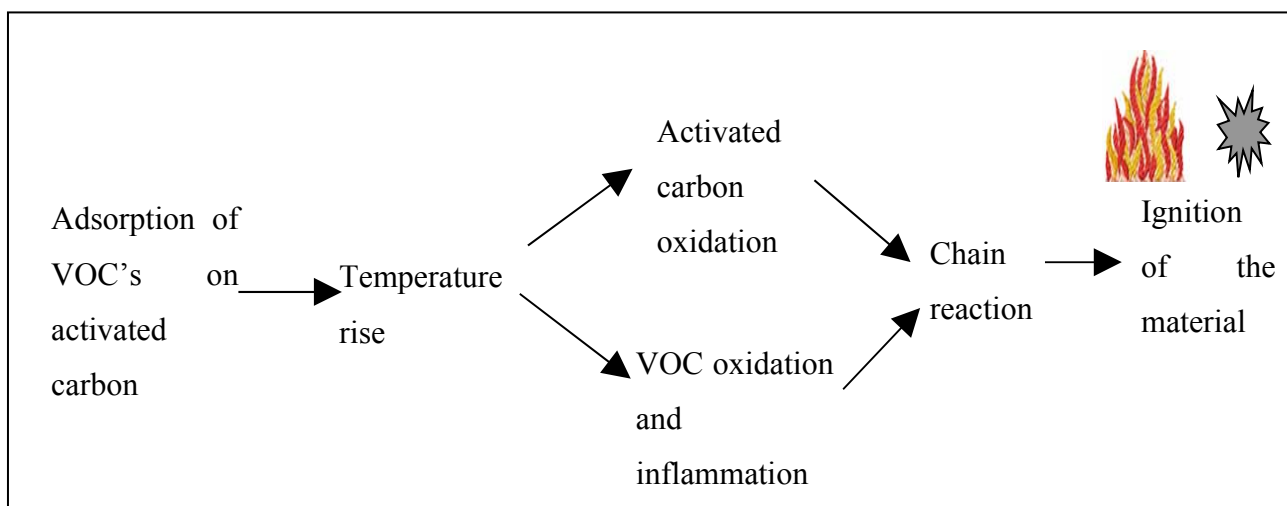


**Figure 2 - :** Steps leading to the ignition of an activated carbon filter with VOC [Delage, 2000].

Delage, [2000] studied extensively about the influence of the nature of VOC on the oxidation and ignition of activated carbons and the schematic representation of the ignition of the activated carbon in the presence of VOC is shown in Figure 2-8. Two reaction pathways for the ignition reactions are possible. If the auto inflammation of the VOC is lower than that of the oxidation temperature of the activated carbon material, then the inflammation of the VOC takes place, which is followed by the ignition of the material. Example for this type of

## ***Chapter 2: Literature Review***

---

mechanism can be found in the VOC systems containing ketone groups like methyl ethyl acetone and methyl isobutyl acetone on activated carbons where they have an oxidation temperature less than 120 °C. The aromatic ketones are easily oxidised than the aliphatic ones and the reactivity of ketones can be lowered by mixing it with less reactive VOC's [Akubuiro and Wagner, 1992].

The second factor that influences the reactivity is the nature of the activated carbon. The oxidation temperature of the activated carbon less than the auto inflammation temperature of the VOC. This type of characteristics is found in hydrocarbons, amines, halogens and alcohols adsorbed onto coconut shell activated carbons. For instance the oxidation of the coconut shell activated carbon (approximately 210 °C) is less than the inflammation of the solvent. Also when a VOC is used in different type of activated carbons, differences in the oxidation temperature is observed which may be explained by the chemical functional groups which interfere in the oxidation reactions and the adsorbent material can take the role of a catalyst in that case [Delage, 2000].

### ***3.1.2.1 VOC OXIDATION MECHANISMS***

Akubuiro and Wagner [1993], proposed a probable mechanism for oxidation of ketones adsorbed onto activated carbons using Fourier transformed infrared spectroscopy. The ketones on oxidation normally form unstable hydroperoxides, which further decomposes to form carboxylic acids, aldehydes and diketones. Two examples are presented here, the first one is an aliphatic ketone namely methylethylacetone and the second one is cyclohexanone which is an aromatic one.

#### ***3.1.2.1.1 Reaction mechanism for methylethylacetone***

Akibuiro, [1993] proposed a mechanism from the identification of the products of oxidation. The reaction starts by the attack of oxygen on the  $\alpha$  carbon of the methylethylacetone. The  $\alpha$  carbon refers to the first carbon after the carbon that attaches to the functional group and in our case it is the carbonyl and it forms  $\alpha$ -hydroperoxide methylethylacetone (product II). In the presence of a strong oxidant, a rupture of the C-C and O-O occurs resulting in the formation of acetaldehyde (product III) and acetic acid (product IV). In the presence of a humid or basic atmosphere, the hydroperoxide transforms into 2,3 butanedione (product V) and water. There are other reactions possible like the 2,3 butanedione can form acetic acid and the acetaldehyde can oxidise to form acetic acid. The products namely carbon dioxide, carbon monoxide and water vapour are formed by further oxidation resulting in the

combustion of the system. All the above reactions are highly exothermic. The heat of the reactions was measured for the system methyl ethyl acetone on Calgon BPL carbon and for the methyl ethyl acetone on Sobonorit B4 system and was found to be 310 and 620 kJ mol<sup>-1</sup> respectively.

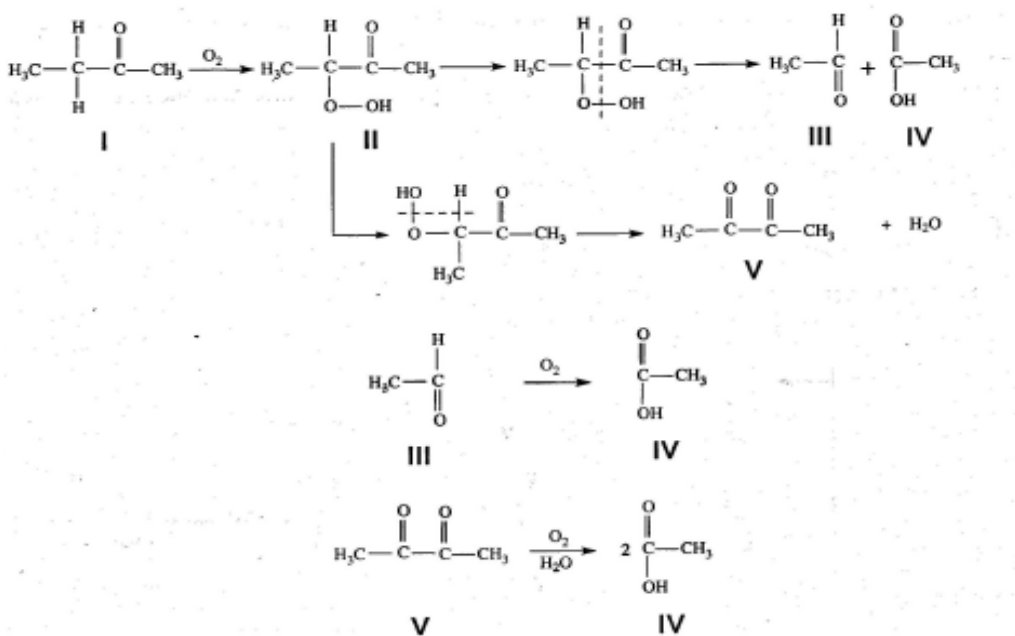


**Figure 2 - :** Probable mechanism of the oxidation of methyl ethyl acetone [Akubuiro, 1993].

### 3.1.2.1.2 Reaction mechanism for cyclohexanone

Like the reaction of methylethylacetone, the oxidation of cyclohexanone starts with the reaction of the  $\alpha$  carbon to form  $\alpha$ -hydroperoxide cyclohexanone (product II) and then decomposes into 1, 2- cyclohexanedione (product III), 2- hydroxycyclohexanone (product IV which exist as a dimer). It may form also adipic aldehyde (product V) and adipic acid (product VI). Hening *et al.*, [1989] proposed in addition the formation of cyclopentanone, phenol and dibenzofurane. The important characteristic of these reactions is the liberation of heat flux which is very important in magnitude of about 2200 kJ mol<sup>-1</sup> for the system namely

cyclohexanone/calgon BPL and cyclohexanone/ Sobonorit B<sub>4</sub> system. The flux generated for cyclohexane is far more superior to the methyl ethyl acetone system.

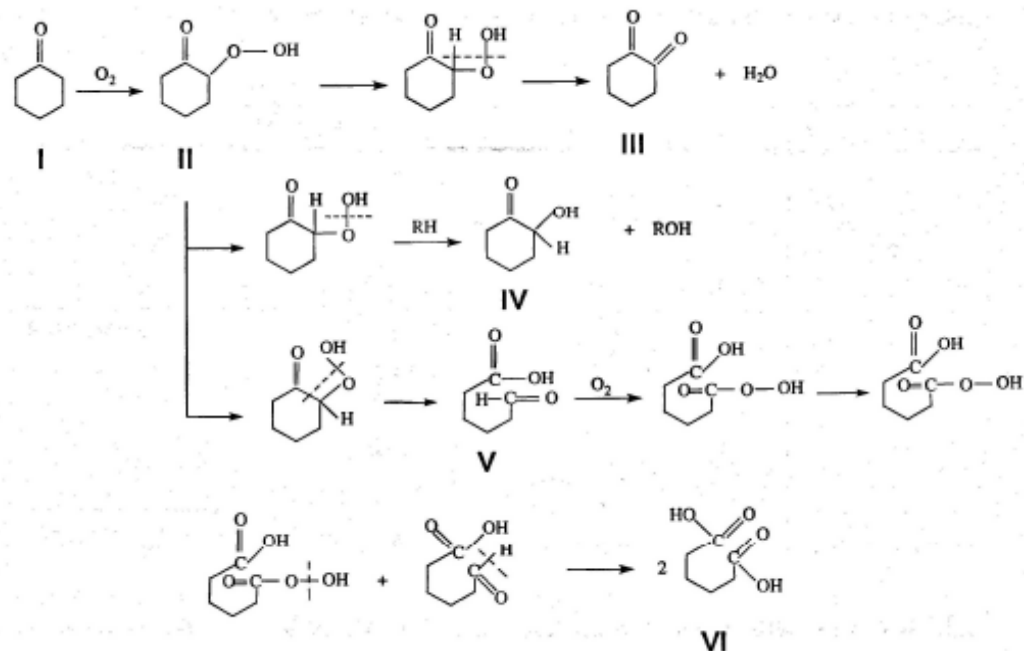


**Figure 2- :** Probable mechanism of the oxidation of cyclohexanone [Akubuiro, 1993].

#### 4 EXPERIMENTAL METHODS ADOPTED TO STUDY OXIDATION PROPERTIES OF ACTIVATED CARBONS

Several test methods can be found in the literature for characterising the oxidation reactivity of activated carbons. These methods enable to determine various parameters representative of the tendency of the carbonaceous materials to ignite. The ignition studies of the activated carbons started with the pioneering works of Bowes and Cameron, [1971] and Cameron and Macdowall, [1972]. The findings of their works later led to the formulation of standard test (IMCO, 1974 and ISO, 1994) which is used widely for assessing the thermal safety of activated carbons. The ignition tests were carried out using cubical heated baskets made of phosphor bronze wire mesh of varying sizes. The baskets are packed with the samples and suspended in an oven preheated to a given constant temperature. The process of self heating was followed by means of chromel/alumel thermocouple placed at the centre and connected to a recorder. If the sample failed to ignite, the experiment is repeated with a fresh sample and with the oven preheated to higher temperature and lower temperature if the sample ignited in the first trial.

## ***Chapter 2: Literature Review***

---

Small scale critical self ignition temperatures and times to ignition at ordinary temperature were deduced from the thermal explosion theory based on the Frank-Kamenetsky model [Frank-Kamenetsky, 1941]. The models based on F-K theory overestimated the parameters by a factor of 5, which is mainly attributed to the experimental conditions differing from the real ones and the hygroscopic nature mainly due to the physisorbed water present in the activated carbons.

A series of studies published by Jones explored criterion for the safe shipment of a series of activated carbons using microcalorimetric measurements. The sample for testing was placed in a steel ampoule, previously stabilized at the set temperature. The ampoule containing the sample and the reference ampoule was then placed in the equilibration position. Thermal equilibration of the samples took place over a one hour period. The ampoules were then lowered into the measuring position and the signal was followed by a potentiometric recorder connected to the instrument. The ampoules were left in the measuring position for several hours and sometimes overnight and the final heat release reading was taken once the value remains stable.

The safety of the activated carbons was assessed on the basis of 2 criteria: the heat release at criticality and the Critical Ignition Temperature (CIT) approach. The heat release rate at criticality and critical ignition temperature are respectively:  $2.10^{-3} \text{ W kg}^{-1}$  at  $38^\circ\text{C}$ , and  $140^\circ\text{C}$  for a 10 cm cube obtained from the Frank-Kamenetsky model. Comparisons were made between q values and CIT values activated carbons of various manufacturing histories and were accordingly assigned safe or unsafe for transportation.

Herbig and Jess [2002] have studied the reactivity and the ignition behaviour of carbonaceous materials like activated carbon, charcoal and coke using fixed bed reactors, fluidised bed reactors, thermogravimetry and oven heating. The experiments were carried out under static and continuous flow conditions. Calculation for the critical parameters like the ignition during transport and storage was made from the Frank-Kamenetsky model. The kinetic parameters (reaction rate constant, activation energy of oxidation) obtained by all the investigated methods were compared and found to be reliable within an acceptable confidence interval. Fast and simple determination of the kinetic data was made by using the fixed bed reactor with a constant flow.

## ***Chapter 2: Literature Review***

---

The characterization of oxidation and ignition process of activated carbons was extensively studied by Suzin *et al.*, 1999. Two regions of interest were defined which describe the oxidation process at relatively low temperature followed by ignition at higher temperature. The limit of the first region is denoted by the Point of Initial Oxidation (PIO). This point corresponds to the minimum temperature above which the carbon starts to oxidize. The surface properties are modified as the advancement of the oxidation reaction reaches a certain value of significance. In the second region, the material ignites in a self-sustaining manner. This region is denoted by the Spontaneous Ignition Temperature (SIT). Thermal analysis techniques consisting of Thermogravimetry and Differential Scanning Calorimetry were used to determine PIO and SIT data of various activated carbon materials. The detailed description of the TG-DSC methods can be found in chapter 3.

The ignition temperature of activated carbons was also determined in the work of Suzin *et al.*, [1999] using the ASTM method (D 3466-76) which consisted in exposing a sample material to a stream of heated air. Sample and air temperatures are increased at a constant rate of 2 or 3°C min<sup>-1</sup> until the carbon ignites. The slope of the sample bed or the outlet temperature profiles from pre and post ignition are linearly extrapolated and the intersection of the two curves is defined the SIT.

Parameter	Activated carbon samples					
	ASZM-T	ASC	ASZM	Coconut shell	Maxsorb	BPL
<i>SIT (°C)</i>						
ASTM	300	265	300	365	>370	>370
DSC	365	330	365	475	410	525
TG	370	335	370	480	455	565
<i>PIO (°C)</i>						
ASTM	150	195	225	210	265	360
DSC	165	220	260	215	295	470
TG	215	290	315	325	385	500

**Table 2 - :** Oxidation and ignition temperatures evaluated by the various methods [Suzin *et al.*, 1999].

The values obtained from the different methods were compared in his work and are shown in Table 2-5. The abbreviations refers to impregnated activated carbon samples with the impregnates ASZM-T (Cu, Ag, Mo, Zn, TEDA), ASC (Cr, Cu, Ag), ASZM (Cu, Ag, Mo, Zn). The ASTM method of determining the SIT and PIO value was found to be closer to those values found in practice but it did not necessarily reflect the minimum ignition

temperature at which the ignition can occur [Suzin *et al.*, 1999]. According to the authors, the ignition temperature is dependant on the physical properties of the filter, impregnates on the carbon and the flow rates of the filtrate. An accurate value of SIT and PIO can be ensured only when they were uniquely determined under application specification conditions for each adsorbent. Hence the different methods found in literature did not perfectly reflect the ideal condition existing in practice. In order to obtain the accurate values of oxidation and ignition temperatures, application conditions resembling the same flow rate, bed dimensions, carbon type, flow rate of the filtrate, etc have to be applied which is very difficult to obtain. The DSC technique seems to be not too far away from the ASTM method, one of the unique advantages is the simplicity of these tests (short experimentation time, less sample quantity, ease in maintaining the test conditions constant, higher repeatability and better instrumentation).

## **5 CONCLUSION**

The literature review gives abundant information on the activated carbon materials, fire incidents associated with them and an overview of the oxidation and ignition mechanisms with outlining the various factors influencing them.

The characteristics of the activated carbon like the surface chemistry, physical structure and the porosity characteristics of the activated carbons were found to be complex and diverse. They are found to be dependant mainly on the origin of the material used and mode of activation employed. The chemically activated carbons were subjected to lower temperatures than the physically activated carbons during their manufacturing stage.

The different incidents of fire and thermal runaways in industries utilizing activated carbons were also assessed. The majority of accidents were associated with the VOC's either during their adsorption or due to the introduction of air into the system of activated carbons saturated with VOC. Fires were also found during the transportation of activated carbons due to their reaction with oxygen in air and it was mainly encountered for the chemically activated and freshly prepared activated carbons and charcoals. The factors influencing the ignition of activated carbon were identified from the various accidents assessed using the reviews from literature.

The mechanisms for the oxidation and ignition of activated carbons mainly by the action of VOC's and air were approached. The surface oxygenated groups and the porous structure play an important role in the oxidation and ignition reactions due to the reactions forming unstable

## ***Chapter 2: Literature Review***

---

complexes, exothermic heat and oxidation products. The VOC's on the other hand liberate exothermic heat due to their adsorption phenomenon. Concerning the different methods found in the literature for the study of oxidation and ignition properties of activated carbons, the experimental results depend on the condition in which the tests were performed. Though the ASTM D3466-76 was closest to the temperatures prevailing in reality, the deviation still existed and hence the experiments should be done in the activated carbon application conditions which are very difficult to achieve in a laboratory scale.

### **6 REFERENCES**

1. Akubiro, E.C. and Wagner "Potential mechanistic roots for the oxidative disintegration of ketones on carbon adsorbents," *Ind. Eng. Chem. Res.*, **32**, 2690-2698 (1993).
2. Balci, S., Ph.D dissertation, Middle East Technical University - METU, Ankara (1992).
3. Bansal, R.C., J.B. Donnet, and N. Stoeckli. Active Carbon, pp. 10-49, Marcel Dekker, New York, (1988).
4. Boehm, H.P., "Some aspects of the surface chemistry of carbon blacks and other carbons," *Carbon*, **32**, 759-769 (1994).
5. Boehm, H.P., "Surface oxides on carbon and their analysis: a critical assessment," *Carbon*, **40**, 145-149 (2002).
6. Bowes, P.C. and A. Cameron, "Self heating and ignition of chemically activated carbon". *J. Appl. Chem. Biotechnol.*, **21**, 244-250 (1971).
7. Bradbury, A.G.W. and F. Shafizadeh, "Role of oxygen in low temperature ignition of cellulose," *Combustion Flame*, **37**, 85-89 (1980).
8. Cameron, A. and J.D. MacDowall, "The self heating of commercial powdered Activated carbons," *J. Appl. Chem. Biotechnol.*, **22**, 1007-1018 (1972).
9. Chapman, M.J. and D.L. Field, "Lessons from carbon bed adsorption losses," *Loss Prev*, **12**, 136-141 (1979).
10. Clemens, A.H. and T.W. Matheson, "The role of moisture in self heating of low rank coals," *Fuel*, **75**, 891-895 (1996).
11. Clemens, A.H., T.W. Matheson, and D.E.Rogers, "Low temperature oxidation studies of dried New Zealand coals," *Fuel*, **50**, 215-221 (1991).
12. Delage, F., Ph.D dissertation, University of Poitiers, Ecole des Mines de Nantes, France (2000).

## ***Chapter 2: Literature Review***

---

13. Delage, F., P. Pré., H. Tezel, and P. Le Cloirec, "Mass transfer and warming during adsorption of high concentrations of VOC on an activated carbon bed: experimental and theoretical analysis," *Environ. Sci Technol.*, **34**, 4816-4821 (2000).
14. Donnet, J.B., E. Custodero., T.K. Wang, and G. Hennebert, "Energy site distribution of carbon black surfaces by inverse gas chromatography at finite concentration condition," *Carbon*, **40(2)**, 163-167 (2002).
15. EPA, Chemical Emergency Preparedness and Prevention office. Fire Hazard from carbon deodorizing systems. EPA 550-F-97-002 e (1997).
16. Figueiredo, J.L., M.F.R. Pereira, M.M.A. Freitas, and J.J.M. Orfao, "Modification of the surface chemistry of activated carbon," *Carbon*, **37**, 1379-1389 (1999).
17. Fortier, H., S. Zhang, and J.R. Dahn, "Simulations of isothermal oven tests of impregnated activated carbons in cylindrical and cubic sample holders," *Carbon*, **42**, 2385-2392 (2004).
18. Frank-Kamenetsky, D.A, "Ignition and extinction of solid surfaces," *C.R. Acad. Sci, URSS*, **30(8)**, 734-737 (1941).
19. Franklin, R.E, "Crystallite growth in graphitizing and non-graphitizing carbons," *Proc. Roy. Soc, London*, **209**, 196-219 (1951).
20. Gartein, V.A. and D.E. Weiss., "Surface chemical structures of activated carbons," *Rev. Pure Appl. Chem.*, **7**, 69 (1957).
21. Gethner, J.S, "Thermal and oxidation chemistry of coal at low temperatures," *Fuel*, **64**, 1443-1446 (1985).
22. Giraudet. S., "Study of energetic interactions during the adsorption of VOC's on activated carbons," Research report, University of Poitiers and Nancy, (2003).

## ***Chapter 2: Literature Review***

---

23. Gregg, S.J. and K.S.W. Sing, Adsorption, surface and porosity, pp 59-73, New York Academic Press (1982).
24. Hayward, D.O. and B.W. Trapnell, "Chemisorption in carbon materials" *Butterworth*, London (1964).
25. Henning, K.D., W.Bongartz, and J. Degel, "Adsorption recovery of problematic solvents," *19<sup>th</sup> Biennial Conference on Carbon*, Pennsylvania State University, USA, June (1989).
26. Herbig, C. and A. Jess, "Determination of reactivity and ignition behaviour of solid fuels based on combustion experiments under static and continuous flow conditions," *Fuel*, **81**, 2387-2395 (2002).
27. Holden, M.J., "Manufacture and uses of activated carbon," *J Eff Water Treat.*, **22**, 27-31 (1982).
28. Itay, M., C.Hill, and D.Glasser, "A study of the low temperature oxidation of coal," *Fuel Process Technol*, **21**, 81-97 (1989).
29. Johnson, J.E. and Woods, F.J, "Flammability of activated charcoal used in air purification," *J. Fire Flamm*, **2**, 141-156 (1971).
30. Jones, J.C., "Towards an alternative criterion for the shipping safety of activated carbons," *J. Loss Prev. Proc. Ind*, **11**, 407-411 (1998).
31. Kerr, J., " US Environmental Protection Agency, Region 4, Enforcement and Compliance Branch, Waste Management Division. Information about Investigation and Corrective Measures Related to the January 15, 1998, Carbon Canister Incident, South Eastern Chemical, Sumter," South Carolina (1998).
32. Kudynska, J. and H.A. Buckmaster, "Low temperature oxidation kinetics of high-volatile bituminous coal studied by dynamic in situ 9 GHz c.w. epr spectroscopy. *Fuel*, **75**, 872-878 (1996).

## ***Chapter 2: Literature Review***

---

33. Le Cloirec. P., Multiscale Analysis of Environmental Technologies – MUST, Ecole de Mines de Nantes (2003).
34. Leon. C.A., J.M. Solar, V. Calemma, and L.R. Radovic, “Evidence for protonation of basal plane sites on carbon,” *Carbon*, **30**, 797-811 (1992).
35. Liotta, R. G., Brons, and J.Isaacs, “Oxidative weathering of Illinois No.6 coal,” *Fuel*, **62**, 781-791 (1983).
36. Long, F.J. and K.Skykes, “The mechanism of the steam-carbon reaction” *Proceedings of the royal society of London, series A mathematical and physical sciences*, **1034**, 377-399 (1948).
37. Lu. Z., Ph.D dissertation, Pennsylvania State University, USA (2006).
38. Mangun, C.L, K.R. Benak, and M.A. Daley, “Oxidation of activated fibers: effect of pore size, surface chemistry and adsorption properties,” *Chem. Mater.*, **11**, 3476-3483(1999).
39. Marine investigation report M01M0017, Transport Safety Board (TSB), Transportation Ministry, Canada (2001).
40. Martin, A.E., “Chemistry of coal utilization,” 2<sup>nd</sup> Supp. vol, John Wiley & sons inc (1981).
41. Mattson, I.S. and H.B. Mark, “Activated carbon surface chemistry and adsorption from solution” Newyork, Marcel Dekker (1971).
42. Miyake, A., S.Ando, T.Ogawa and Y.Lizuka, “Influence of atmospheric conditions on the spontaneous ignition behaviour of activated carbon,” *J. Therm. Anal. Calorimetry*, **80**, 519-523 (2005).
43. Naujokas, A.A., “Spontaneous combustion of carbon beds,” *Plant/Operations Progress*, **4**, 120-126 (1985).
44. Nelson, C.R., “Coal weathering: chemical processes and pathways” *Elsevier*, 1-32 (1989).

## ***Chapter 2: Literature Review***

---

45. Proctor, A. and P.Sherwood, "XPS studies of carbon surface," *Surface and Interface Analysis*, **4(5)**, 213 (1982).
46. Oberlin, A., High resolution TEM studies of carbonization and graphitization, in Chemistry and physics of carbon, vol. 22, edited by Peter A. Thrower, New York, Marcel Dekker, Inc (1989).
47. Oberlin, A., "Carbonization and graphitization" *Carbon*, **22**, 521-541 (1984).
48. Procter, A. and M.A., Sherwood, "Data analysis techniques in X-ray Photoelectron spectroscopy," *Anal. Chem.*, **54**, 13-18 (1982).
49. Puri, B.R., "Chemistry and Physics of Carbon," Marcel Dekker, New York (1970).
50. Puri, B.R. and R.C. Bansal, "Studies in surface chemistry of carbon blacks," *Carbon*, **3**, 523-539 (1966).
51. Reinoso, F.R., "The role of carbon materials in heterogeneous catalysis" *Carbon*, **36**, 159-175 (1998).
52. Selitti, C., J.K. Keonig, and H. Ishida, "Surface characterization of graphitized carbon fibers by attenuated total reflection fourier transformed IR-spectroscopy," *Carbon*, **28**, 221-228 (1990).
53. Smisek, M. and S.Cerny, "Active carbon: Manufacture, Properties and Applications," *Elsevier Publishing Company*, Amsterdam, The Netherlands (1970).
54. Standard test method for autoignition temperature of liquid petroleum products. ASTM-D 2155-66 (1982).
55. Standard test method for ignition of granular activated carbon. ASTM-D 3466-76 (reapproved 1993).
56. Suzin, Y., L.C. Buettner and C.A. LeDuc, "Behaviour of impregnated activated carbons heated to the point of oxidation," *Carbon*, **11**, 1557-1566 (1998).

## **Chapter 2: Literature Review**

---

57. Suzin, Y., L.C. Buettner and C.A. LeDuc, "Characterizing the ignition process of activated carbon," *Carbon*, **37**, 335-346 (1999).
58. Takeuchi, Y., M.Mizutani, and H. Ikeda, "Adsorption of binary and tertiary organic solvent vapour in air by a fixed bed of granular activated carbon," *J. Chem. Eng. Jpn*, **24**, 411-417 (1991).
59. van der Merwe, M.M. and T.J. Bandosz J, "A study of metal impregnated carbons: the influence of oxygen content in the activated carbon matrix," *J. Colloid Interface Sci*, **282**, 102-108 (2005).
60. Walker P.L., J. Rusinko, and L.G. Austin, "Gas reaction of carbon" *Adv. Catalysis*, **11**, 134-221 (1959).
61. Wang, H., Z.B. Dlugogorski, and E.M. Kennedy, "Coal oxidation at low temperatures: oxygen consumption, oxidation products, reaction mechanism and kinetic modelling," *Progress in Energy and Combustion Sci*, **29**, 487-513 (2003).
62. Wildman, J., "Practical problems in solvent recovery using activated carbon", *Proceedings of an international conference on carbon.*, University of Newcastle Upon Tyne, United Kingdom, September (1988).
63. Wolff. W.F., " A model of Active Carbon," *J. Phys. Chem*, **63**, 653-659 (1959).
64. Zerbonia, R.A.,C.M. Brockman., P.R. Peterson, and D. Housely, "Carbon bed fires and the use of carbon canisters for air emissions control on fixed roof tanks," *J. Air Waste Management Assoc*, **51**, 1617-1627 (2001).
65. Zielke, U., K.J. Huttinger, and W.P. Hoffman, "Surface oxidized carbon fibers 1. Surface structure and chemistry," *Carbon*, **34(8)**, 983-998 (1996).
66. Website references - <http://aria.environnement.gouv.fr/>

---

## **Chapter 3**

---

### **Materials and Experimental Methods**

---

#### **3. MATERIALS AND EXPERIMENTAL METHODS**

In order to study the thermal behaviour of activated carbons experimental procedures were performed. This chapter reports the experimental methods for material characterization. The first section outlines the choice of the carbon samples used for the study with details about their manufacture and origin. The second section concentrates on the different characterization techniques describing the instrumentation, theory, experimental methodology and the calculation procedures.

The material characterization consists of four main parts. The first part is on the thermal analysis study for determining the oxidation and ignition properties of the carbons samples. It is mainly carried out using thermogravimetry coupled with differential scanning calorimetry (TG-DSC).

This part consists in the study of the measurement porosity properties mainly using N<sub>2</sub> adsorption and mercury porosimetry techniques. The third part focuses on the chemical composition of the carbon samples and ash content analysis. The chemical composition is studied using the Boehm's titration and the elementary analysis methods, whereas the ash content analysis is carried out using ASTM and SEM-X methods. This final part of this chapter describes the structural characteristics analysed using High Resolution Transmission Electron Microscopy (HRTEM) and Scanning Electron Microscopy (SEM) techniques. The qualitative and quantitative data's from the images were obtained.

We remember the objective of this study is first to measure the different material properties of the carbon samples and to analyse and study their influence on the oxidation and ignition characteristics.

## ***Chapter 3: Materials and experimental methods***

---

### **7 INVENTORY**

#### **7.1.1 ACTIVATED CARBON SAMPLES**

Various activated carbon samples were selected differing from each other by the nature of the raw material and the mode of activation applied. They were provided either by commercial suppliers or prepared in the laboratory. The activated carbon samples have diversified origin which includes natural raw materials like coconut shell, peat, coke, wood, olive stone and synthetic products like coal tar pitch and polyacrylo nitrile.

The activated samples from the two modes of activation were chosen to study the effect of the activation on the properties of the activated carbons and their role on the stability towards oxidation and ignition. Activated carbon samples impregnated with metals like copper and chromium were also chosen for this study. The objective is to study the influence of the metal impregnates on the oxidation and ignition characteristics. The physically activated coconut shell sample NC with the suffix Cu and Cr represents the impregnated activated carbons. Apart from the impregnated metals activated carbons rich in nitrogen content from the coal tar pitch and polyacrylo nitrile origin were chosen for the study. The main is to study the influence of the nitrogenated functions on the reactivity of the activated carbons. The carbonized samples were mainly chosen in order to enable us to compare the characteristics of the activated and non-activated carbon samples.

#### **7.1.1.1 PHYSICALLY ACTIVATED CARBONS**

The physically activated carbon samples used for this study were manufactured mostly using steam at about 800-1000 °C. The preparation of the CTP and PAN samples are documented in detail in the work of Grzyb *et al.*, 2004 ; Machnikowski *et al.*, 2005. The starting materials for the samples rich in nitrogen content were polyacrylonitrile (PAN), the oxidized form of poly(4-vinylpyridine) cross linked with 25 wt.% of divinylbenzene (PVPOx) and coal-tar pitch (CTP). The polymers were synthesized in the laboratory from the respective monomers (Aldrich). To produce PAN powder, 80 g of acrylonitrile was added to a glass flask containing 160 cm<sup>3</sup> of an aqueous solution of 1.6 g of ammonium persulphate and 1.12 g of sodium thiosulphate. The resultant solution was heated under reflux conditions at 70 °C for 1 h. Next, the precipitate was separated by filtration, washed with 0.1 N K<sub>2</sub>CO<sub>3</sub> and dried. For the synthesis of

## ***Chapter 3: Materials and experimental methods***

---

polyvinylpyridine (PVP) cross-linked with divinylbenzene (DVB), 21 g of 4-vinylpyridine and 4.4 g of DVB were heated at 70 °C for 1 h under reflux conditions in the presence of 0.21 g of benzoil peroxide as an initiator. The crystalline product of the reaction was filtered, washed with 0.1 N K<sub>2</sub>CO<sub>3</sub> and dried. CTP used in the study was quinoline insoluble free (QI-free) pitch with a softening point (Mettler) of 99.6 °C. The pitch was produced from a commercial coke oven tar, which was centrifugated prior to distillation to remove particulate matter.

Coal-tar pitch was selected as an inexpensive and practically ash-free carbon precursor, which permits blends preparation in a liquid phase [Grzyb *et al.*, 2003]. The blends of CTP and PAN or PVPox of various components weight ratio were prepared by dissolution/dispersion of polymer powder (particle size <60 µm) in the liquid pitch at 250 °C for 0.5 h with a vigorous stirring. The numbers in the extension of the sample names indicate the amount of each constituent used in the blend. For example, the sample CTP-PAN-3:1-A contains 75 % of CTP and 25 % of PAN in the blend and the letter ‘A’ means that the sample is activated.

### ***7.1.1.2 CHEMICALLY ACTIVATED CARBONS***

The chemical activation was performed using concentrated solution of H<sub>3</sub>PO<sub>4</sub>. The temperature range for the chemical activation of the carbon samples were between 450 –600 °C. For example the temperature of activation for the BC-120 sample was about 450 °C and for the GF-40 sample it was 600 °C.

### ***7.1.1.3 CARBONIZED SAMPLES***

The raw carbonized samples are also chosen for the study. These samples are not activated, but were heated from 800-1000 °C in an inert gas. The samples chosen includes non-activated carbonised samples with the extension ‘C’ and the carbonized coconut shell sample as shown in the table 3-1.

### ***Chapter 3: Materials and experimental methods***

---

<b>Sample name</b>	<b>Manufacturer</b>	<b>Raw material</b>	<b>Mode of activation</b>	<b>Activation agent used</b>
NC-50	PICA	Coconut shell	Physical	Steam
NC-60	PICA	Coconut shell	Physical	Steam at 900 °C
NC-100	PICA	Coconut shell	Physical	Steam at 950 °C
RB-2	NORIT	Peat	Physical	Steam
BPL	CHEMVIRON	Coal	Physical	Steam under vacuum
GF-40	NORIT	Olive stone	Chemical	H <sub>3</sub> PO <sub>4</sub>
BC-120	PICA	Wood	Chemical	H <sub>3</sub> PO <sub>4</sub> at 450 °C
PICABIOL	PICA	Wood	Chemical	H <sub>3</sub> PO <sub>4</sub>
NC-70-Cu	PICA	Coconut shell	Physical	Steam
NC-70-CuCr	PICA	Coconut shell	Physical	Steam
CTP-A	LCSM Nancy	Coal tar pitch	Physical	Steam at 800 °C
CTP-PAN-3 :1-A	LCSM Nancy	Coal tar pitch and polyacrylonitrile	Physical	Steam at 800 °C
CTP-PAN-1 :1-A	LCSM Nancy	Coal tar pitch and polyacrylonitrile	Physical	Steam at 800 °C
PAN-A	LCSM Nancy	Polyacrylonitrile	Physical	Steam at 800 °C
PAN-C	LCSM Nancy	Polyacrylonitrile	Non-activated	-
CTP-PAN-3 :1-C	LCSM Nancy	Coal tar pitch and polyacrylonitrile	Non-activated	-
CTP-C	LCSM Nancy	Coal tar pitch	Non-activated	-
CTP-PAN-1 :1-C	LCSM Nancy	Coal tar pitch and polyacrylonitrile	Non-activated	-
Carbonized coconut shell	PICA	Coconut shell	Non-activated	-

**Table 3 - : General characteristics of carbon samples selected for the study**

\*LCSM – Laboratoire de Chimie du Solide Mineral.

### **8 OXIDATION PROPERTIES AND REACTIVITY STUDIES**

This section deals with the introduction to thermal analysis particularly that of calorimetry and thermogravimetry techniques. The oxidation and ignition characteristics of the activated carbon in this study are obtained using thermal analysis techniques. In this section, the description about the apparatus used, sample preparation and experimental procedures is discussed and finally heat flux and mass data treatment for determination of oxidation and ignition properties.

#### **8.1.1 TG-DSC ANALYSIS**

Thermal analysis in its broadest sense refers to measurement of the changes in properties of substances in a controlled temperature system [Starink, 2004]. The signals measured can include heat flows, temperature changes, mass changes, evolved gases and many other parameters that characterize properties or reactions of interest. Some of the phenomena which can be investigated by thermal analysis methods and equipments are thermal stability, chemical reactivity, dimensional changes and phase transitions [Sestak, 2004].

On the contrary of isothermal calorimetry, differential scanning calorimetry uses a non-isothermal mode of operation, which is temperature scan. Differential scanning technique is applied to a wide range of materials and substances and offer many advantages compared to the isothermal techniques. The advantages of non-isothermal methods are mainly speed, convenience, accuracy and versatility [Starink, 2004]. But some drawbacks are also associated with these methods. The changing temperatures will influence reaction rates which are sometimes in a complex manner and this complicates the non-isothermal technique when compared with the isothermal ones. Apart from this, temperature non homogeneities in the apparatus or in the sample can upset the controlled sample conditions aimed for.

Thermogravimetry technique measures the mass change of the material sample. Thermogravimetry analysis can be operated in isothermal and non-isothermal mode. Due to the advent of technology and instrumentation, one or more thermal analysis techniques are coupled together to record more than one property change at the same time. The most common one is the calorimetry coupled with the thermogravimetry technique. The differential scanning calorimetry

## ***Chapter 3: Materials and experimental methods***

---

(DSC) coupled to thermogravimetry analysis techniques have attained scientific importance due to their novelty in determining the instability and thermal runaway potential of materials [Surianarayanan *et al.*, 2001]. This combination is made used in this study for the characterisation of reactivity parameters of activated carbons and taken up briefly in the next section.

### **8.1.2 APPARATUS SETERAM ATG-DSC- 111**

The schematic representation of the ATG-DSC apparatus (Seteram-111) is shown in figure 3-1. The two analyzers ATG and DSC are coupled together with an online PC loaded with the SETSOFT software to control, monitor and treat the recorded signals. A small sample mass of about 3-10 mg was used. The apparatus provides with a good reproducibility and sensitivity of mass and heat flux measurements. The reproducibility of the apparatus between the trials is very high, unless the measurement conditions are not altered. The percentage of errors for calculating the oxidation and ignition curves varies from 5 -10 %.

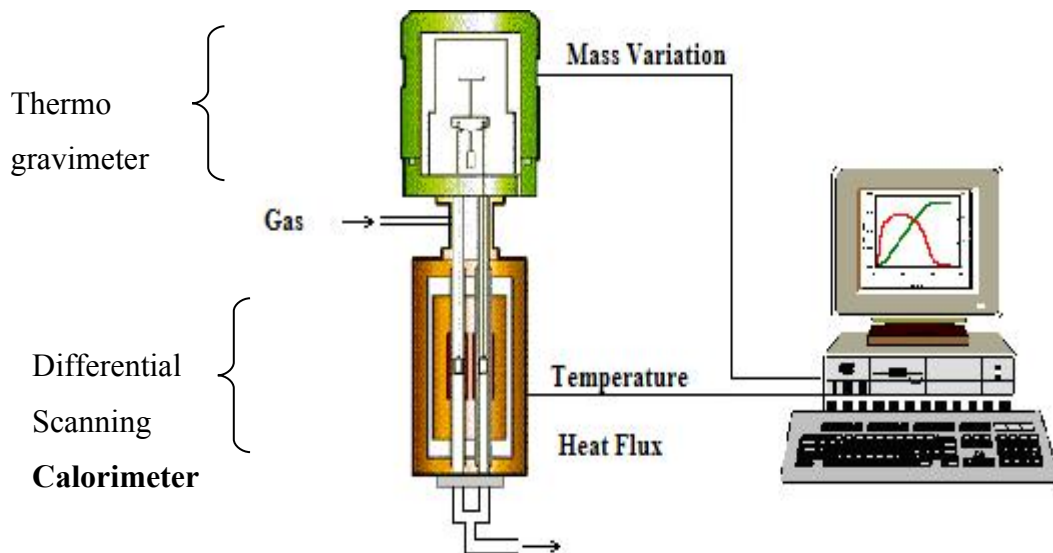


**Figure 3 - :** Schematic representation of the Thermogravimetry coupled with Differential Scanning Calorimeter [ATG-DSC Setaram-111].

## ***Chapter 3: Materials and experimental methods***

---

### ***8.1.2.1 THERMOGRAVIMETER (TG)***

Thermogravimetric analysis is carried out by following the weight loss undergone by the material during the temperature control programmation. Measurements of the changes in the sample mass are made using a thermobalance. The schematic representation of the thermobalance system is shown in Figure 3-2. The thermobalance consists of two crucibles attached to a metal hook hanging from the beam. The hooks are thin metallic rod usually made of platinum. Of the two crucibles one is used for the reference and the other is used for the sample. The principle of the thermobalance is to measure the force necessary to displace the balance to initial position due to mass variation of the sample. The balance is placed in a closed system so that the experiments can be conducted under different atmospheres like oxygen, nitrogen, helium and argon. The characteristic signal obtained here is the evolution of mass in mg.

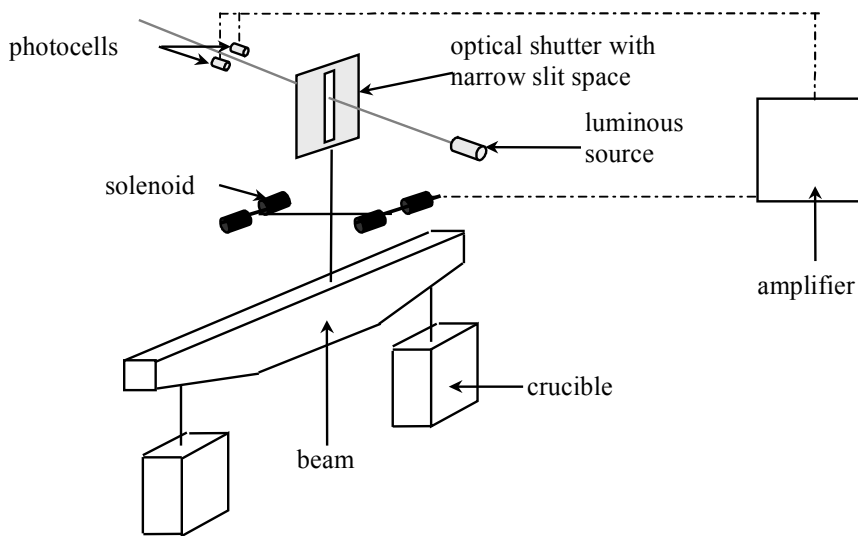


**Figure 3 - :** Schematic representation of a microbalance [ATG-DSC Setaram-111]

### ***8.1.2.2 DIFFERENTIAL SCANNING CALORIMETER (DSC)***

Differential scanning calorimetry measures the heat flow rate (power) evolved from the sample under a controlled temperature treatment and under a controlled atmosphere. The word 'differential' refers to measurements based on the determination of the relative behaviour of a

## ***Chapter 3: Materials and experimental methods***

---

substance when compared to a reference material. The main feature of the DSC technique is that they can be calibrated such that the heat evolved from the sample can be directly measured quantitatively. There are two types of DSC commonly found based on the heating arrangement of the sample namely the Power compensation DSC and the Heat flux DSC. The DSC used in this study is the power compensated DSC and the description of the system is discussed below.

### ***8.1.2.2.1 Power compensated DSC***

In power-compensated calorimeters, separate heaters are used for the sample and reference. Both the sample and reference are maintained at the same temperature while monitoring the electrical power used by their heaters, whereas in the heat flux DSC the heat is transferred to the sample and the reference using a single disk. A schematic representation of the power compensated DSC setup is shown in Figure 3-3, where the sample cell S and the reference cell R are heated using separate heating elements. The heating elements are kept very small (weighing about 1 g) in order to ensure that heating, cooling, and thermal equilibration can occur as quickly as possible. The sample and reference are located above their respective heaters, and the temperatures are monitored using electronic temperature sensors located just beneath the samples. Generally platinum resistance thermometers are used due to the high melting point of platinum. The differential thermal power is supplied to the heaters to maintain the temperature of the sample and reference at the programmed value.

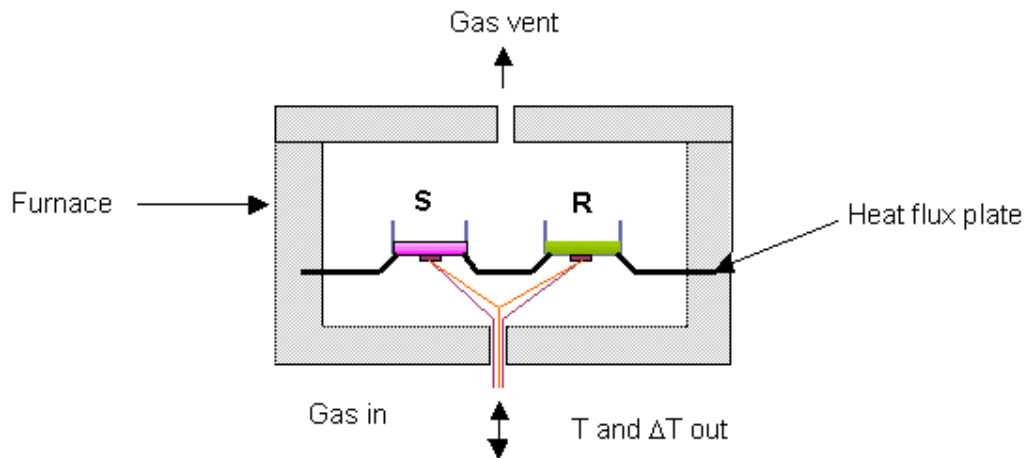


**Figure 3 - :** Schematic representation of a power compensated DSC [figures from Sestak, 2004].

### **8.1.3 EXPERIMENTAL PROCEDURES**

#### **8.1.3.1 SAMPLE PREPARATION**

The samples to be tested are first crushed and sieved using ordinary filter cloth in order to remove the influence of the particle size on the reactivity of activated carbons and to maintain the uniformity of the sample particles. The average diameter of the particles was 50 µm. About 3-5 mg of the crushed sample is loaded in the crucible and the gas flow rate is maintained at a rate of around 1 L/h and with the heating rate of 5 K.min<sup>-1</sup> [Suzin *et al.*, 1999]. The gas used for the oxidation test contains 79 and 21 percentage of helium and oxygen respectively. The flow rate of the carrier gas and the heating selected were found to be the optimum conditions for measuring the PIO and SIT [Suzin *et al.*, 1999]

#### **8.1.3.2 TEMPERATURE PROGRAMMATION**

The heating is programmed with a ramp signal at a constant rate of temperature increase and the system is maintained at a constant temperature using an isotherm giving a stipulated time interval. For the determination of oxidation and ignition parameters, the sample is submitted to a controlled temperature rise, according to the steps described in Figure 3-4.

1. An isotherm for about 5 minutes at 30 °C is maintained in order to eliminate the disturbances caused at the start of the heating and therefore to stabilise the signals.
2. The system is then heated from 20° C to 105° C using a ramp at 5 K/min.
3. This is followed by a 2<sup>nd</sup> isotherm at 105 °C for 30 minutes, the main purpose of this isotherm is to remove the physisorbed moisture content present in the samples acquired during the handling. [Suzin *et al.*, 1999].
4. The sample is then heated from 105 °C to 650 °C at the same heating rate of 5 ° K/min.
5. The final step is the cooling of the sample from 650 °C to 100° C at the rate of 10 K. min<sup>-1</sup> using a cooling ramp.

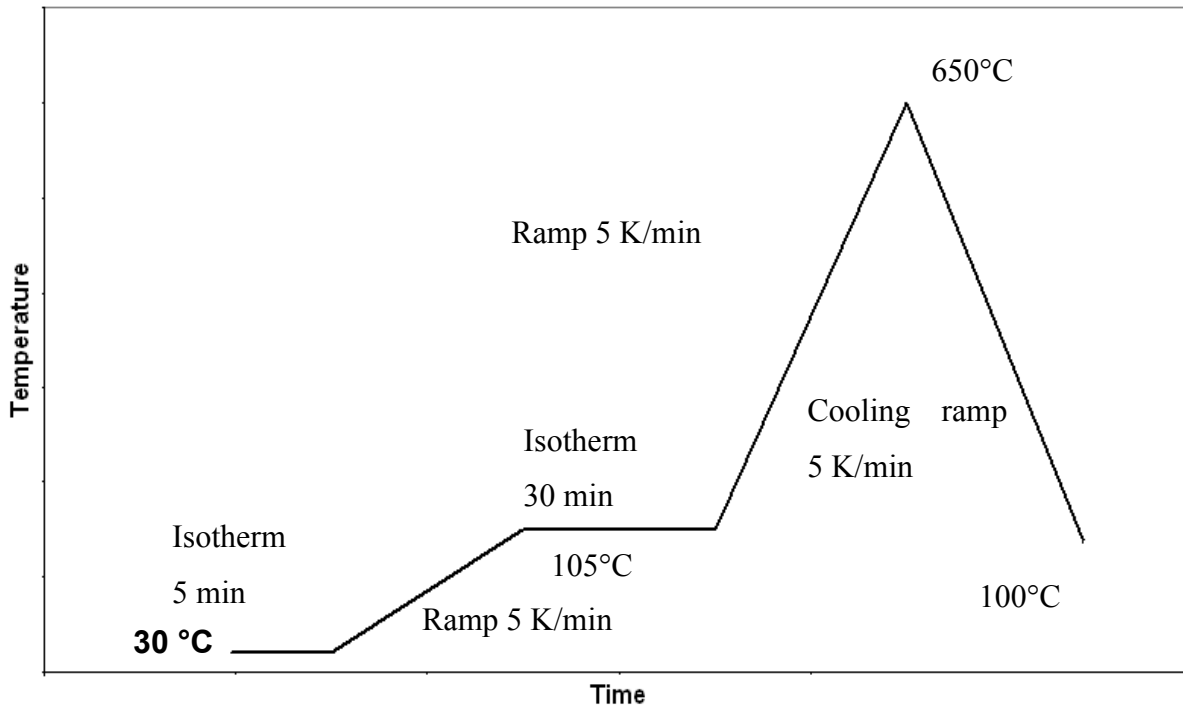


**Figure 3 - :** Temperature programmation used for the oxidation and ignition characteristics of activated carbon.

#### **8.1.3.2.1 Signal corrections**

Auxiliary experiments are carried out in order to eliminate the errors incorporated in the TG-DSC signals due to temperature gradients, convection current and air buoyancy. When the crucible containing the sample is heated in gaseous atmosphere, its apparent weight changes with the temperature increase due to change in the weight of the displaced gas. The sample then appears to gain weight on heating. Corrections curves have to be done to compensate for the above said effects.

Blank tests are carried out with empty crucible both in air and inert atmosphere. Due to high sensitivity and buoyancy effects of the equipment the variations of mass and heat flux signals are normally found even for the empty crucible measurements. So in order to eliminate these errors, signals from the blank experiments are subtracted from the experimentation carried out with the samples. The oxidation heat curve is calculated from Equation 3.11.

$$\Delta H(\text{oxidation}) = \left[ \left( \frac{\Phi_{\text{air}} - \Phi_{\text{blank/air}}}{m_s} \right) - \left( \frac{\Phi_{\text{ref/He}} - \Phi_{\text{blank/He}}}{m_s} \right) \right] \quad (3.11)$$

Where,  $\tilde{\Delta}H$  (oxidation) = Heat flux/unit mass of the sample (mW/mg)

$\Phi_{\text{air}}$ : Heat flux of the sample in air (mW)

$\Phi_{\text{blank/air}}$ : Heat flux of the empty crucible in air (mW)

$\Phi_{\text{blank/He}}$ : Heat flux of the sample under helium (mW)

$\Phi_{\text{Blank/He}}$ : Heat flux of the empty crucible under helium (mW)

$m_s$ : Mass of the sample of activated carbon in (mg)

The Equation 3.11 represents the heat flux expressed in unit mass after subtraction of all the potential errors arising in the TG-DSC system. The blank experimental heat flux measured is subtracted from the air and reference experiments to correct for the errors due to empty crucible measurements. Then the reference experiments are subtracted from the air measurements to correct for the air buoyancy effects. The experiment is repeated three times to check for the repeatability and the calculation of the error percentage.

### **8.1.4 TG-DSC THERMOGRAMS**

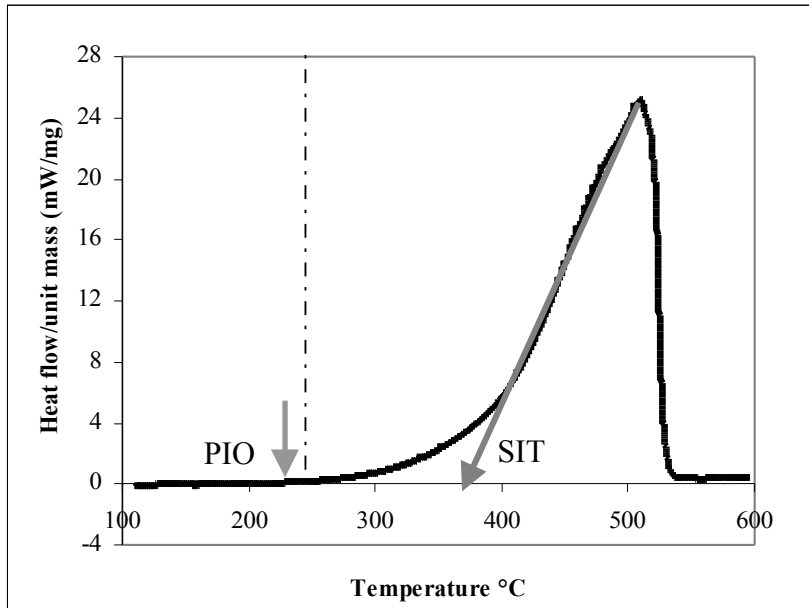
Determination of oxidation and ignition temperatures of activated carbons using thermal analysis techniques was studied by Suzin *et al.*, [1999]. The author points out two regions of interest for the heat flux curves (Figure 3-5) associated to oxidation process at relatively low temperature range, and spontaneous ignition at high temperature. The first region where the carbon starts significantly to oxidize is denoted by the Point of Initial Oxidation (PIO). The second region where the material ignites in a self-sustaining manner is denoted by Spontaneous Ignition Temperature (SIT).

According to Suzin *et al.* [1999], the SIT can be determined from the temperature where the tangent to the point of inflection intersects the heat flux curve baseline (Figure 3-5). The SIT defines the limit beyond which the combustion of the sample takes place, and leads to the consumption of the carbon matrix as observed on the mass curve in Figure 3-7. The PIO represents the point beyond which the exothermic reactions become significant: a low oxidation process takes place with partial oxidation of the carbon and the organic components. The PIO

## ***Chapter 3: Materials and experimental methods***

---

was extracted from the net heat flux curve by locating the initial point of monotonic deviation



from the baseline [deviation of 2 % from the running average of 5 prior points].

**Figure 3 - :** DSC thermogram of an activated carbon samples showing PIO and SIT.

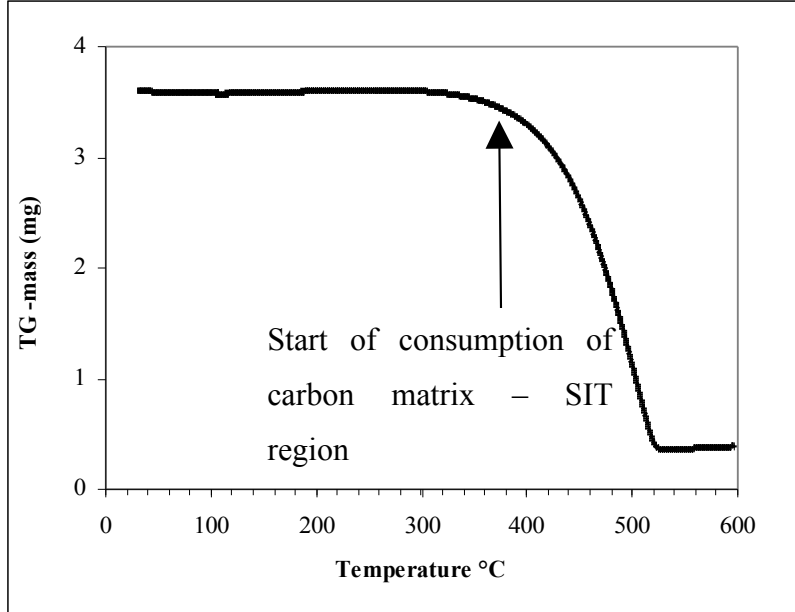


**Figure 3 - :** TG thermogram of an activated carbon samples showing the evolution of mass with temperature.

### 8.1.5 KINETIC PARAMETERS FROM DSC AND TG CURVES

The kinetic parameters for both oxidation and combustion reactions were estimated from the Arrhenius equation applied to the DSC and TG curves respectively. The DSC and the TG thermograms of the carbon sample, recorded during their oxidation and combustion of the samples is expressed in terms of activation energy and frequency factor using the Arrhenius equation [Jones, 1998 ; Kizgut and Yilmaz, 2003].

#### 8.1.5.1 OXIDATION KINETICS FROM THE DSC CURVES

The heat flux per unit mass of the sample ( $\frac{\Phi}{m}$ ) is written in the form of the Arrhenius equation.

There is a considerable heat flux evolved once the oxidation reactions start and hence the kinetic parameters are calculated between the oxidation and the ignition regions for the activated carbons. A zero order reaction is assumed here, where the reaction is assumed to be independent of the concentration of the reactants taking the form

$$\frac{\Phi}{m} = Ae^{-\frac{AE}{RT}} \quad (3.12)$$

Where  $\frac{\Phi}{m}$  : Heat flux/unit mass of the carbon sample ( $\text{mW}\cdot\text{mg}^{-1}$ ),

AE: Activation energy expressed in ( $\text{kJ}\cdot\text{mole}^{-1}$ ),

A: Pre-exponential factor ( $\text{mW}\cdot\text{mg}^{-1}$ ),

T: Temperature of the sample (K),

R: Ideal gas constant ( $8.314 \text{ J}\cdot\text{K}^{-1}\cdot\text{mol}^{-1}$ ),

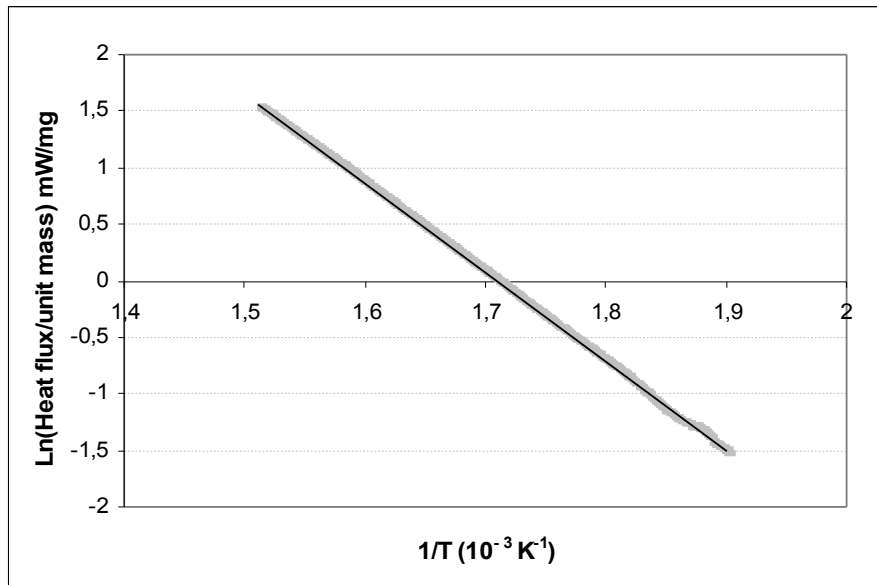
Equation (3.12) is transformed into logarithmic form and a plot of the natural logarithmic function of the ratio of the heat flux/unit mass  $\ln(\Phi/m)$  with time versus inverse of temperature in Kelvin ( $1/T$ ) is made as shown in Figure 3-7. A straight line with a slope of  $(-AE/R)$ , giving the magnitude of the activation energy is obtained. The activation energy was calculated in the range between SIT and PIO values.

$$\ln\left(\frac{\Phi}{m}\right) = \ln(A) - \frac{AE}{RT} \quad (3.13)$$

## ***Chapter 3: Materials and experimental methods***

---

**Figure 3 - :** Arrhenius plot on DSC curve of the activated carbon sample NC-60



Deviation of the experimental data from the straight line trend indicates the degree of inaccuracy of the assumption of the zero order reaction in our case. A good regression correlation of about 0.99 is obtained here indicating the accuracy of the model.

### ***8.1.5.2 COMBUSTION KINETICS FROM THE TG-CURVES***

In the same manner, the mass loss with respect to temperature is written in the Arrhenius form to calculate the kinetic parameters. The mass loss takes place mostly once the ignition reactions starts, hence the combustion kinetic are determined from the TG curves. In the PIO region, there is negligible mass variation to study the oxidation kinetics using the TG curve.

The rate of decomposition can be evaluated by using the Arrhenius equation:

$$\frac{dw}{dt} = A \exp\left(-\frac{E_a}{RT}\right)w \quad (3.14)$$

$dw/dt$ : Change of mass/temperature of the carbon sample ( $\text{mW} \cdot \text{C}^{-1}$ ),

$E_a$ : Activation energy expressed in ( $\text{kJ} \cdot \text{mole}^{-1}$ ),

$A$ : Pre-exponential factor ( $\text{mW} \cdot \text{C}^{-1}$ ),

$T$ : Temperature of the sample (K).

Taking natural logarithm on both sides of the equation 4.13, we get

## ***Chapter 3: Materials and experimental methods***

---

$$\ln\left(\frac{dw}{dt} \frac{1}{w}\right) = \ln A - \frac{Ea}{RT} \quad (3.15)$$

Plot of the natural log function of the ratio of the weight loss with temperature ( $dw/dt$ ) against  $1/T$  is then a straight line with a slope of  $(-Ea/R)$  as shown in Figure 4-25, giving the magnitude of the activation energy. Deviation of the experimental data from the straight line trend indicates the degree of inaccuracy of the first order reaction assumption. For the whole of the AC samples, such an assumption appears reasonable as the regression correlation was 0.99.

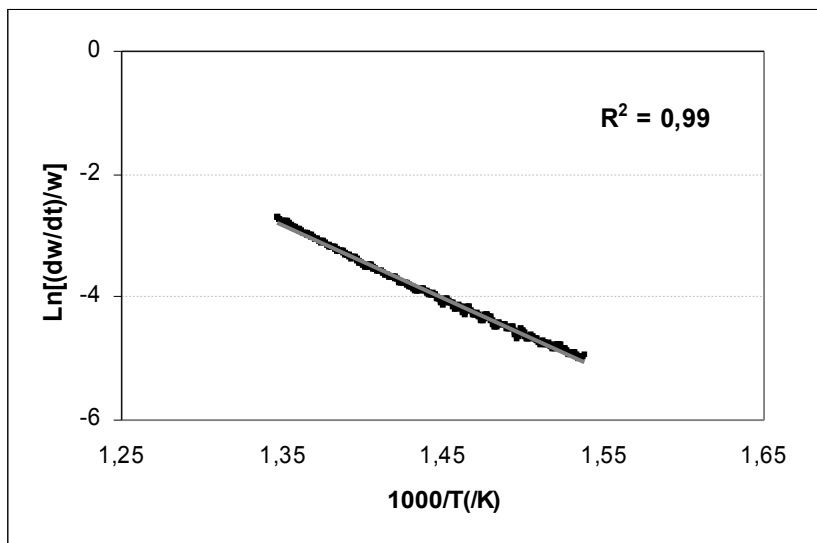


**Figure 3 - :** Arrhenius plot on TG curve of the AC sample NC-60.

### **8.1.6 OPERATING CONDITIONS**

The operating conditions like the heating rate, flow rate of the carrier gas and the percentage of oxygen composition also influence the values of the PIO and SIT. The operating parameters like the heating rate fixed at  $5 \text{ K}.\text{min}^{-1}$ , flow rate of  $1 \text{ L}.\text{hr}^{-1}$  and the concentration of the oxygen gas as 21 % are changed to study the effect of the operating conditions on the reactivity of activated carbons.

## **9 CHARACTERIZATION OF POROUS PROPERTIES OF CARBONS**

This section deals with the theory and methods used to characterize porous activated carbon adsorbents used in this study. It includes adsorption isotherms, determination of adsorbent

## ***Chapter 3: Materials and experimental methods***

---

surface area, pore volume and micropore size distributions using N<sub>2</sub> adsorption and mercury porosimetry techniques.

### **9.1.1 NITROGEN ADSORPTION ANALYSIS**

There are numerous techniques and methods available for the physical characterization of the pore structure of the activated carbons. The pore sizes of the activated carbon vary by nature from macro, meso to micropores and there is no single technique to provide information for all ranges of pores. In many cases, a combination of different methods is used [Senel, 1994]. The adsorption of gases and vapours by standard gravimetric or volumetric techniques and mercury porosimetry are classical and convenient approaches for the characterization of porosity in activated carbon [Kenneth Sing, 1998]. Other complementary techniques such as small angle scattering (X-rays or neutrons), transmission electron microscopy are also used for the characterization of pores [Senel, 1994]. A short description about the phenomena of adsorption and adsorption isotherms is given before going into the details of the characterisation by nitrogen adsorption.

#### **9.1.1.1 ISOTHERM MODELS**

When a gas is confined in a closed space, in presence of an out gassed solid (adsorbent), adsorption takes place [IUPAC, 1985]. Adsorption is brought about by the interaction between the solid and the molecule in the fluid phase. The sizeable part of the total volume of activated carbons is taken up by the pores which may be connected to the surface. Only pores which are open play a role in the adsorption studies whereas the remaining ones are not reachable by the fluid under study. Figure 3-9 shows the diversity in the distribution of the porous structure of activated carbons comprising micro, meso and macropores with the adsorption of the gases on to the different pores.

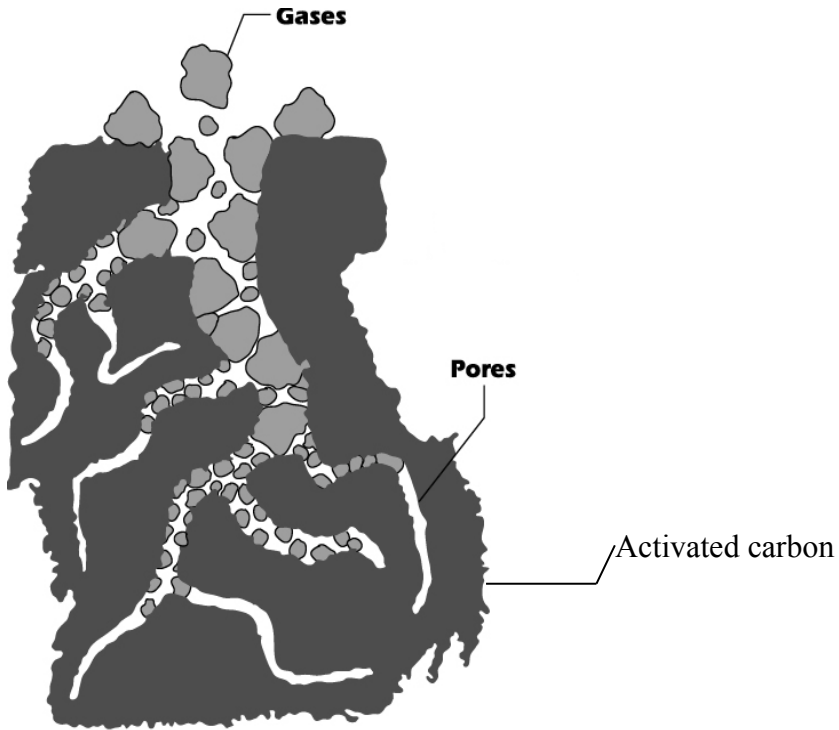


**Figure 3 - :** Micro, meso and macropore regions of activated carbons along with a gaseous adsorbate [Balci, 1992]

The amount adsorbed on a solid surface depends upon the temperature, the pressure and the interaction potential between the vapour and the surface. The adsorbed gas results in a pressure reduction as well as an increase in the mass of the solid in the enclosed volume. These effects are exploited both in volumetric and gravimetric measuring techniques. The plot of the volume or mass adsorbed, versus the measured pressure or relative pressure (quotient of the measured pressure and the saturation vapour pressure at measurement temperature) is called “adsorption isotherm” [IUPAC, 1985]. Isotherms give information about surface and porosity [Roquerol *et al.*, 1999].

According to Brauner *et al.*, 1940, most of the adsorption isotherms fit into one of the five types shown in Figure 3-10. Later, isotherms were universally agreed upon and validated by IUPAC and the number of isotherm types was increased to six.

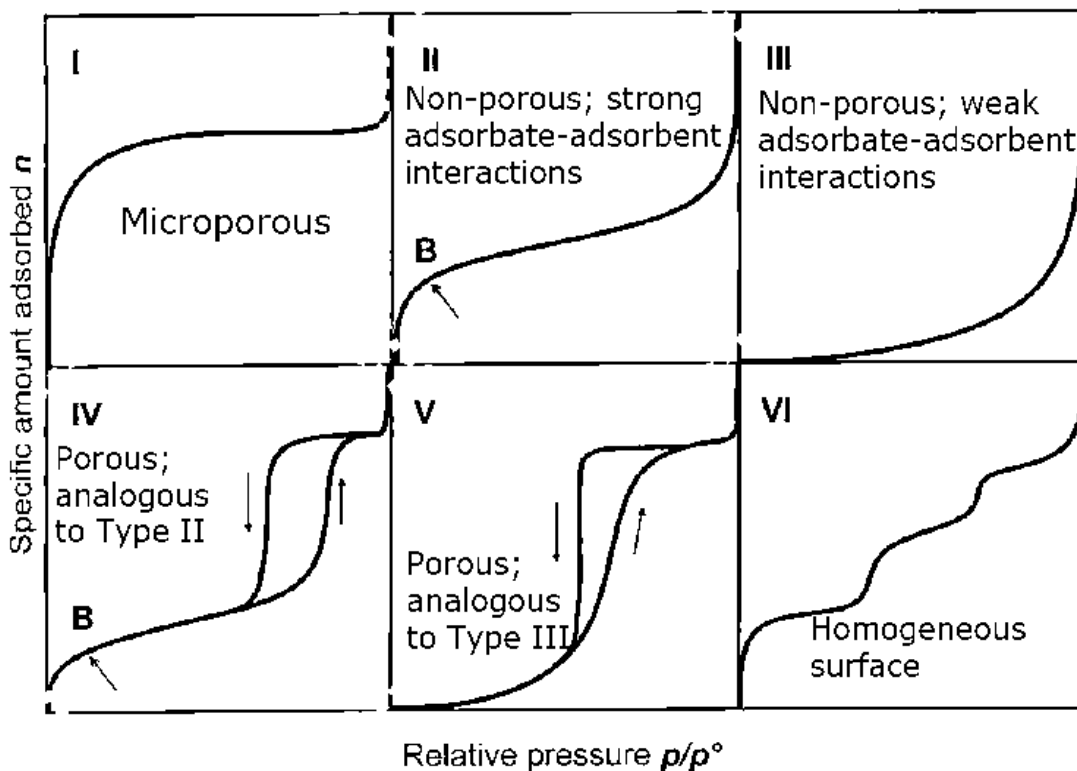


**Figure 3 - :** Classification of adsorption isotherms [IUPAC, 1985].

The type I isotherm indicates that the pores of the solid are mainly microporous (pore width below 2 nm). The curve is concave to the relative pressure ( $p/p_0$ ) axis. It rises sharply at low pressures and reaches a plateau where the amount adsorbed per unit mass of the solid approaches a limiting value  $p/p_0 - 1$ . The plateau is interpreted as a sign of small external surface area. Adsorption is then controlled by the micropore volume filling.

The type-II isotherm exhibits a concave shape only at low relative pressures, followed by a linear range and then ends with a slightly convex shape at relative pressures close to unity. This shape results from the rapid growth of the adsorbate layer when the relative pressures rise. Once saturated vapour pressure is reached, the adsorbate changes from the gaseous form into the liquid or solid phase. The beginning of the linear range can be interpreted as the completion of an adsorbed monolayer and as a transition to multilayer adsorption. Type-II adsorption isotherms are attributed to non-porous and macroporous substances (pore width larger than 50 nm).

## ***Chapter 3: Materials and experimental methods***

---

The type IV isotherm, whose initial region closely resembles the type II isotherm, it exhibits the existence of a hysteresis, indicating the presence of mesopores (between 2 and 50 nm). The hysteresis loop is usually associated with the filling and emptying of mesopores by capillary condensation and evaporation. The shape of this hysteresis varies from one adsorbent to another. The type III and type V isotherms show pronounced convex slope, revealing weak adsorbate-adsorbent interactions. Type V isotherms differ from type III by reaching a saturated pressure and by the existence of a hysteresis loop associated to pore filling and emptying. The hysteresis loop is indicative of a porous adsorbent.

In addition to the five isotherm types, the type VI isotherm is also found. Type VI isotherms are also called a step isotherm representing the stepwise multilayer adsorption on a uniform non-porous surface. The step represents the monolayer capacity for each adsorbed layer and in the simplest case remains nearly constant for two or three adsorbed layers. The best examples of the type VI isotherms are those obtained with argon and krypton on graphitised carbons at liquid nitrogen temperature.

### ***9.1.1.2 EVALUATION APPROACHES***

A large number of approaches based on kinetics, thermodynamics and empiricism are available for interpretation and further evaluation of adsorption isotherms. The BET method is used for the evaluation of the microporosity.

#### ***9.1.1.2.1 Braunauer, Emmett and Teller (BET) isotherm***

Although BET theory [Brauner et al., 1940] was derived over sixty years ago, it is still widely used today because of its simplicity and its ability to accommodate the different isotherm types. The BET model extends the monolayer Langmuir model to multilayer adsorption. It assumes that the surface is homogeneous and that the different layers of molecules do not interact. Each adsorbed molecule in the monolayer is assumed to be an adsorption site for the second layer and so on as the relative pressure increases, until bulk condensation occurs.

In the region of relative pressures near the completion of monolayer, the BET theory and experimental isotherms do agree very well leading to a powerful and extremely useful method for

## ***Chapter 3: Materials and experimental methods***

---

the estimation of surface areas of various materials including activated carbon, coal and coal chars as well. In the final form it is given as:

$$\frac{P}{V[P_o - P]} = \frac{1}{V_m C} + \frac{C - 1}{V_m C} \frac{P}{P_o} \quad (3.23)$$

Where V, the volume adsorbed, at the relative equilibrium pressure P/Po, and the monolayer capacity respectively, C is a constant, which is related exponentially to the heat of adsorption at the first and subsequent layers by the equation

$$C = \exp[(q_1 - q_2)/RT] \quad (3.24)$$

Where  $q_1$  is the heat of adsorption of the first layer,  $q_2$  is the heat of adsorption of the second and subsequent layers. According to the above equation, a plot of P/V(P-Po) versus P/Po should yield a straight line, usually in the range of  $0.05 < P/Po < 0.35$ .

The BET equation usually gives a good representation of the frequently appearing type II and IV isotherms within the range of relative pressures 0.05 – 0.2. At higher relative pressures, the BET equation is usually inaccurate because of capillary condensation effect, whilst at P/Po values below or about 0.05; the amount of adsorbed gas is too small to be measured with sufficient accuracy. The specific surface area is then derived from the equation 3.25,

$$S_{BET} = \frac{V_m N_A A_m}{V_{mol}} \quad (3.25)$$

where  $V_m$  is the volume of the monolayer,  $N_A$  is the Avogadro's constant,  $V_{mol}$  is the molar volume of the gas. The mean cross sectional area  $A_m$  of any adsorbed gas molecule can be estimated from the density of the condensed phase of the gas and. area occupied by one molecule of adsorbate gas.

Several adsorbates may be used to determine surface area of an adsorbent, the most common being nitrogen at 77 K. Other commonly used adsorbates include benzene at 293 K and CO<sub>2</sub> at 198, 273 or 293 K. Mclellon and Harnsberger [1967] compiled a list of adsorbate molecular areas, some of which are presented in Table 3-3.

## ***Chapter 3: Materials and experimental methods***

---

Adsorbate molecule	Cross sectional area ( $\sigma$ ) [Å <sup>2</sup> ]	Molecular dimension (Lennard Jones) [Å]
Water (H <sub>2</sub> O)	12.5	2.64
Nitrogen (N <sub>2</sub> )	16.2	3.80
Acetone (C <sub>3</sub> H <sub>6</sub> O)	16.7	4.60
Carbon-di-oxide (CO <sub>2</sub> )	22	3.94
Benzene (C <sub>6</sub> H <sub>6</sub> )	43	5.35

**Table 3 - :** Adsorbate molecules and their dimensions [Mclellon and Harnsberger, 1967]

A criticism of the BET theory is the assumption that all adsorption sites on the solid surface are energetically homogeneous. In reality, most adsorption surfaces are energetically heterogeneous. Another criticism is that the model suggests adsorbate – adsorbate interactions, which are not negligible when an adsorption layer is near completion and the average separation of the molecules is small in relation to their size [Gregg and Sing, 1982].

### ***9.1.1.2.2 Microporosity analysis by t-plot***

The t-plot or De Boer plot [Lecloux, 1971, Olivier, 1995] can be used to determine the micropore volume. According to this method, the nitrogen adsorption isotherm obtained from the porous solid is compared to the isotherm of the non-porous solid of the same origin. The deviation behaviour is illustrated in Figure 3-11. Lippens *et al.*, [1965] established that for a large variety of non-porous solids, an empirical relation binding (t) to P/P<sub>0</sub> as shown in equation 3.26 with V<sub>ads</sub> = f (t).

$$\log\left(\frac{P}{P_0}\right) = f(t) = f\left(3.54 \cdot \frac{V_{ads}}{V_{mono}}\right) \quad (3.26)$$

Here t represents the thickness of the layer which is adsorbed under the absence of the capillary condensation on a solid non porous for the same value of P/P<sub>0</sub>. Hence the method consist in making a linear regression of the form V<sub>ads</sub> =  $\alpha + \beta \cdot t$  on the linear part of the curve V<sub>ads</sub> = f (t).

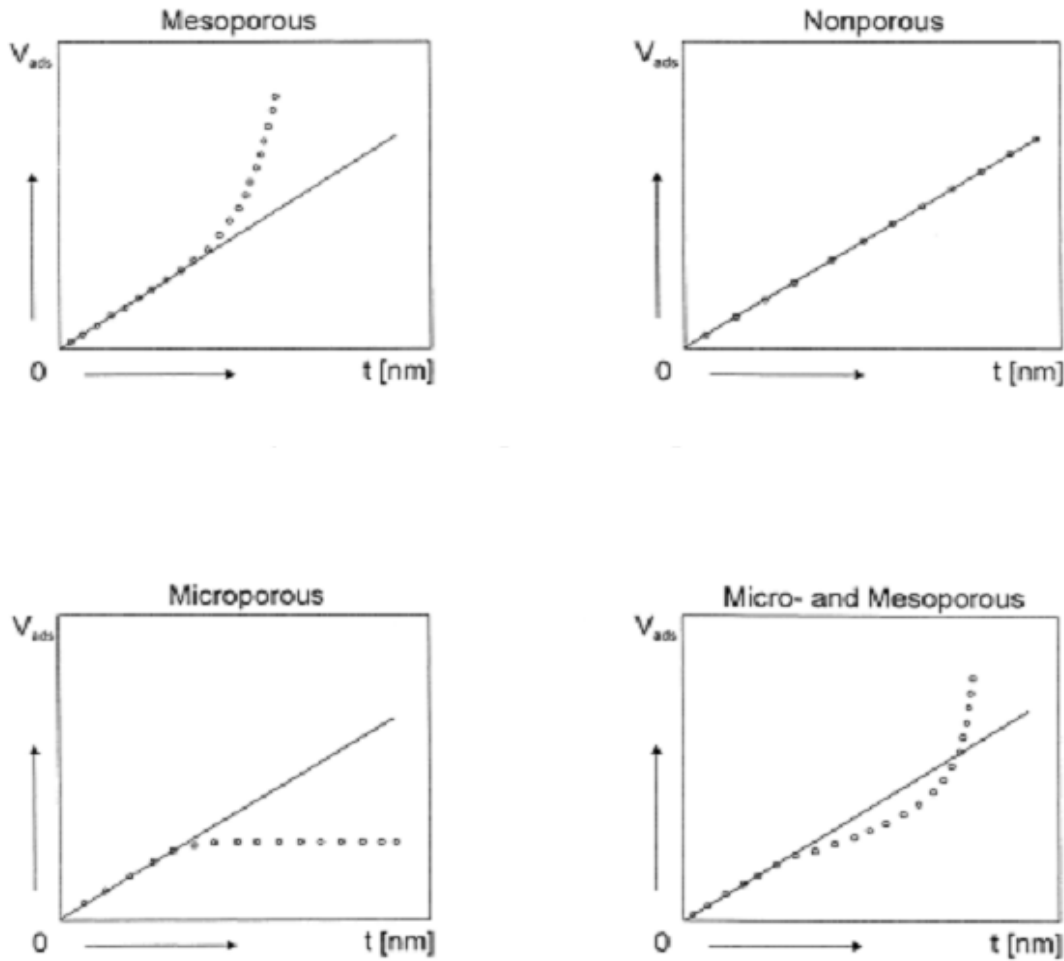


Figure 3 - : t-plots of micro, meso and non-porous test materials [Senel, 1994]

The value of 't' is calculated from the Harkins & Jura equation 3.27 [Lecloux, 1971]

$$t = \left[ \frac{13.990}{0.0340 - \log\left(\frac{P}{P_0}\right)} \right]^{0.5} \quad (3.27)$$

The rest of the parameters like the external surface area, microporous surface and microporous volume are calculated from the following relations

The microporous volume

$$V_{\text{micro}} = \alpha \cdot D \quad (3.28)$$

Where,  $\alpha$ : ordinate of the linear regression at the origin ( $\text{cm}^3/\text{g}$ ),

$\beta$ : slope of the linear regression ( $\text{cm}^3/\text{g.A}$ ).

D: conversion factor of the density,

## ***Chapter 3: Materials and experimental methods***

---

$V_{\text{micro}}$ : microporous volume ( $\text{cm}^3/\text{g}$ )

### **9.1.1.3 DFT METHOD**

The Density Functional Theory is used for the evaluation of pore size distributions. Techniques based on statistical mechanics were proven to be more consistent than the traditional Kelvin equation based on the methods for fitting isotherm data, particularly in the low pressure range where incomplete surface coverage occurs. These methods are not limited by macro thermodynamic concepts such as surface tension; therefore they may be extended to any pore size [Olivier, 1995]. The pore size distributions are normally derived from the experimental nitrogen adsorption data. These data were combined with theoretical sorption isotherms for a range of pore sizes to solve the adsorption integral. The integral equation describes the pore distributions as the integral of the product of a kernel function and a distribution function. The kernel function reflects the adsorption isotherm for a porous adsorbent of a given pore width [Lastoskie, 1993].

The distribution function indicates the respective step width of the kernel function in a given quantity (e.g. pressure). The overall distribution, called Fredholm integral, results for the determination of the pore volume as a function of pressure shown in equation 3.29 [Lastoskie, 1993].

$$V_{\text{ads}}(p) = \int dW \cdot q(p, W) f(W) \quad (3.29)$$

Where  $V_{\text{ads}}$  is the adsorbed volume;  $W$ , the pore width;  $q(p, W)$  is the kernel function, and  $f(W)$  is the associated distribution function. To match this expression to experimental adsorption isotherms, the integral is substituted by a sum:

$$V_{\text{ads}} = \sum q(p, W_i) f(W_i) \quad (3.30)$$

The kernel function,  $q(p, W)$ , then is described by a matrix,  $q(p, W_i)$ , of the adsorbed volume for a given number of pressure levels,  $p$ , and a fixed pore width. The actual calculation of the pore volume per pore width is preceded by an interpolation of the measured pressure levels to the given ones. The quality of the interpolation as well as the number and distribution of the given pressure levels decisively influence the accuracy of the pore distributions obtained and in particular the pore volume determined.

## ***Chapter 3: Materials and experimental methods***

---

The shape of an adsorption isotherm for a given adsorptive reflects the porous properties of the sorbent. Parameters measured by different evaluation approaches are given in table 3-4 and precaution has to be taken while interpreting the results.

<b>Method</b>	<b>Derivable Information</b>
BET	Specific surface area
t-plot or De Boer plot	Micropore volume and surface, external surface area
DFT (Density Functional Theory)	Pore size distribution and total pore volume

**Table 3 - :** Porosity information obtained from different approaches

### ***9.1.1.4 EXPERIMENTAL ASPECTS CHARACTERIZATION BY NITROGEN ADSORPTION TECHNIQUE***

A commercial volumetric gas adsorption “ASAP 2010” analyser manufactured by Micrometrics instrument corporation, USA was used for measuring the surface area and pore size distributions using N<sub>2</sub> adsorption and desorption data at –195.6 °C.



**Figure 3 - :** Gas adsorption Micrometers ASAP 2010 analyser

Before obtaining the adsorption or desorption isotherms the activated carbon samples were degassed for 48 hours at 250 °C to remove any moisture or adsorbed contaminants present in the activated carbon samples. The outgassed samples were then weighed and subjected to adsorption

## ***Chapter 3: Materials and experimental methods***

---

of nitrogen gas. The sample holder is immersed in liquid nitrogen at  $-195.6\text{ }^{\circ}\text{C}$  during the adsorption of nitrogen. The different equations and pressure ranges were applied:

- The BET model and the DFT method were applied in the pressure range from 0.01 to 0.2.
- The t-plot characteristics were obtained for the microporosity in the pressure ranges  $10^{-7}$  to 0.01.

### ***9.1.1.5 ADVANTAGES AND LIMITATIONS OF NITROGEN GAS ADSORPTION***

Many parameters that describe the pore structure of a sample, for example pore volume, specific surface area and pore size distribution can be determined by a single method. One of the drawbacks is that the time used for a single analysis can take hours. The pore diameter range that can be determined is from 0.3 to 200 nm, where the micropore range is well covered by this method when compared to porosimetry techniques.

With nitrogen adsorption, only open pores are determined, the slit shaped pore model is normally assumed in pore size distribution measurements. The desorption isotherm in the characterisation of pore size distribution may be affected by the pore network; when pressure is reduced, liquid will evaporate from large open pores, but pores connected to the surface with narrower channels remain filled [Allen 1997]. This induces changes in the shape of the pore size distribution.

### ***9.1.2 MERCURY POROSIMETRY***

Washburn in 1921 first suggested the use of mercury intrusion under pressure to determine the pore size distribution of porous solids. The principle of this technique is to force the mercury to fill smaller and smaller pores. An important property of mercury is that it exhibits a contact angle of greater than  $90^{\circ}$  with most materials. This means that mercury will neither penetrate the openings of particles nor pore space within the material unless forced.

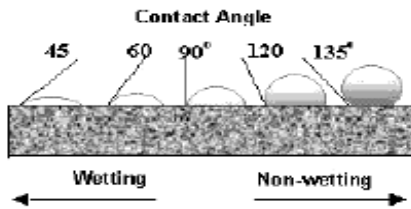


**Figure 3 - :** The different angles of contact are illustrated for wetting and non-wetting liquids [Westermarck, 2000].

Mercury porosimetry is based on the Washburn equation. The volume of mercury penetrated into the solid is measured as a function of the applied pressure which is related by the Washburn equation as,

$$r_p = \frac{-2\gamma \cos\theta}{P} \quad (3.31)$$

Generally used values for surface tension and contact angle of mercury are  $480 \text{ mNm}^{-1}$  and  $140^\circ$  respectively. where  $r_p$  is the radius of circular pore,  $\gamma$  is the surface tension of mercury in the pore,  $\theta$  is the angle of wetting of the pore wall by mercury  $P$  is the total pressure exerted under which mercury is made to penetrate the pores. From this, the pore volume and pore surface area distributions can be calculated. The lower limit of this technique is approximately  $80 \text{ \AA}$ .

#### **9.1.2.1 DENSITY AND TOTAL PORE VOLUME DETERMINATIONS**

The total pore volume and the porosity of activated carbon can be determined by using the combination of apparent and true density measurements. Apparent density is defined as the weight of the solid divided by the volume of the solid including the internal pores of the solid. True density is defined as the ratio of the mass to volume occupied, where the contribution to the volume made by pores and internal voids are excluded. The calculation of the apparent and true densities using the Hg porosimetry technique is shown below:

$$\text{Volume of Hg (cm}^3\text{)} = \frac{W - W_p - W_s}{\rho_{Hg}} \quad (3.32)$$

$W_p$ : mass of the empty penetrometer (g),

$W_s$ : mass of the sample (g),

$W$ : mass of the penetrometer + sample + Hg (low pressure analysis) (g).

## ***Chapter 3: Materials and experimental methods***

---

The true volume of the sample (without porosity) is calculated using Equation (3.33)

$$V_{\text{True}} = V_p - V_{Hg} \quad (3.33)$$

This is then followed by the calculation of the true density

$$\rho_{\text{True}} = \frac{W_s}{V_p - V_{Hg}} \quad (3.34)$$

$V_p$ : volume of the empty penetrometer ( $\text{cm}^3$ ),

$V_{Hg}$  : volume of the mercury ( $\text{cm}^3$ ),

The apparent volume of the sample (including porosity).

$$V_{\text{app}} = V_{\text{True}} - V \quad (3.35)$$

Where  $V$  is the total volume of the mercury filling the pores, obtained from the high pressure analysis.

$$\rho_{\text{app}} = \frac{W_s}{V_{\text{True}} - V} \quad (3.36)$$

$$\text{Total pore volume } (\text{cm}^3 \cdot \text{g}^{-1}) = \frac{1}{\rho_{\text{True}}} - \frac{1}{\rho_{\text{app}}} \quad (3.37)$$

$$\text{Total porosity} = 1 - \frac{\rho_{Hg}}{\rho_{He}} \quad (3.38)$$

### ***9.1.2.2 EXPERIMENTAL ASPECTS OF CHARACTERIZATION BY MERCURY POROSIMETRY TECHNIQUE***

The pore size distribution measurements are carried out using Micrometrics Auto pore IV 9500 mercury porosimetry analyser. The characterization of the material's porosity is done by applying various levels of pressure to a sample immersed in mercury. The pressure required to intrude mercury into the sample's pores is inversely proportional to the size of the pores. The analysis is carried out in two stages, the low pressure analysis followed by the high pressure one.

Low Pressure: measurement: 0 to 50 psia (345 kPa)

Pore Diameter: 200 - 3.6  $\mu\text{m}$

High Pressure: from atmospheric pressure to 33,000 psia (228 MPa)

Pore Diameter: 8 - 200  $\mu\text{m}$

## ***Chapter 3: Materials and experimental methods***

---

### ***9.1.2.2.1 Analysis Technique***

To perform an analysis, the sample is loaded into a penetrometer, which consists of a sample cup connected to a metal-clad precision-bore glass capillary stem. The penetrometer is sealed and placed in a low pressure port, where the sample is evacuated to remove air and moisture – the user controls the speed of the evacuation and there's no need for a separate preparation unit. The penetrometer's cup and capillary stem are then automatically backfilled with mercury. Excess mercury is automatically drained back into the internal reservoir; only a small amount remains in the penetrometer.

As pressure on the filled penetrometer increases, mercury intrudes into the sample's pores, beginning with those pores of largest diameter. This requires that mercury move from the capillary stem into the cup, resulting in a decreased capacitance between the now shorter mercury column inside the stem and the metal cladding on the outer surface of the stem.

The instrument automatically collects low pressure measurements over the range of pressures specified by the operator. Then, the penetrometer is moved to the high pressure chamber, where high pressure measurements are taken. Data are automatically deduced using the low and high pressure data points, along with values entered by the operator, such as the weight of the sample and the weight of the penetrometer loaded with mercury.

### ***9.1.2.3 ADVANTAGES AND LIMITATIONS OF MERCURY POROSIMETRY***

Mercury porosimetry is rather a rapid method, the measurement time being a matter of few hours. The sample must be dry, because mercury cannot intrude into the sample when voids are filled with another liquid [Ek *et al.*, 1995]. Samples with a fine pore structure are difficult to degas, and adsorbed layers reduce effective pore diameter and pore radius values [Allen, 1997].

During measurement, high pressures to force mercury into small pores may compress the sample [Webb and Orr, 1997]. This effect can be shown especially in samples containing closed pores of small or medium size. These compression effects added to a rise in temperature [van Brakel *et al.*, 1981] can be eliminated with the use of hydraulic oil as a medium for transferring pressure.

## ***Chapter 3: Materials and experimental methods***

---

Usually, constant surface tension and contact angle data are used for mercury. However, contact angle may differ depending on the surface of the sample. Contact angle can be determined for each material studied, and a corrected value can be used in determinations. The diameter of the pore opening determines the pressure when mercury is intruded into the sample. Large pores with a small opening are thus filled at high pressures, and detected as smaller pores than they actually are. Pore size distributions obtained with incremental and continuous mode differ, and the results obtained with these two methods are thus not comparable. In incremental mode, the pressure is increased by steps. In the continuous mode, the pressure is increased continuously at a predetermined rate.

### **9.1.3 COMPARISON OF NITROGEN ADSORPTION AND MERCURY POROSIMETRY TECHNIQUES**

In mercury porosimetry and nitrogen adsorption, two different physical interactions take place. Both methods are based on surface tension, capillary forces and pressure. With mercury porosimetry, large pores are determined first during the intrusion phase. During nitrogen adsorption, the smallest pores are first filled [Webb and Orr, 1997]. The pore size range of high-pressure mercury porosimetry is wider (pore diameter 8 nm – 14 µm) than that of nitrogen adsorption (0.3 – 200 nm). Mercury porosimetry determines larger pores that are out of the detection range of nitrogen adsorption (Figure 3-14). By using nitrogen adsorption, the smallest pores that are out of range of mercury porosimetry can be determined.

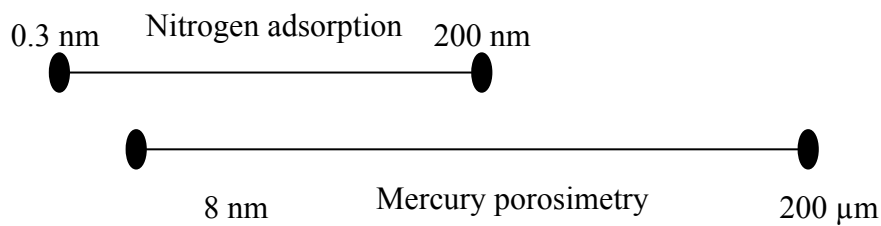


**Figure 3 - :** Pore diameter ranges determined with mercury porosimetry and nitrogen adsorption.

### **9.1.4 CHEMICAL COMPOSITION ANALYSIS**

#### **9.1.4.1 BOEHM'S METHOD**

The method of the neutralisation of the acids and the bases is dealt here to predict the presence of various surface groups and their nature. The acidity constants of the individual groups will differ

## ***Chapter 3: Materials and experimental methods***

---

from several orders of magnitude and this neutralisation behaviour helps in the identification of various groups.

All the functional groups determined by this method account for much less than the total oxygen content of the samples; they account for only about 50%. It is not clearly explained as to how the rest of the oxygen is bound. But there may be a possibility of the existence of the ether type of oxygen or the less reactive functional groups (*H.P.Boehm, 1990*)

### ***9.1.4.1.1 Protocol of the experiment***

The degassing of the carbon sample is done for the removal of the physically adsorbed gases and water vapour on the carbon surface. It is done at a temperature of 110° C for 48 hours. About 1 g of the carbon is sample is taken, for which 50 cm<sup>3</sup> of the neutralisation solution is added with strength of 0.1 normal. It is agitated for about 48 hours and 10 cm<sup>3</sup> filtrate is titrated with HCl of 0.1N. Phenolphthalein is added to the titration if the solutions are Na<sub>2</sub>CO<sub>3</sub> and NaHCO<sub>3</sub>. If the solutions of NaOH or NaOC<sub>2</sub>H<sub>5</sub> are used drops of phenolphthalein is added as indicator. The quantity of base that was neutralised is given below

$$\text{Concentration of the neutralised solution meq/g} = [N_{\text{base}} - \frac{N_{HCl} \cdot V_{HCl} (\text{cm}^3)}{10}] \cdot 50 \quad (3.39)$$

The concentrations of the individual groups are given below :

$$G1 = C[\text{NaHCO}_3]$$

$$GII = C[\text{Na}_2\text{CO}_3] - C[\text{NaHCO}_3]$$

$$GIII = C[\text{NaOH}] - C[\text{Na}_2\text{CO}_3]$$

$$GIV = C[\text{NaOC}_2\text{H}_5] - C[\text{NaOH}]$$

Similarly the basic surface oxides can also be found out by the same procedure. 1 g of the carbon is sample is taken, for which 50 cm<sup>3</sup> of the neutralisation solution namely Hcl is added with strength of 0.1 normal. It is agitated for about 48 hours and 10 cm<sup>3</sup> filtrate is titrated with NaOH of 0.1N with phenolphthalein added to the titration as an indicator.

## ***Chapter 3: Materials and experimental methods***

---

### ***9.1.4.2 ELEMENTARY ANALYSIS***

The elemental composition of the activated carbons is measured using Thermofinnigan Flash EA-1112 CHNS-O elementary analyzer. CHNS-O stand for carbon, hydrogen, nitrogen, sulphur and oxygen which could be present in the activated carbons.

Elemental analysis is based on dynamic flash combustion. The analysis involves two different setup one for the CHNS analysis, and the other for O analysis. The CHNS analysis is carried out by oxidation of the sample in an oxygen rich environment and O analysis is carried out by pyrolysis of the sample. The sample preparation consists of placing a few milligrams of the solid in a tin capsule and closing it well by folding the capsule. The capsule is then dropped into the quartz tube at 950 °C with constant helium flow (carrier gas). A few seconds before the sample drops into the combustion tube, the stream is enriched with high purity of oxygen to achieve a strong oxidizing environment which guarantees almost complete combustion/oxidation of the samples. The combustion gas mixture is then driven through an oxidation catalyst zone, then through a subsequent copper zone which reduces nitrogen oxides and sulphurous anhydride ( $\text{SO}_3$ ) eventually formed during combustion to elemental nitrogen and sulphurous anhydride ( $\text{SO}_2$ ) and retains the oxygen excess. The resulting four components of the combustion mixture are detected by a thermal conductivity detector in the sequence  $\text{N}_2$ ,  $\text{CO}_2$ ,  $\text{H}_2\text{O}$  and  $\text{SO}_2$ .

In case of oxygen which is analyzed separately, the sample undergoes immediate pyrolysis in a helium stream and the temperature is maintained around 1050° C for this process. This ensures quantitative conversion of organic oxygen into carbon monoxide separated on a GC column packed with molecular sieves. The results can be directly obtained from the analyser.

### ***9.1.4.3 DETERMINATION OF ASH CONTENT***

The ASTM standard test method D 2866-94 was used for measuring the total ash content of activated carbons. The experiment was carried out using a temperature controlled muffle furnace. The empty crucible was placed in the furnace at 650 °C for an hour, then cooled to room temperature in a dessicator. It was then weighed to check for any variations in the mass of the crucible. Sufficiently dried activated carbon sample is taken in the crucible and placed in the furnace at 650 °C. Ashing will require from 3 to 16 h depending upon the size and the type of the

## ***Chapter 3: Materials and experimental methods***

---

activated carbon. Ashing can be considered complete when a constant weight is reached. The crucible is cooled and placed in a dessicator and weighed to the nearest 0.1 mg.

### **9.1.5 STRUCTURAL CHARACTERIZATION**

This section gives a short overview of the different microscopic techniques used for structural characterization of the activated carbons. The structural and nanotextural characterization was carried out by Scanning Electron Microscopy and High Resolution Transmission Electron Microscopy (HRTEM) techniques.

#### **9.1.5.1 HIGH RESOLUTION TRANSMISSION ELECTRON MICROSCOPY (HRTEM)**

##### ***9.1.5.1.1 Introduction***

The characteristics at the nanometric scale of the activated carbons were studied using a high resolution transmission electron microscope (HRTEM). Electron microscopy techniques use beams of electrons instead of the light radiations used in classical optical microscopy techniques [Reimer, 1997 ; Williams and Carter, 1996]. According to quantum mechanics, an electron beam with a high velocity will become wave like and the wavelengths are inversely proportional to the electron beam velocity. Thus, a higher electron beam velocity will produce much shorter wavelengths, which in turn results in higher magnifications and spatial resolution.

The HRTEM operates with the beam of electrons transmitted directly (without the loss of energy) or diffracted in a non-elastic manner (with loss of energy). If the objects are amorphous or crystalline then at the origin of the diffused beam, only the objects which posses the range of periodicities or atomic planes will give diffracted beams. Their existence is governed by the Bragg's law:

$$2d \sin (\theta) = n \lambda \quad (3.40)$$

where  $d$  represents the angle of incidence (this is formed by the incidental beam and the normal for the considered periodicity),  $\lambda$  is the wavelength associated with the electrons in movement and  $n$  the order of diffraction. In the case of electrons, the associated wavelength (calculated by means of de Broglie's relation) is extremely short: 0.0037 nm and 0.00254 nm for electrons accelerated under 100 kV and 200 kV respectively.

## ***Chapter 3: Materials and experimental methods***

---

The resolution of transmission electron microscopy is until about 0.1 nm and a raw magnification range between 1000-1,000,000 X depending on the model of the microscope and the imaging mode. This makes TEM an excellent tool for characterisation of the nanostructures i.e. organization at the nanometre scale. The wavelength of the electrons can be reduced to values suitable for imaging atomic features by accelerating electrons through high voltages (> 100 kV). The lenses in a TEM are electromagnetic, which makes it possible to change the strength of the lenses and to adjust the magnification and defocus without physically changing or moving the lenses. However such lenses are not thin and the spherical aberration is a serious defect which hardly limits the resolution.

### ***9.1.5.1.2 Instrumentation***

The nanostructural characterization of the activated carbons was carried out using a Jeol 2011 HRTEM (acceleration voltage 200 kV, resolution in the lattice fringe mode 0.14 nm). The schematic representation of the conventional TEM is shown in the figure 3-15. The TEM is equipped with a gun which is a LaB<sub>6</sub> crystal which is the source of the electrons and act as a cathode with respect to the anodes. Electrons are emitted by the heating of the LaB<sub>6</sub> crystals and accelerated to about (200 keV).

The LaB<sub>6</sub> crystals produce a high coherent beam, which is essential for a high resolution TEM. Condenser lenses are placed between the source and the specimen that forces the electron into a quasi parallel beam before they interact with a very small area of the specimen. The first image is generated by the objective lens which is then sent to the intermediate lens unit which is responsible for the coupling of the magnifying unit (projector lens) to the first image generated. The projector lenses are mainly responsible for the image magnification.

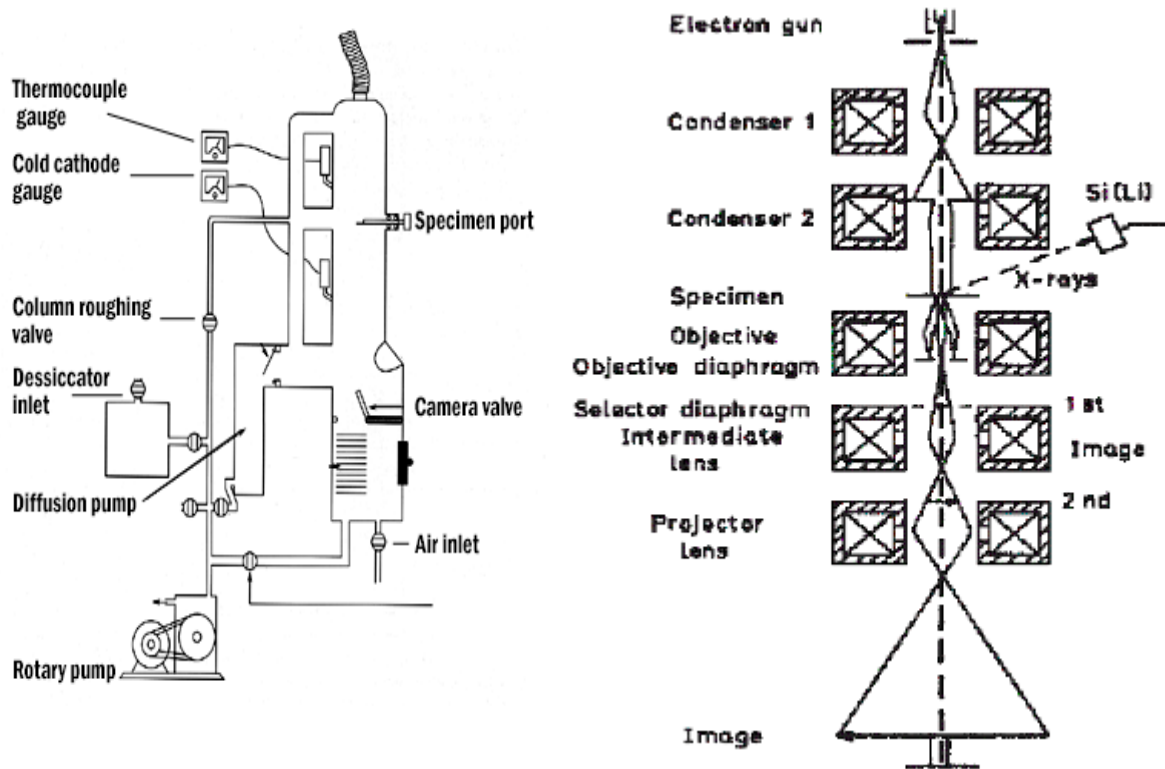


**Figure 3 - :** Schematic representation of the vacuum unit and the lens unit [figures from Muller, 2005].

Basically TEM is a diffraction technique and the microscope is operated in two modes as shown in Figure 3-16. The diffraction mode, which will produce a diffraction pattern of the probed specimen in the objective focal plane, on the viewing screen, and imaging mode which results in an image of the specimen on the objective image plane. Controlling the strength of the intermediate lenses shifts between these two modes. In the diffraction mode, the object of the intermediate lenses is chosen as the back focal plane of the objective lens. In imaging mode, the object of the intermediate lens is the image plane of the objective lens.

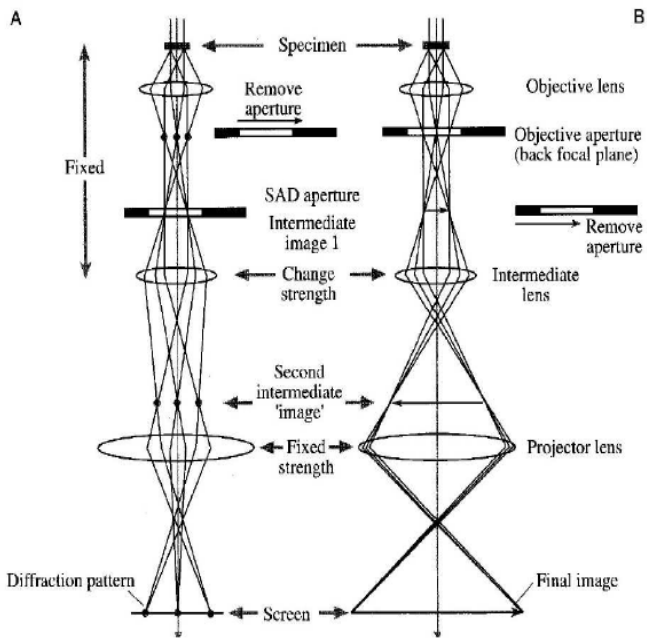


**Figure 3 - :** Light wave patterns in both diffraction and imaging pattern [Muller, 2005].

For digital image recording, a CCD camera coupled to the imaging filter is used to depict the intensity of variations of the transmitted electron beam. As electrons interact strongly with the sample material and it has to be transmitted through them, a very thin sample has to be used for the analysis. The maximum thickness suitable depends on the system of interest, but as a rule of thumb the thickness must not exceed 100 nm. The requirement of thin specimens is a major limitation of TEM. Consequently, for very disordered materials like activated carbons thickness of less than a few nm are required to avoid the superimpositions preventing image interpretation and analysis. As the image obtained is the projection on a 2D plane of the information (atomic planes on the Bragg angle i.e. parallel to the incident electron beam) collected in a 3D volume.

In general, two types of contrast are observed in a transmission electron microscope operating in imaging mode. The mass-thickness contrast or diffraction contrast, which is observed in low magnification images, and the phase contrast which accounts for atomic resolution in high magnification images. The thickness contrast/diffraction contrast is induced by electrons that are scattered off-axis by elastic scattering as they pass through the specimen with a typical scattering angle of 10 mrad. As the thickness increases, more electrons are scattered off-axis. Electrons scattered through angles larger than the objective aperture (back focal plane) are intercepted

## ***Chapter 3: Materials and experimental methods***

---

resulting in high mass-thickness areas to appear darker than low mass-thickness areas. This type of contrast can be enhanced by decreasing the size of the objective aperture, although the total image intensity decreases. The phase contrast is produced by interference between the scattered wave and the incident wave at the image point. This contrast gives detailed structural information of the specimen at an atomic level.

### ***9.1.5.1.3 Analysis and treatment of the image***

The samples were first grounded in a small agata mortar, dispersed in ethanol and a drop of solution was then deposited on a classical TEM copper grid, previously covered by a holey amorphous carbon film. The raw HRTEM images were recorded on classical negatives and a part of this image is sampled and digitalised (256 grey levels, resolution 4000 pixels per inch). The quantitative procedure for the analysis of the HRTEM images involves

1. Background noise reduction performed through a filtration of the Fourier Transform (FT) of the raw HRTEM images.
2. Thresholding and binarisation of the filtered image.
3. Skeletonization of the image.
4. Computerised extraction of the quantified structural and microtextural data from the skeletons.

Software of HRTEM analysis specially developed was used to obtain quantitative structural information [Rouzaud and Clinard, 2002]. With the help of an improved version of the visolog (Noesis) commercial software, an homogenous image without background noise is first obtained, and then binarised and skeletonized; each fringe is now one pixel-large (the size of one pixel for this work : 0.017 nm). The skeletonized pixel based image is then transformed into a vectorial image and each fringe is analysed individually in relation to its neighbours, thanks to the lab-made software. Careful analysis is done taking into account different criterions to avoid artefacts (for instance fringes smaller than 0.25 nm, i.e. the size of a single aromatic ring, were considered without physical sense and eliminated). Pairs of fringes were here considered as stacked layers to form coherent domains (i.e. Basic Structural Units or BSU), only if their angle is smaller than 15° and their interlayer spacing narrower than 0.6 nm [Rouzaud, 2004]. An example of a single basic structural unit chosen for the analysis is shown in Figure 3-17. The software allows to obtain de-averaged data on fringe length, interlayer spacing and number of stacked layers in a

## ***Chapter 3: Materials and experimental methods***

---

coherent domain with great advantage than the usual X-ray diffraction techniques which give poor information on averaged data.

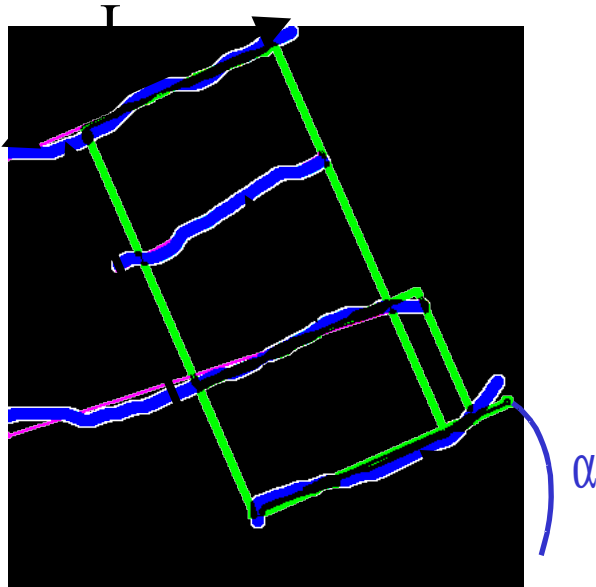


**Figure 3 - :** HRTEM image analysis: structural analysis showing coherent domain limits: L is the individual fringe length,  $L_a$  is the width of the coherent domain,  $L_c$  is its height related to  $d$  which is the interlayer spacing and N is the number of stacked layers within a domain [Rouzaud and Christian, 2002]

L: layer length

d: interlayer spacing

$L_a$ : domain diameter

$L_c$ : domain height

$\alpha$ : disorientation degree

### ***9.1.5.2 SCANNING ELECTRON MICROSCOPY (SEM)***

High resolution images of the sample surface can be obtained by Scanning Electron microscopy. The SEM image mainly shows the surface features and has lesser magnification than TEM image. The details of the porous structure in the macro and mesopore range can be obtained using the SEM technique.

### ***9.1.5.2.1 Instrumentation***

Scanning electron microscopy (SEM) is a method for high-resolution imaging of surfaces. SEM also uses electrons for imaging. A typical SEM has a resolution of  $0.01 \mu\text{m}$  and a magnification of 100-600,000 X depending upon the model of the apparatus. The SEM is an instrument that produces a largely magnified image by using electrons instead of light to form an image. A beam of electrons is produced at the top of the microscope by an electron gun. The electron beam follows a vertical path through the microscope, which is held within a vacuum. The beam travels through electromagnetic fields and lenses, which focus the beam down toward the sample. Once the beam hits the sample, electrons and X-rays are ejected from the sample. Detectors collect these X-rays, backscattered electrons, and secondary electrons and convert them into a signal that is sent to a screen similar to a television screen.

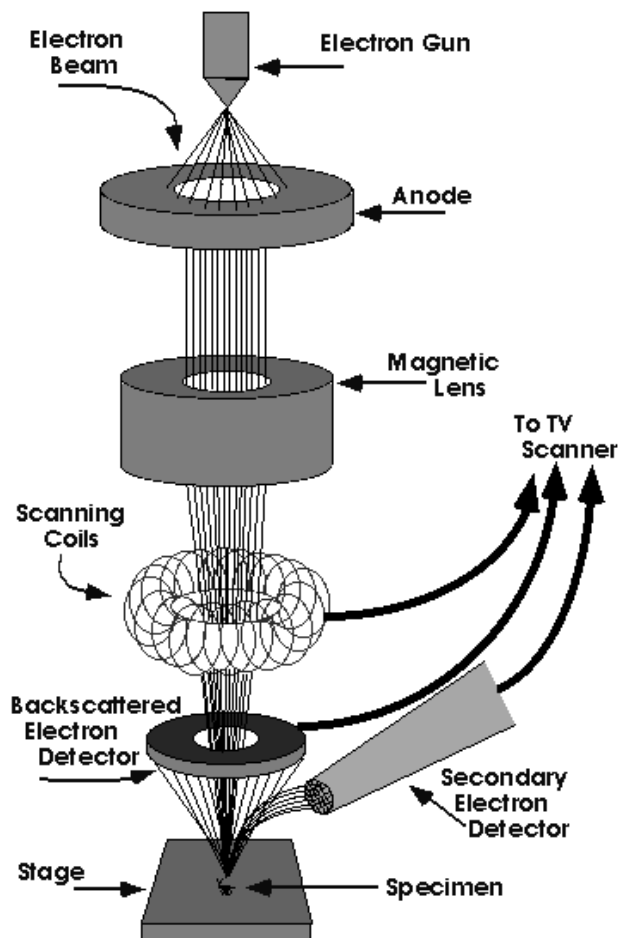


**Figure 3 - :** Working principle and parts of a Scanning electron microscope [Iowa State University SEM Homepage]

## ***Chapter 3: Materials and experimental methods***

---

The variation of the specimen topography will result in marked variation of the beam strength of the secondary electrons. Imaging is typically obtained using secondary electrons for the best resolution of the fine surface topographical features. The sample to be examined should be electrically conductive, this is the reason why a thin layer of metallic surface coating (usually gold) is applied on the non-conductive specimen surface. Samples that conduct electricity are the easiest to study because the unimpeded flow of electrons to the ground minimises the artefacts associated with the build up of charge.

## **10 CONCLUSIONS**

In this chapter, the different characterization techniques for the measurement of textural, chemical and nanostructural properties of the activated carbon samples has been seen.

In the thermal analysis part, TG-DSC is used for the study of oxidation and ignition parameters although the ASTM method gives lower oxidation and ignition values as they tend to mimic the application conditions, but in reality ideal application oriented conditions does not exist. Moreover the TG-DSC seems to be an efficient method with regards to the analysis and comparison of large number of samples maintaining the same experimental conditions. The other advantage is the exploitation of more number of properties like heat flux, mass evolution leading to the reaction kinetics. Two parameters namely PIO and SIT characterizing low temperature oxidation and ignition reactions were measured.

With regards to the characterization of porosity using nitrogen adsorption and mercury porosimetry techniques, the various parameters and the evaluation approaches are outlined with the measurement conditions. As far as activated carbon samples are concerned the nitrogen adsorption technique is more suitable due to their higher specific surface areas and microporous nature.

The chemical composition of the activated carbons is characterized using the elementary analysis techniques giving the composition of carbon, hydrogen, nitrogen and oxygen content. In addition to these, the ash content of the activated carbons was measured using the ASTM method as it is found from the literature sources that it has an influence on the oxidation and ignition characteristics of activated carbons.

Finally the structural and nanostructural characterization was studied using SEM and TEM apparatus giving the surface features and the quantified nanostructural data.

## ***Chapter 3: Materials and experimental methods***

---

### **11 REFERENCES**

1. Allen, T., Particle Size Measurement, pp.251, 5<sup>th</sup> Ed, Chapman & Hall, New York, 1997.
2. Balci, S., Middle East Technical University – METU, Ankara, Turkey (1992).
3. Brauner, S., L.S. Demming., W.L. Demming, and E.Teller, *J. Am. Chem. Soc*, **62**, 1723 (1940).
4. Ek, R., H. Lennholm, R. Davidson, C. Nystrom and G.Ragnarsson, “. Pore swelling in beads made of cellulose s and fragments,” *Int. J. Pharm*, **122**, 49-56 (1995).
5. Gregg, S.J. and K.Sing, Adsorption, Surface area and Porosity, Academic Press, London, 1982.
6. Grzyb, B., H. Machnikowska, and J.V. Weber, “Mechanism of co-pyrolysis of coal tar pitch with polyvinyl pyridine” *J. Anal. Appl. Pyrolysis*, **72**, 121 (2004).
7. Grzyb, B., H. Machnikowska, J.V. Weber, A. Koch, and O. Heintz, “Mechanism of co-pyrolysis of coal tar pitch with polyacrylonitrile” *J. Anal. Appl. Pyrolysis*, **67**, 77 (2003).
8. IUPAC Recommendations, “Reporting physisorption data for gas/solid systems with spherical reference to determination of surface area and porosity,” *Pure & Appl. Chem*, **57**, 603-619 (1985).
9. Jones, J.C., “Towards an alternative criterion for the shipping safety of activated carbons,” *J. Loss Prev. Proc. Ind*, **11**, 407-411 (1998).
10. Kenneth Sing, S.W., “Adsorption methods for the characterisation of porous materials,” *Adv. Colloid Interface Sci*, **76-77**, 3-11 (1998).
11. Langmuir, I., *J. Am. Chem. Soc*, **40**, 1361 (1918).
12. Lastoskie, C., K.E.Gubbins, and N.Quirke, “Pore size distribution analysis of microporous carbon: A density functional theory approach,” *J. Phys. Chem*, **97**, 4786-4796 (1993).

### **Chapter 3: Materials and experimental methods**

---

13. Lecloux, A., "Exploitation of adsorption and desorption isotherms of nitrogen for the study of textural properties of porous solids," Mémoires société des sciences de Liège, pp169-209, tome I, fasc. 4. Belgium, 1971.
14. Lippens, B.C. and J.H. Boer; *J. Catalysis*, **4**, 319 (1965).
15. Livingstone, H.K., *J. Colloid. Sci*, **4**, 1447 (1949).
16. Machnikowski, J., B. Grzyb, H. Machnikowska, and J.V. Weber, "Surface chemistry of porous carbons from N-polymers and their blends with pitch" *Microporous Mesoporous Mater*, **82**, 113 (2005).
17. Mc Clellan, A.L. and H.F. Harnsberger, *J. Colloid Interface Sci*, **23**, 577 (1967).
18. Muller, J.O., Ph.D dissertation, University of Berlin, Germany (2005).
19. Olivier, J.P., "Modelling physical adsorption on porous and nanoporous solids using density functional theory," *J. Porous Mater*, **2**, 9-17 (1995).
20. Olivier, J.P., "The determination of surface heterogeneity using model isotherms calculated by density functional theory, 5<sup>th</sup> International Conference on the Fundamentals of adsorption, (1995).
21. Reimer, L., Transmission Electron Microscopy, 4<sup>th</sup> Edition, Springer (1997).
22. Roquerol, F., J. Roquerol, and K.Sing, Adsorption by Powders and Porous Solids, Academic Press, London, 1999.
23. Rouzaud, J.N. and C.Clinard, "Quantitative high-resolution transmission electron microscopy: a promising tool for carbon materials characterization," *Carbon*, **78**, 229-235 (2002).
24. Rouzaud, J.N., "The multiscale organization as a fingerprint of the formation conditions of carbons; a TEM study," Extended Abstracts Carbon, Providence, Rhode Island, USA, 2004.
25. Senel, G.I., Ph.D dissertation, Middle East Technical University – METU, Ankara, Turkey (1994).

### **Chapter 3: Materials and experimental methods**

---

26. Sestak, J. Heat, Thermal analysis and Society, pp.174-198, Nucleus HK, Czech Republic (2004).
27. Standard test method for total ash content of activated carbon. ASTM D 2866-94 (1999).
28. Starink, M.J., "The analysis of Al based alloys by calorimetry: Quantitative analysis of reactions and reaction kinetics," *Int. Mater. Rev.*, **49**, 191-226 (2004).
29. Surianarayanan.M., R.Vijayaraghavan, G. Swaminathan, and P.G. Rao, "Microcalorimetry and its role in thermal hazard quantification," *Current Science*, **80**, 738-747 (2001).
30. Suzin, Y., L.C. Buettner, and C.A. LeDuc, "Characterizing the ignition process of activated carbon," *Carbon*, **37**, 335-346 (1999).
31. van Brakel, J., S. Modry, and Svatá, M, 'Mercury porosimetry: state of art' *Powder Technol.* **29**, 1 – 12 (1981).
32. Washburn, E.W., "Note on the method of determining the distribution of pore sizes in a porous material", *Proc. Nat. Acad. Sci.*, **7**, 115-117 (1921).
33. Webb, P.A. and C. Orr., Analytical methods in fine particle technology, Micrometrics Instrument Corporation Report, Norcross, 1997.
34. Westermark, S., Phd dissertation, University of Helsinki, Finland (2000).
35. William, D.B. and C.B. Carter, Transmission Electron Microscopy: A text book in Materials Science, Plenum Press, 1996.

#### Website references

1. <http://mse.iastate.edu/microscopy/home.html> - Iowa State University SEM Homepage.

---

## **Chapter 4**

---

### **Results and discussions**

---

#### **4. RESULTS AND DISCUSSIONS**

This chapter essentially deals with the results of experimental studies discussed in Chapter-3. It consists of 4 major sections. The first part describes the experimental results obtained from various characterization techniques. This includes surface characterization using N<sub>2</sub> adsorption and Hg porosimetry followed by elementary and ash content analysis. Then the results of the structural properties obtained by Scanning Electron Microscopy (SEM) and High Resolution Transmission Electron Microscopy (HRTEM) are analyzed. The 2<sup>nd</sup> part describes the oxidation and ignition reactivity of activated carbons determined from thermal analysis techniques, namely Thermogravimetry coupled with Differential Scanning Calorimetry (TG-DSC).

In the 3<sup>rd</sup> part of this chapter, a qualitative analysis is conducted in order to enlighten the relationship between textural, nanostructural and chemical composition of AC's and their reactivity in the presence of oxygen and VOC's. Further the reactivity of the activated carbons is studied changing the operating conditions like the oxygen concentration of the ambient gas, flow rate of the carrier gas and the heating rate. At last, a statistical study was applied using Multiple Linear Regression (MLR) in order to establish quantitative structure reactivity relationships.

#### **12 CHARACTERIZATION OF ACTIVATED CARBONS**

In this section, the physico-chemical characteristics of activated carbons obtained from the various characterization techniques described in Chapter 3 are discussed.

##### **12.1.1 CHEMICAL COMPOSITION**

According to the procedure explained in section 3.4.4, the elemental analysis data of the nineteen activated carbons are given in Table 4-1. The composition of C, H, N, O elements are given in weight percentages. No sulphur was detected in the activated carbon samples. Ratios of H, N and O with respect to carbon are also expressed.

## ***Chapter 4: Results and Discussions***

---

<b>Sample name</b>	<b>Raw material</b>	<b>C (%)</b>	<b>H (%)</b>	<b>N (%)</b>	<b>O (%)</b>	<b>O/C (%)</b>	<b>H/C (%)</b>	<b>N/C (%)</b>
NC-50 <sup>(PA)</sup>	Coconut shell	93.8	0.5	0	1.6	1.7	0.5	0
NC-60 <sup>(PA)</sup>	Coconut shell	91.8	0.3	0.1	3.3	3.6	0.3	0.1
NC-100 <sup>(PA)</sup>	Coconut shell	91.1	0.5	0	3	3.3	0.6	0
RB-2 <sup>(PA)</sup>	Peat	88	0.3	0.2	5.2	5.9	0.3	0.2
BPL <sup>(PA)</sup>	Coal	88	0.2	0.3	3.6	4.1	0.2	0.3
NC-70-Cu <sup>(PA)</sup>	Coconut shell	80	0.5	0.5	6.7	8.4	0.6	0.6
NC-70-CuCr <sup>(PA)</sup>	Coconut shell	73.2	2.6	0.7	9.1	12.4	3.6	1
CTP-A <sup>(PA)</sup>	Coal tar pitch	92.7	0.8	0.7	1.6	1.7	0.9	0.8
CTP-PAN-3 :1-A <sup>(PA)</sup>	Coal tar pitch and PAN	85.7	1.1	4.8	2.7	3.15	1.3	5.6
CTP-PAN-1 :1-A <sup>(PA)</sup>	Coal tar pitch and PAN	84.3	1	8	6.2	7.3	1.2	9.3
PAN-A <sup>(PA)</sup>	PAN	76.6	1.3	11.2	10.5	13.7	1.7	14.6
GF-40 <sup>(CA)</sup>	Olive stone	70.8	2	0.2	24.5	34.6	2.8	0.3
BC-120 <sup>(CA)</sup>	Wood	69.5	1.9	0.1	24.6	35.4	2.7	0.1
PICABIOL <sup>(CA)</sup>	Wood	68	1.8	0	27.6	40.6	2.6	0
PAN-C <sup>(C)</sup>	PAN	77.6	0.9	16	4.9	6.3	1.2	20.6
CTP-PAN-3 :1-C <sup>(C)</sup>	Coal tar pitch and PAN	90.1	1.2	6.4	2.2	2.5	1.3	7.1
CTP-C <sup>(C)</sup>	Coal tar pitch	88.7	1.1	0.7	0.6	0.7	1.2	0.8
CTP-PAN-1 :1-C <sup>(C)</sup>	Coal tar pitch and PAN	82.7	0.9	11.1	2.7	3.3	1.1	13.4
Carbonized coconut shell-C <sup>(C)</sup>	Coconut shell	82.6	2.6	0.1	10.3	12.5	3.2	0.12

**Table 4 - :** Elemental composition of the activated carbon samples.

PA: Physically activated carbons

C: Carbonized samples which are non-activated

CA: Chemically activated carbons

## ***Chapter 4: Results and Discussions***

---

### ***12.1.1.1 CARBON CONTENT***

Data reported in Table 4-1 indicate that the carbon content varies from 70 to 95 %. The highest percentage of carbon is found in the physically activated carbons with NC-50 having about 94 %. The lowest carbon contents are found in the three chemically activated carbon samples varying slightly around 70%.

### ***12.1.1.2 OXYGEN AND HYDROGEN CONTENT***

As discussed earlier in the literature review (Chapter-2), the oxygen and hydrogen elements are combined with the atoms of carbon by chemical bonds. They are normally associated together in the form of surface functional groups. The trends for O and H ratios are analysed together with the help of Figure 4-1. The highest percentage of oxygen is found in the chemically activated carbons (GF-40, BC-120 and Picabiol) with the O/C ratio in the Picabiol sample ranging up to 40 %. The higher percentage of the O/C is mainly due to  $H_3PO_4$  activation which incorporates the oxygenated groups. Moreover the chemical activation is carried out at very low temperatures ( $450\text{-}600\ ^\circ C$ ) so that the sample retains much of the volatile matter and oxygenated surface groups.

Moderate amount of oxygen content are found in the PAN and coal tar pitch blended samples, ranging from 6-13 %. Literature sources [Yi, 2002] have shown that PAN as such does not contain much oxygen content and most of the oxygen content may have been introduced by the activation agent (steam,  $CO_2$  or a combination of both). This is evident from the O/C ratio of PAN-C (carbonized) sample which is about 6 % half that of the activated PAN sample amounting to 13.7 % after activation.

Finally the commercially prepared steam activated carbons have low O/C ratio ranging from 2-6 % for the coconut shell, peat and coal based activated carbons (NC series, BPL and RB-2). For the coconut shell based activated carbons, the process of activation decreases the O/C ratio. It is evident from the comparison between the carbonized coconut shell to that of NC-50, NC-60 and NC-100. The value of O/C decreases from about 12 % to around 3 % after activation.

The hydrogen content is associated with the oxygen content. It is found that the hydrogen to carbon ratio follows the same trend like that of oxygen to carbon ratio.

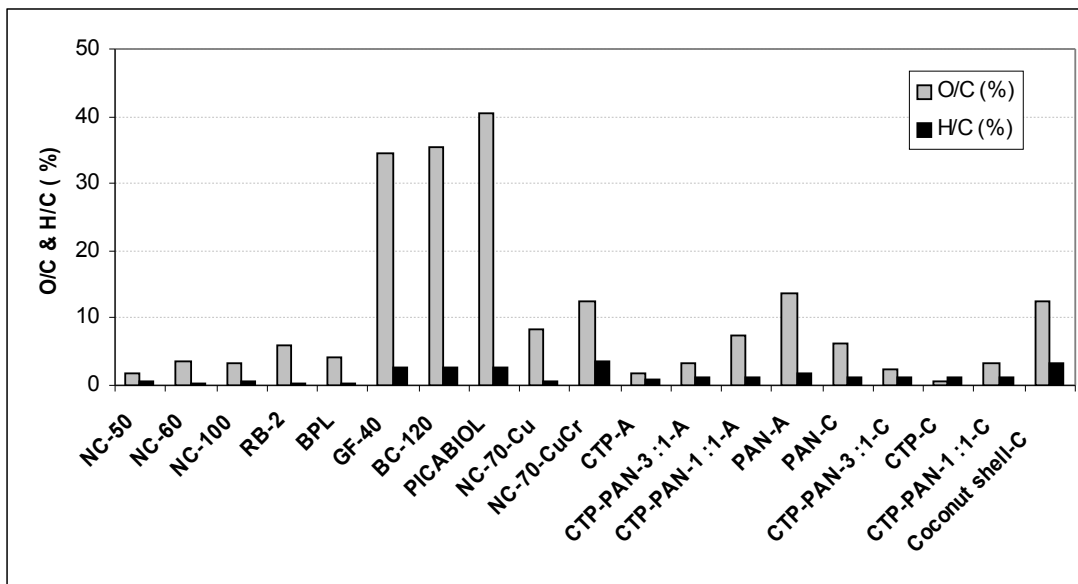


**Figure 4 - :** Oxygen and hydrogen ratios obtained by elemental analysis.

#### 12.1.1.3 NITROGEN CONTENT

Significant amounts of the element N are only found in the samples prepared from CTP (coal tar pitch) and PAN (polyacrylonitrile) samples whilst the other activated carbon samples contain negligible amounts of nitrogen. The forms of nitrogen substituted for carbon in the graphene layer of the CTP and the PAN samples are shown in Figure 4-2.

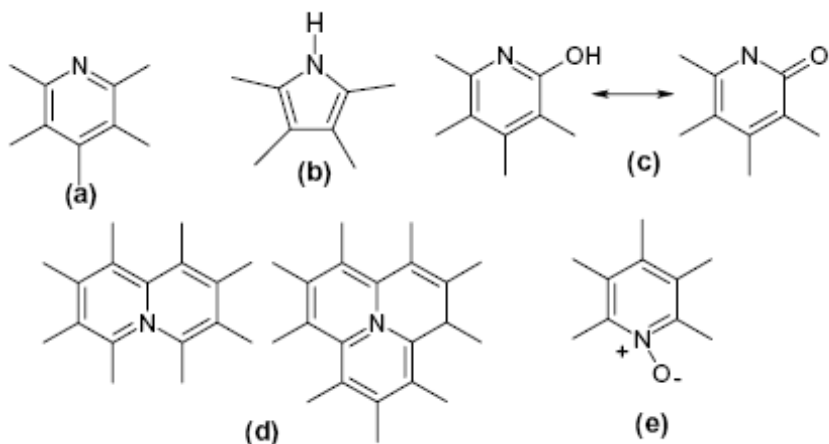


**Figure 4 - :** Forms of nitrogen substituted for carbon in graphene layer: pyridinic (a), pyrrolic (b), pyridonic (c), quaternary “valey” and “center” (d), pyridine N-oxide (e). [Grzyb *et al.*, 2005].

The highest amount of N/C ratio is found in the carbonized PAN sample and reaches about 20 %. After activation this ratio is reduced to about 14 %. Literature sources [Yi, 2002] show that nitrogen groups are eliminated from the PAN during the course of activation. According

## ***Chapter 4: Results and Discussions***

---

to Wang *et al.*, 1996, the activating agent preferentially reacts with the edges of the carbon structure which leads to the removal of species present in them. Nitrogen functional groups are eliminated due to the activation process.

The N/C ratio of the PAN and CTP blended samples depends on the proportion of the PAN in the blend. The activated sample blend consisting of 50 % PAN and 50 % CTP contains about 10 % N/C ratio. The sample blend containing 25 % PAN and 75 % CTP contains a N/C ratio reduced to about 6 %. Thus the nitrogen content varies according to the percentage of PAN added to the blend.

### **12.1.2 BOEHM'S METHOD**

The acidic and basic surface functional groups of some of the activated carbons measured using the Boehm's titration is given below in Table 4-2. The results show that there is a significant amount of the surface oxygenated groups for the samples GF-40 and BC-120. The chemical activation mode increased the number of the surface oxygenated groups. This coincides with the elementary analysis results with the chemically activated carbon samples showing higher oxygen to carbon ratio. The experimental error observed for the measurement of the surface functional groups is greater than 25 %. The results of the Boehm titrations is not taken up for further analysis due to the uncertainty in the results.

	<b>GF-40</b>	<b>NC-60</b>	<b>NC-100</b>	<b>BC-120</b>	<b>BPL</b>	<b>RB-2</b>
<b>Acidic complexes (méq.L<sup>-1</sup>)</b>						
<b>GI</b>	0,20	0	0	0,652	0	0
<b>GII</b>	0,62	0,06	0,27	0,12	0,16	0,09
<b>GIII</b>	0,49	0,4	0,2	0,8	0,18	0,07
<b>GIV</b>	0,32	0,9	0,4	1,5	0	0
<b>Basic complex (méq.L<sup>-1</sup>)</b>						
	0,65	0,5	0,55	0,2	0,50	0,62

**Table 4 - :** Surface functional groups of activated carbons.

## ***Chapter 4: Results and Discussions***

---

### **12.1.3 ASH AND MINERAL CONTENT**

The ash content of the activated carbon samples was measured by the ASTM D-2866 method and the mineral analysis was carried out using the SEM-X ray technique. The results of these two analysis are discussed in this section.

#### ***12.1.3.1 ASH CONTENT***

Ash content is representative of mineral impurities present in carbon precursors or derived from impregnation. Consequently the ash content varies the nature of the carbon precursor and with the activation mode applied. The ash content values measured are given in Table 4-3. The ash levels were higher for the steam activated carbons namely RB-2 and BPL with 5 % ash content. The coconut shell activated carbons contained about 2% ash. Finally the acid activated carbons like GF-40, BC-120 and Picabiol possess the lowest amounts of ash, ranging from 0.3 to 0.4 %. From the literature [Baker *et al.*, 1992], it was found that the ash content in physically activated carbons ranges mostly from 1 to 10 %, whilst the acid activated carbons contain negligible amounts of ash.

<b>Sample</b>	<b>Precursor</b>	<b>Ash content (%)</b>	<b>Ash content (g)</b>
NC-50 <sup>(PA)</sup>	Coconut shell	1.9	0.01
NC-60 <sup>(PA)</sup>	Coconut shell	1.65	0.008
NC-100 <sup>(PA)</sup>	Coconut shell	2.2	0.011
RB-2 <sup>(PA)</sup>	Peat	4.7	0.024
BPL <sup>(PA)</sup>	Coal	4.5	0.023
GF-40 <sup>(CA)</sup>	Olive stone	0.4	0.002
BC-120 <sup>(CA)</sup>	Wood	0.3	0.0015
Picabiol <sup>(CA)</sup>	Wood	0.3	0.0015

**Table 4 - :** Ash content of activated carbon samples measured by ASTM method.

PA: Physically activated carbons

C: Carbonized samples which are non-activated

CA: Chemically activated carbons

#### ***12.1.3.2 MINERAL ANALYSIS***

The ash content was qualitatively analyzed using the SEM-X ray technique. The results are shown in Table 4-4 and the figures depicting the elemental peaks can be found in Appendix-A. The elemental weight fractions of different constituents can be seen in Table 4-3. There are differences between the coconut shell based samples and peat and coal based. The exceptional

## ***Chapter 4: Results and Discussions***

---

difference between the carbons exists in the presence of K. It may be seen from the Appendix-A that the coconut shell activated carbons namely NC-50 and NC-60 show a strong signal for K which is followed by other constituents like Ca, Mg, Al, S. The presence of potassium in the coconut shell activated carbons is in the following order NC-50 >NC-60 >NC-100. The higher percentage of K for the coconut based carbons can be related to the activation or neutralization process during the manufacture where hydroxide of potassium is added to increase the microporosity in the carbons during activation step [Amarasekera *et al.*, 1998].

The peat and coal based activated carbon samples show lower amounts of K content, but higher for Al, S, Ca, Na etc. The higher amounts of Al, Mg, S and P may indicate the presence of clay in these samples.

Element	Coconut shell			Peat	Coal
Sample	NC-50	NC-60	NC-100	RB-2	BPL
K (Elt wt %)	22.7	15.5	10.60	4.60	1.40

## ***Chapter 4: Results and Discussions***

---

Ca (Elt wt %)	5.60	3.70	0.50	2.80	1.30
S (Elt wt %)	0.13	1.60	0	3.30	0.82
P (Elt wt %)	0.70	1.20	0.40	0.60	0.22
Al (Elt wt %)	0.30	0.10	3.70	1.40	8.80
Mg (Elt wt %)	1.80	2.50	0.30	1.03	0.30
Na (Elt wt %)	4.90	4.04	3.90	2.30	0.30
Fe (Elt wt %)	0.23	0.21	0.50	2.40	4.50

**Table 4 - :** Results from ash content elemental analysis by X-ray spectra from SEM scans.

### **12.1.4 POROSITY**

The porosity characteristics of the AC samples otherwise termed as the textural properties were characterized from nitrogen adsorption at 77 K and mercury porosimetry.

#### ***12.1.4.1 ANALYSIS OF NITROGEN ADSORPTION DATA***

Nitrogen adsorption measurements were carried out only with the activated carbon samples, as the non-activated ones have negligible porosity. Appendix-B shows the adsorption and desorption isotherms of N<sub>2</sub> at 77 K obtained for the various activated carbons used in this study. These isotherms give a first hand description of the kind of porosity present in the activated carbon samples. Adsorption isotherms of the physically activated carbons exhibit conformity to the type I isotherm with complete reversibility observed throughout the entire pressure range. On the other hand, the chemically activated carbon samples exhibit an hysteresis between the adsorption and the desorption isotherms in the upper pressure range, characteristic of type IV isotherms and that can be related to the presence of greater fraction of mesopores in the adsorbent [Brauner *et al.*, 1940]. From Appendix-B, we find that for the samples GF-40 and BC-120 the N<sub>2</sub> adsorbed continues to increase indicating the filling of the mesopores.

At saturation (P/P<sub>0</sub> = 1), adsorption isotherms of the chemically activated carbon samples BC-120 and GF-40 have N<sub>2</sub> adsorption capacities significantly higher when compared to other

## ***Chapter 4: Results and Discussions***

activated carbon samples whilst in the physically activated series NC-100, exhibits the highest adsorption capacity at saturation.

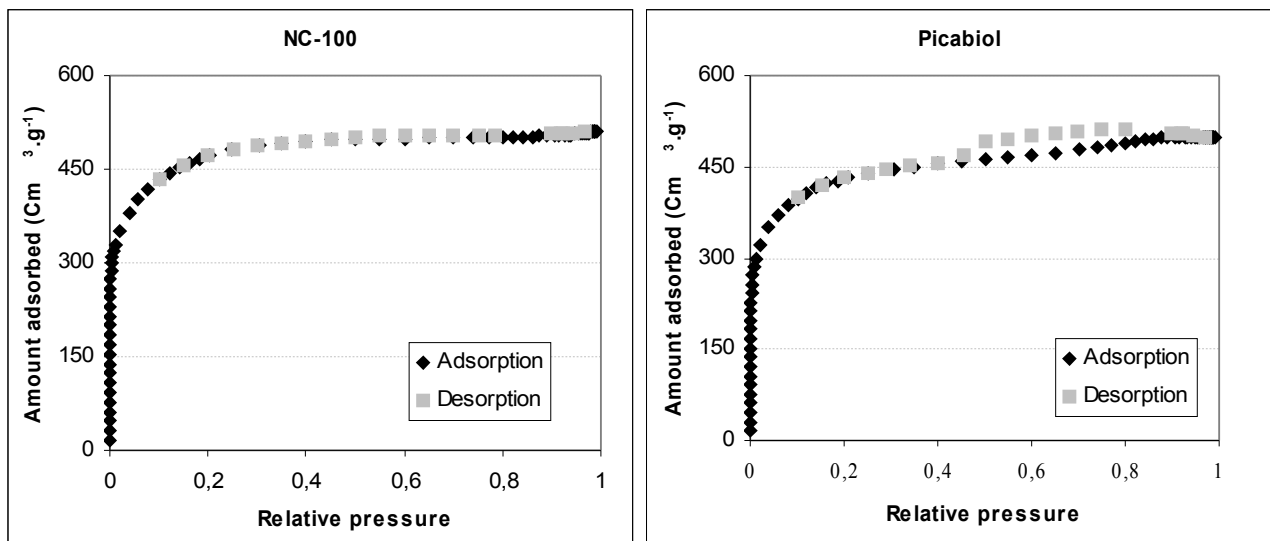
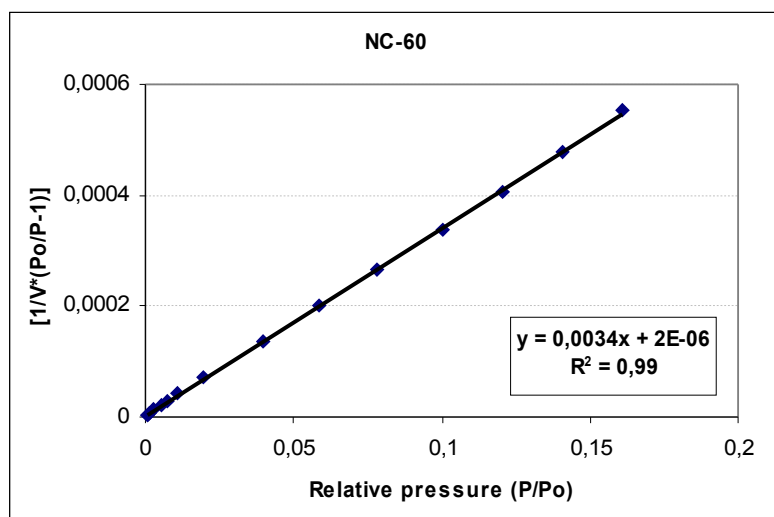


**Figure 4 - :** Adsorption isotherms of N<sub>2</sub> at 77 K for the activated carbon samples NC-100 and Picabiol.

### ***12.1.4.2 SPECIFIC SURFACE AREA***

Specific surface areas of AC samples were successfully derived from the BET model which

fits the experimental data well, as shown in Appendix-C. By plotting  $\frac{1}{V_A [P_0 / P - 1]} \text{ vs } \frac{P}{P_0}$ , linear relationship was obtained with a R<sup>2</sup> coefficient of determination in all cases of about 0.99. An example of the plot for the sample NC-60 is shown in Figure 4-4.



## ***Chapter 4: Results and Discussions***

---

**Figure 4 - :** Plot of  $\frac{1}{V[P_0 / P - 1]} \text{ vs } \frac{P}{P_0}$  for the calculation of specific surface area.

Specific surface area data can be found in Appendix-F. The distribution of the specific surface areas among the activated carbon samples is shown in Figure 4-5. The commercially prepared chemically activated sample BC-120 had the largest specific surface area with  $1975 \text{ m}^2 \cdot \text{g}^{-1}$ . The other acid activated carbons namely Picabiol and GF-40 also had higher specific surface areas of about  $1600 \text{ m}^2 \cdot \text{g}^{-1}$ . The higher surface area of the chemically activated carbons are mainly attributed to the chemical agent used for the activation. The phosphoric acid creates a highly porous structure thanks to the charring and aromatization of the carbon skeleton [Bansal, 1988].

The specific surface area of the steam activated carbons varied greatly from 1000 for the RB-2 sample until  $1800 \text{ m}^2 \cdot \text{g}^{-1}$  for the NC-100 sample. One can notice an increase in the  $S_{\text{BET}}$  with respect to the activation times. The  $S_{\text{BET}}$  of the three coconut shell samples is in the following order  $\text{NC-100} > \text{NC-60} > \text{NC-50}$ , with NC-50 having the lowest activation time.

On the other hand, Coal Tar Pitch and the PAN samples possessed low specific surface areas ranging from  $100-500 \text{ m}^2 \cdot \text{g}^{-1}$ .

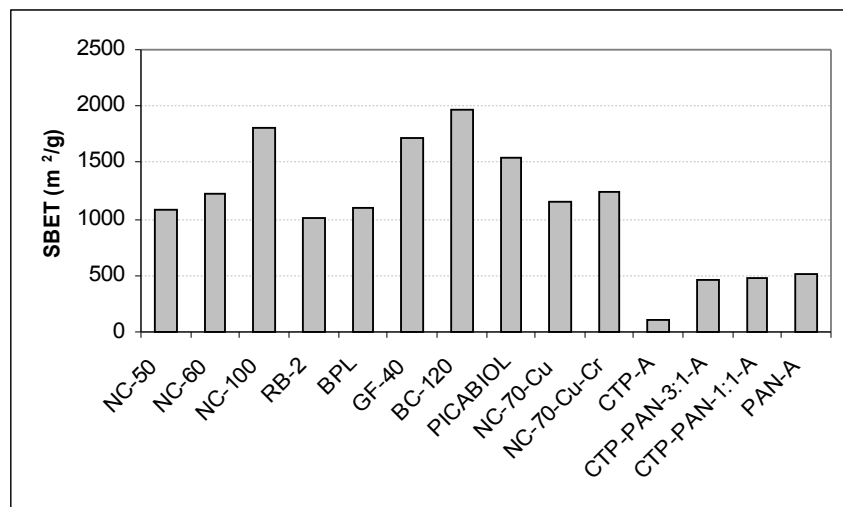


**Figure 4 - :** Specific surface area of the activated carbon samples.

### ***12.1.4.3 PORE SIZE DISTRIBUTION***

The pore size distribution is obtained using the Density Functional Theory (DFT) on the  $\text{N}_2$  adsorption data at 77 K. The pore size distribution of the activated carbon samples is given in

## ***Chapter 4: Results and Discussions***

---

Appendix-D and an example of that of NC-60 is shown in Figure 4-6. The pores are mainly distributed in the micropore region for the physically activated carbons, which is around 20 Å, whereas for the chemically activated carbons the fraction of mesopores is significative.

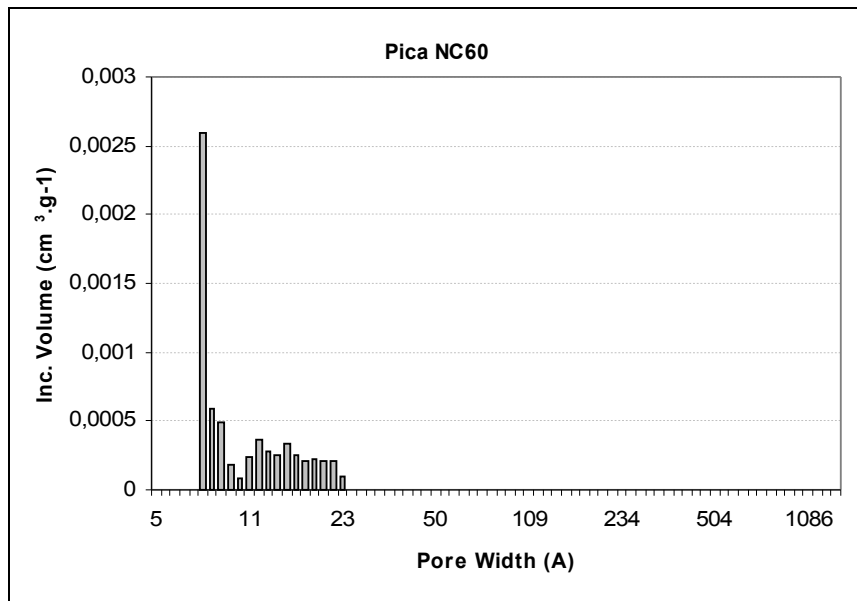


**Figure 4 - :** Pore size distribution of the activated carbon sample NC-60 by DFT method.

Average widths of micropores derived from DFT are presented in Appendix-G. Little variations are observed between the values reported both for physically and chemically AC samples. Samples data being within the range [0.92-1.38]. Chemically AC samples show slightly larger average diameter than the physically activated carbons.

### ***12.1.4.4 POROUS VOLUMES***

Data related to the micropore, mesopore and the macropore volumes of the activated carbons are discussed in this section.

#### ***12.1.4.4.1 Microporous volume***

## ***Chapter 4: Results and Discussions***

---

The micropore volume is derived from the t-plot using the procedure explained in section 3.4.1.2.3. Appendix-E presents t-plots obtained for the different AC samples and an example is shown in Figure 4-7. t-plots obtained for the activated carbons are representative of microporous materials, with the upper part of the curve bending from the straight line passing through the origin in comparison to the non-porous solid (section 3.4.1.2.3).

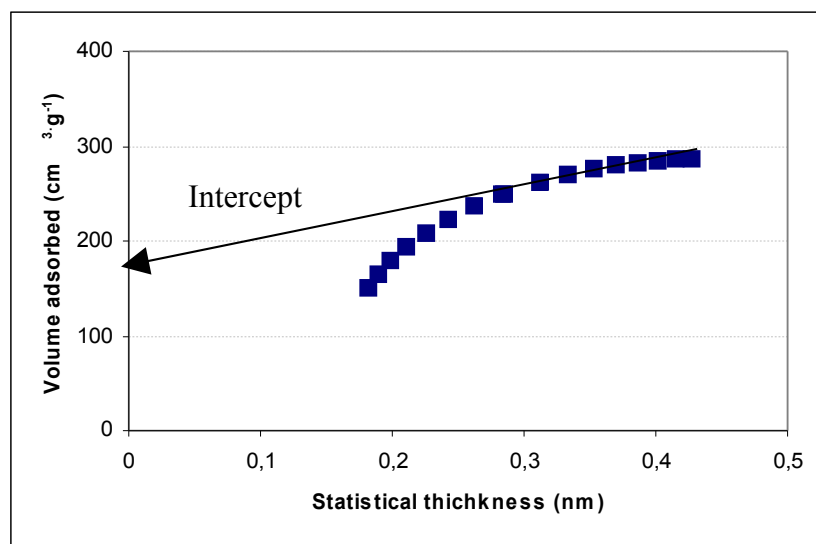


**Figure 4 - :** t-plot for the activated carbon sample NC-50.

The distribution of the micropore volume among the activated carbon samples is shown in Figure 4-8. The micropore volume is evenly distributed among the commercially prepared activated carbons, ranging from  $0.2\text{--}0.35\text{ cm}^3\text{.g}^{-1}$ . The only sample with a very low micropore volume ( $0.04\text{ cm}^3\text{.g}^{-1}$ ) is the laboratory prepared coal tar pitch activated carbon sample. Variations observed cannot be directly linked to  $S_{BET}$  data. Certain activated samples, like PICABIOL show high specific surface area but relatively low micropore volume, and the inverse trend is found for the samples RB-2 and NC-50.

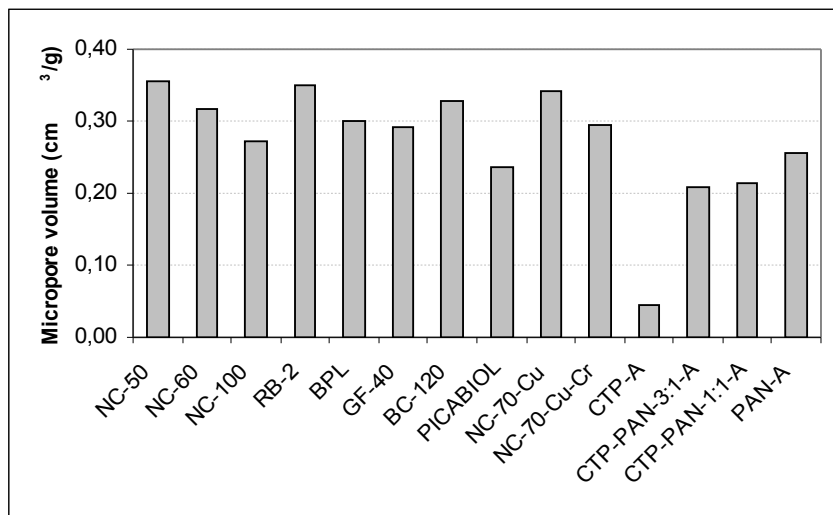


**Figure 4 - :** Micropore volumes determined from t-plots of the activated carbon samples used for the study.

#### 12.1.4.4.2 Meso and macroporous volume

Volumes of pores greater than 80 Å (meso and macropore) were measured from mercury intrusion technique. The experimental values are shown in Table 4-5, comparison between samples can be made from Figure 4-9.

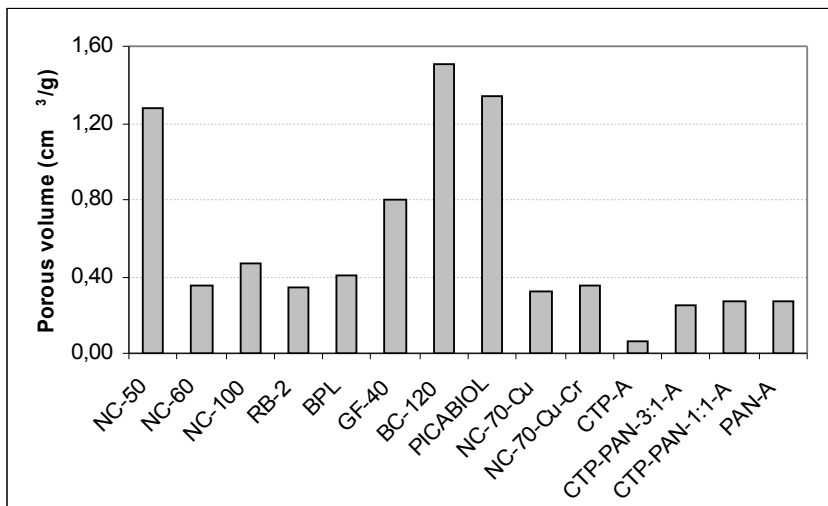


**Figure 4 - :** Meso-macro porous volumes of the activated carbon samples.

Porous volumes are found to be higher for chemically activated carbon samples than for physically activated ones. Typically physically AC's develop largest pore volumes within the range  $[0.25-0.5] \text{ cm}^3 \cdot \text{g}^{-1}$ , whereas for chemically activated samples, values range from  $0.8-1.5 \text{ cm}^3 \cdot \text{g}^{-1}$ . The only deviation to this trend is the NC-50, a coconut based physically activated carbon having a large mesopore volume of about  $1.20 \text{ cm}^3 \cdot \text{g}^{-1}$ . This may be due to the short

## ***Chapter 4: Results and Discussions***

---

activation time applied compared to other samples NC-60, NC-100. In a similar way, sample NC-50 has a lower specific surface area.

**Table 4 - :** Porous volumes obtained from mercury porosimetry technique.

<b>Sample</b>	<b>Precursor</b>	<b>Meso-macro porous volumes (cm<sup>3</sup>. g<sup>-1</sup>)</b>
NC-50 <sup>(PA)</sup>	Coconut shell	1.20
NC-60 <sup>(PA)</sup>	Coconut shell	0.35
NC-100 <sup>(PA)</sup>	Coconut shell	0.47
RB-2 <sup>(PA)</sup>	Peat	0.34
BPL <sup>(PA)</sup>	Coal	0.40
CTP-A <sup>(PA)</sup>	Coal tar pitch	0.07
CTP-PAN-3 :1-A <sup>(PA)</sup>	Coal tar pitch and PAN	0.25
CTP-PAN-1 :1-A <sup>(PA)</sup>	Coal tar pitch and PAN	0.27
PAN-A <sup>(PA)</sup>	PAN	0.27
GF-40 <sup>(CA)</sup>	Olive stone	0.80
BC-120 <sup>(CA)</sup>	Wood	1.50
PICABIOL <sup>(CA)</sup>	Wood	1.34
NC-70-Cu <sup>(PA)</sup>	Coconut shell	0.33
NC-70-Cucr <sup>(PA)</sup>	Coconut shell	0.35

### **12.1.5 STRUCTURAL PROPERTIES**

Results of the structural characterization made using Scanning Electron Microscopy (SEM) technique and the High Resolution Transmission Electron Microscopy (HRTEM) is discussed in this section.

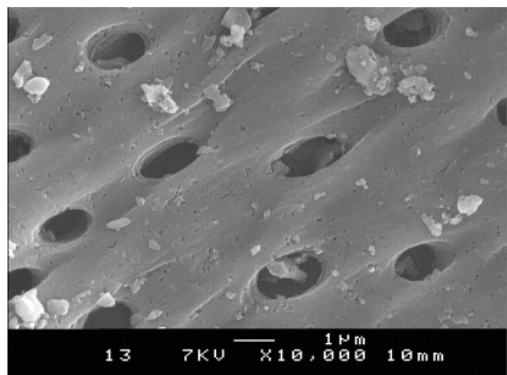
#### ***12.1.5.1 SEM IMAGES***

The porous structure of activated carbons was observed using a Scanning Electron Microscope (SEM). SEM micrographs for a few activated carbons are shown in Figure 4-10 and in Appendix-G. A magnification ranging from 1000 X to 50,000 X was used for the better visualization of the images above which the surface features could not be clearly visualized.

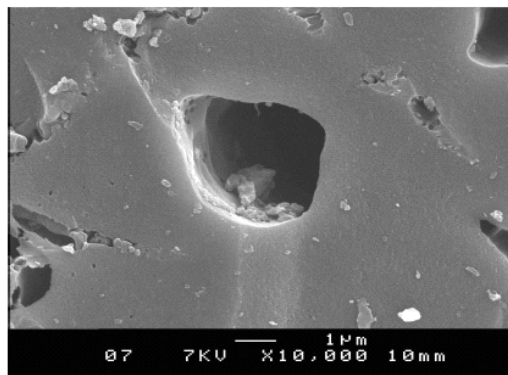
## ***Chapter 4: Results and Discussions***

---

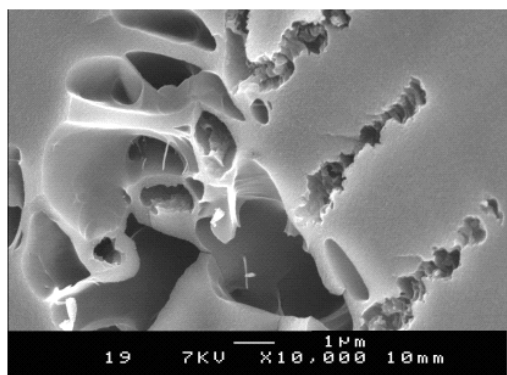
The SEM micrographs show the different types of morphology among the activated carbon samples. The coconut shell activated carbons like NC-100 and NC-60 show a hard and pitted surface with macropores arranged in an orderly fashion. On the other hand the surface of the chemically activated carbon (BC-120) is smooth with irregularly shaped macropores or cavities distinctly different from the coconut shell samples. The physically activated RB-2 sample showed fibrous surface with macropores more or less regular in shape and finally the BPL sample resembled a flaky structure obtained from the coal precursor and the surface features, like macropores and cavities, could not be observed.



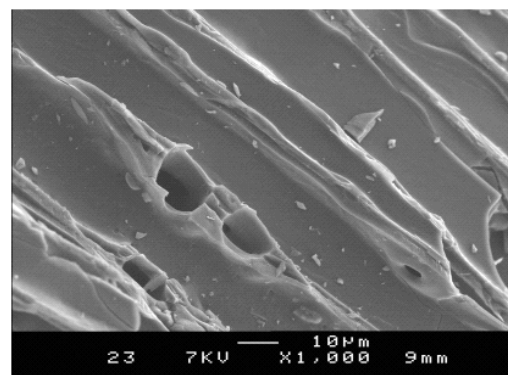
NC-100



NC-60



BC-120



RB-2

**Figure 4 - :** SEM micrographs of some activated carbon samples.

From SEM observation of the activated carbon samples only macropore, pits and cavities could be observed whereas the micro and mesopores could not be distinguished with the magnification obtained from the SEM

### ***12.1.5.2 HRTEM IMAGE ANALYSIS***

The raw HRTEM images of the activated carbons are illustrated in Figure 4-11 and in Appendix-H. The aim is to study and compare the nanostructural arrangement of the different activated carbons with respect to the precursor, mode of preparation and their physical and chemical properties

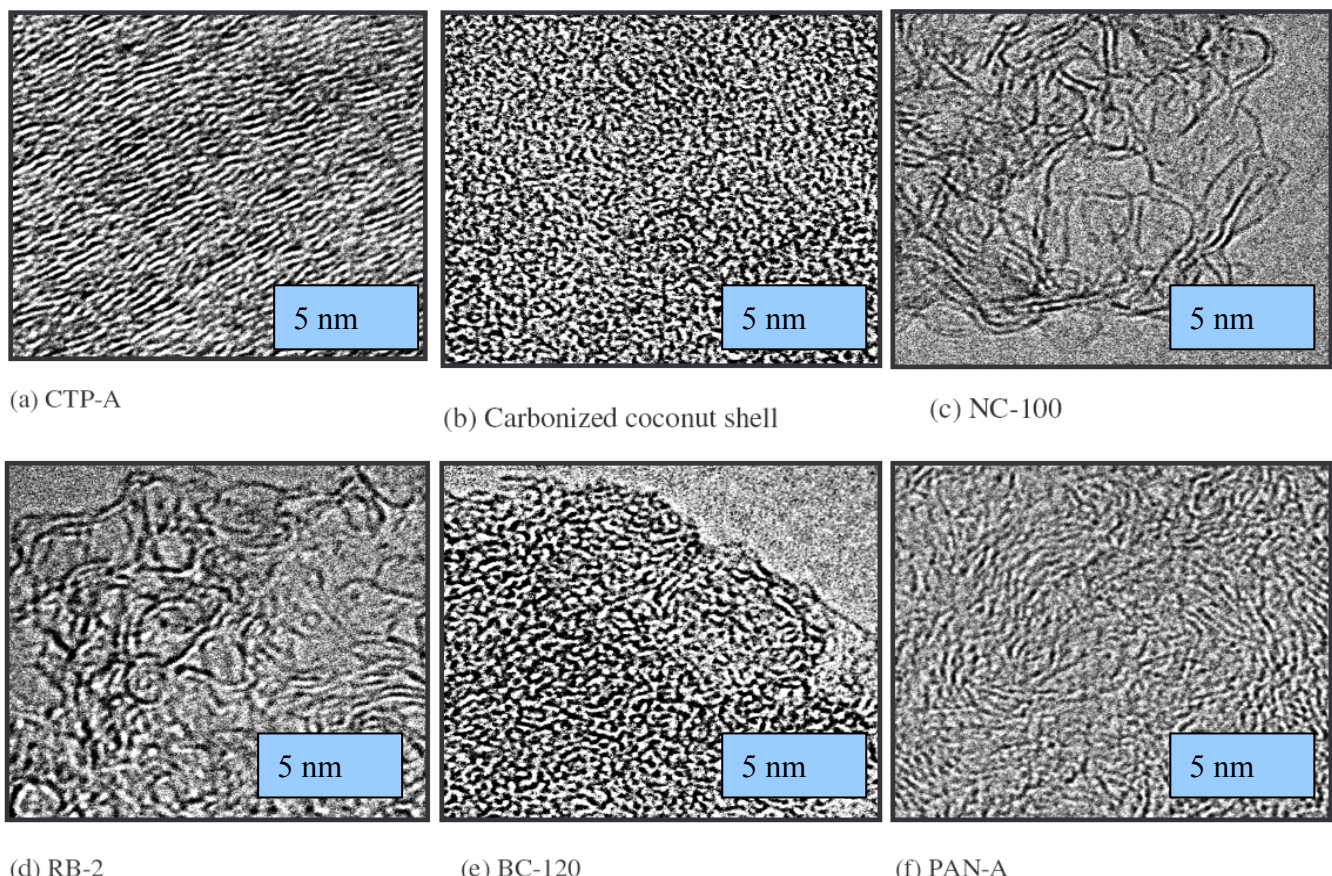


**Figure 4 - :** HRTEM images of some of the carbon samples used for the study (image size 16 nm X 16 nm).

#### ***12.1.5.2.1 Visual observations***

From the visual observation of the HRTEM images (Figure 4-11), the differences in the structural organization among the carbon samples are clearly observed. Three distinct characteristics can be distinguished: the fringe length ( $L$ ), interlayer spacing ( $d$ ) and number of stacked layers ( $N$ ) in a coherent domain. The first group of carbon samples have short fringe length and the graphitic layers are randomly arranged in an isolated fashion without appreciable stacking of the layers ( $> 60\% \text{ NSL}$ , i.e. non stacked layers). This feature is mainly seen in the chemically activated carbons, namely GF-40, Picabiol and BC-120. The

## ***Chapter 4: Results and Discussions***

---

main reason is being attributed to the mode of activation with a chemical agent and the low temperatures experienced during the process of manufacture. Aromatisation, i.e. formation of polyaromatic layers, and activation, i.e. grafting of oxygenated groups on the layers boundaries, occur concomitantly. Consequently, small and highly cross linked layers, are formed rendering difficult the layer stacking. Therefore, in comparison with physically activated carbons, length of the graphitic layers (L) and number of stacked layers (N) are small, whereas interlayer spacing (d) and % NSL (non stacked layers) are high. Another important feature is that these samples have a high O/C ratio.

The second group of carbon samples show long graphitic sheets, weakly stacked. The graphitic sheets slightly bent as the layer edges tend to weld (free radical recombination) constituting spaces between them as seen in activated carbon samples like NC-60, BPL, NC-100 and RB-2. The micropores and the mesopores are found to be large and elongated as in the case of NC-100 and RB-2. The samples were physically activated at around 800 – 1000 °C and exhibit low oxygen to carbon ratio. The burn-off of the shortest and the distorted layers take place at such high temperature.

The third group of carbon sample contains mainly the coal tar pitch and polyacrylonitrile samples which exhibit a lamellar nanostructure of the graphitic layers which tend to be parallel to each other and better stacked compared to the first and second group of samples. The best example of this type of material is the CTP based activated carbon. This is due to CTP precursor which leads to a well ordered graphitisable coke with well stacked nanometre-sized layers giving a lamellar nanostructure [Rouzaud, 2004], and to the physical activation which do not induce noticeable cross-linking responsible for strong alteration of this nanostructure. The PAN precursor forming a non-graphitizable char give activated carbons which show a structure noticeably more disorganised than the CTP sample. The CTP-PAN samples which are a mixture of CTP and PAN precursors give physically activated carbons which take a character depending on the composition of the mixture.

### ***12.1.5.2.2 Quantitative image analysis (dimensional analysis)***

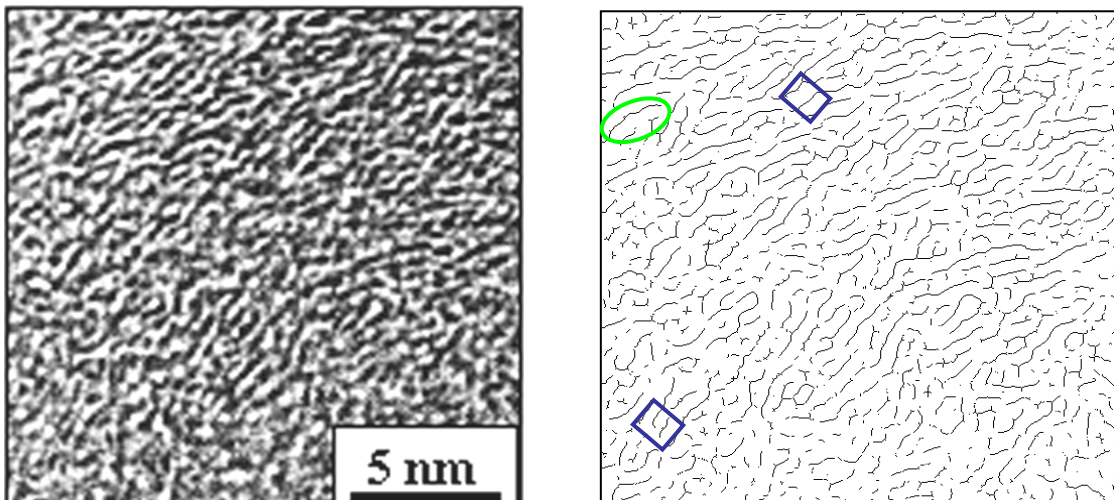
From the skeletonized images shown in Figure 4-12, a computerized interface was used to obtain the structural and microtextural data. The Basic Structural Unit (BSU) is first defined from the skeletonized image according to some preset conditions. To specify the presence of BSU (i.e. stacked layers), a set of parallel layers were defined according to adjustable parameters as the tolerance of misorientation ( $\pm 15^\circ$ ). When the above said defined BSU is

## ***Chapter 4: Results and Discussions***

---

detected, this interfringe spacing  $d_{002}$  its height  $L_c$  and its length  $L_a$  were determined as shown in Figure 4-13. The amount of single fringes was also determined. Then the corresponding mean data were calculated for all the BSU's. Histograms of orientation can be built from the data. The length of each individual fringe was measured and an average fringe length  $L$  is obtained.  $L$  corresponds to a mean of the aromatic layer sizes of each individual.

**Figure 4 - :** Analysis of high resolution TEM images of activated carbons : raw images



(on the left) and skeletonized images (on the right).

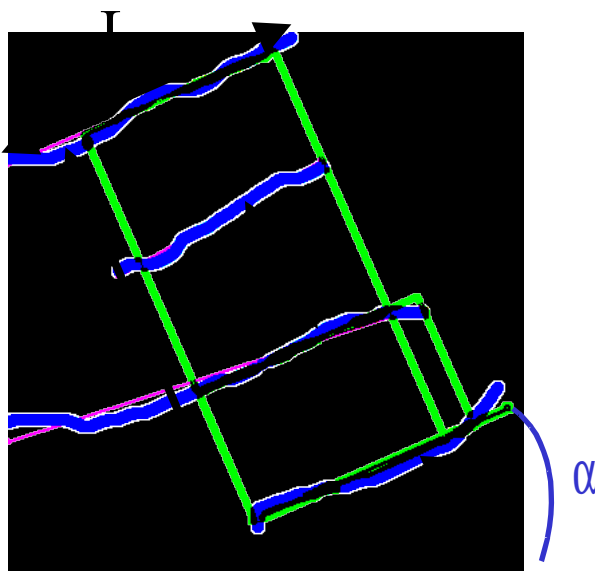


**Figure 4 - :** HRTEM image analysis. structural analysis showing coherent domain limits:  $L$  is the individual fringe length,  $L_a$  is the width of the coherent domain,  $L_c$  is its height related to  $d$  which is the interlayer spacing and  $N$  is the number of stacked layers within a domain [Rouzaud and Clinard, 2002].

Sample	% Non Stacked Layers	$L > 1$ ring ( $\text{\AA}$ )	$L > 2$ rings ( $\text{\AA}$ )	$L > 3$ rings ( $\text{\AA}$ )	$L_a$ ( $\text{\AA}$ )	$L_c$ ( $\text{\AA}$ )	$N$	$d_{avg}$ ( $\text{\AA}$ )
--------	----------------------	-------------------------------	--------------------------------	--------------------------------	------------------------	------------------------	-----	----------------------------

## ***Chapter 4: Results and Discussions***

---

RB-2 <sup>(PA)</sup>	57	5.8	8.4	14.5	4.6	6	2.5	4.2
PAN-A <sup>(PA)</sup>	59	6.4	9	14.7	3.9	5.3	2.4	3.9
PAN-C <sup>(PA)</sup>	47	6.3	8.8	14.4	4.3	6.9	2.8	3.8
CTP-A <sup>(PA)</sup>	14	9.7	12.3	18.1	7.2	10.3	3.7	3.8
CTP-1 :1-A <sup>(PA)</sup>	60	5.8	8.4	13.8	3.8	5.6	2.5	3.9
NC-60 <sup>(PA)</sup>	53	6.3	8.9	14.4	4.4	5.9	2.5	4.0
NC-100 <sup>(PA)</sup>	51	6.1	9.1	16.5	4.7	5.4	3.9	3.9
NC-50 <sup>(PA)</sup>	50	5.6	8.4	14.5	4.2	6	2.6	3.8
BPL <sup>(PA)</sup>	46	6	8.6	15	3.9	5.6	2.5	3.8
BC-120 <sup>(CA)</sup>	65	5.5	7.7	13.3	3.5	4.9	2.2	3.9
GF-40 <sup>(CA)</sup>	74	5.4	7.7	12.6	3	4.7	2.2	4
Picabiol <sup>(CA)</sup>	66	4.8	7.1	13.2	3.4	4.5	2.1	4.1
Coconut shell <sup>(C)</sup>	82	4.4	6.6	12.3	2.3	3.9	2.1	3.8

**Table 4 - :** Average structural parameters of carbon samples obtained from image analysis

PA: Physically activated carbons

C: Carbonized samples which are non-activated

CA: Chemically activated carbons

### ***12.1.5.2.3 Arrangement of graphitic layers***

The tendency of stacking of the graphitic layers among the activated carbons is shown in Figure 4-14. It is found that the % NSL is very low for the physically activated carbons compared to the chemically activated ones. The coal tar pitch sample has the lowest value with just 14 % of non stacked layers indicating that 86 % of the graphitic layers are found to be stacked. On the other hand, it can be observed that for the carbonized coconut shell and the

## ***Chapter 4: Results and Discussions***

---

chemically activated carbons the % NSL is high and amounts to about 80 %. The other physically activated carbons are found to be placed in between these two types of samples.

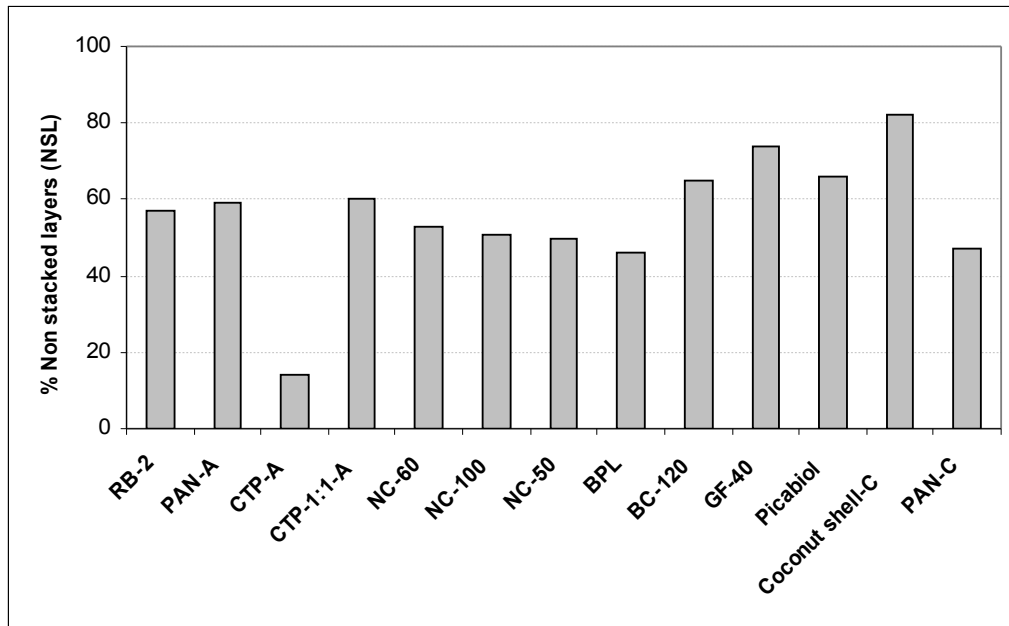


**Figure 4 - :** Graphitic layers stacking trends among the activated carbon samples.

### ***12.1.5.2.4 Graphitic layer length***

The distribution of the length of the graphitic sheets namely  $L > 1$  ring ( $\text{\AA}$ ),  $L > 2$  rings ( $\text{\AA}$ ) and  $L > 3$  rings ( $\text{\AA}$ ) among the activated carbons is shown in Figure 4-15. It is generally found that the graphitic layer for the physically activated carbons is longer than the chemically activated carbons. The activated carbons having shorter graphite layers had generally higher O/C ratio.

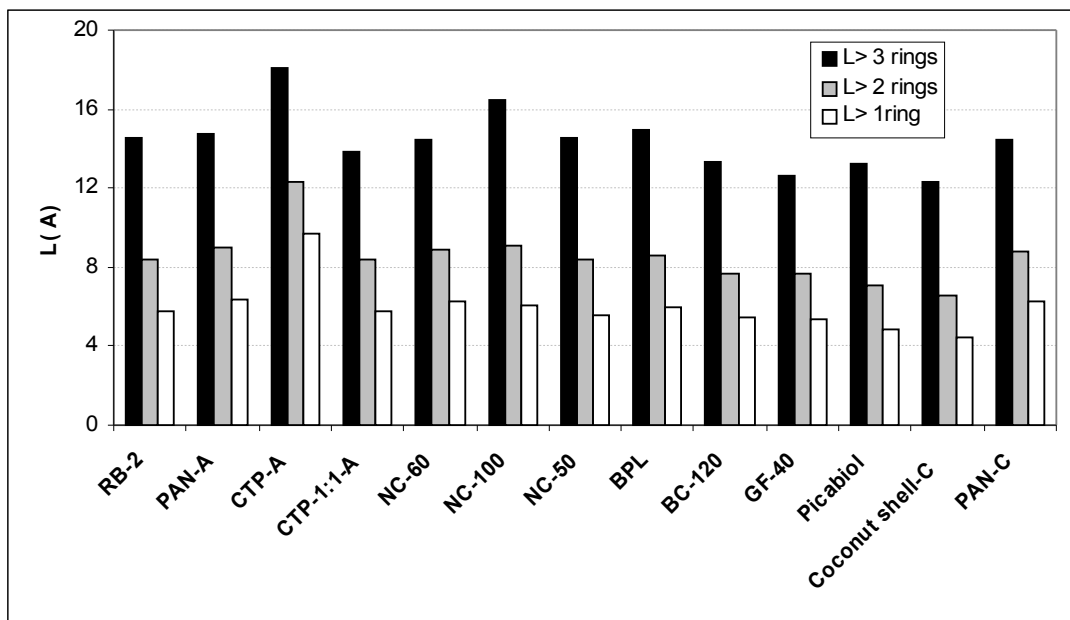


**Figure 4 - :** Distribution of graphitic layer lengths among the carbon samples.

#### 12.1.6 COMPARISON OF MICROPOROUS DIMENSIONS

The micropore dimensions obtained from the DFT is compared to that obtained from the HRTEM image analysis technique. The micropore widths obtained from the two procedures are shown in Table 4-7. Large variations are found and micropore dimensions obtained by DFT are larger than the ones determined from the HRTEM technique. Estimations of the micropore width from the DFT uses the experimental nitrogen adsorption data with consideration of fluid-fluid and the fluid solid interactions.

Using the HRTEM observations, micropore dimensions are calculated from the distance between two graphitic layers. The HRTEM technique measures the distance of the fringe  $< 7 \text{ \AA}$ . The nitrogen adsorption technique assumes the pores to be slit shaped whereas it is not the case found in the visualization of the images. For these reasons it is difficult to compare the micropore dimensions derived from these two methods as they have their own limitations.

## ***Chapter 4: Results and Discussions***

---

<b>Sample</b>	<b>DFT method (nm)</b>	<b>HRTEM technique (nm)</b>
NC-50 <sup>(PA)</sup>	1.35	0.38
NC-60 <sup>(PA)</sup>	0.97	0.40
NC-10 <sup>(PA)</sup>	1.11	0.39
RB-2 <sup>(PA)</sup>	0.92	0.42
BPL <sup>(PA)</sup>	0.93	0.38
CTP-A <sup>(PA)</sup>	1.30	0.38
CTP-PAN-1:1-A <sup>(PA)</sup>	1.11	0.39
PAN-A <sup>(PA)</sup>	1.15	0.39
GF-40 <sup>(CA)</sup>	1.15	0.40
BC-120 <sup>(CA)</sup>	1.12	0.39
Picabiol <sup>(CA)</sup>	1.38	0.41

**Table 4 - :** Comparison of micropore dimensions of activated carbons obtained from HRTEM and DFT analysis

#### **12.1.7 CONCLUSIONS**

Important conclusions can be drawn from the characterization of the activated carbons. The mode of activation and the origin of the material have a deep impact on the surface properties of the material.

Chemically activated carbons are characterized with high oxygen to carbon ratios, negligible nitrogen contents and low ash contents. Physically activated commercial samples have low oxygen to carbon ratios, negligible nitrogen to carbon ratios with high ash contents. The physically activated carbon samples prepared in the laboratory show diverse characteristics depending on the precursor material and activation conditions. PAN samples show high nitrogen and oxygen to carbon ratios whereas the coal tar pitch samples show scarce amounts of oxygen and nitrogen to carbon ratios.

The chemically activated carbons are mesoporous in nature and exhibit high specific surface area. The physically activated samples show a wide range of specific surface areas and are microporous in nature, but the degree of activation actually controls the extent of the specific surface area of the physically activated coconut shell. The NC-100 sample submitted to longer activation times than NC-50 and NC-60 shows higher specific surface area. The coal tar pitch and PAN activated sample possess low specific surface area.

Finally the structural characterization has illustrated the effects of the activation mode and the nature of precursor on the organization and dimensions of the graphitic layers. Chemically activated and carbonized carbons show highly disordered and short graphitic layers. On the contrary, physically activated carbons show longer graphitic sheets, well ordered. At last

## ***Chapter 4: Results and Discussions***

---

deviations observed between micropore widths measured from N<sub>2</sub> adsorption and HRTEM underline uncertainties and difficulties to determine absolute structural data.

### **13 REACTIVITY STUDIES**

The main objective of this section is to evaluate the oxidation and ignition reactivity of the activated carbons in the presence of oxygen in order to better understand the mechanisms of oxidation and ignition.

#### **13.1.1 OXIDATION AT LOW TEMPERATURES**

Oxidation of activated carbons, particularly at low temperatures > 100 °C, is studied in this section. The TG-DSC thermograms are used in order to characterize the reactivity of the materials.

##### ***13.1.1.1 POINT OF INITIAL OXIDATION (PIO)***

The Point of Initial Oxidation (PIO) corresponds to the initiation of the oxidation reaction and is pointed out when the heat flux release becomes significant as shown in Figure 4-17. PIO data derived from the DSC curves according to the procedure explained in section 3.2.4 (Chapter-3) are given in Table 4-8. The Figure 4-17 shows the DSC thermogram of the sample NC-60. The heat flux curve remains stable to a temperature of about 200 °C and above which there is an augmentation in its magnitude.

The DSC curves used for the measurement of PIO have a high repeatability as shown in the Figure 4-17 indicating the accuracy between the tests using the same experimental conditions. The percentage of error in the measurement of PIO is around 10 %. The repeatability and accuracy of heat flux change measurements are major advantages of the use of TG-DSC system for determination of reactivity parameters.

From the table 4-8, it appears that the metal impregnated and the chemically activated carbon samples have a low PIO, less than 200°C indicating early start of the oxidation reactions. For physically activated carbon samples, the PIO varies widely from moderate temperature, around 200 °C for the coconut shell activated carbon to elevated temperature, as high as 300 °C for the coal tar pitch activated carbon. Depending on the nature of the precursor, non activated carbon materials exhibit very different PIO, from 175 °C for the non activated

## ***Chapter 4: Results and Discussions***

---

coconut shell sample to 380 °C for the coal tar pitch non-activated carbon. The variation in the oxidation reactivity among the activated carbons can be briefly discussed using the TG and DSC curves.

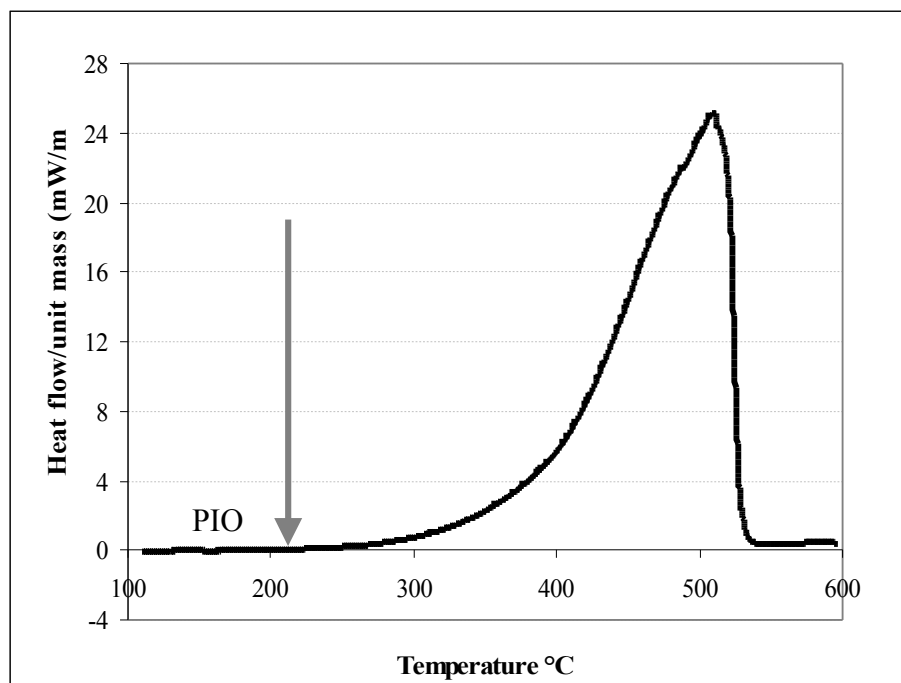
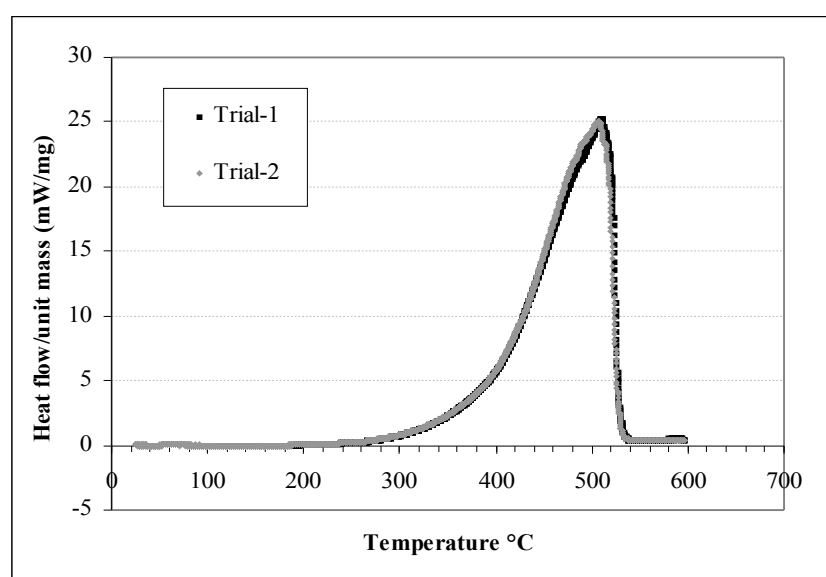


**Figure 4 - :** DSC thermogram of a physically activated carbon sample NC-60 characterizing the PIO.



## ***Chapter 4: Results and Discussions***

---

**Figure 4 - :** Repeatability test for the DSC curves of the activated carbon sample NC-60.

<b>Sample</b>	<b>Activation mode</b>	<b>Precursor</b>	<b>PIO °C</b>
NC-50	Physical	Coconut shell	220
NC-60	Physical	Coconut shell	203
NC-100	Physical	Coconut shell	240
BPL	Physical	Peat	253
RB-2	Physical	Coal	260
CTP-A	Physical	Coal tar pitch	309
CTP-PAN-3:1-A	Physical	Coal tar pitch and PAN	264
CTP-PAN-1:1-A	Physical	Coal tar pitch and PAN	235
PAN-A	Physical	Polyacrylonitrile	225
GF-40	Chemical	Olive stone	183
BC-120	Chemical	Wood	178
Picabiol	Chemical	Wood	168
PAN-C	Non-activated	Polyacrylonitrile	315
CTP-PAN-3:1-C	Non-activated	Coal tar pitch and PAN	267
CTP-C	Non-activated	Coal tar pitch	380
CTP-PAN-1:1-C	Non-activated	Coal tar pitch and PAN	307
Carbonised coconut shell	Non-activated	Coconut shell	175
NC-70- Cu	Physical	Coconut shell	133

## ***Chapter 4: Results and Discussions***

NC-70 -CuCr	Physical	Coconut shell	125
-------------	----------	---------------	-----

**Table 4 - :** Point of Initial Oxidation (PIO) obtained from DSC.

### ***13.1.1.2 DSC CURVE ANALYSIS***

Interesting information can be drawn from the analysis of the DSC curves. Figure 4-18, shows the heat flux releases measured for the three chemically activated commercial carbons: BC-120, Picabiol and GF-40. The chemically activated carbons have a low PIO, and consequently the DSC curves show an early rise and perturbations in the low temperature ranges (less than 350 °C). These perturbations mainly occur because of the presence of large amounts of surface oxygenated groups which react with oxygen in air. Small lags are observed regarding the relative positioning of the heat curves among the three chemically activated carbons indicating that they behave more or less identically.

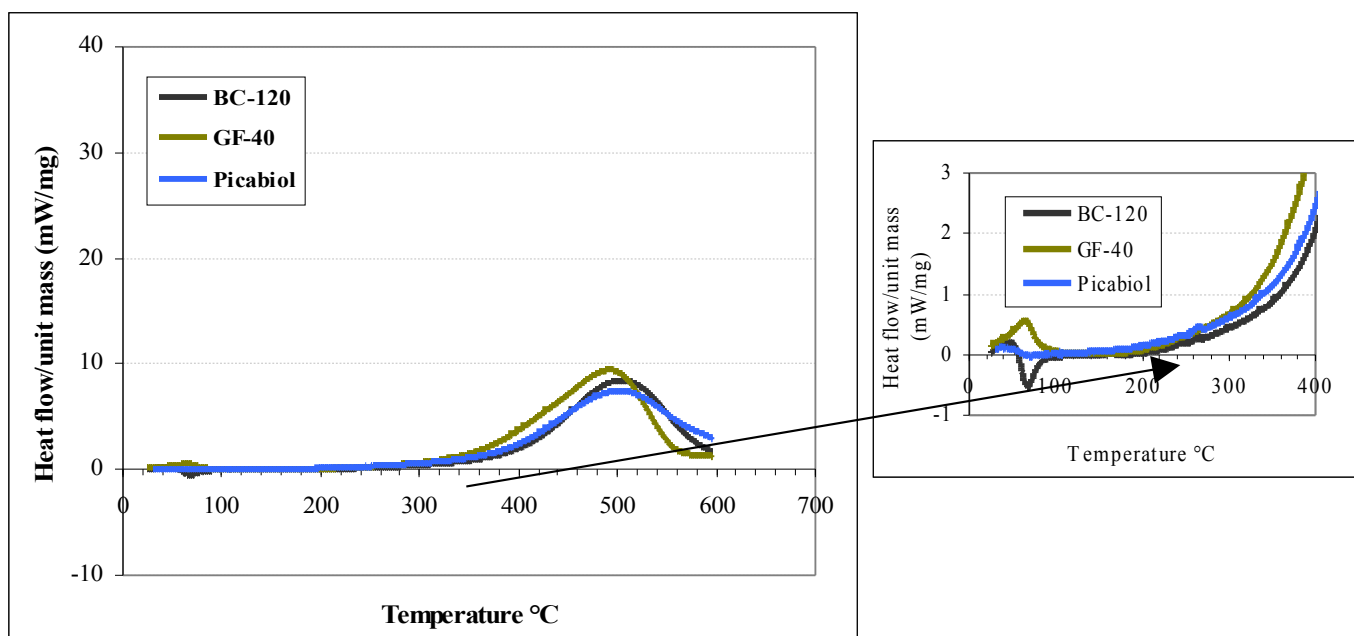


**Figure 4 - :** Heat flux curves of commercially prepared chemically activated carbons

Another interesting feature noticed in the DSC thermograms of chemically activated carbons is the presence of small heat flux peaks of negligible magnitude in the temperature range less than 100 °C. This is probably due to the desorption of water or devolatilization reactions.

The heat flux curves of the commercially physically activated samples are shown in Figure 4-19. Notable differences can be observed among the samples. The activated carbon samples NC-50 and NC-60 exhibit an earlier increase in the heat flux release compared to

## ***Chapter 4: Results and Discussions***

---

other sample NC-100, RB-2 and BPL. Unlike the chemically activated carbons, there is a lag in the positioning of the heat curves among the activated carbon samples. The time lag observed is relevant of the better stability of the activated carbon samples. The most stable materials show greatest magnitudes of heat flux release at high temperature above 400°C, indicating fastest combustion.

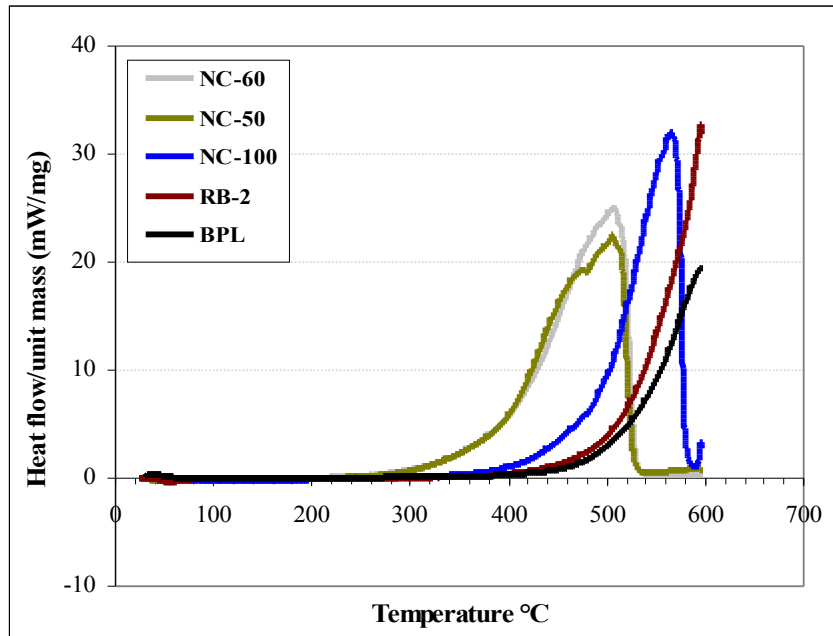


**Figure 4 - :** Heat flux curves of commercially prepared physically activated carbons.

The laboratory prepared coal tar pitch and PAN samples are the most stable compared to all the other activated carbon samples studied. From Figure 4-20, we find that the increase in the heat flux curve is observed at a temperature greater than 400°C. The CTP-A sample shows the highest heat flux peak at a temperature close to 600°C.

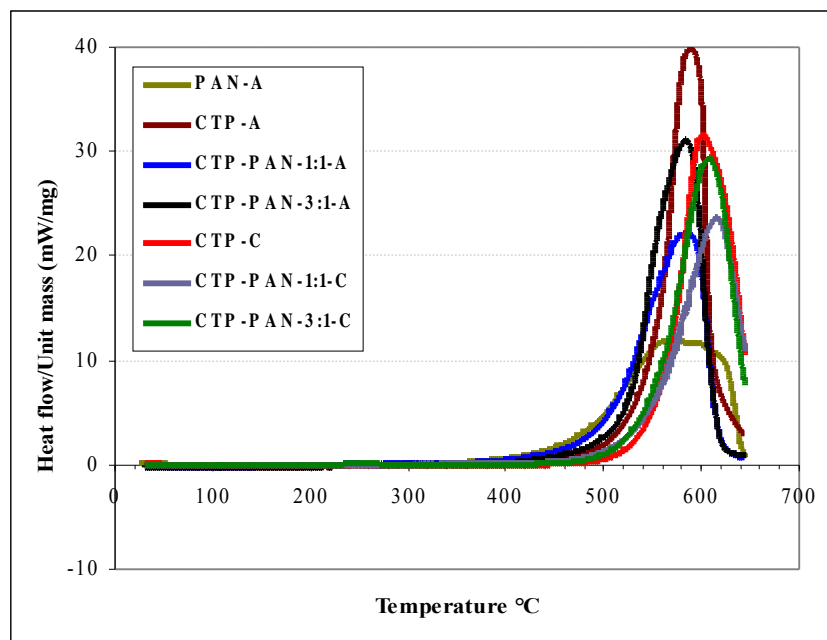


**Figure 4 - :** Heat flux curves of laboratory prepared activated carbons.

#### **13.1.1.3 TG-CURVES**

Simultaneously with the heat flux, the mass variation with respect to temperature was recorded using the thermogravimetric analyser. Examples of decomposition curves obtained for the physically activated NC-60 and chemically activated GF-40 are shown in Figure 4-21. In the initial oxidation stage, a significant amount of mass loss is observed for the chemically activated carbons that is not apparent in the physically activated carbons. This may be related to the consumption of the abundant oxygenated groups in the chemically activated carbons, which react rapidly with air forming unstable complexes, and further decompose into oxidation products like H<sub>2</sub>O, CO and CO<sub>2</sub> along with exothermic. At higher temperatures, further mass losses takes place in the ignition region resulting from the consumption of the carbon matrix. Another hypothesis for the higher mass loss in the chemically activated carbons is the decompostion of the phosphate groups from these samples which is present due to the phosphoric acid activation.

The mass loss for the different activated carbon samples are given in Table 4-9.

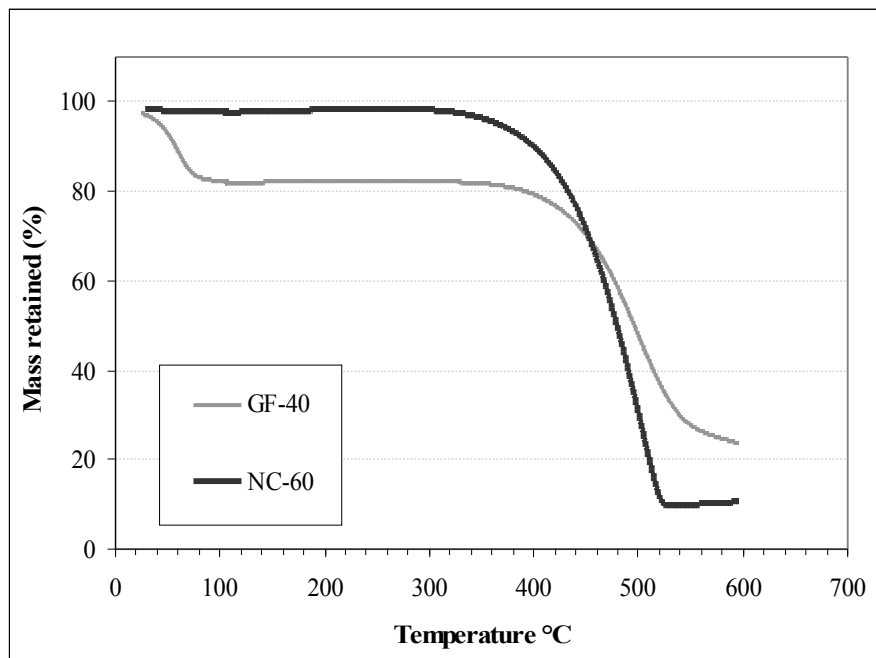


**Figure 4 - :** Decomposition curve of the activated carbon sample NC-60.

Sample	Precursor	Mass loss at PIO (%)
NC-50 <sup>(PA)</sup>	Coconut shell	6,7
NC-60 <sup>(PA)</sup>	Coconut shell	2,0
NC-100 <sup>(PA)</sup>	Coconut shell	3,3
RB-2 <sup>(PA)</sup>	Peat	5,7
BPL <sup>(PA)</sup>	Coal	1,0
CTP-A <sup>(PA)</sup>	Coal tar pitch	0,2
PAN-1:1-A <sup>(PA)</sup>	Coal tar pitch and PAN	8,0
PAN-3:1-A <sup>(PA)</sup>	Coal tar pitch and PAN	5,1
PAN-A <sup>(PA)</sup>	PAN	9,1

## ***Chapter 4: Results and Discussions***

---

GF-40 <sup>(CA)</sup>	Olive stone	17,0
Picabiol <sup>(CA)</sup>	Wood	9,6
BC-120 <sup>(CA)</sup>	Wood	18,0

**Table 4 - :** Mass loss (%) at PIO for the activated carbon samples

### ***13.1.1.4 OXIDATION KINETICS***

The kinetic model characterizing the oxidation process between the PIO and the SIT were estimated from 0 order reaction assumption. Data representing the heat flux per unit mass of the carbon sample, were related to the kinetic constant according to the Arrhenius equation [Jones, 1998].

$$\frac{\phi}{m} = A e^{-\frac{E_a}{RT}} \quad (4.11)$$

$\frac{\phi}{m}$

Where  $m$  : Heat flux/unit mass of the carbon sample ( $\text{mW} \cdot \text{mg}^{-1}$ )

$E_a$ : Activation energy expressed in ( $\text{kJ} \cdot \text{mole}^{-1}$ )

$A$ : Pre-exponential factor ( $\text{mW} \cdot \text{mg}^{-1}$ )

$T$ : Temperature of the sample (K)

$$\ln\left(\frac{\phi}{m}\right) = \ln(A) - \frac{E_a}{RT} \quad (4.12)$$

Equation (4.11) was transformed into logarithmic form in order to determine the parameters of the straight line function of the inverse of the temperature, giving the values of the activation energy  $E_a$  as shown in Figure 4-22.

## ***Chapter 4: Results and Discussions***

---

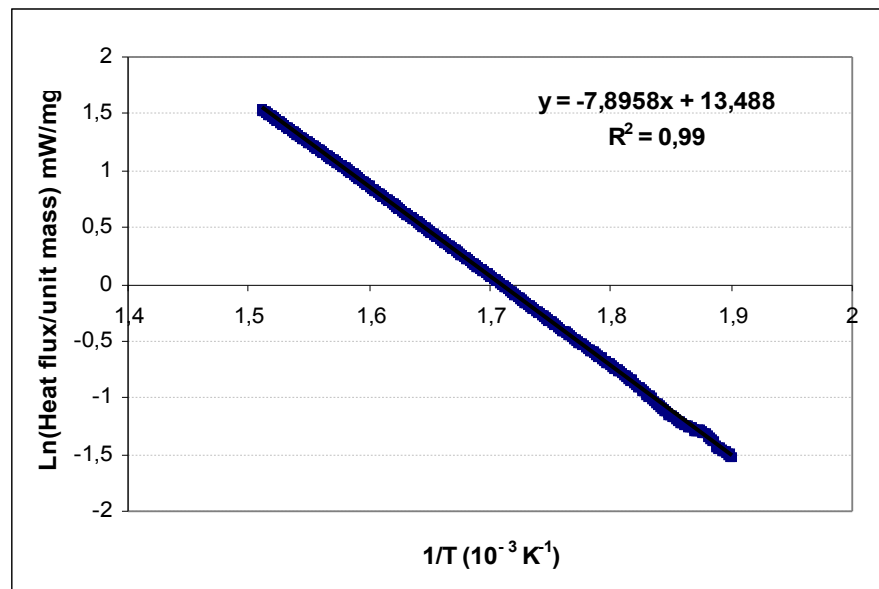


**Figure 4 - :** Arrhenius plot of the activated carbon sample NC-60

Deviation of the experimental data from the straight line trend indicates the degree of inaccuracy of the assumption of the zero order reaction. A good regression correlation of about 0.99 is obtained for all the samples tested indicating the accuracy of the 0 order reaction model. Moreover if the heat flux curve is recalculated from the kinetic model, a very good agreement is obtained coinciding with the experimental data as shown in Figure 4-23.

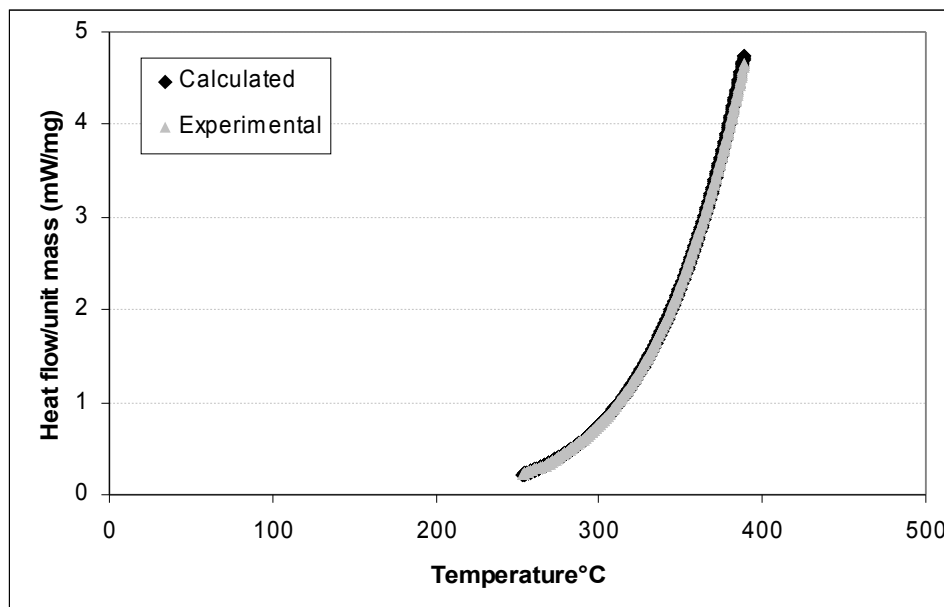


**Figure 4 - :** Comparison of experimental and calculated heat flux curves validating oxidation kinetic model.

## ***Chapter 4: Results and Discussions***

---

The kinetic parameters associated to the temperature domain of validity of the 0 order model can be found in Table 4-10. It can be noticed that both the activation energy and the pre-exponential factor of the chemically activated carbons are much lower than that of physically activated carbons. The lowest value of the activation energy is thus found for the PICABIOL sample with 33 kJ/mole, whilst the highest values is found for the Coal Tar Pitch carbonized sample, with 222 kJ/mole.

Lower activation energy values indicate start of the oxidation reaction at lower temperatures. Low activation energy values indicate faster acceleration of the reaction rate with the temperature increase. Results reported in Table 4-9 are thus coherent with the previous observations obtained from the DSC curve analysis and PIO evaluations.

<b>Sample</b>	<b>Activation energy (<math>E_a</math>) (kJ/mole)</b>	<b>Ln (A)</b>	<b>Temperature range °C</b>
NC-50 <sup>(PA)</sup>	71	14.6	227-400
NC-60 <sup>(PA)</sup>	65	13.4	188-400
NC-100 <sup>(PA)</sup>	75	13.6	271-480
BPL <sup>(PA)</sup>	104	17.2	408-520
RB-2 <sup>(PA)</sup>	85	14.6	322-516
CTP-A <sup>(PA)</sup>	136	21.8	397-517
CTP-PAN-3:1-A <sup>(PA)</sup>	118	19.3	358-520
CTP-PAN-1:1-A <sup>(PA)</sup>	79	13.4	332-485
PAN-A <sup>(PA)</sup>	74	12.8	281-475

## ***Chapter 4: Results and Discussions***

---

GF-40 <sup>(CA)</sup>	49	9.7	170-400
BC-120 <sup>(CA)</sup>	46	8.7	208-400
Picabiol <sup>(CA)</sup>	33	6.6	160-380
PAN-C <sup>(C)</sup>	124	18.7	354-500
CTP-PAN-3:1-C <sup>(C)</sup>	202	31.5	421-550
CTP-C <sup>(C)</sup>	222	34.1	424-575
CTP-PAN-1:1-C <sup>(C)</sup>	141	22.5	426-575
Carbonised coconut shell	45	10.2	219-400
NC-70-Cu <sup>(PA)</sup>	39	9.2	175-290
NC-70-CuCr <sup>(PA)</sup>	32	8.6	154-285

**Table 4 - :** Kinetic parameters for the oxidation carbon samples from DSC curve

### **13.1.2 IGNITION STUDIES**

The ignition of the activated carbon samples was studied from TG and DSC curves.

#### ***13.1.2.1 SPONTANEOUS IGNITION TEMPERATURE (SIT)***

The spontaneous ignition temperature SIT was determined as discussed in Section 3.2.3 and 3.2.4. The SIT values derived from the DSC curves are presented in Table 4 -11. An example of the application of the tangential method to the heat flux curve is shown in Figure 4-24.

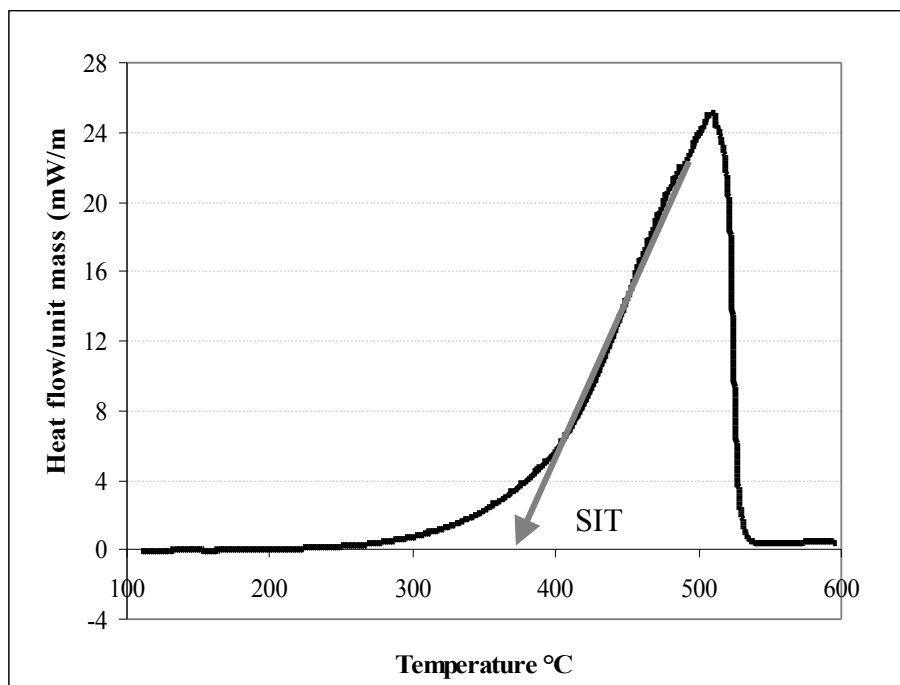


**Figure 4 - :** DSC thermogram for a physically activated carbon sample, showing the determination of SIT.

The SIT values of the activated carbons range from 300°C to 600°C. From the data reported, it is found that the physically activated carbons like BPL, RB-2, coal tar pitch and the PAN samples have a higher SIT than the chemically and the coconut shell activated carbons. These results are consistent with the previous trends observed for the PIO variations.

Sample	Activation mode	Precursor	SIT °C
NC-50	Physical	Coconut shell	380
NC-60	Physical	Coconut shell	388
NC-100	Physical	Coconut shell	475
BPL	Physical	Peat	516
RB-2	Physical	Coal	515

## ***Chapter 4: Results and Discussions***

---

CTP-A	Physical	Coal tar pitch	544
CTP-PAN-3:1-A	Physical	Coal tar pitch and PAN	520
CTP-PAN-1:1-A	Physical	Coal tar pitch and PAN	498
PAN-A	Physical	Polyacrylonitrile	457
GF-40	Chemical	Olive stone	347
BC-120	Chemical	Wood	377
Picabiol	Chemical	Wood	367
PAN-C	Non-activated	Polyacrylonitrile	501
CTP-PAN-3:1-C	Non-activated	Coal tar pitch and PAN	546
CTP-C	Non-activated	Coal tar pitch	558
CTP-PAN-1:1-C	Non-activated	Coal tar pitch and PAN	540
Carbonised coconut shell	Non-activated	Coconut shell	370
NC-70- Cu	Physical	Coconut shell	325
NC-70 -CuCr	Physical	Coconut shell	316

**Table 4 - :** SIT of the activated carbon samples obtained from the DSC curves

### ***13.1.2.2 COMBUSTION KINETICS***

The mass losses of the carbon samples observed at high temperatures are representative of the ignition process. Hence the burning behaviour of the carbon materials was characterized from the TG data. The integral method of the mass loss with respect to temperature is used in order to determine the combustion kinetics. The main region of the sample weight loss, arising from the conversion of the organic matter to gas, occurs above 300°C. It is assumed by different authors that the decomposition of the solid carbon matrix is initiated at the defective regions within the porous structure of the material [Zaghib *et al.*, 2001; Jiang *et al.*, 2000]. Kinetic information is important to better understand the decomposition mechanisms. Assuming that the kinetics of the combustion process follows a first order rate [Kizgut and Yilmaz, 2003], the rate of decomposition can be expressed as follows:

## Chapter 4: Results and Discussions

$$\frac{dw}{dt} = A \exp\left(-\frac{E_a}{RT}\right) w \quad (4.13)$$

$dw/dt$ : Heat flux/unit mass of the carbon sample ( $\text{mW} \cdot \text{°C}^{-1}$ )

$E_a$ : Activation energy expressed in ( $\text{kJ} \cdot \text{mole}^{-1}$ )

A: Frequency factor ( $\text{mW} \cdot \text{°C}^{-1}$ )

T: Temperature of the sample (K)

Plot of the natural logarithmic function of the ratio of the weight loss with temperature ( $dw/dt$ ) versus  $1/T$  should give a straight line equivalent to  $(-E_a/R)$  as shown in Figure 4-25. The linear regression coefficient  $R^2$  indicates the degree of inaccuracy of the first order reaction assumption. For the whole of the AC samples, such an assumption appears reasonable as the  $R^2$  was in all cases above 0.99.

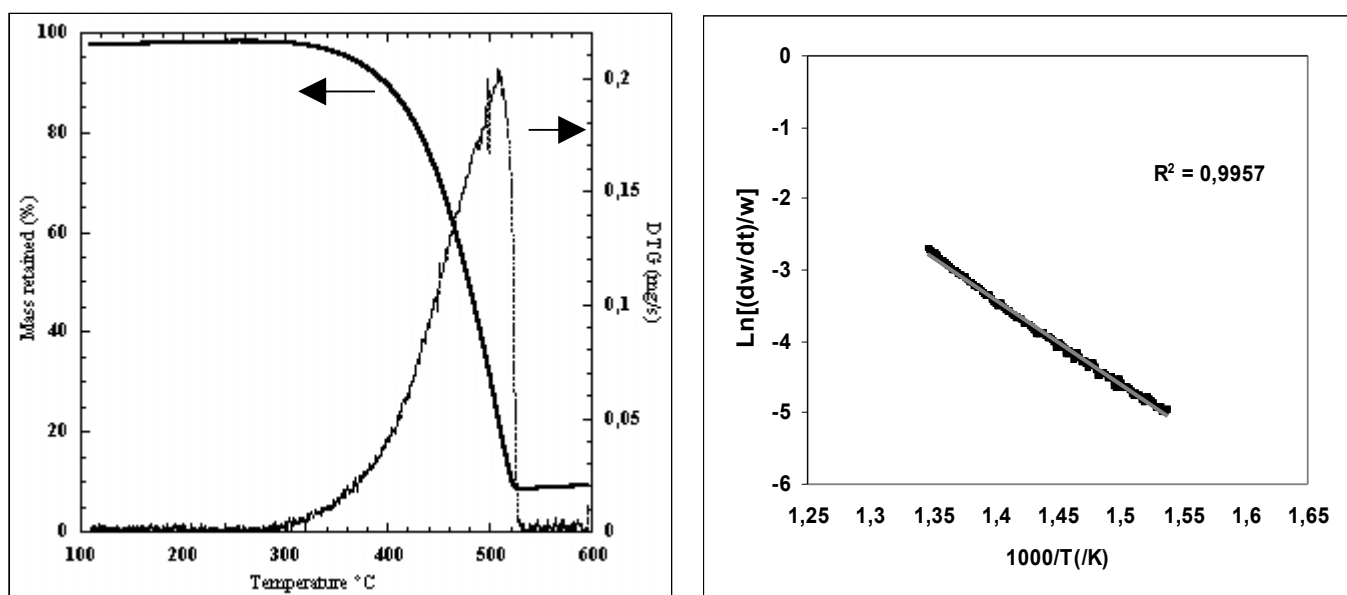
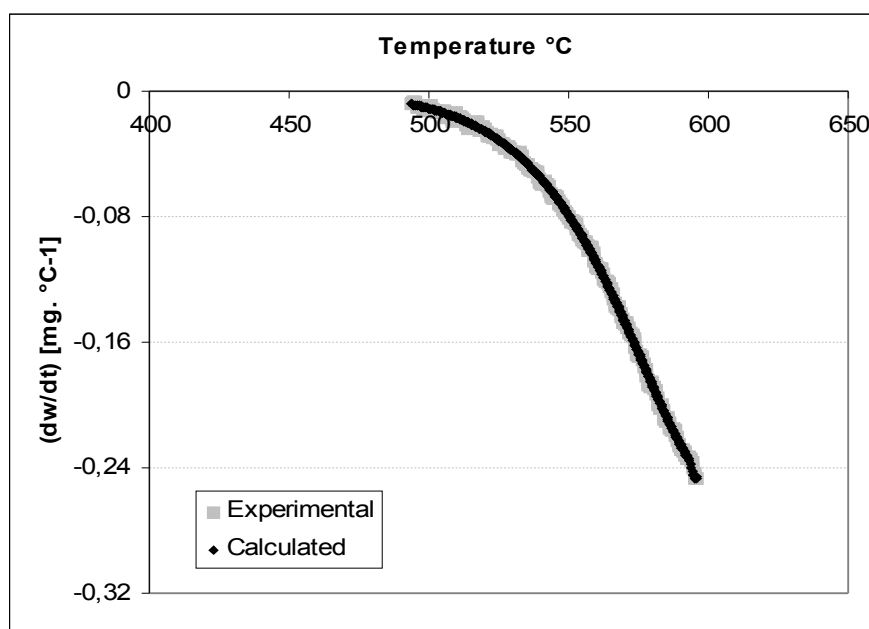


**Figure 4 - :** Decomposition curves and Arrhenius plots of activated carbon samples.



## ***Chapter 4: Results and Discussions***

---

**Figure 4 - :** Comparison of experimental and calculated heat flux curves validating combustion kinetic model.

Calculation of the mass loss curve ( $dw/dt$ ) from the first order kinetic model shows a very good match with the experimental data (Figure 4-26). The activation energy of the carbon matrix combustion reactions was found to vary between 70 kJ.mole<sup>-1</sup> for the metal impregnated samples to 300 kJ.mole<sup>-1</sup> for the coal tar pitch activated carbon sample.

<b>Sample</b>	<b>Activation energy (E<sub>a</sub>) (kJ/mole)</b>	<b>Ln (A)</b>	<b>Temperature range °C</b>
NC-50	106	14.7	390-490
NC-60	106	14.4	390-495
NC-100	132	17.1	400-550
BPL	219	28.3	490-595
RB-2	205	27.1	490-570

## ***Chapter 4: Results and Discussions***

---

CTP-A	299	21,8	495-595
CTP-PAN-3:1-A	233	19,3	480-595
CTP-PAN-1:1-A	204	13,4	450-580
PAN-A	138	12,8	460-590
GF-40	103	9,9	360-500
BC-120	104	8,7	430-520
Picabiol	104	6,6	422-497
PAN-C	164	18,8	354-500
CTP-PAN-3:1-C	237	31,5	421-550
CTP-C	302	34,1	424-575
CTP-PAN-1:1-C	216	22,5	426-575
Carbonised coconut shell	89	10,2	219-400
NC-70-Cu	70	5.8	200- 375
NC-70-CuCr	62	4.3	195-365

**Table 4 - :** Kinetic parameters of the combustion process from TG curves.

### **13.1.3 CONCLUSIONS**

The oxidation reactivity and ignition process of the activated carbon samples were studied. Significant variations were observed with respect to the mode of activation and the origin of the activated carbon material. The chemically activated carbon samples show a higher reactivity in air with lower values of PIO and SIT. They are accompanied by early oxidation and greater mass loss. The magnitude of heat flux remains small for this type of samples within the ignition region. The physically activated carbons showed varying oxidation and ignition properties: the coconut shell activated carbons (NC-50 and NC-60) are the most sensitive to oxygen reactions, whereas the physically activated peat, coal based and the coal tar pitch samples have a greater stability towards oxidation.

These trends were complemented with the quantitative assessment of the kinetic parameters using the TG and DSC curves. The activation energy data area consistent with the

## ***Chapter 4: Results and Discussions***

comparisons made between the different types of material tested from the PIO and SIT results.

### **14 INFLUENCE OF THE ACTIVATED CARBON PROPERTIES ON THEIR REACTIVITY**

The influence of the material properties on the oxidation reactivity and ignition is qualitatively analysed in this section.

#### **14.1.1 INFLUENCE OF THE SURFACE OXYGENATED GROUPS**

Effects of the elementary composition namely oxygen and hydrogen, nitrogen on the point of initial oxidation and spontaneous ignition temperature are qualitatively analysed.

##### ***14.1.1.1 OXYGEN AND HYDROGEN CONTENT***

The influence of oxygen to carbon ratio contained in the material on the reactivity can be studied from Figure 4-27, which plots of (O/C) versus PIO and SIT. The trends for 12 activated

carbon samples are analysed, with the exemption of the metal impregnated samples and the carbonized non-activated samples. It is found that when the O/C ratio increases, both PIO and SIT decreases. The chemically activated carbons, namely BC-120, GF-40 and Picabiol have consequently far lower PIO and SIT values compared to the physically activated carbons.

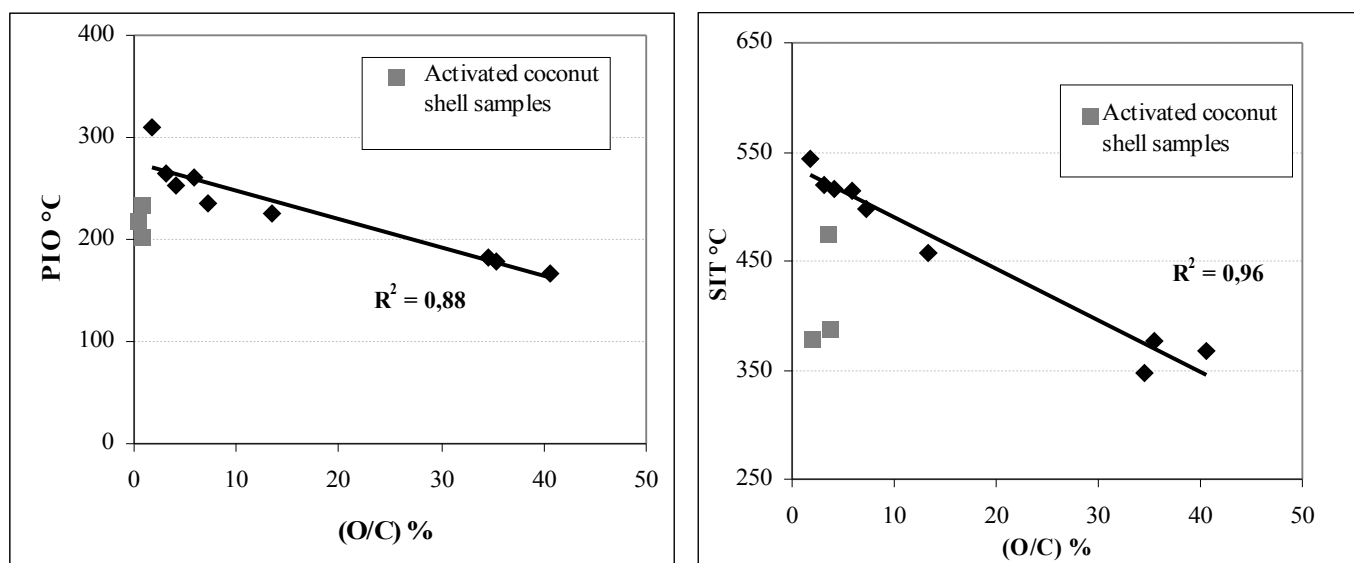


**Figure 4 - :** Influence of oxygen to carbon ratio on PIO and SIT.

## ***Chapter 4: Results and Discussions***

---

Such a relationship is being attributed to the involvement of the oxygenated surface functional groups in the oxidation reactions under air. The oxygen atoms in activated carbons are actually present in the form of surface oxygenated groups, like carboxyl, hydroxyl, carbonyl and ether groups. Some of the oxygen content may come from the material itself or from its activation mode. When activated carbons are exposed to air and heated, the surface oxygenated groups react with air to form desorbable products like CO<sub>2</sub>, CO, H<sub>2</sub>O and intermediate complexes accompanied by exothermic heat [Hardman *et al.*, 1983]. Furthermore, the oxygenated groups are bonded to the edge sites which have a greater reactivity than the basal plane of the graphene layers and hence react rapidly on exposure to air.

The above trend can be well illustrated using the CTP and PAN samples. It can be seen in Figure 4-28, that an increase in the O/C ratio in the carbon samples increases their reactivity in air with a decrease in the PIO and SIT values. For example the coal tar pitch activated sample CTP-A having an O/C ratio of about 1.72 % has a PIO and SIT value of about 309 °C and 544 °C respectively. These values are reduced to 225 °C and 457 °C for the activated PAN sample (PAN-A) having an O/C ratio of 13.4 %. There is a decrease of about 100 °C in the values of PIO and SIT as we move from CTP-A to PAN-A.

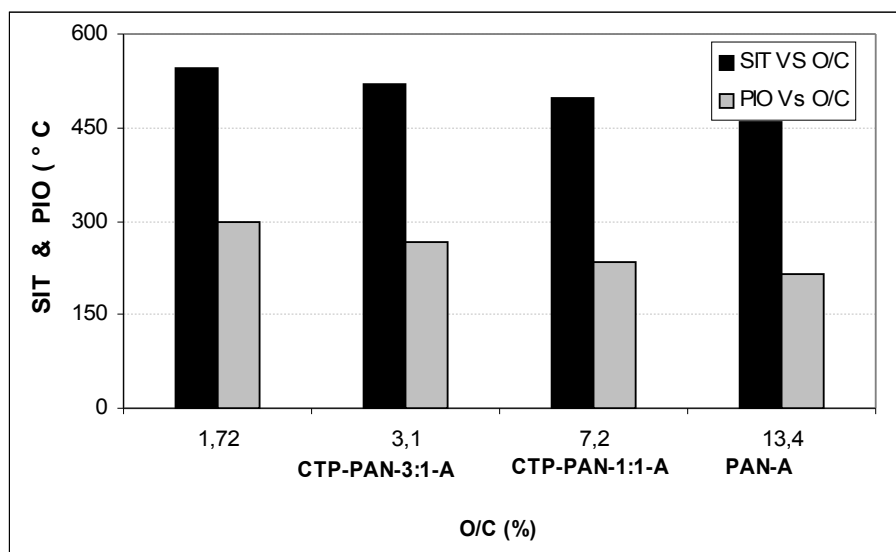


**Figure 4 - :** Influence of O/C ratio on the PIO and SIT for the coal tar pitch and PAN samples.

However, considering at Figure 4-27, there are exceptions to these trends with the activated coconut shell samples, whose PIO and SIT values are lower than expected. Such deviations which may be due to higher affinity for the chemisorption of oxygen, or the presence of a

## ***Chapter 4: Results and Discussions***

---

higher potassium content which enhances the reactivity of the material [Bandosz and van der Merwe, 2005]. Letting apart the three activated coconut shell samples, regression coefficient of 0.96 and 0.88 were obtained between PIO, SIT and O/C ratio

In order to verify that a decrease in the oxygen content of the carbon matrix makes the activated carbons more stable and less reactive, a Temperature Programmed Desorption (TPD) was carried out. The activated carbon samples were heated under an inert atmosphere (helium) until about 750 °C. The oxygen content of the samples was then priorly determined by elemental analysis taking care that the samples were not exposed to air, and a Temperature Programmed Oxidation (TPO) in an atmosphere of oxygen was applied.

After heat treatment under inert atmosphere, a decrease in the oxygen content of the activated carbon samples due to the liberation of the oxygen adsorbed on the surface and contained in the surface oxygenated groups was observed. There was approximately 10-15 % reduction in the oxygen to carbon ratio in the chemically activated carbons and about 2-5 % in the physically activated carbons as shown in Figure 4-29.

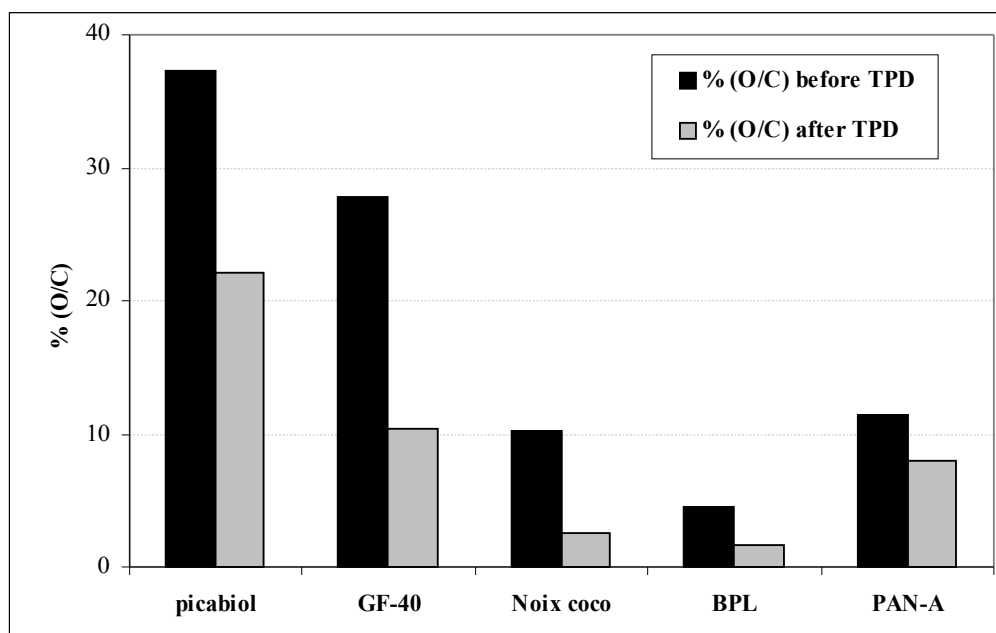


**Figure 4 - :** Comparison of O/C ratio of some of the activated carbon samples before and after TPD.

A comparison of the PIO and SIT before and after TPD shows a considerable increase in the PIO and SIT values after TPD (Appendix-J). The increase was much higher for PIO than SIT. There was an increase of about 50-100 °C in the PIO values as shown in Figure 4-30.

## ***Chapter 4: Results and Discussions***

---

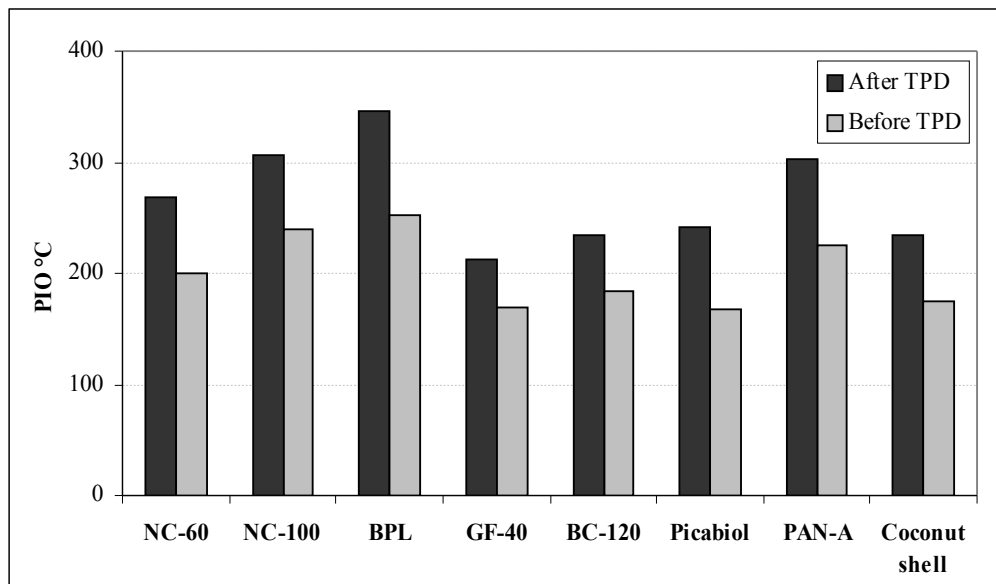


**Figure 4 - :** Comparison of PIO of the activated carbon samples before and after TPD.

This tendency was not only observed for the chemically activated carbons but also for the physically activated carbons indicating that the oxygen present in small quantities in physically activated carbons play a role in the initial stage of the oxidation process.

The TPD brought about very small changes in the SIT values of the samples like BPL and NC-100 as compared to the chemically activated carbons. It is likely that for these materials, because of their initial very low oxygen content, the combustion process is not dictated by oxygenated surface group's concentration.

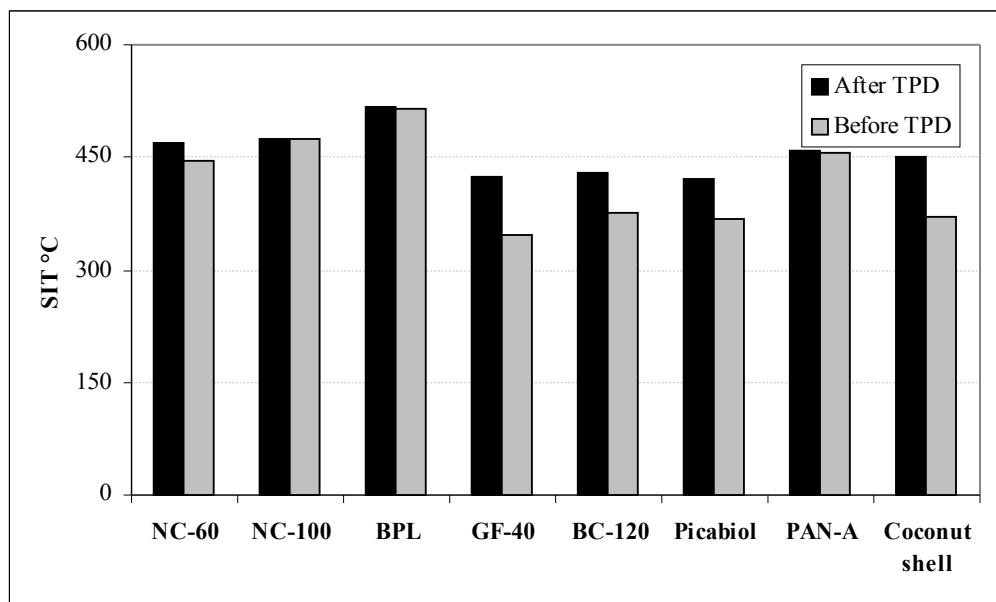


**Figure 4 - :** Comparison of SIT of the activated carbon samples before and after TPD.

### **14.1.1.2 NITROGEN CONTENT**

The nitrogen rich activated carbons are generally found to be more resistant and stable towards oxidation and ignition. The high temperature treatment involved in the activated carbon preparation makes thermally stable nitrogen substituted for carbon in the ring system. In nitrogen rich samples, the influence of nitrogen alone could not be well established as an increase in the N/C ratio increases the O/C ratio. For samples like PAN-A, the effect is being masked by the presence of oxygen. The comparison of the PIO and SIT data between nitrogen rich and nitrogen poor samples is shown in Figure 4-32 and 4-33.

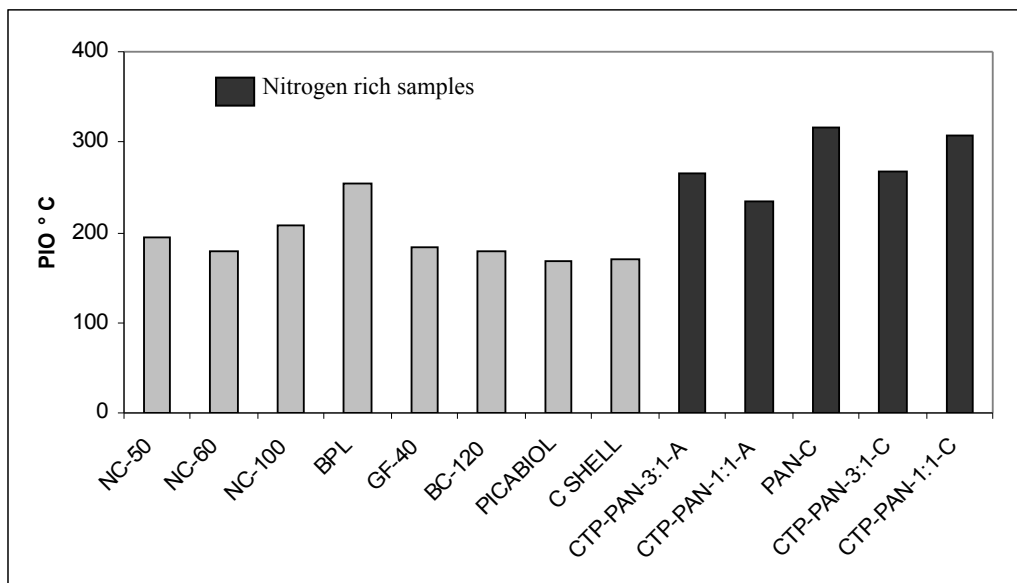


**Figure 4 - :** Comparison of PIO between activated carbon samples rich in nitrogen content with the samples having scarce nitrogen content

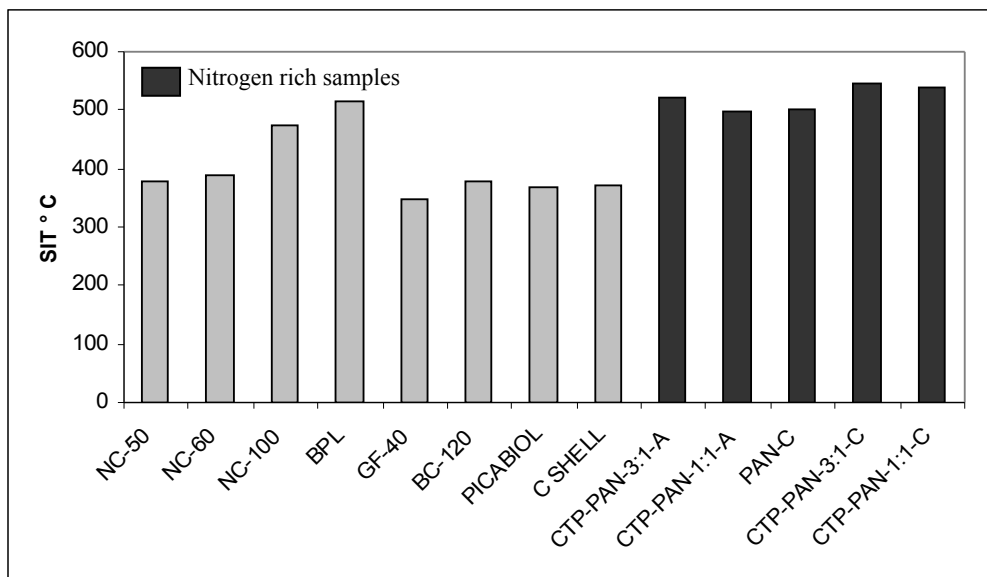


**Figure 4 - :** Comparison of SIT between activated carbon samples rich in nitrogen content with the samples having scarce nitrogen content

#### 14.1.2 EFFECT OF MINERAL MATTER

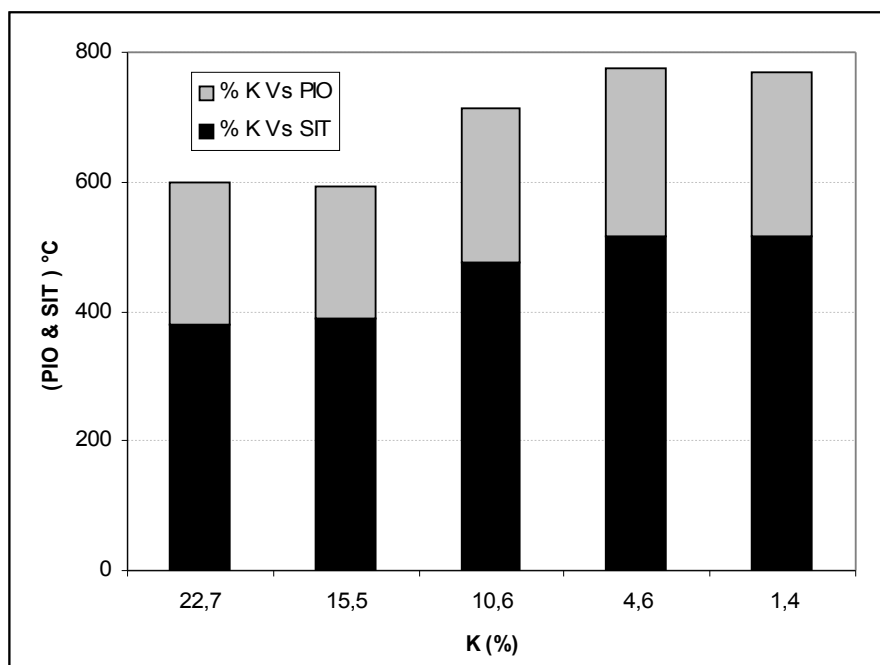


**Figure 4 - :** Influence of potassium content on the PIO and SIT

## ***Chapter 4: Results and Discussions***

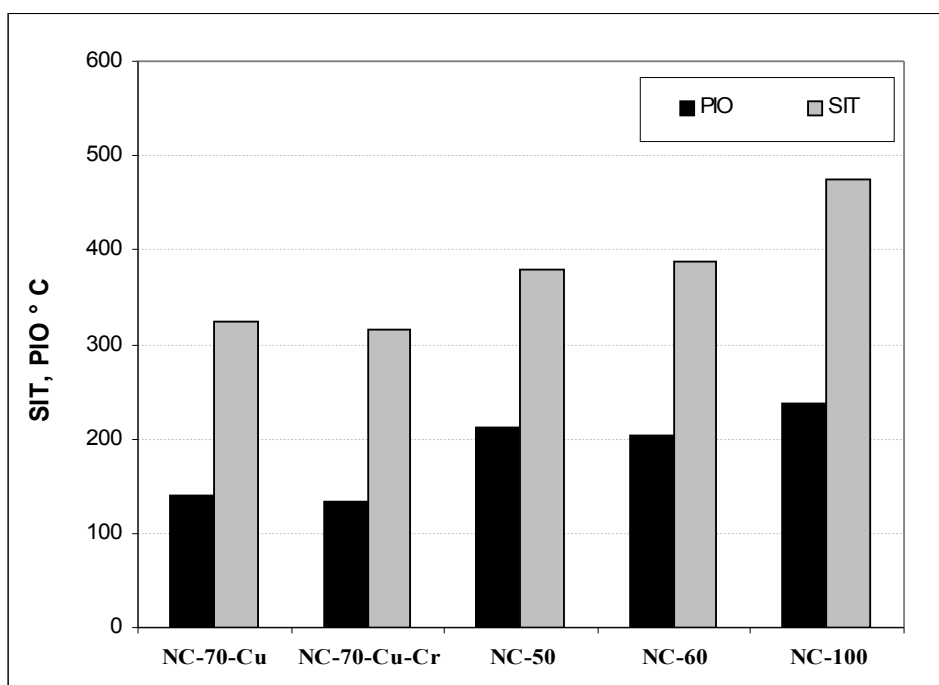
---

The influence of K content on the PIO and SIT is shown in Figure 4-34. An increase in the K content decreases the PIO and SIT of the activated carbons. The higher potassium content is mainly found in the coconut shell activated carbons which explains also the deviation observed in Figure 4-27. The experimental work of Bandosz and Van der Merwe, [2005] showed that the coconut shell activated carbons are susceptible to ignition reactions when compared to the peat based activated carbons. Mineral matters like potassium provide direct catalytic activity to the surface which depends on the amount present, chemical form and the degree of dispersion [Lu, 2002; Bandosz and Van der Merwe, 2005]. The high presence of potassium in the carbon samples is due to the activation and neutralization process encountered during their manufacture [Amarasekara *et al.*, 1998].

### **14.1.3 INFLUENCE OF IMPREGNATION**

The influence of the impregnation of metals on the activated carbon samples can be studied by comparing PIO and SIT between the impregnated and non-impregnated samples. Activated carbons are impregnated with metals to capture high vapour pressure substances. The oxidation and ignition parameters are compared between the non-impregnated samples particularly NC-50, NC-60 and NC-100 with coconut shell as origin with that of NC-70 impregnated with copper and chromium having the same material as origin.

From the bar graph in Figure 4-35, it is found that the impregnated samples have higher reactivity in the presence of oxygen than the non impregnated ones. The main reasons for the early ignition of the impregnated active carbons is being attributed to the surface oxidation of the impregnates with high local temperature causing nearby carbons to oxidize in the presence of oxygen. [Suzin *et al.*, 1998]. The presence of metal impregnates may also have a catalytic



## ***Chapter 4: Results and Discussions***

---

effect on the oxidation reactions between oxygen and carbon, thereby decreasing the stability of the impregnated activated carbons [Zhang *et al.*, 2003 ; Suzin *et al.*, 1998].

**Figure 4 - :** Effect of impregnation of copper and chromium on PIO and SIT of the activated carbons.

### **14.1.4 EFFECT OF TEXTURAL AND STRUCTURAL PROPERTIES**

The influence of the textural properties like the  $S_{BET}$  and meso-macro porous volumes on the oxidation and ignition reactivity of the activated carbons is analysed quantitatively using the graphical analysis.

#### ***14.1.4.1 INFLUENCE OF TEXTURAL PROPERTIES***

The influence of the textural properties, i.e. the specific surface area ( $S_{BET}$ ), the porous volume ( $V_{porous}$ ), the width of the micropore ( $W_{micro}$ ) and volume of micropores ( $V_{micro}$ ) on the PIO and SIT was attempted to be pointed out by plotting the porosity parameters vs PIO and SIT. However, except the porous volume, no appreciable relationships were found between the different textural properties and the PIO and SIT data. In Figure 4-36, a tendency towards decrease of PIO and SIT with an increase in the macro-meso porous volume of the material can be noted. A low coefficient of determination is obtained with the maximum  $R^2$  equals to

## ***Chapter 4: Results and Discussions***

0.60. One can assume that the large porous volume facilitate the diffusion of the oxygen molecules in air to the carbon surface, enhancing by this way the oxidation reactions.

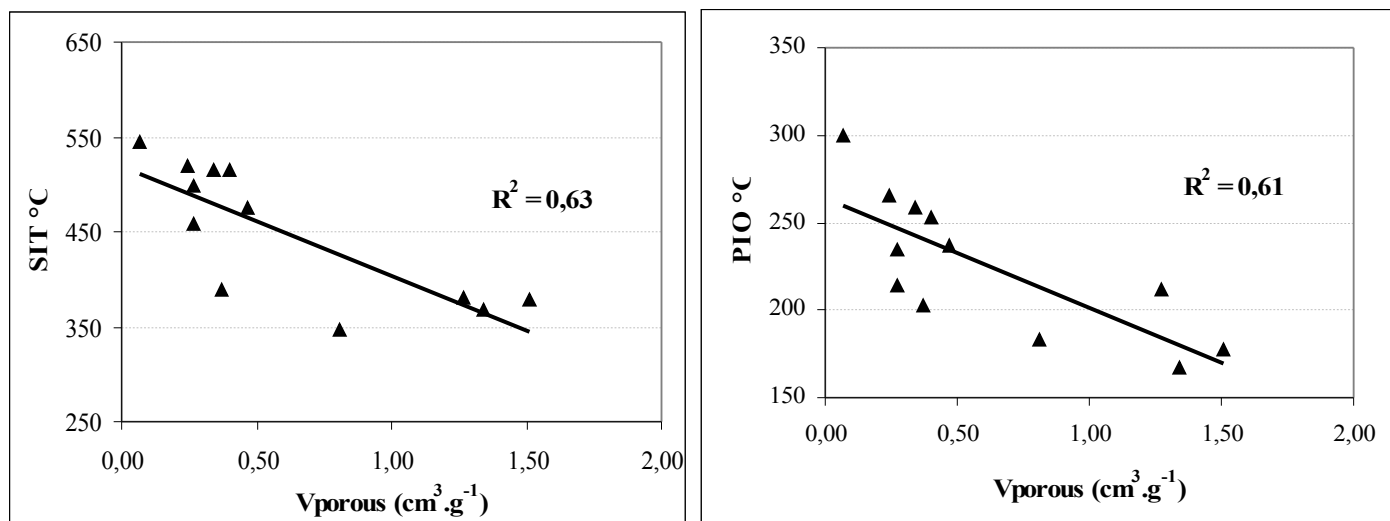


**Figure 4 - :** Textural properties of the carbon samples and their influence on activation energy signifying the oxidation reactions.

### ***14.1.4.2 INFLUENCE OF QUANTITATIVE STRUCTURAL PROPERTIES***

The influence of the quantitative structural data on the reactivity of the activated carbon was also analysed. The only well established tendency is the one relating graphitic layers having fringe length greater than 1 ring Å and the activation energy of the initial stage of the oxidation reaction. A linear regression coefficient of about 0.80 was obtained for  $L > 1$  ring and  $E_a$ . In Figure 4-37, it is demonstrated that the graphitic layer length, the higher the activation energy, thus the greater stability towards oxidation in air. The samples having shorter graphitic layer length were more reactive towards oxidation reactions. This result is attributed to the presence of short distorted layers containing surface oxygenated groups at their boundaries which may be responsible for the early oxidation of the activated carbons.

Other trends observed from the quantitative data like the % of non-stacked layers, N the number of stacked layers in a domain and length of the graphitic layers  $L > 2$  and 3 rings on the reactivity PIO yielded low coefficients.

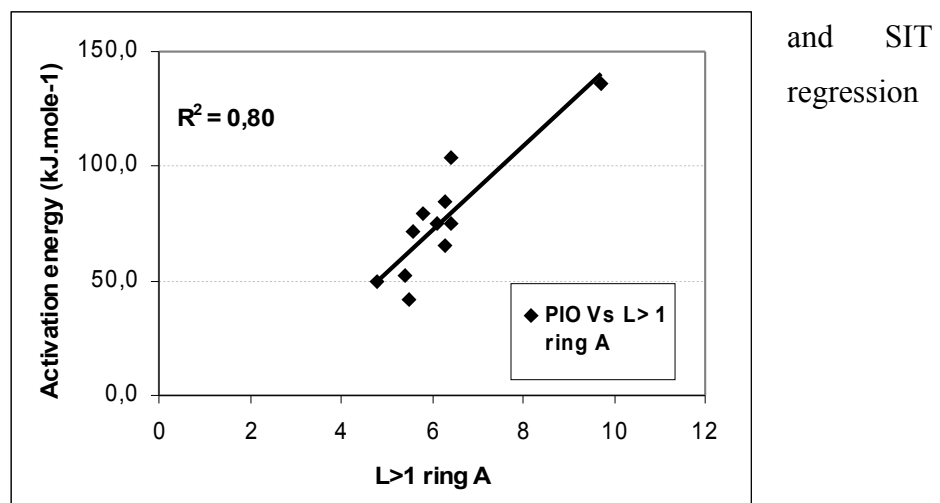


**Figure 4 - :** Influence of the graphitic layer length on the activation energy of the oxidation reactions.

### **15 INFLUENCE OF THE OPERATING CONDITIONS**

Operating conditions, such as oxygen content in the ambient environment air flow rates, heating rate and adsorbed VOC may have a direct influence on the reactivity and reaction rates of activated carbon. These effects are analyzed in detail in the following part.

#### **15.1.1 INFLUENCE OF OXYGEN CONCENTRATION IN THE AMBIENT GAS**

The main objective of varying the concentration of oxygen in the ambient gas was to study the contribution of diffusion phenomena oxidation and ignition mechanisms. The oxidation tests were performed using different oxygen concentration levels namely: 10 %, 21 %, 40 %, 70 % and 100 %. Four different activated carbon samples were used: the physically activated carbons (NC-60 and PAN-A), the carbonized non-activated coconut shell and the chemically activated carbon sample (GF-40). The influence of the oxygen concentration in the ambient environment on the PIO and on the SIT was analysed. The changes in PIO and SIT values with respect to oxygen concentration are shown in Figure 4 -38 and 4-39. PIO and SIT data for the activated carbons tested at different concentrations are given in Appendix-K. The corresponding TG and DSC curves are shown in Appendix-L and M.

At 100 % oxygen concentration, the NC-60 and carbonized coconut shell samples show abnormal increase in the heat flux, exceeding the security threshold of the apparatus, and an automatic shutdown was observed. This phenomenon is associated to the very high reactivity and thermal runaway reactions. Hence the PIO and SIT values for these samples at 100 % oxygen concentration could not be measured

### ***15.1.1.1 EFFECT ON PIO***

For all the samples studied, a change in the slope of the curve in the oxygen concentration range less than 21 % and greater than 21 % was observed (Figure 4-38). The reactivity of the material decreases strongly, at 10 % oxygen concentration level, when the environment is poor in oxygen. The reactivity of the carbon samples increases when the ambient oxygen concentration is increased. The oxygen in the ambient gas plays an important role on the initiation of oxidation reactions of the material. A decrease in the concentration of the oxygen slows down the reaction with the oxygenated groups. This may be related to the reduction in the concentration of free radicals formed from cohesions between oxygen molecules and surface oxygenated groups. Such reductions slow the propagation of the chain reactions in the gaseous phase. Another important observation is that at oxygen concentration levels greater than 21 %, no significant changes in PIO of the samples rich in surface oxygenated groups like the chemically activated GF-40 and the carbonized coconut shell samples. For these samples oxygen contained in the material in the form of surface oxygenated groups is no more a limiting reactant of the oxidation process.

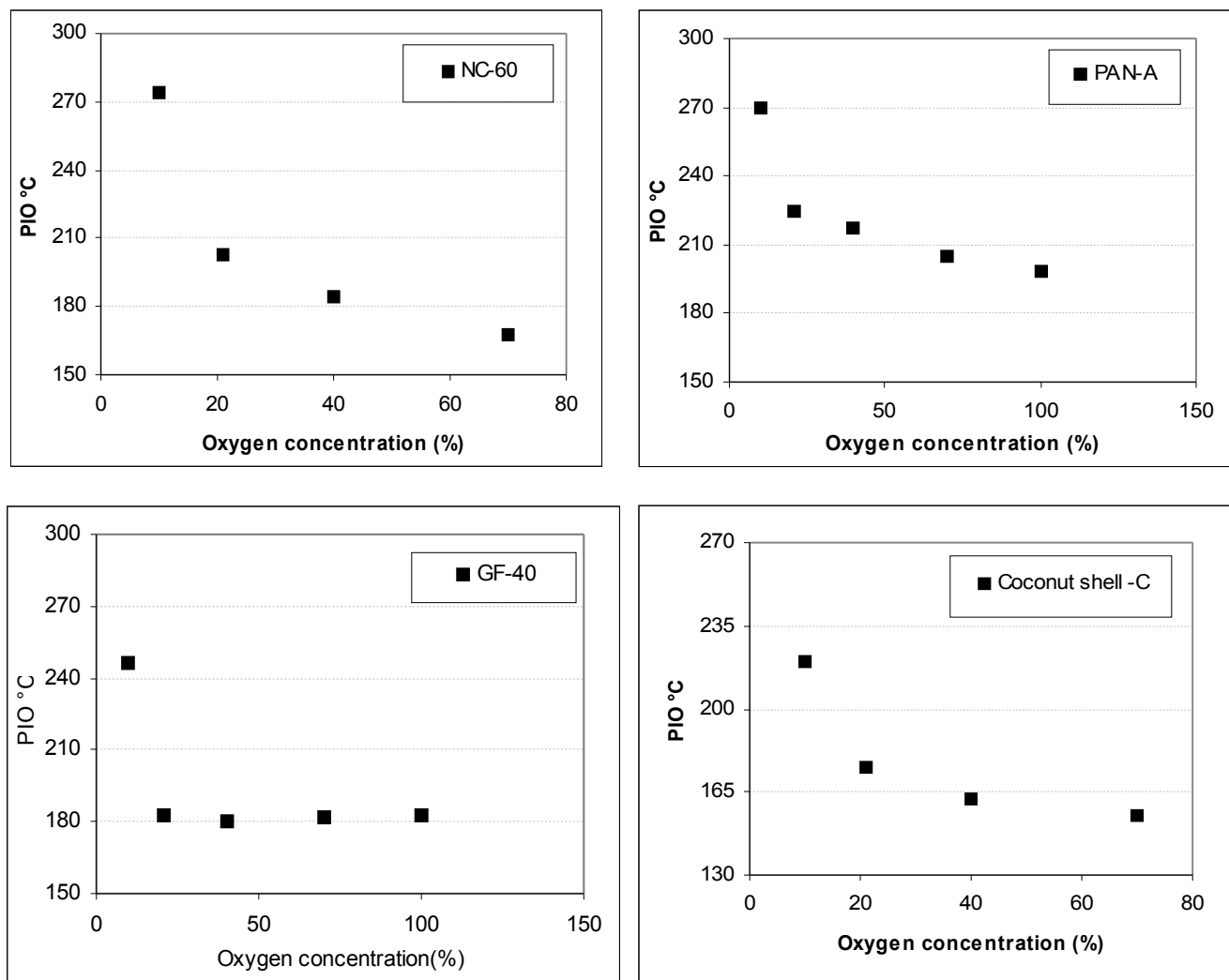


**Figure 4 - :** Influence of oxygen concentration on the PIO.

#### **15.1.1.2 EFFECT ON SIT**

On the entire oxygen concentration range studied, the increase in the concentration of oxygen has a notable effect except for the carbonized coconut shell sample [Figure 4-39]. The diffusion of oxygen in the pores of the material controls the then phenomenon of inflammation. The porous characteristics have an influence on the inflammation because they are responsible for the transportation of oxygen till the reactivity site.

By examining the DSC curves in Appendix-L, it is observed an increase in the magnitude of the heat flux as the concentration, when oxygen increases from 10 % to 100 %, indicating the increase in the rate of the oxidation and combustion reactions. However for the GF-40 chemically activated carbon, there is a lag between the heat flux curves and the magnitude remains the same.

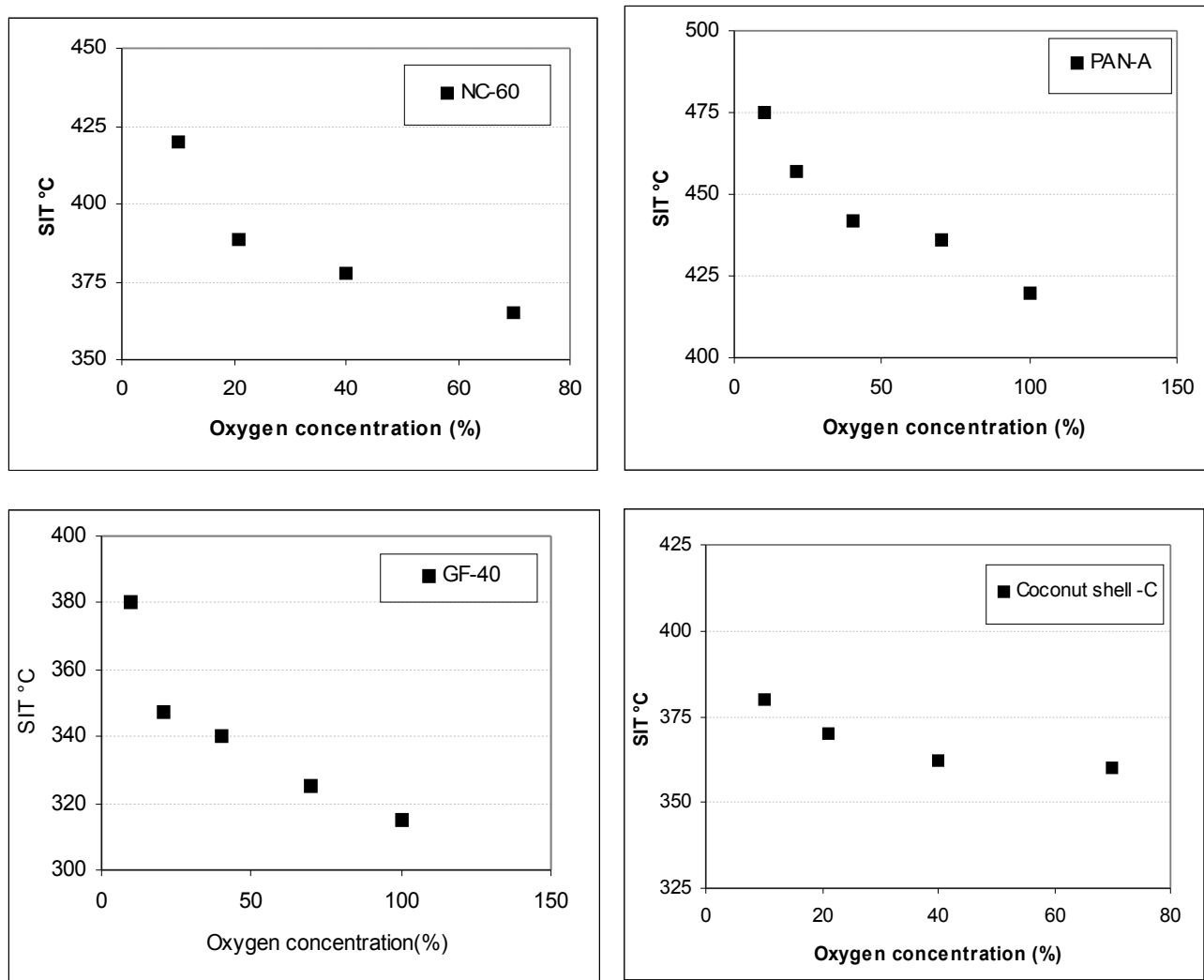


**Figure 4 - :** Influence of oxygen concentration on the SIT.

Furthermore, at concentrations of 10 and 21 %, the PIO of the GF-40 sample has lower SIT and PIO than the physically activated NC-60 sample. But when the concentration of oxygen increases, a reversing trend is observed, and the PIO of the NC-60 sample becomes lower than that of GF-40. This shows that the reactivity of the materials is specific to given oxygen concentration in the surrounding gas

#### 15.1.2 INFLUENCE OF FLOW RATE

The influence of the gas flow rate on the determination of PIO and SIT is studied in this section. Flow rates were maintained at  $1.2 \text{ L.hr}^{-1}$  and  $2.4 \text{ L.hr}^{-1}$ . PIO and SIT data are reported given in Appendix -N.

## ***Chapter 4: Results and Discussions***

---

Figure 4-40 shows the oxidation and ignition trends when flow rate of the carrier gas is increased. As the flow rate increases from  $1.2 \text{ L.hr}^{-1}$  to  $2.4 \text{ L.hr}^{-1}$  there is a decrease in the PIO and SIT values. The decrease is found to be more significant for the PIO than for the SIT. There is approximately about  $20^\circ\text{C}$  decrease in the PIO values as the flow rate is doubled. This is mainly due to the increase in the amount of oxygen available for the reaction. In the ignition region, an increase in the gas flow rate does not have a significant effect.

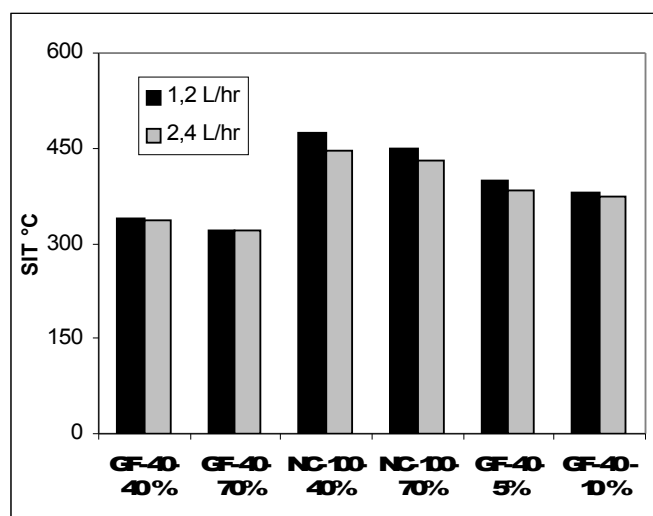
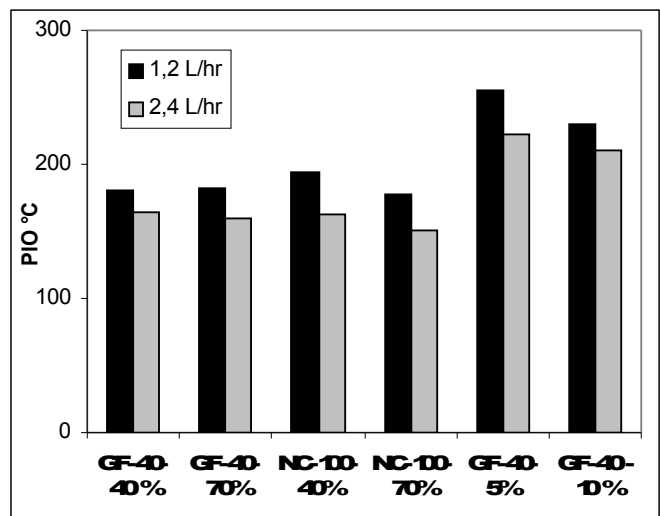


**Figure 4 - :** Comparison of PIO and SIT at 2 different flow rates.

## ***Chapter 4: Results and Discussions***

---

These results show that in practice, if an increase of the gas flow rate leads to acceleration of the oxidation reactions in the initial stages, the temperature at which bed ignition occurs is likely to not vary a lot. The increase in the self heating rate of the bed may also be compensated by heat dissipation resulting from convection. The results obtained are in conjunction with the work of Naujokas, [1985] and Delage [2000] showing that high gas velocities can cause a dissipation of the heat, thereby reducing the risk of oxidation and thermal runaway of the carbon beds.

### **15.1.3 INFLUENCE OF HEATING RATE**

The PIO and SIT measurements were performed at different heating rates: 2, 5 and 8 K/min. The concentration of oxygen in air was maintained at 21 %. The values of PIO and SIT of the activated carbon samples measured at different heating rates are given in Appendix-O.

Comparing the PIO obtained for a same material at different heating rates (Figure 4-41), a decrease in the PIO with the increase in the heating rate from 2 K. $\text{min}^{-1}$  to 8 K.  $\text{min}^{-1}$  is observed. The decrease in the PIO is in the range of 50 °C which means that the rate of initial oxidation stage is accelerated with the heating rate. As the temperature increases the rate of oxygen consumption increases leading to early oxidation of the activated carbons. In practice, oxidation reactions occur earlier and faster in confined or externally heated systems. However the heating rate has almost no influence on the temperature at which ignition is observed. Thus, the differences in the SIT data reported were not more than 10 °C.

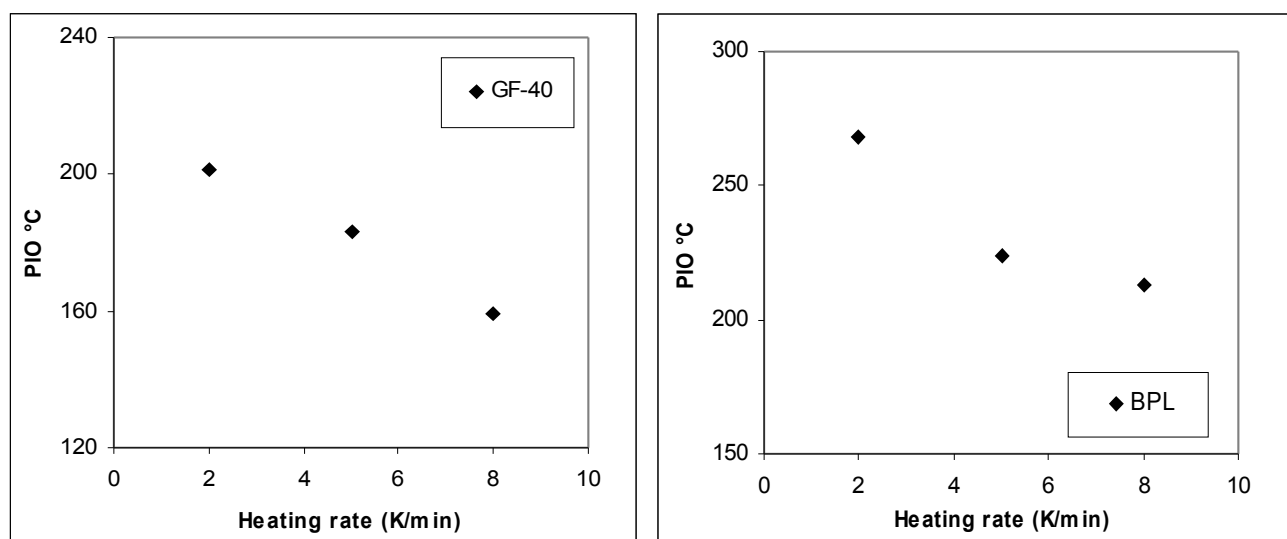


**Figure 4 - :** Influence of heating rate on the PIO of the activated carbon samples

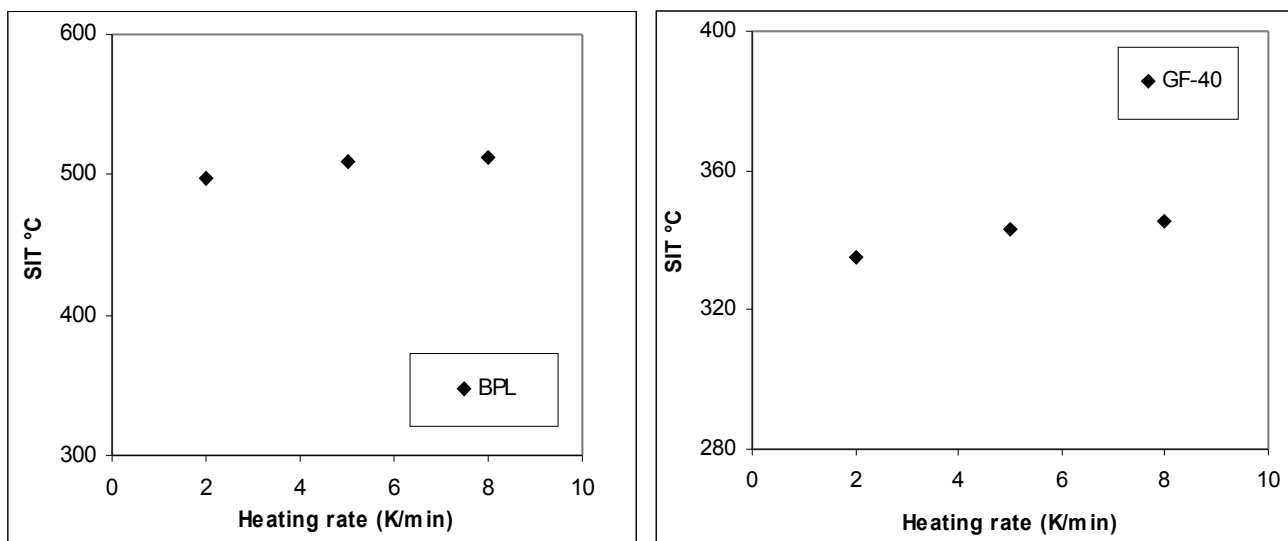


**Figure 4 - :** Influence of heating rate on the SIT of the activated carbon samples.

#### 15.1.4 INFLUENCE OF ADSORBED VOC's

From the literature sources [Naujokas, 1985 ; Delage, 2000] discussed in Chapter-1, it was found that the Volatile Organic Compounds (VOC's) may have a great influence on the reactivity of activated carbons.

Results of the experimental work carried out in the laboratory of Ecole des Mines de Nantes by Delage *et al.*, (2000) is utilized in this work. VOC saturation was achieved using the TG-DSC system, coupled to a system for solvent injection. The increase in the mass of the sample enable to follow the progressive saturation of the material with VOC. Once the saturation point is reached there is no further increase in the mass of the sample. The PIO and SIT were measured for saturated activated carbon samples.

##### 15.1.4.1 NATURE OF VOC's

The physically activated carbon NC-60 was used to analyze the influence of the nature of VOC's on the oxidation properties of activated carbons [Delage, 2000]. NC-60 is one of the most commonly used samples for the adsorption of the VOC's and the experimental work was done before the present study and hence the experimental results of the NC-60 alone is taken up here. Fifteen different types of VOC's were chosen for the study, to saturate NC-60 samples. Oxidation tests were performed in the presence of air. The PIO of the NC-60 samples saturated with the different VOC's and the self ignition temperatures of the corresponding solvent are reported in Table 4-13.

## ***Chapter 4: Results and Discussions***

---

<b>COV</b>	<b>Molecular formula</b>	<b>PIO °C</b>	<b>T<sub>i</sub> COV (°C)</b>
Methyl isobutyl acetone	C <sub>6</sub> H <sub>12</sub> O	107	448
Methyl ethyl acetone	C <sub>4</sub> H <sub>8</sub> O	118	404
Acetone	C <sub>3</sub> H <sub>6</sub> O	129	465
Tetrahydrofuran	C <sub>4</sub> H <sub>8</sub> O	136	321
Isobutyl vinyl ether	C <sub>6</sub> H <sub>12</sub> O	136	311
Ethyl acetate	CH <sub>3</sub> CH <sub>2</sub> OC(O)CH <sub>3</sub>	145	426
Isopropyl ether	(CH <sub>3</sub> ) <sub>2</sub> CHOCH(CH <sub>3</sub> ) <sub>2</sub>	156	238
Methylethyldioxalane	C <sub>9</sub> H <sub>18</sub> O <sub>2</sub>	158	387
Toluene	C <sub>7</sub> H <sub>8</sub>	> Tox (AC)	480
Cyclohexane	C <sub>6</sub> H <sub>12</sub>	> Tox (AC)	245
1,2 dichloro ethane	C <sub>2</sub> H <sub>4</sub> Cl <sub>2</sub>	> Tox (AC)	413
Ethanol	C <sub>2</sub> H <sub>6</sub> O	> Tox (AC)	363
Chloroform	CHCl <sub>3</sub>	> Tox (AC)	249
Triethylamine	C <sub>6</sub> H <sub>15</sub> N	> Tox (AC)	228
Hexane	C <sub>6</sub> H <sub>14</sub>	> Tox (AC)	228

## ***Chapter 4: Results and Discussions***

---

**Table 4 - :** Oxidation temperatures of NC-60 sample saturated with different types of VOC's.

**T<sub>ox</sub> (AC):** Denotes that oxidation of the sample takes place at a temperature above the PIO of the non saturated activated carbon (i.e. 204°C, PIO of the NC-60).

From Table 4-13, two scenarios are distinguished. The first scenario corresponds to the case where oxidation occurs at a temperature lower than that of the material not containing the VOC. Such a scenario was found for the VOC's ranging from methyl isobutyl acetone to methyl ethyl dioxalane in Table 4-13. These VOC's contain oxygen groups which may be easily brought about the oxidation reactions. Literature sources also show that aromatic ketones are easily oxidised than aliphatic ones [Akubuiro and Wagner, 1993]. These ketonic groups form hydroperoxides further decomposing into carboxylic acids, aldehydes and diketones facilitating the oxidation reactions.

The second scenario corresponds to the case where sample oxidation takes place at a temperature equal to or above the PIO measured for the sample without organic adsorbate. Organic compounds like hydrocarbons, amines, halogens and alcohols belong to these category.

The oxidation behaviour of two other activated carbon samples saturated with a ketone group of VOC is reported in Table 4-14. Before VOC adsorption, PIO of RB-2 and BPL are found to be close to each other. However, PIO measured for the saturated material show great differences. It is seen that the two samples RB-2 and BPL have different oxidation temperatures for the same VOC. For example the BPL sample show a very low oxidation temperature for the organic compound methyl ethyl acetone compared to RB-2. BPL, which can be considered as more stable in the presence of air is found to be the least stable sample in the presence of methyl ethyl acetone. Such results due to the differences in the nature of chemical functional groups and in the ash content of the BPL samples, which may play a catalytic role.

VOC	Sample	PIO (°C)	PIO (°C) without VOC's
<i>Acetone</i>	RB-2	153	260
	BPL	125	253.2

## ***Chapter 4: Results and Discussions***

---

<i>Methyl ethyl acetone</i>	RB-2	137	260
	BPL	76	253.2

**Table 4 - :** Oxidation temperatures of RB-2 and BPL sample saturated with ketones.

## **16 STATISTICAL ANALYSIS**

In this section, we attempt to establish quantitative relationships between the influent surface properties of the activated carbons and their oxidation and ignition parameters. For that purpose a statistical analysis was carried out based on the use of MLR.

### **16.1.1 MULTIPLE LINEAR REGRESSION (MLR)**

Multiple regression analysis is one of the most widely statistical tools used. They were successfully used to establish quantitative relationships between the adsorption energies or capacities and some internal properties of activated carbons[Giraudet *et al.*, 2007]. It attempts to relate linearly two or more explicative variables, also called *predictors* with the observed response data called *predictand*. MLR enables to analyse simultaneously the dependencies of the response studied with all the influent variables. It helps to identify the hidden links and to discard apparent but in existing links.

Multiple Linear Regressions are assessed from least squares analysis. The model established is fit in such a way that the sum-of-squares of the differences between observed and predicted response variables is minimized. In the process of fitting or estimating the model, statistics are computed that summarize the accuracy of the regression model. A MLR may be represented by a model equation of the type (4.15). The model expresses the value of the observed data or predictand variable as a linear function of one or more predictor variables and an error term:

$$y_i = b_0 + b_1 x_{i,1} + b_2 x_{i,2} + \dots + b_k x_{i,k} + e_i \quad (4.15)$$

Where  $b_0$ : regression constant.

$b_k$ : coefficient on the  $k^{\text{th}}$  predictor.

$y_i$ : predictand in  $i$

$k$ : total number of predictors.

$e_i$ : error term.

## ***Chapter 4: Results and Discussions***

---

The model (4.15) is estimated by least squares, which yields parameter estimates such that the sum of squares of errors is minimized. The resulting prediction equation (4.16) is given below

$$\hat{y}_i = \hat{b}_0 + \hat{b}_1 x_{i,1} + \hat{b}_2 x_{i,2} + \dots + \hat{b}_K x_{i,K} \quad (4.16)$$

Where the variables are defined as in equation (4.15) except that “ $\hat{\cdot}$ ” denotes the estimated values.

### ***16.1.1.1 RESIDUALS***

The error term in equation (4.15) is unknown because the true model is unknown. Once the model is estimated, the regression residuals are defined as

$$\hat{e}_i = y_i - \hat{y}_i \quad (4.17)$$

$y_i$  = observed value of the predictand

$\hat{y}_i$  = predicted value of the predictand

The residuals measure the closeness of fit of the predicted and observed values. The variance of the residuals measures the “size” of the error, and is small if the model fits the data well.

### ***16.1.1.2 SUM OF SQUARE TERMS***

Several regression statistics are computed as functions of the sum of squares terms:

$$SSE = \sum_{i=1}^n \hat{e}_i^2 \quad \text{sum of squares, error}$$

$$SST = \sum_{i=1}^n (y_i - \bar{y})^2 \quad \text{sum of squares, total}$$

$$SSR = \sum_{i=1}^n (\hat{y}_i - \bar{y})^2 \quad \text{sum of squares, regression}$$

$\hat{y}_i$  = regression prediction for the  $i^{\text{th}}$  case,

$\bar{y}$  = average of total  $y_i$

### ***16.1.1.3 ASSESSMENT OF MLR PREDICTIVE ABILITY***

The predictive ability of the Multiple Linear Regression is assessed from the Coefficient of determination ( $R^2$ ), adjusted coefficient of determination ( $R^2-a$ ) and the standard error of the estimates.

#### **4.5.1.3.1 Coefficient of Multiple determinations ( $R^2$ )**

The explanatory power of the regression is summarized by its  $R^2$  value, computed from the sums of squares terms as

$$R^2 = \frac{SSR}{SST} = 1 - \frac{SSE}{SST} = 1 - \frac{\sum \left( y_i - \hat{y}_i \right)^2}{\sum \left( y_i - \bar{y} \right)^2} \quad (4.18)$$

The  $R^2$  also called as coefficient of determination, is often described as the proportion of variance “accounted for”, “explained”, or “described” by regression [Garson, 2003]. An  $R^2$  of 1.0 indicates that the regression line perfectly fits the data.  $R^2$  alone does not indicate the goodness of the fit. Sometimes when the predictor variables are calculated by ordinary least squares regression there may be a very high increase in the  $R^2$  value without having a real significance. In this case  $R^2$  increases as we increase the number of the predictor variables in the model increases. In this case a more pertinent approach leads to the calculation of the adjusted  $R^2$  along with the  $R^2$ .

The adjusted  $R^2$  is written in mathematical form as shown in equation (4.19)

$$R_a^2 = 1 - \frac{\sum (Y_i - \hat{Y}_i)^2}{\sum (Y_i - \bar{Y})^2} \frac{(n - 1)}{(n - k - 1)} \quad (4.19)$$

Where  $n$  is sample size and  $k$  is the number of predictor variables in the model not counting the constant term [Garson, 2003]. Unlike the coefficient of determination,  $R^2$ -a may decrease if variables entered in the model do not add significant effects to the model fit [Neter *et al.*, 1990]. The adjusted  $R^2$  increases only if the new term improves the model more than would be expected by chance. The adjusted  $R^2$  can be negative, and will always be less than or equal to  $R^2$ .

#### **16.1.1.3.1 Standard error of the estimate**

The residual mean square (MSE) is the sample estimate of the variance of the regression residuals. The value of the error term is sometimes written as  $\sigma_e^2$  while the sample estimate is given by

$$S_e^2 = MSE \quad (4.20)$$

Where MSE is the residual mean square obtained from the ANOVA table. The square root of the residual mean square is called the *root-mean-square error* (RMSE), or the *standard error of the estimate*

$$s_e = \sqrt{s_e^2} = \sqrt{MSE} \quad (4.21)$$

## ***Chapter 4: Results and Discussions***

---

### ***16.1.1.4 HYPOTHESIS TESTING***

The hypothesis tests are used to verify the significance of the predictor variables, individually and as a whole, in the regression model. The Fisher test (F-test) and the student test (t-test) are used for this purpose.

#### ***16.1.1.4.1 F-Test***

The *F* test is used to test the significance of  $R^2$ , which is the same as testing the significance of the regression model as a whole [Neter *et al.*, 1990]. The *F*-ratio, or *overall F*, which is computed from the mean squared terms in the ANOVA table, estimates the statistical significance of the regression equation. The F-test is referred to as the test for overall significance.

The null hypothesis may be stated as follows:

$$H_0: \beta_1 = 0 \quad H_A: \beta_1 \neq 0$$
$$F_{\text{obs}} = \frac{MSR}{MSE} = \frac{SSR / k}{SSE / (n - k - 1)}$$
$$F_{\text{obs}} \geq F_{\alpha, k, n-k-1}$$

Suppose that no significant regression may be drawn from the  $m$  independent variables considered in the model, and then the full model reduces to the intercept term  $\hat{\alpha}_0$  indicating that  $H_0$  is true. In this case the  $F$  observed  $< F$  critical (from F-table with critical probability alpha,  $k$  predictor variables and  $(n-k-1)$  degrees of freedom).

$H_a$ : At least one of the parameters is not equal to zero

The *F*-ratio is given from the ANOVA table

$$F = \frac{MSR}{MSE}$$

In terms of  $R^2$  it is written as

$$F = \frac{R^2 m}{1 - R^2 (n - m - 1)}$$

this value can be obtained from the ANOVA table.

#### ***16.1.1.4.2 t-Test***

T-tests are used to assess the significance of individual  $b$  coefficients, specifically testing the null hypothesis that the regression coefficient is zero. The t-test is conducted for each of the

## ***Chapter 4: Results and Discussions***

---

independent variables in the model and it is also called as the test of individual significance.

Hypothesis:

$$H_0: \beta_1 = \beta_1^0 \quad H_A: \beta_1 \neq \beta_1^0$$
$$TS: t_{obs} = \frac{b_1 - \beta_1^0}{S_{b_1}} \quad S_{b_1} = \frac{S_{YX}}{\sqrt{\sum_{i=1}^n (X_i - \bar{X})^2}}$$
$$RR: |t_{obs}| \geq t_{\frac{\alpha}{2}, n-2}$$

If  $t_i$  is greater  $t_{critical}$ , then we can reject the null hypothesis and conclude that the estimated coefficients are significant and different from zero otherwise the null hypothesis is not rejected.

### ***16.1.1.5 MULTICOLLINEARITY***

“Multicollinearity” is a term reserved to describe the case when the intercorrelation of predictor variables is high. It has been noted that the variance of the estimated regression coefficients depends on the intercorrelation of predictors. There are negative effects of multicollinearity. The variance of the predictor coefficients can be inflated so much that the predictor variables are not statistically significant – even though the overall regression equation is strong and the predictive ability is good. Secondly, the relative magnitudes and even the signs of the predictor coefficients may defy interpretation.

Signs of multicollinearity include:

1. High correlation between pairs of predictor variables.
2. Regression coefficients whose signs or magnitudes do not make good physical sense
3. Statistically non-significant regression coefficients on important predictors
4. Extreme sensitivity of sign or magnitude of regression coefficients to insertion or deletion of a predictor variable.

The multicollinearity is measured using functions parameters like the matrix correlation and the variance inflation factors.

#### ***16.1.1.5.1 Matrix correlation***

It is also called as the Pearson’s correlation which is the measure of the correlation between two variables X and Y. The matrix correlation reflects the degree of linear relationship between two variables. It ranges from 0 to 1. A correlation of 1 means that there is a perfect

## ***Chapter 4: Results and Discussions***

---

positive linear relationship between variables and a correlation of 0 means there is no linear relationship between the two variables.

### ***16.1.1.5.2 Variance Inflation Factor (VIF).***

The Variance Inflation Factor (VIF) is used to identify multicollinearity among the predictor variables. “Variance Inflation” refers here to the mentioned effect of multicollinearity on the variance of estimated regression coefficients. Accordingly, the VIF is based on the multiple coefficient of determination in regression of each predictor in multivariate linear regression on all the other predictors:

$$VIF_i = \frac{1}{1 - R_i^2}$$

Where  $R_i^2$  is the multiple coefficient of determination in a regression of the  $i^{\text{th}}$  predictor on all other predictors, and  $VIF_i$  is the variance inflation factor associated with the  $i^{\text{th}}$  predictor. Note that if the  $i^{\text{th}}$  predictor is independent of the other predictors, the variance inflation factor is one, while if the  $i^{\text{th}}$  predictor can be almost perfectly predicted from the other predictors, the variance inflation factor approaches infinity.

### ***16.1.1.6 ANALYSIS OF RESIDUALS***

Analysis of residuals consists of examining graphs and statistics of the regression residuals to check that model assumptions are satisfied. Some frequently used residuals tests are listed below.

#### ***16.1.1.6.1 Scatter plot of residuals against predicted values.***

The residuals are assumed to be uncorrelated with the predicted values of the observed data or predictand. Violation is indicated by some noticeable pattern of dependence in the scatter plots. For example, the residuals might have an increasing or decreasing linear trend.

#### ***16.1.1.6.2 Scatter plots of residuals against individual predictors.***

The residuals should be uncorrelated with the individual predictors. Presence of noticeable patterns of the dependence in the scatter plots would indicate that the presence of errors in the model.

#### ***16.1.1.6.3 Histogram of residuals.***

## ***Chapter 4: Results and Discussions***

---

The residuals should be normally distributed. Accordingly, the histogram of residuals should resemble a normal Probability Distribution Function (PDF). But a random sample from a normal distribution will be only approximately normal, and so the some departures from normality in the appearance of the histogram are expected – especially for small sample size.

### ***16.1.1.7 STEPWISE MULTIPLE LINEAR REGRESSION***

The regression analysis was carried out using MINITAB-14 software. The type of the multiple linear regression carried out here is the *stepwise multiple regression* which is also called as the *statistical regression* which consists of successive addition of the predictor variables. In the first stage the best regression is obtained with a single predictor variable. Successive variables are added one by one at each stage to get a better regression coefficient and satisfying all the statistical conditions [Brasquet, 1998 ; Cougnaud *et al.*, 2005]. The predictor variables that were considered through this analysis are oxygen to carbon ratio – (O/C) %, specific surface area – (SBET)  $\text{m}^2\cdot\text{g}^{-1}$ , porous volume – (Vporous)  $\text{cm}^3\cdot\text{g}^{-1}$ , volume of micropore – (Vmicro)  $\text{cm}^3\cdot\text{g}^{-1}$ , width of the micropore-(Wmicro) nm, length of the graphitic layers (L>1 ring Å and L> 2 ring Å).

Eleven samples are chosen for this study. The carbonized samples are not taken up because of their negligible porosity characteristics. The metal impregnated samples are also not taken up as the metal impregnates have a large influence on the reactivity of the material masking the influence of the other properties. The K content of the physically activated carbons is available as the chemically activated carbons did not produce enough content for the analysis of the K in these samples. Hence the K content is also not taken up as a predictor variable. The nitrogen to carbon ratio (N/C) was not considered as a predictor variable because of a non uniform distribution of the data within the variation range. A huge difference is obtained between the highest and the lowest N/C contents obtained for the chemically and the physically activated carbons.

Multicollinearity among the predictor variables was checked before carrying out the regression analysis. It represents the interdependence among the predictor variables and increases the statistical errors in regression analysis. The multicollinearity character was tested by the use of a correlation matrix [Brasquet, 1998; Brasquet and Le Cloirec, 2001].

	O/C (%)	S <sub>BET</sub> (m <sup>2</sup> /g)	Vporous (cm <sup>3</sup> /g)	Wmicro (nm)	Vmicro (cm <sup>3</sup> /g)	L > 2 rings Å
S <sub>BET</sub> (m <sup>2</sup> /g)	0.60					
Vporous (cm <sup>3</sup> /g)	0.68	0.69				
Wmicro (nm)	0.47	0.21	0.51			
Vmicro(cm <sup>3</sup> /g)	0.55	0.12	-0.17	-0.37		
L > 2 rings (Å)	-0.62	-0.68	-0.65	-0.21	0.27	
L > 1 ring (Å)	-0.50	-0.67	-0.61	-0.18	0.31	0.98

**Table 4 - :** Matrix of correlation for the predictor variables.

From Table 4-15, we find that L> 2 ring Å correlated strongly with L> 1 ring (Å). Hence fringe greater than 1 ring (Å) and 2 rings (Å) are considered one at a time during regression analysis. The regression obtained from stepwise methods are

$$\text{PIO} = 148.8 + 16.7 \text{ L}>1 \text{ ring} - 1.62 \text{ O/C} \quad (4.22)$$

With PIO in (°C), L> 1 ring in (Å) and O/C in (%).

$$S = 13 \text{ °C}, R^2 = 0.93, adj R^2 = 0.91 \quad (4.23)$$

Predictor	Coefficient	T	P
Constant	148,8	5.66	0.001
L> 1 ring A	16.7	4.39	0.003
O/C	-1.62	-5.02	0.002

## ***Chapter 4: Results and Discussions***

---

**Table 4 - :** Coefficients obtained from the regression equation

From the Table 4-16, we find that the individual coefficients have a probability less than 0.05. The value of  $T > 2$  indicate that they are significant coefficients and satisfy the hypothesis of t-test.

<b>Source</b>	<b>DF</b>	<b>Sum of squares</b>	<b>CM</b>	<b>F</b>	<b>P</b>
<b>Regression</b>	2	15435.9	7717.9	44.26	0.000
<b>Residual error</b>	7	1220.6			
<b>Total</b>	9	16656.4			

**Table 4 - :** Analysis of variance

Table 4-17 describing the analysis of variance indicates significance of the MLR model as a whole as the value of F obtained is above the critical value of 19.38. The residual plots of the predicted data and their histogram are shown in Appendix-P. The residual plots of the predicted values and the independent variables show a scattered trend indicating the goodness of the fit.

The best MLR obtained relates the PIO with O/C ratio and graphitic layer length ( $L > 1\text{ring } \text{\AA}$ ). The combination of the two predictor variables explained changes in the PIO values measured for the AC samples. The accuracy of the model is given by the  $R^2$  value equal to 0.93 and the standard error of fits S of 13 °C. The only sample which deviated from the regression equation was NC-60. The precision between the calculated and the measured PIO is around 5 % and the deviation of the NC-60 sample is shown in Figure 4-44.

The magnitude of the individual properties cannot be directly interpreted from the regression equation due to the differences in the units of the predictor variables. As the predictor variables are in different units of measurement, the regression equation was computed again with the standardized data. The coefficients resulting from the standardized data (subtracted from the mean and divided by standard deviation) are called “beta coefficients”, and can be

## ***Chapter 4: Results and Discussions***

used directly for predicting the magnitude of the predictor variables on the response variables [Brasquet, 1998 ; Giraudeau *et al.*, 2006].

$$\text{PIO} = -0,6 \text{ O/C (\%)} + 0,5 \text{ L >1 ring (A)} \quad (4.24)$$

$$S = 13 \text{ }^{\circ}\text{C}, R^2 = 0.93, \text{adj } R^2 = 0.91$$

From the beta coefficients, we find that the O/C ratio is slightly more influent than the graphitic layer length for the activated carbons considered.

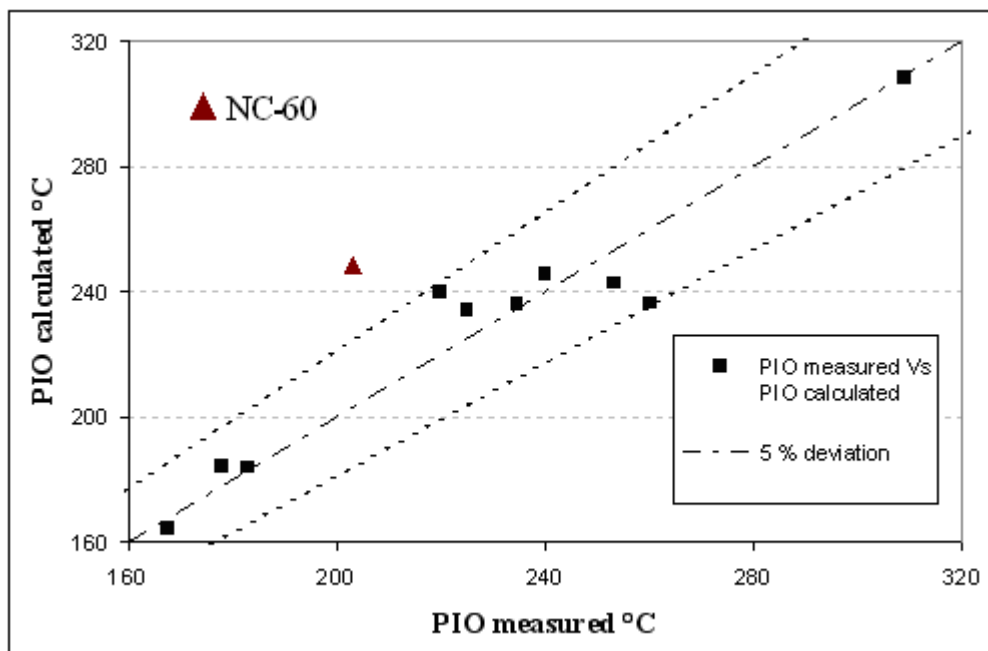


**Figure 4 - :** Result of the prediction ability of the best multiple linear regression for PIO.

These results confirm the major influence of these surface properties on the oxidation reactivity of the materials. The higher the O/C content and the shorter the length of the graphitic layers the lower is the PIO.

The results of statistical correlation are in accord with the qualitative analysis that the oxygen to carbon and length of the graphitic layer influences the oxidation reactivity of activated carbons. The correlations also explains the mechanism of the oxidation discussed in the

## ***Chapter 4: Results and Discussions***

---

literature with the commencement of the oxidation of the surface oxygenated groups at lower temperature which is followed by the formation and decomposition of the unstable radicals liberating heat and oxidation products. Also from the image analysis, it was found that the graphitic layers are short and distorted with grafting of oxygenated groups on the layer boundaries which are prone to oxidation easily.

Regarding the SIT, the regression equation obtained involves two predictor variable which is the O/C content and porous volume:  $SIT\ ^\circ C = 514 - 1.02\ O/C\ (%) - 87.7\ V_{porous}\ (\text{cm}^3\cdot\text{g}^{-1})$ , with  $R^2$  of 0.78 and the adj  $R^2$  of 0.72. But the regression equation could not be validated because of a high standard error deviation ( $S = 45^\circ C$ ) and the value of the adjusted  $R^2$  is reduced drastically with insignificant coefficients as seen in Table 4-18.

Predictor	Coefficient	T	P
Constant	514	5.66	0.001
$V_{porous}$	87.7	-2.25	0.06
O/C	-1.02	-0.8	0.45

**Table 4 - :** Coefficients obtained from the regression equation

The standardized equation obtained for the SIT was

$$SIT\ ^\circ C = -0.226\ O/C\ (%) - 0.637\ V_{porous}\ (\text{cm}^3\cdot\text{g}^{-1})$$

Hence the SIT was very explained with the oxygen to carbon ratio with  $SIT = 537 - 4.7\ O/C\ (%)$  and all additional variables do not improve the predictive ability of the regression equation.

## **17 CONCLUSION**

The measurement of the PIO and SIT have been made with 19 different carbon samples having different source of origin and mode of activation. The PIO of the carbon samples varied from 150 to about 350 °C whereas the SIT of varied from 200 to 500 °C. The kinetic model has been established from the heat flux and the mass loss curves. The early oxidation process was derived from the heat flux curve taking a zero order reaction, whereas the ignition reactivity was derived from the heat flux curves with an order 1 for the reaction.

## ***Chapter 4: Results and Discussions***

---

The chemical composition of the activated carbon has an effect on their reactivity towards oxygen in air. The materials containing significant amounts oxygen and potassium are the most sensitive to oxidation. Thus chemical activation by an acid agent produces carbons containing high contents of surface oxygenated surface groups, which initiate the oxidation reactions by reacting with oxygen in air to form radical active sites. For such materials, the point of initial oxidation is as low as 170°C. The nature of the mineral matter initially present in the precursor may also influence the reactivity. Among the materials tested, physically activated carbons manufactured from coconut shell were found to contain noticeable amounts of potassium that is supposed to act as a catalyst which enhances their reactivity compared to other physically activated samples.

The influence of the external conditions on the oxidation process was enlightened. Low concentrations of oxygen in air strongly slows down the initiation of the oxidation reactions. By enriching the oxygen content above its value in air the PIO does not change greatly but the ignition process speeds up, and its rate is controlled by the diffusion of oxygen molecule within the pores. An increase in the gas flow rate contributes to the acceleration of the oxidation reactions in the early stage but does not affect the self ignition temperature.

Atlast the presence of VOC adsorbed in the material may cause an earlier starting of the oxidation reactions. Activated carbons saturated with oxygen groups compounds and especially ketones exhibit PIO value reduced by 50-100°C. These results are in consistent with our previous results regarding the effect of the oxygen surface groups on the oxidation process.

The quantitative analysis performed by setting up multiple linear regressions discriminates the influent surface properties and assess their weight on the reactivity parameters. The quantitative analysis of the surface properties confirms that the chemical composition notably the oxygen to carbon ratio in the form of surface oxygenated groups, play a significant role in the oxidation and ignition process. Oxygen to carbon ratio influences both PIO and SIT, but their influence is felt more in PIO than in SIT, but the impact of these variable is higher on the PIO than on the SIT. The textural properties (specific surface area, porous volume and the width of the micropore) could not be discriminated as influent properties. However nanometric structural dimension of the basic structural units namely L>1 ring was found to play an important role on the oxidation mechanisms. Short fringe lengths contribute to develop a greater number of reaction sites, thus accelerating the initial oxidation rate and reducing the PIO.

## **18 REFERENCES**

1. Akubuiro, E.C. and Wagner, "Potential mechanistic roots for the oxidative disintegration of ketones on carbon adsorbents," *Ind. Eng. Chem. Res.*, **32**, 2690-2698 (1993).
2. Amarasekera, G., M.J. Scarlett, and D.E. Mainwaring, "Development of microporosity in carbons derived from alkali digested coal," *Carbon*, **36**, 1071-1078 (1998).
3. Baker, F.S., C.E. Miller, and D.E. Tolles, Activated carbon. Kirk-Othmer encyclopedia of Chemical Technology, 4<sup>th</sup> Edition, Volume No. 4 p. 1015. New York Wiley & Sons (1992).
4. Bansal, R.C., J.B. Donnet, and N. Stoeckli. Active Carbon, pp. 10-49, Marcel Dekker, New York, (1988).
5. Brasquet, C.F. "Process of adsorption on activated carbon tissues, water treatment applications," Ph.D dissertation, University of Pau and des Pays de l'Adour, Ecole des Mines de Nantes, France, 1998.
6. Brasquet, C.F. and P. Le Cloirec, "Neural networks modelling of inorganics removal by activated carbon cloths," *J. Environ. Eng.*, **127**, 889-894 (2001).
6. Brauner, S., L.S. Demming., W.L. Demming, and E.Teller, *J. Am. Chem. Soc.*, **62**, 1723 (1940).
8. Cougnaud, A., C.F. Brasquet, and P. Le Cloirec, "Removal of pesticides from aqueous solution: Quantitative relationship between activated carbon characteristics and adsorption properties," *Environ. Technol.*, **26 (8)**, 857-866 (2005).
7. Delage, F., "Warming of activated carbon beds during adsorption of volatile organic compounds: experimental and theoretical study," Ph.D dissertation, University of Poitiers, Ecole des Mines de Nantes, France (2000).

## ***Chapter 4: Results and Discussions***

---

8. Delage, F., P. Pre, and P. Le Cloirec, "Mass transfer and warming during adsorption of high concentrations of VOC's on an activated carbon bed: experimental and theoretical analysis," *Eviron. Sci. Technol.*, **34**, 4816-4821 (2000).
9. Garson, D., Multiple Regressions. North Carolina State University.  
<http://www2.chass.ncsu.edu/garson/pa765/regress.htm>, July 2003.
10. Giraudeau, S., P. Pré., H. Tezel, and P. Le Cloirec, "Estimation of the coupled influence of the porosity characteristics of activated carbons and the molecular properties of VOCs on the adsorption energy," *Carbon*, **44**, 2413-2421 (2006).
11. Hardman, J.S., C.J. Lawman, and P.J. Street, "Further studies of the spontaneous behaviour of activated carbon," *Fuel*, **62**, 632-638 (1983).
12. Jones, J.C., "Towards an alternative criterion for the shipping safety of activated carbons," *Journal of Loss Prevention in Process Industries*, **11**, 407-411 (1998).
13. Jiang, W., G. Nadeau., K. Zaghib, and K. Kinoshita, "Thermal analysis of the oxidation of natural graphite – effect of particle size," *Thermochim. Acta*, **351**, 85-93 (2000).
14. Kizgut, S. and S.Yilmaz "Characterization and non-isothermal decomposition kinetics of some Turkish bituminous coals by thermal analysis," *Fuel Process. Technol* **85**, 103-111 (2003).
15. Lu. Z., Ph.D dissertation, Pennsylvania State University, USA (2006).
16. Montgomery, D.C., E.A. Peck, and G.G, "Vining introduction to linear regression analysis" 3<sup>rd</sup> Ed., J. Wiley (2001).
17. Naujokas, A.A., "Spontaneous combustion of carbon beds," *Plant/Operations Progress*, **4**, 120-126 (1985).
18. Neter, J., W. Wasserman, and M.H. Kutner, "Applied Linear Statistical Models: Regression, Analysis of Variance and Experimental Designs" 3<sup>rd</sup> ed., Richard Irwin, Inc, (1990).

## ***Chapter 4: Results and Discussions***

---

19. Rouzaud, J.N. and C. Christian, “Quantitative high-resolution transmission electron microscopy: a promising tool for carbon materials characterization,” *Carbon*, **78**, 229-235 (2002).
20. Rouzaud, J.N., “The multiscale organization as a fingerprint of the formation conditions of carbons; a TEM study,” Extended Abstracts Carbon, Providence, Rhode Island, USA, (2004).
21. Suzin, Y., L.C. Buettner, and C.A. LeDuc, “Behaviour of impregnated activated carbons heated to the point of oxidation,” *Carbon*, **11**, 1557-1566 (1998).
22. van der Merwe, M.M. and T.J. Bandosz J, “A study of metal impregnated carbons: the influence of oxygen content in the activated carbon matrix,” *J. Colloid Interface Sci*, **282**, 102-108 (2005).
23. Wang, P.H., Z.R., Yue, and J. Liu, “Conversion of polyacrylonitrile fibers to activated carbon fibers: effect of activation,” *Journal of Applied Polymer Science*, **60**, 923-929 (1996).
24. Yi, S.L, Ph.D dissertation, University of Illinois at Urbana-Champaign, USA (2000).
25. Zaghib, K., X. Song, and K. Kinoshita, “Thermal analysis of the oxidation of natural graphite: Isothermal kinetic studies,” *Thermochim. Act*, **371**, 57-64 (2001).
26. Zhang, S., S.A. Stewart, T.D. Hatchard, and J.R.Dahn, “Thermal runaway predictions fro impregnated activated carbons from isothermal DSC measurements,” *Carbon*, **41**, 903-913 (2003).



---

## **CONCLUSIONS AND PERSPECTIVES**

---

The phenomenon of self heating of activated carbons is the result of several complex physical and chemical processes. Attempts have been made in this work to elucidate the dependence of the various material properties and operating conditions influencing the oxidation and ignition reactivity. A novelty in this work is the quantification of the influence of these properties on the oxidation and ignition reactivity using statistical correlations. Conclusions can be drawn from this study under three main topics: characterization of the surface properties of the activated carbons, oxidation reactivity and mechanisms and quantitative influence on the material characteristics on its reactivity and practical applications in the perspective of process safety.

### Surface properties of the activated carbons

The results showed that the mode of activation and the precursor predominantly influence the surface properties of activated carbons. The chemical activation rendered the carbons more mesoporous with higher specific surface area, greater amounts of oxygenated functional groups on the surface, and negligible ash content. The structural organization of these carbons is highly disordered and characterized with shorter graphitic layers. On the other hand the physically activated carbons show diversified characteristics as both the commercial and laboratory prepared samples were analyzed. In general the physically activated carbons possessed lower oxygenated surface groups with higher ash content. The specific surface area varied with respect to the activation conditions and the precursor sample. The commercial samples possess higher surface area than the samples prepared in the laboratory. The HRTEM observations show that the physically activated carbons have well organized graphitic layers which are longer than that of the chemically activated carbons.

### Reactivity studies

The study of the oxidation and ignition reactivity of the activated carbons in air was characterized by two parameters namely PIO for the oxidation region and SIT for the ignition region. These values were shown to vary with the method of measurement applied and external conditions (flow rate, heating rate, oxygen composition in the gas). The purpose was

## ***Conclusions and perspectives***

---

to make quantitative comparisons with the various samples and point out the influent surface properties on the reactivity of the materials. Kinetic analysis were undertaken for the both the oxidation and ignition regions. The temperatures of PIO and SIT were slightly higher than that of the ASTM-D 3466-76 method. But the results are used for understanding the influence of the properties affecting the reactivity and not for measuring the accurate oxidation and ignition temperatures.

### Influence of material properties and operating conditions on the reactivity of activated carbons

The influence of the material properties and operating conditions on the reactivity parameters of the activated carbons were analysed qualitatively and quantitatively. The qualitative analysis gave general trends of the effect of the chemical composition and the porosity characteristics over the reactivity parameters. The oxygen to carbon ratio showed a greater influence as single influent parameter on the oxidation ignition characteristics with the exceptions of coconut shell activated carbons. The porosity characteristics like the specific surface area, porous volume and the width of the micropore had very little influence on the reactivity parameters, instead they were better explained with the help of the structural properties namely the graphitic layer length. It was found that the stable activated carbons have lower percentage of non-stacked layers and higher number of stacked layers in a domain which probably limit the accessibility of oxygen to active sites. The activated carbon having longer graphitic layers had higher oxidation and ignition temperatures.

The VOC's had a profound impact in reducing the oxidation and ignition temperatures of the activated carbons. The oxidation and the ignition temperatures depended on the nature of the VOC's. Certain type of VOC's like the aromatic ketones were more reactive than amines, hydrocarbons and alkanes. The VOC's undergo oxidation reactions on the surface of the activated carbons liberating exothermic heat initiating the oxidation and ignition reactions. Certain activated carbons like the coconut shell activated carbons with lower PIO undergo oxidation reactions well before the oxidation of the VOC's. Hence the characteristics of the activated carbon should be also taken into account while studying the influence of VOC's on the reactivity of activated carbons.

The operating conditions like the increase in the oxygen composition decreases the oxidation and ignition temperatures. The reactivity of activated carbons is greatly reduced in oxygen deficient environment. The activated carbons which are less reactive at 21 % oxygen

## ***Conclusions and perspectives***

---

concentration showed drastic increase at 100 % oxygen concentration which was observed especially for the coconut shell activated carbons. Thus the reactivity is specific to the operating conditions

An increase in oxygen flow rate does not enhance significantly the internal diffusion of the oxygen molecules in the micropores. The increase in the self heating rate of the bed may also be compensated by heat dissipation resulting from convection. . However the heating rate has almost no influence on the temperature at which ignition is observed as the differences in the SIT data reported were not more than 10 °C.

The quantitative analysis performed using a multiple linear regression discriminated the influent variables affecting the reactivity parameters giving their magnitude of influence. The chemical composition notably the oxygen to carbon ratio in the form of surface oxygenated groups and the graphitic layer length had an important role on the oxidation and ignition of activated carbons confirming the results of qualitative analysis. The increase of oxygen to carbon ratio and the decrease of the graphitic layer length of the activated carbons increase the reactivity of the material.

These results could be of great importance industrially as they can help in selecting the materials which are of lesser oxidation and ignition risks. It can also help the manufacturers to adjust their process of fabrication to obtain a material with lesser risk considering the final properties of the material which would be obtained. Finally the correlations and the kinetic information data could be used in complex models for predicting the risk of oxidation and ignition

### **Perspectives**

The results of this work can be used mainly in the process of fabrication and in the aspects of process engineering. Certain properties can be looked into while manufacturing activated carbons that can increase the oxidation stability. In the process point of view extra care has to be taken to certain materials during their operation, transport and storage due to their vulnerability for oxidation and ignition. The results of this work may be integrated with the kinetic models simulating industrial units. A multiple linear regression model has been attempted in this work and this may be further extended to non linear regression model using the database of values of the different characteristics of the materials. Finally an indepth knowledge is required about the structural morphology of the activated carbons in order to answer the different ambiguities on the structural aspects.

---

## **Resumé en Français**

---

### **CHAPITRE – 1**

### **INTRODUCTION GÉNÉRALE**

Les charbons actifs sont des matériaux à base de carbone utilisés largement en catalyse hétérogène, pour la filtration d'effluents industriels, dans les équipements de protection personnelle pour atmosphères contaminées. Ils sont généralement utilisés pour le traitement de Composés Organiques Volatiles et des odeurs. Ces Composés Organiques Volatiles peuvent agir directement sur la santé humaine, les écosystèmes et le réchauffement de la planète. Aussi, les limites d'émission dans l'atmosphère sont de plus en plus sévères, la réglementation limite de plus en plus leurs rejets dans l'atmosphère. La réglementation française définit les Composés Organiques Volatiles (COV) comme tout composé organique, à l'exclusion du méthane, ayant une pression de vapeur de 10 Pa ou plus à une température de 293.15 K, ou ayant une volatilité qui correspond les conditions d'utilisation particulières (arrêté du 29 mai 2000). Les émissions de Composés Organiques Volatiles proviennent des processus industriels impliquant des solvants (produits chimiques de base, le dégraissage des métaux, l'utilisation de Cholorofluorocarbone, la production de peinture, les colles et les adhésifs et d'autres industries incluant des raffineries et des pétroliers, ainsi que la production des alcools.

La politique environnementale plus stricte et les engagements pris par des industriels ont permis de diminuer les émissions et ont engendré des améliorations dans les procédés de traitement pour la réduction des polluants dans l'air. Les principaux résultats concernent l'utilisation de différentes techniques de traitement de pollution impliquant des charbons actifs particulièrement dans la réduction des Composés Organiques Volatiles. Cependant l'utilisation, le stockage et le transport des charbons actifs présentent également des risques d'inflammation : ils agit de l'inflammation du matériau. Le risque est réel lors de l'utilisation des charbons actifs pour l'adsorption des Composés Organiques Volatiles, de l'élimination des odeurs et pour la récupération des solvants. L'adsorption est un phénomène exothermique,

## ***Resumé en Français***

---

le transfert gaz-solide s'accompagne d'un dégagement de chaleur. Si ce phénomène peut paraître anecdotique lorsque le fluide possède une grande inertie thermique, comme dans le domaine du traitement de l'eau, il n'en est pas de même pour le traitement d'air chargé en Composés Organiques Volatiles. Les systèmes de traitement de l'air chargés de Composés Organiques Volatiles ont une probabilité plus grande de risques d'inflammation et d'oxydation. Aussi le charbon actif étant un matériau combustible, l'échauffement du filtre peut poser des problèmes de sûreté avec comme risque l'inflammation de l'adsorber.

De ce point de vue, les objectifs principaux de la thèse sont d'étudier les propriétés des matériaux carbonés ainsi que le mode d'activation influençant leur réactivité à des températures élevées en présence d'air et des Composés Organiques Volatiles. L'autre objectif est de déduire des corrélations statistiques quantitatives rapprochant les propriétés des matériaux et les paramètres caractérisant d'oxydation et l'inflammation des charbons actifs.

Cette thèse est présentée en trois chapitres principaux. Le premier chapitre consiste en une revue bibliographique sur les charbons actifs, particulièrement la méthode de fabrication avec les propriétés physiques et chimiques associées. Il inclut aussi une revue sur les différents accidents industriels impliquant les charbons actifs survenus en France et dans le monde entier. Ces incidents donnent une indication sur les divers facteurs responsables de l'oxydation et de l'inflammation des charbons actifs. Cette partie présente aussi les mécanismes d'oxydation et d'inflammation des charbons actifs, ainsi que les différentes méthodes expérimentales nécessaires pour caractériser leur réactivité. En bref, ce chapitre donne une vue globale sur les matériaux, les principaux facteurs responsables des divers incidents thermiques ainsi que les mécanismes d'oxydation et d'inflammation des charbons actifs.

Le deuxième chapitre donne une description plus fine des matériaux et des procédures expérimentales. Les diverses techniques de caractérisation pour mesurer les propriétés (incluant la texture, la structure et la composition chimique) des matériaux sont analysées. Les caractéristiques thermiques consistent de la mesure des températures d'oxydation et d'inflammation des charbons actifs. Finalement, le dernier chapitre fait une analyse des résultats des différentes techniques de caractérisation, suivie par la déduction des corrélations statistiques rapprochant les propriétés importantes des charbons actifs avec les paramètres de réactivité.

## **CHAPITRE 2**

## **ETUDE BIBLIOGRAPHIQUE**

L'objectif principal de ce chapitre est de faire une revue synthétisée sur les charbons actifs pour mieux connaître leurs caractéristiques et leur réactivité d'oxydation et d'inflammation. Les différentes circonstances et les propriétés menant à l'oxydation et à l'inflammation des charbons actifs sont discutées.

Ce chapitre est composé de quatre sous parties. La première partie donne une description des charbons actifs : les matières premières utilisées pour leur fabrication, les méthodes de production et leurs caractéristiques (la texture, la structure, et la composition chimique, particulièrement celle de surface). La deuxième et la troisième partie donnent un compte-rendu des accidents thermiques associés aux charbons actifs, en précisant les détails de la nature de l'incident et des circonstances dans lesquelles ils ont eu lieu. Dans ces parties, on retrouve les mécanismes d'oxydation et d'inflammation des charbons actifs en présence de l'air et des Composés Organiques Volatiles. La dernière partie de ce chapitre traite des études expérimentales et la détermination des paramètres d'oxydation et d'inflammation des charbons actifs.

### **Le charbon actif**

#### **Fabrication des charbons actifs**

Presque toutes les matières carbonées peuvent servir de précurseur à la préparation de charbon actif,. Cependant, en pratique, le bois, les coquilles de noix, les noyaux de fruits, la tourbe, le charbon, etc.. sont des produits peu chers qui possèdent une forte teneur en carbone et sont les plus utilisés mondialement (cf. Tableau 1). Mais les produits finaux sont différents selon la nature de la matière première utilisée, selon la nature du procédé d'activation et selon les conditions dans lesquels cette activation a été réalisée.

---

Matière Première	Masses Utilisées (tonnes par an)
------------------	----------------------------------

## *Resumé en Français*

---

Bois	130 000
Houille	100 000
Lignite	50 000
Noix de coco	35 000
Tourbe	35 000
Autres	10 000

**Tableau 1 : Matières premières utilisées pour la fabrication de charbon actif**

La production de charbon actif peut se faire selon deux modes d'activation :

- L'activation chimique : cette procédure est utilisée habituellement pour le bois ou la tourbe. Le produit finement divisé est mélangé avec une solution concentrée de chlorure de zinc, d'acide phosphorique ou d'acide sulfurique qui dégrade la cellulose de la matière. Le mélange est séché et pyrolysé dans un four entre 400 et 700°C. Le produit est ensuite lavé pour enlever l'agent activant. La création de la structure poreuse vient de la déshydratation de la cellulose durant la pyrolyse.
- L'activation physique : elle implique habituellement deux étapes. Tout d'abord, la pyrolyse (carbonisation) de la matière première avant l'activation. Cette carbonisation se fait en l'absence d'air pour enlever les constituants non carbonés et pour produire une masse plus importante de charbon avec une faible porosité. Cette phase influe peu sur la structure poreuse du produit final. Le charbon doit ensuite subir une activation en présence de vapeur d'eau ou de dioxyde de carbone ou d'un mélange des deux. Ces deux gaz sont des agents oxydants doux pour des températures d'environ 800-1000°C.

### **Structure des carbons actifs**

Les carbons actifs ont une structure consistant en des couches ou feuillets de cycles aromatiques condensés, entassés en couches non polaires. Les feuillets sont pourvus de défauts, de dislocations, de discontinuités et les atomes de carbone présents en bordure des couches ont des valences incomplètes et des électrons non-appariés. Cela confère au charbon actif un potentiel énergétique très fort, avec une très forte réactivité de ces atomes de carbone. Les carbons actifs sont la plupart du temps associés à des quantités non négligeables d'hétéroatomes, en particulier l'oxygène qui possèdent une affinité très forte avec les sites réactifs du charbon<sup>1</sup>. Ces hétéroatomes proviennent soit du matériau de départ, soit font partie

## ***Resumé en Français***

---

de la structure chimique finale et sont issus de liaisons chimiques avec la surface durant l'activation ou pendant d'autres traitements. Ces hétéroatomes sont liés aux bordures des feuillets aromatiques et forment des composés de surface (complexes de surface) ou ils peuvent être intégrés dans les couches carbonées et former des hétérocycles.

De plus, la structure en feuillets du charbon actif confère à sa porosité une forme particulière puisque les pores sont dits en ‘fente’ (espaces entre deux plans). La taille des pores est donc définie comme la distance disponible entre deux parois opposées. Les pores sont souvent classés en trois catégories suivant leur taille.

- Les *macropores* dont l'épaisseur est supérieure à 50 nm ;
- Les *mésopores* pour des épaisseurs comprises entre 2 et 50 nm ;
- Les *micropores* dont l'épaisseur est inférieure à 2 nm.

### **L'adsorption sur charbon actif**

#### Mécanismes de l'adsorption

L'adsorption est un phénomène de surface qui résulte du transfert de matière entre une phase gazeuse (l'adsorbat) et une phase solide (l'adsorbant). Ce transfert se déroule en plusieurs étapes :

1. Transport du composé de la phase gazeuse vers la couche limite entourant la particule (diffusion extragranulaire) ;
2. Transport du composé dans la couche limite entourant le grain (diffusion externe) ;
3. Diffusion du composé dans le volume poreux ;
4. Adsorption du composé en surface de l'adsorbant par le biais d'interactions physiques ou chimiques ;
5. Diffusion de surface, le composé adsorbé pouvant se déplacer d'un site d'adsorption à un autre
6. Libération de chaleur consécutive à l'adsorption. La quantité de chaleur libérée est fonction de l'intensité des interactions entre l'adsorbat et l'adsorbant.

Pour discuter des mécanismes fondamentaux de l'adsorption, il est utile de distinguer l'adsorption physique (physisorption) qui fait intervenir uniquement de faibles forces intermoléculaires et l'adsorption chimique (chimisorption) qui consiste en la formation d'une liaison chimique entre la molécule d'adsorbat et la surface de l'adsorbant.

## ***Resumé en Français***

---

Quelques caractéristiques distinctives de ces deux mécanismes sont rassemblées dans le tableau suivant :

Physisorption	Chimisorption
Phénomène général	Dépend de la réactivité de l'adsorbat et de l'adsorbant
Faible spécificité	Très forte spécificité
Adsorption en mono- ou multicouche(s)	Adsorption en monocouche uniquement (molécules chimisorbées liée aux parties réactives de la surface)
Pas de dissociation possible de l'adsorbat	Dissociation possible de l'adsorbat
Pas d'énergie d'activation	Réaction qui nécessite une énergie d'activation
Phénomène rapide et réversible	Phénomène qui peut être lent et irréversible
Pas de transfert d'électron malgré la polarisation de la molécule adsorbée	Transfert d'électron(s) qui conduit à la formation d'une liaison chimique entre la molécule et la surface

*Tableau 2 : Différences entre physisorption et chimisorption*

En phase gaz, l'adsorption sur charbon actif fait toujours intervenir de manière prépondérante la physisorption puisque ce matériau est principalement apolaire et possède peu de complexes de surface capables de créer des liaisons chimiques.

L'énergie dégagée par l'adsorption donne une mesure directe de la force de la liaison entre l'adsorbat et l'adsorbant.

L'adsorption physique à partir d'une phase gazeuse est systématiquement exothermique. Une simple explication thermodynamique peut le montrer. En effet, comme la molécule adsorbée a tout au plus deux degrés de liberté pour une translation et comme le

## ***Resumé en Français***

---

degré de rotation de l'espèce adsorbée est toujours inférieur à celui de cette molécule dans la phase gazeuse, l'entropie échangée lors de l'adsorption est négative ( $\Delta S = S_{\text{ads}} - S_{\text{gaz}}$ ).

Pour que l'adsorption puisse avoir lieu, il faut que l'enthalpie libre  $\Delta G$  soit aussi négative ; or  $\Delta G = \Delta H - T\Delta S$ , donc  $\Delta H$  est aussi négative, d'où une réaction exothermique

### *Remplissage des pores*

L'adsorption sur charbon actif dans les pores les plus petits (micropores) peut se faire sur plusieurs couches d'adsorbat et peut être interprétée comme de la condensation sur les parois poreuses à une pression critique de condensation  $P_c$

Dans les pores de plus grandes dimensions (mésopores), Ruthven et Rouquerol et al. décrivent la progression dans un matériau adsorbant d'une adsorption multicouches vers une condensation capillaire. Ce phénomène est expliqué par l'effet de la tension de surface sur la pression de saturation de la vapeur, comme le montre l'équation de Kelvin, page suivante, établie à partir de considérations thermodynamiques.

$$\frac{P_v}{P_s} = \exp\left(\frac{-\gamma V_m \cos \theta}{r_c R T}\right)$$

Où  $P_v$  : Pression de vapeur saturante du composé lors de la condensation capillaire (Pa) ;

$P_s$  : Pression de vapeur saturante pour le liquide pur à la même température sur une surface plane (Pa) ;

$\gamma$  : tension de surface ( $\text{N.m}^{-1}$ ) ;

$\theta$  : angle de contact ( $^\circ$ ) ;

$V_m$  : volume molaire de la phase adsorbée ( $\text{m}^3.\text{mol}^{-1}$ ) ;

$r_c$  : rayon du pore où a lieu la condensation (m) ;

$R$  : constante des gaz parfaits ( $R=8,314 \text{ J.mol}^{-1}.\text{K}^{-1}$ ) ;

$T$  : température absolue (K).

Dobruskin décrit le processus de remplissage des mésopores de la façon suivante :

- ♦ Après le remplissage des micropores, l'adsorption du composé commence sur les parois mésoporeuses, qui consistent en des molécules d'adsorbat compressées. En effet, il est supposé soit que les molécules adsorbées, compressées dans les micropores, forment la surface des mésopores, soit que la surface est constituée d'atomes de carbone recouverts par un film pré-adsorbé (pendant le remplissage des micropores). De toute manière, les conclusions sont dans un cas comme dans l'autre

## ***Resumé en Français***

---

similaires puisque la plus grande contribution à l'énergie d'adsorption totale provient des interactions avec la première couche de molécules adsorbées.

- ♦ Quand le recouvrement de la surface par une monocouche d'adsorbat atteint la pression critique de condensation, la condensation en surface est initiée. Finalement, le volume mésoporeux est entièrement rempli d'une phase condensée.

D'un point de vue énergétique, il est important de noter l'intérêt que représente l'enthalpie de condensation qui reflète le dégagement énergétique lié au changement de phase vapeur/liquide.

Rouquerol *et al.* affirme que l'énergie mise en jeu dans l'adsorption sur charbon actif est toujours plus grande que l'énergie de condensation de l'adsorbat.

## **Forces et potentiels d'interactions intermoléculaires**

### **Définitions**

Les liaisons physiques résultent de forces intermoléculaires s'exerçant entre atomes et molécules distincts, contrairement aux liaisons chimiques qui mettent en jeu des forces intramoléculaires faisant intervenir un changement complet des orbitales électroniques. Dans les liaisons physiques, les distributions électroniques sont peu perturbées. On emploie le terme d'interactions pour parler indifféremment des forces intermoléculaires ou du potentiel, c'est-à-dire de l'énergie potentielle intermoléculaire, qui est généralement la quantité utilisée dans les calculs. Elle se définit comme l'énergie  $\Phi(r)$  résultant des interactions à une séparation  $r$  des molécules.

La force intermoléculaire est reliée à l'énergie par la relation :

$$\Phi(r) = \int_{\infty}^r F(r') dr'$$
$$F(r) = -\frac{d\Phi}{dr}$$

De même, le potentiel est égal au travail des forces nécessaire pour amener les molécules à la distance ( $r$ ) l'une de l'autre en partant de l'infini :

On désigne par  $r_m$ , la séparation au minimum de la fonction  $\Phi(r)$ . La force intermoléculaire est alors attractive lorsque  $r > r_m$  et répulsive pour  $r < r_m$ .

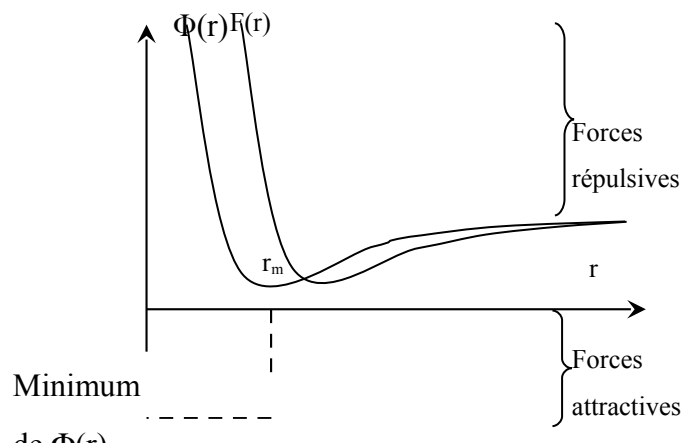


*Fig.2 : Courbes du potentiel intermoléculaire  $\Phi(r)$  et de la résultante des forces d'interaction  $F(r)$  en fonction de la distance intermoléculaire*

### 1.2.2. Expressions des potentiels énergétiques

#### 1.2.2.1. Forces répulsives

A courte distance, l'interpénétration des nuages électroniques conduit à une répulsion qui croît très rapidement lorsque les molécules se rapprochent. L'énergie de répulsion est souvent exprimée sous la forme :

$$\Phi_R = \frac{B}{r^{12}}$$

avec  $B$  : constante

#### 1.2.2.2. Forces dipolaires (Keesom)

Deux molécules polaires, c'est-à-dire possédant un moment dipolaire permanent, subissent une interaction attractive. L'expression du potentiel énergétique correspondant a été

$$\Phi_K = -\frac{1}{3(4\pi\epsilon_0\epsilon)^2} \frac{1}{k_B T} \frac{\mu_1^2 \mu_2^2}{r^6}$$

établie par Keesom :

avec  $\epsilon_0$  : permittivité du vide ( $\epsilon_0 = 8,854 \cdot 10^{12} \text{ C}^2 \text{ J}^{-1} \text{ m}^{-1}$ ) ;

$\epsilon$  : constante diélectrique du milieu ;

$k_B$  : constante de Boltzmann ( $k_B = 1,381 \cdot 10^{23} \text{ J.K}^{-1}$ ) ;

## ***Resumé en Français***

---

$\mu_1, \mu_2$  : moments dipolaires des molécules qui interagissent (Db) ;  
 $r$  : distance séparant les deux molécules (m).

### ***1.2.2.3. Forces de polarisation (Debye)***

Les forces de polarisation sont mises en œuvre entre un dipôle permanent et un dipôle induit. L'attraction provient de la polarisation induite d'une molécule non polaire quand elle pénètre dans le champ électrique créé par une autre molécule polaire.

Le potentiel correspondant est exprimé par Debye<sup>[17]</sup> :

$$\Phi_D = - \frac{1}{(4\pi\epsilon_0\epsilon)^2} \frac{\alpha \cdot \mu^2}{r^6}$$

avec  $\alpha$  : polarisabilité de la molécule non polaire ( $m^3$ ) ;  
 $\mu$  : moment dipolaire du dipôle permanent (Db).

### ***1.2.2.4. forces de dispersion (London)***

Les forces dispersives de London caractérisent les interactions entre deux dipôles induits. Sous l'effet d'un champ électrique créé par le voisinage d'une molécule, le nuage électronique de cette molécule peut se déformer temporairement, ce qui conduit à l'apparition d'un moment dipolaire temporaire induit. Ce moment dipolaire induit provoque alors l'apparition d'un moment dipolaire induit de la molécule voisine, il se forme ainsi une force attractive entre ces deux molécules. Cette interaction est fluctuante mais elle conduit à une attraction permanente.

L'expression du potentiel énergétique de dispersion est :

$$\Phi_L = - \frac{A}{r^6}$$

Plusieurs expressions de la constante A sont habituellement citées<sup>[9]</sup> :

- London :  $A_L = \frac{3}{2} \alpha_1 \alpha_2 I$       où       $\frac{1}{I} = \frac{1}{PI_1} + \frac{1}{PI_2}$

avec  $PI_1, PI_2$ : potentiels d'ionisation des molécules interagissantes (Db) ;  
 $\alpha_1, \alpha_2$  : polarisabilité des deux molécules ( $m^3$ ).

- Slater-Kirkwood :  $A_{SK} = \frac{3e\hbar}{4\pi\sqrt{m}} \left( \frac{\alpha_1 \alpha_2}{\sqrt{\alpha_1/N_1} + \sqrt{\alpha_2/N_2}} \right)$

avec  $e$  : charge de l'électron ( $e=1,602.10^{-19}$  C) ;

## **Resumé en Français**

---

c : vitesse de la lumière ( $c=2,99792 \cdot 10^8 \text{ m.s}^{-1}$ ) ;

m : masse de l'électron ( $m=9,109 \cdot 10^{-31} \text{ kg}$ ) ;

h : constante de Plank ( $h=6,626 \cdot 10^{-34} \text{ J.s}$ ) ;

$N_1, N_2$  : nombre d'électrons de la couche de valence.

- Kirkwood-Müller : 
$$A_{KM} = 6mc^2 \frac{\alpha_1 \alpha_2}{(\alpha_1/\chi_1) + (\alpha_2/\chi_2)}$$

avec  $\chi_1, \chi_2$  : susceptibilités magnétiques des deux molécules.

### 1.2.2.5. Potentiel global pour une surface apolaire

Le charbon actif étant reconnu comme généralement apolaire avec assez peu de sites en surface capables de créer des liaisons chimiques, les forces qui prédominent sont les forces de physisorption et spécialement celles de dispersion de London. Les forces attractives sont ainsi le plus souvent réduites au seul terme dispersif pour caractériser le potentiel attractif.

Pour une molécule située à une distance  $r$  de l'atome, en supposant que les contributions de répulsion et de dispersion s'ajoutent, le potentiel global s'exprime alors :

$$\Phi = -\frac{A}{r^6} + \frac{B}{r^{12}}$$

Cette relation est connue sous le nom de potentiel (12-6) de Lennard-Jones.

L'expression de la constante A la plus couramment utilisée est celle de London du paragraphe précédent.

### **1.2.3. Calcul théorique de l'enthalpie d'adsorption à faible recouvrement**

A faible recouvrement, tout effet d'interaction entre molécules adsorbées voisines peut être négligé. Une relation simple existe alors entre l'énergie potentielle moyenne d'une

$$\bar{\Phi} \approx \Delta H$$

molécule et la chaleur d'adsorption<sup>[9]</sup> :

Les forces de dispersion étant additives, il est alors possible de déduire l'énergie potentielle globale par intégration, en considérant toutes les positions possibles de la molécule adsorbée. En pratique, en considérant que les molécules sont majoritairement localisées autour de  $r_m$ , correspondant au potentiel minimum, l'approximation suivante est souvent retenue :

$$\bar{\Phi} = \Phi_{min} \approx \Delta H_{ads}$$

Suivant cette hypothèse, pour évaluer  $\Delta H_{ads}$  on recherche le minimum de la fonction  $\Phi$  d'une molécule adsorbée.

## ***Resumé en Français***

Pour déduire le potentiel global d'une molécule adsorbée située à une distance  $z$  de la surface, les contributions attractives et répulsives individuelles de chaque atome d'adsorbant sont évaluées, puis sommées.

Des approximations sont faites pour réaliser ce calcul. Par exemple, on considère le solide constitué d'un empilement de couches d'atomes. Pour chacune d'entre elles, on calcule séparément l'énergie potentielle avec une molécule d'adsorbat située à une distance  $z$  de la surface. On répète le calcul en faisant varier  $z$  et le niveau de la couche d'atomes d'adsorbant pour obtenir le profil normal du potentiel. La valeur minimale du potentiel global ainsi calculée, correspondant à une distance  $z_e$ , donne alors une bonne approximation de  $\Delta H_{\text{ads}}$ .

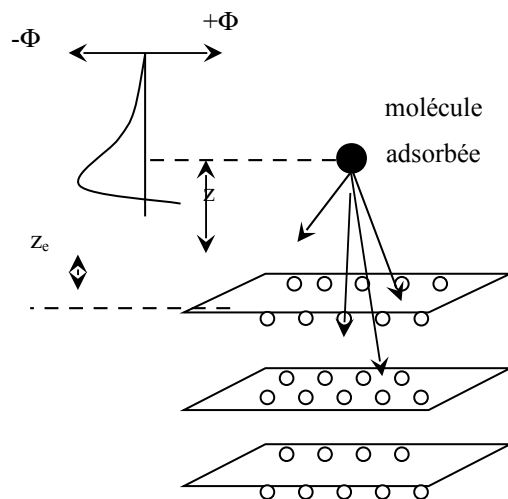


Fig. 3 :Diagramme schématique du potentiel énergétique d'une molécule approchant la surface d'un solide

Les calculs menés par Ross et Olivier sur l'adsorption de gaz rares sur du graphite montrent la concordance entre valeurs de potentiels calculées et enthalpies d'adsorption mesurées expérimentalement.

Notons que cette approche par le calcul n'a été validée que dans les conditions de faible recouvrement de la surface. Les phénomènes de condensation et les interactions possibles entre molécules adsorbées ne sont alors pas prises en compte.

## **Echauffement de lits de charbon actif**

Delage a émis l'hypothèse que le potentiel d'inflammation d'un filtre de charbon actif dépendait de trois facteurs :

## **Resumé en Français**

---

- La température à laquelle les composés organiques peuvent se décomposer en sous-produits de réaction.
- La température d'oxydation des charbons actifs.
- La température d'auto-inflammation du composé.

Par exemple dans le cas de la 3-méthylbutan-2-one, pour une concentration de 150 g.m<sup>-3</sup>, Delage observe une hausse de température de 450 °C en moins de 30 secondes. L'élévation de température devient alors supérieure à la température d'oxydation du charbon actif (comprises entre 200 et 400°C) et le lit s'enflamme. L'hypothèse émise est que l'échauffement provient de l'oxydation de la 3-méthylbutan-2-one en hyperoxydes qui se décomposent alors en acides acétiques, acétaldéhydes et butan-2,3-dione. Or ces réactions sont très énergétiques puisque les chaleurs de réactions sont généralement supérieures à 200 kJ.mol<sup>-1</sup>.

### **UTILISATION :**

Les charbons actifs sous différentes formes sont utilisés dans un but adsorbant pour réduire les polluants de rejets industriels. Certains des gaz filtrés sont les chlorofluorocarbones dans les rejets de mousse, vapeur d'essence ainsi que SO<sub>2</sub> qui provient des fumées. On les utilise pour le traitement des rejets de vapeur de solvant dans des industries comme des fabriques de papier, peinture ou métal, et également pour traiter les effluents biochimiques des unités de fermentation. Ils trouvent une utilisation importante au niveau du matériel de protection comme les masques à gaz utilisés au niveau militaire et industriel.

Leurs applications interviennent dans le traitement des eaux et rejets. Ils sont utilisés pour enlever goûts, odeurs, et matières organiques dans l'eau de consommation.

Les charbons actifs sont également utilisés comme support de catalyseurs pour beaucoup de réactions industrielles importantes ainsi qu'en tant que supports pour d'autres matériaux.

### **Oxydation des charbons actifs – risques d'inflammation**

L'intérêt  
pour

l'oxydation et l'inflammation caractéristique des charbons actifs a gagné en importance suite

## ***Resumé en Français***

---

à plusieurs accidents qui se sont produits au cours de leur transport, stockage et de leur utilisation dans les filtres.

### **INFLAMMATION**

Les différents cas d'accidents du à l'inflammation imprévue de charbon actifs sont présentés dans les paragraphes suivants.

#### ***TRANSPORT :***

Six accidents liés au transport de charbons actifs en container par bateau se sont produits durant la période de mai 1962 à mai 1963, ces incidents ont eu lieu en moyenne 3 à 4 semaines après le chargement des charbons actifs. Ces accidents semblent être dus au processus d'auto inflammation des charbons actifs. L'exposition permanente de ces charbons à l'air entraîne une oxydation lente qui conduit à la chauffe du matériau et peut déboucher sur une inflammation. A la suite de ces accidents, des tests ont été élaborés pour garantir le contrôle et la sécurité du transport du charbon actif.

#### ***STOCKAGE***

Des accidents se sont également produits sur des lits de charbon au repos. Par exemple dans une usine de produits chimiques industriels (Vierzon 27/09/2003) les housses en polyéthylène d'un stock de charbons actifs se sont enflammés. Le stockage des charbons se faisait en extérieur, le feu s'est répandu à une centaine de big-bags de charbons actifs, 51 tones de charbon actif ont été détruites et le coût s'élève à 7 Keuros de pertes (*source www.aria.ecologie.gouv.fr*)

#### ***LITS ADSORBANTS EN SERVICE***

Le processus d'adsorption est exothermique par nature, la température des charbons augmente rapidement surtout si la concentration en COV est importante. L'inflammation des charbons actifs est toujours due à une augmentation de la température du matériau non contrôlée (*F. Delage* ). Le premier accident de combustion de lit de charbon s'est produit dans une petite unité avec un charbon dont l'origine était la noix de coco qui servait à récupérer du cyclohexane à la fin des années 1940. (*Roy Sanders* ). Les feux sont principalement dus à une utilisation des matériaux absorbants pour des conditions dans lesquelles la chaleur

## **Resumé en Français**

---

d'oxydation dépasse la chaleur perdue par le système de refroidissement. Certains débuts d'oxydation se font à basses températures, ceci dépend de la nature du matériau d'origine.

### **CARACTÉRISATION EXPÉRIMENTALE DE LA RÉACTIVITÉ DES CHARBONS ACTIFS :**

Des travaux de recherche ont été réalisés pour améliorer la sécurité et éviter les inflammations de charbons. Différentes procédures de caractérisation de l'oxydation et de l'inflammation des charbons actifs ont été proposées. L'un des tests standards existant consiste à soumettre le matériau mis sous la forme d'un panier cubique de dimensions 10 cm à 140°C. Si l'inflammation spontanée du matériau est observée, cela indique qu'il n'est pas sécuritaire de le transporter dans un container de 3 m<sup>3</sup>, s'il ne brûle pas on peut le transporter ou le stocker dans un container de taille plus grande. (*Jones J.C.*)

Afin de comparer la réactivité à l'air de différents charbons actifs, *Suzin et al* ont mis en évidence deux températures caractéristiques. Le PIO (Point of Initial Oxydation), est la température minimale au delà de laquelle on observe un phénomène exothermique qui résulte de la transformation chimique partielle des composés oxygénés de surface du charbon actif. Le SIT (Spontaneous Ignition Temperature) est la température d'inflammation du matériau, qui s'accompagne la gazéification du carbone solide en dioxyde de carbone.

Ces deux températures caractéristiques peuvent être déterminées par analyse thermogravimétrique couplée à une calorimétrie différentielle à balayage. Les mesures réalisées permettent de déterminer le flux de chaleur dégagé et la perte de masse en fonction de l'augmentation de la température du matériau.

### **Mécanismes d'oxydation et d'inflammation**

Le paragraphe suivant explique les mécanismes d'oxydation et d'inflammation des charbons actifs. Basé sur des études sur l'exothermicité des charbons actifs à base de bois [Johnson and woods, 1971] et sur les charbons actifs [Cameron, 1971], il a été admis pendant une longue période de temps que le réchauffement est principalement une conséquence de l'oxydation du carbone. Cette oxydation est relativement lente et diffère de l'adsorption rapide d'oxygène par des charbons récemment préparés et exposés à l'oxygène. L'oxydation des composés organiques aussi introduit une hausse de température, qui accélère les vitesses de réaction,

## ***Resumé en Français***

---

quand la température est assez haute; le carbone lui-même commence à être oxydé et contribue aux nouvelles augmentations de température. Les points chauds sont d'abord développés dans le lit des charbons actifs. L'inflammation arrive quand l'oxygène suffisamment adsorbé se transformer en complexes oxygénés. Les points chauds, causent l'oxydation rapide du carbone avec la libération de monoxyde de carbone (CO) et di oxyde de carbone (CO<sub>2</sub>).

Les mécanismes d'oxydation et d'inflammation sont étudiés selon deux cas de figure, soit en présence d'air soit en présence de Composés Organiques Volatiles.

### **Etude de l'oxydation en présence d'oxygène**

Le processus d'oxydation à basse température est un phénomène complexe qui a lieu dans les conditions ambiantes de température jusqu'à une température de environ 300 °C. Parmi les matériaux carbonés, on explique bien l'oxydation basse température des charbons. Abondante littérature est disponible sur les processus d'oxydation à basse température du charbon, mais les mécanismes pour les charbons actifs ne sont pas très écrits et connus.

En littérature [Wang et al., 2003] l'oxydation et l'inflammation de matériaux carbonés poreux comme les charbons actifs en présence d'oxygène généralement dépeints sont selon les étapes suivantes:

1. Transport d'oxygène de l'environnement jusqu'à la surface du matériau carboné. Le transfert d'oxygène a lieu ici au niveau du film entourant la particule par le transfert massif convectif et ensuite par le processus de diffusion dans le film.
2. L'étape de diffusion où l'oxygène pénètre dans les pores des charbons actifs.
3. L'interaction de l'oxygène avec la surface suivie la formation de complexes intermédiaires, d'émission de chaleur et des produits gazeux.
4. L'oxydation rapide et réactions de décomposition menant à l'inflammation du matériau.

### **La consommation d'oxygène**

L'étape principale du processus d'oxydation est la consommation d'oxygène. L'oxygène consommé est alors converti en produits d'oxydation. L'oxygène peut être physiquement ou chimiquement adsorbé sur la surface des charbons actifs. L'adsorption physique est semblable à celui du processus de condensation, ici les molécules d'oxygène sont castrées à la surface par les forces d'attraction faibles (interactions de van der Waals) et ils peuvent facilement être enlevés de surface. L'adsorption physique aboutit à la formation d'une ou de plusieurs

## ***Resumé en Français***

---

couches de molécules adsorbées et la chaleur d'adsorption est du même ordre que la chaleur de vaporisation.

Au contraire, le processus de chimisorption implique des forces plus élevées sont beaucoup plus fortes. Seulement certains sites particuliers en surface interne des pores peuvent attirer les molécules d'oxygène et les tenir par les forces de valence entre les atomes [Hayward *et al.*, 1964]. Les processus de chimisorption sont limités à la monocouche des molécules et la chaleur de chimisorption est relativement plus haute que celle de physisorption. Les matériaux comme les charbons actifs possèdent des structures plus désordonnées qui aboutissent à la grande propension pour la chimisorption de l'oxygène. Les bords des charbons actifs contiennent des atomes de carbones non saturés, qui forment les sites pour l'attachement des hétéro atomes et jouent ainsi un rôle significatif dans la chimisorption. Le taux d'assimilation d'oxygène à la température ambiante est très lent et peut être analysé en mesurant la masse gagnée avec le temps [Itay *et al.*, 1989].

Des régimes de réaction différents peuvent dominer la consommation d'oxygène selon le processus de transfert de masse et les propriétés physiques et chimiques. Ces régimes incluent la diffusion externe, la diffusion interne et des réactions chimiques. Le transport de masse externe d'oxygène peut être le facteur limitant notamment un film d'eau est trouvé sur la surface de particule.

Les régimes de réaction sont imposés par la taille de particule. Pour de grandes particules, la vitesse d'oxydation est contrôlée par la diffusion d'oxygène dans les pores. Quand la taille de particule est très petite, la vitesse de réaction est principalement chimiquement contrôlée, comme l'oxygène se répand profondément dans les pores de charbon y créant une concentration du gaz égale dans la phase dense. Le régime de réaction est caractérisé par l'indépendance apparente du taux de consommation d'oxygène avec la taille de particules.

### **Les mécanismes réactionnels et produits d'oxydation**

Les produits principaux de l'oxydation de matériaux carbonés sont les oxydes de carbone et l'eau. Différents auteurs ont proposé différents mécanismes des réactionnels pour le processus d'oxydation avec l'air. Ces mécanismes sont basés sur les produits formés et les conditions de

## ***Resumé en Français***

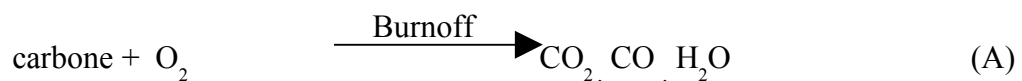
---

température et la pression. Les réactions d'oxydation ont été largement étudiées pour des matériaux carbonés comme le charbon et étendus à d'autres matériaux aussi. Ils sont regroupés en deux réactions parallèles principales: la direct burnoff réaction et la réaction de sorption.

### *1. La Direct burn off reaction*

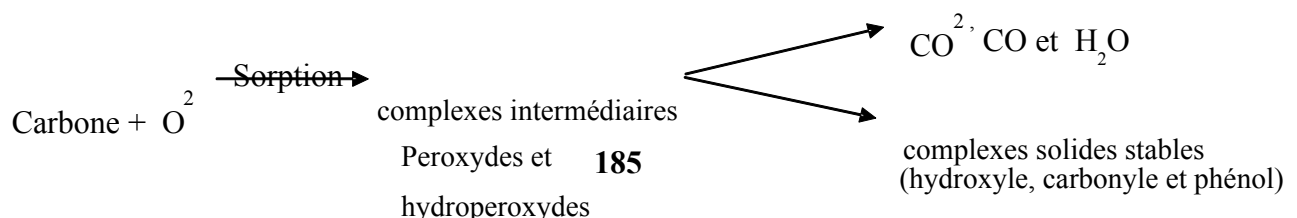
La réaction a été largement décrite en littérature, mais aucune preuve directe n'est citée pour confirmer le mécanisme. Wang et al. [2003] a soutenu le mécanisme de direct burn off réaction sur la base des preuves expérimentales conduites en comparant les taux de production d'oxydes carboniques du processus d'oxydation et des expériences de désorption en utilisant un réacteur de flux isotherme.

Le conclusion de ses travaux c'est la présence d'oxygène commence non seulement la réaction de chimisorption, mais aboutit aussi à la présence du direct burn off réaction. La réaction suggérée ressemble à celle de la combustion directe des carburants solides, qui ont lieu aux températures aussi hautes que 300 °C. Les prévues des mécanismes n'ont pas encore été apportes. Le direct burn off réaction est présenté dans l'équation A.



### *2. Réactions de sorption*

Le processus de chimisorption d'oxygène a lieu dans les pores des matériaux carbonés pour former des complexes instables d'oxygène. Les intermédiaires instables peuvent être des peroxydes et ou des hydro peroxydes. La décomposition des complexes oxygénés instables a lieu avec la libération des oxydes de carbone et l'eau ou la formation de fonctions stables comme les hydroxyles (OH), les carboxyles (-COOH) ou des groupes de phénoliques. Ces groupements oxygénés stables sont dégradés à la température élevée. Il ya une certaine quantité de chaleur exothermique est dégagée pendant la décomposition de ces complexes stables.

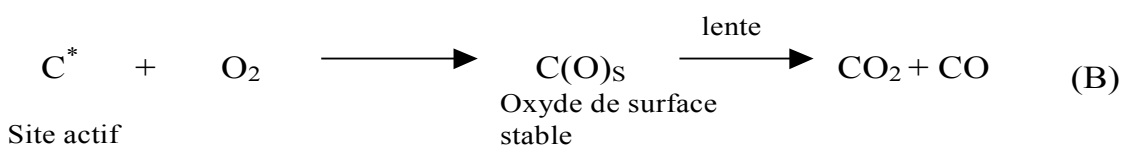


### **Etapes réactionnelles dans une séquence de chimisorption**

La chimisorption commence par la formation de complexes intermédiaires comme des peroxydes suite à une réaction entre la molécule d'oxygène et un centre carbonique libre. Ces complexes intermédiaires sont des espèces fortement instables et se décomposent en d'autres produits dans une courte période de temps. Ces espèces peuvent être détectées par des techniques comme la titration, bien que les résultats restent toujours un point de discussion. Les peroxydes formés sont convertis en hydro peroxydes (-O-O-H) avec le déplacement d'atome hydrogène de l'aliphatique ou la structure aromatique [Kudynska et Buckmaster, 1996]. Cette étape est confirmée par l'énergie de dissociation d'environ 377 kJ/mol qui est semblable à l'énergie de clivage de la liaison C-H [Nelson, 1989].

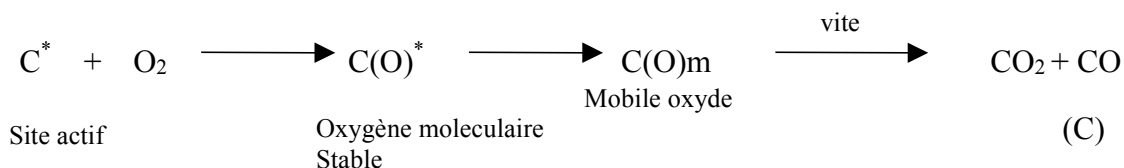
La formation d'hydro peroxydes est suivie par le déplacement du radical pour former un hydroxyle (OH) et des groupes d'éther (C-O-C) [Liotta et al., 1983]. Le carboxyle et l'aldéhyde peuvent être les produits de la décomposition thermique de l'espèce hydroxyle [Clemens et al., 1991] ou par la thermolyse des hydro peroxydes [Gethner et al., 1985]. Dans l'ensemble il y a trois groupes fonctionnels principaux, OH (hydroxyle), carbonyle (C=O) et le carboxyle (COOH) et on pense que ceux-ci peuvent être formés des peroxydes (-O-O-). Plusieurs chercheurs ont proposé des mécanismes différents pour l'évolution des produits d'oxydation à savoir ce di oxyde de carbone (CO<sub>2</sub>), mon oxyde de carbone (CO) et l'eau (H<sub>2</sub>O) comme produits de décomposition des complexes oxygénés solides.

Certains ont suggéré que les oxydes carboniques étaient directement formés des hydro peroxydes à basse température par un processus de thermolyses. Bradbury et Shafizader, [1980] ont expliqué le mécanisme impliquant la chimisorption de l'oxygène menant à l'inflammation dans des matériaux cellulosiques avec l'aide de sites actifs. Les auteurs ont proposé deux mécanismes de réaction semblables à la séquence de sorption décrite par l'équation B et l'équation C.



## *Resumé en Français*

---



Selon les auteurs, les matériaux cellulaires subissent l'oxydation directe aux basses températures et les réactions sont très lentes. Le premier processus décrit dans eq. (B) représente la formation d'un oxyde de surface plutôt stable par chimisorption à un site actif et suivie par une désorption lente pour donner le di oxyde de carbone ( $\text{CO}_2$ ) et le monoxyde de carbone (CO). Il peut nécessiter jusqu'à 1000 °C pour la réaction de désorption dans la condition inerte du gaz. Le deuxième processus eq. (C) représente un oxyde mobile de durée de vie très courte par une réaction d'oxygène moléculaire stabilisée qui est responsable de la majorité des gaz carboniques d'oxydes formés pendant la combustion. Quand le gaz d'oxygène a été remplacé par l'air dans les expériences, les taux de chimisorption ont été réduits par un facteur de 5 et les températures d'inflammation ont été augmentées par 100 °C.

A part la formation de groupements oxygénés de surface par l'interaction avec l'oxygène dans l'air, certains groupements oxygénés de surface sont déjà présents dans les matériaux de carbons actifs. Ces groupes peuvent agir directement avec l'oxygène dans l'air pour donner les produits d'oxydation qui sont le plus généralement trouvé dans ce carbone chimiquement activé préparé récemment [Cameron et Macdowall, 1972]. L'existence d'un grand nombre de sites de réaction et de possibles mécanismes indique la complexité du processus d'oxydation des carbons actifs.

### **Mécanisme d'oxydation et réactions d'inflammation en présence des COV**

L'oxydation et l'inflammation du charbon actif en présence de composés organiques volatiles ont lieu plus rapidement que l'interaction avec l'oxygène. La réactivité dépend de la nature du carbone actif et le type des composés organiques volatiles. La chaleur libérée pendant les réactions d'adsorption est supérieure à 200 kJ.mol<sup>-1</sup> et peut aller jusqu'à 1000 kJ.mol<sup>-1</sup>. De telles hautes valeurs de chaleur exothermiques rendent les carbons actifs susceptibles pour des réactions d'inflammation.

## *Resumé en Français*

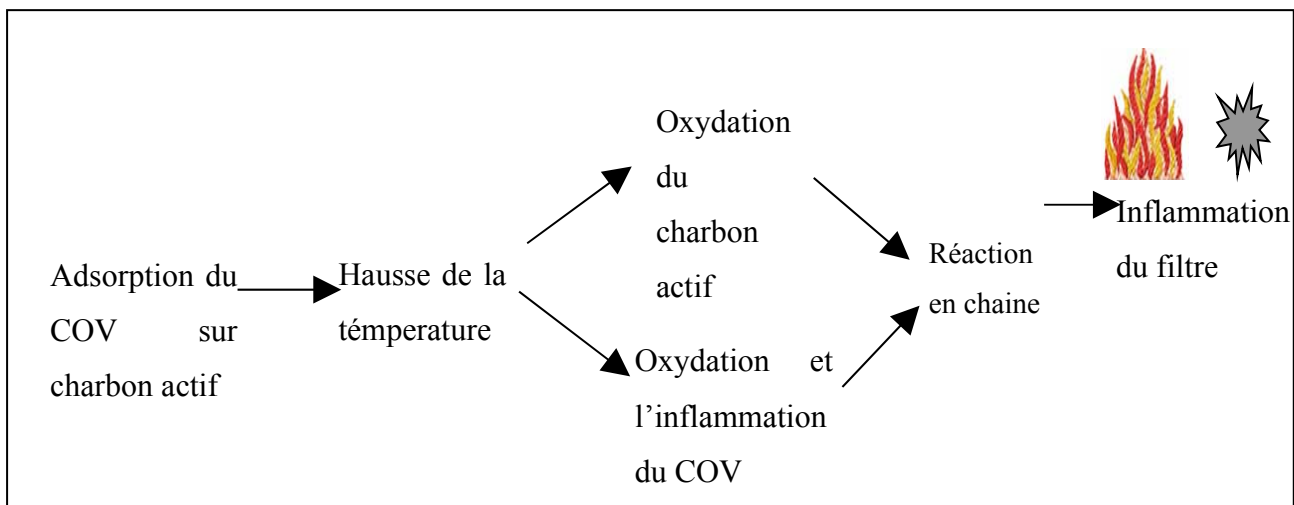


Figure A : Séquence menant à l'inflammation d'un filtre de charbon actif

Delage, [2000] a étudié largement l'influence de la nature de composés organiques volatiles sur l'oxydation et l'inflammation des charbons actifs en présence de composés organiques volatiles comme montrés dans la Figure A. Deux cas de réaction sont possibles pour les réactions d'inflammation des charbons actifs. Si la température d'auto-inflammation du composés organiques volatiles est inférieure la température d'oxydation du charbon actif, l'inflammation du composés organiques volatiles a lieu d'abord, qui est suivie par l'inflammation du matériaux. L'exemple pour ce type de mécanisme peut être rencontré dans les mélanges de composés organiques volatiles contenant des cétones comme le méthyléthylcétone et le méthylisobutylcétone sur des charbons actifs où ils ont une température d'oxydation inférieure à 120 °C. Les cétones aromatiques sont plus facilement oxydées que les aliphatiques et la réactivité des cétones peut être baissée en le mélangeant avec des composés organiques volatiles moins réactifs [Akubuiro et Wagner, 1992].

Le deuxième facteur qui influence la réactivité est la nature du charbon actif. Dans ce cas la température d'oxydation du charbon actif moins que la température d'auto-inflammation du composés organiques volatiles. Ce type de comportement est trouvé pour les hydrocarbures, amines, halogènes et alcools adsorbés sur des charbons actifs à base de noix de coco. Par exemple l'oxydation des charbons actifs à base de noix coco (environ 210 °C) est moins importante que la température d'inflammation de solvant. Aussi quand un composés organiques volatiles est utilisé avec le type différent de carbones activés, les différences de température d'oxydation sont observées que l'on peut expliquer par le fait que les groupements

## **Resumé en Français**

oxygénés de surface de l'adsorbant peuvent prendre le rôle d'un catalyseur dans ce cas [Delage, 2000].

### **18.1.0.0.1 Approche des mécanismes des réactionnels d'oxydation**

Akubuiro, [1993] a proposé un mécanisme de l'identification des produits d'oxydation. Les démarques de réaction par l'attaque d'une molécule d'oxygène sur le carbone en alpha de la méthyléthylcétone. Le carbone alpha se réfère au premier carbone attaché au groupe fonctionnel et dans notre cas c'est le carbonyle et il forme l'alpha-hydroperoxyde méthyléthylcétone (le produit II). En présence d'un oxydant fort, une rupture du C-C et O-O aboutit à la formation d'acétaldéhyde (le produit III) et d'acide acétique (le produit IV) . La présence d'une atmosphère humide ou de base, l'hydroperoxyde se transforme en 2,3 butanedione (le produit V) et l'eau. Il y a d'autres réactions possibles : la 2,3 butanedione peut former l'acide acétique et l'acétaldéhyde. Les produits à savoir le dioxyde de carbone, le monoxyde de carbone et la vapeur d'eau sont formés par la nouvelle oxydation aboutissant à la combustion du système. Tout au-dessus des réactions sont fortement exothermiques. La chaleur de réaction a été mesurée des charbons actifs comme Calgon BPL et sur Sobonorit B4 saturés en méthyléthylcétone et sont trouvés entre 310 et 620 kJ mol<sup>-1</sup> respectivement.

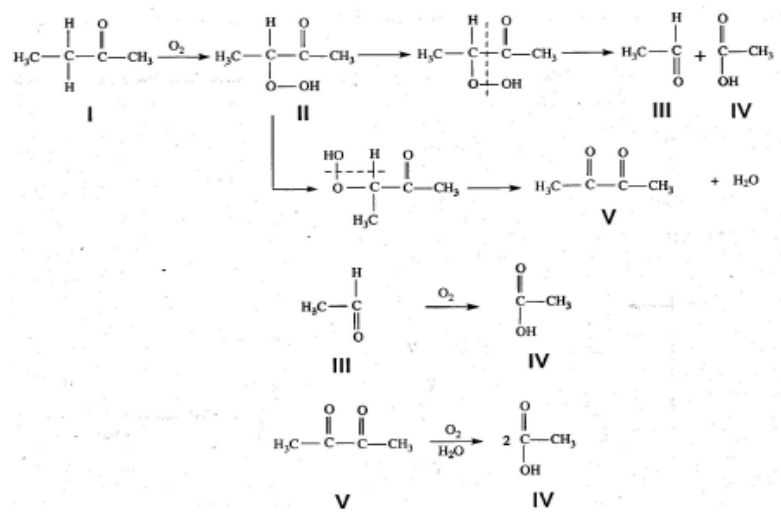


Figure B : Mécanisme probable d'oxydation de la méthyléthylcétone (Akubuiro, 1993).

### **Le mécanisme de réaction pour le cyclohexanone**

Comme la réaction de méthyléthylcétone, l'oxydation de cyclohexanone commence par la réaction d'un carbone pour former l'alpha-hydroperoxyde de cyclohexanone (le produit II) et

## **Resumé en Français**

se décompose ensuite en 1, 2-cyclohexanedione (le produit III), 2-hydroxycyclohexanone (le produit IV qui existe comme un dimère). Il peut former aussi l'aldéhyde adipique (le produit V) et l'acide adipique (le produit VI). Hening et al., [1989] ont proposé de plus la formation de la cyclopentanone, le phénol et le dibenzofurane. L'importante caractéristique de ces réactions est la libération d'un important flux de chaleur d'environ 2200 kJ mol<sup>-1</sup> pour le système des carbons actifs/composés organiques volatiles notamment cyclohexanone/calgon BPL et cyclohexanone/Sobonorit B4. Le flux chaleur produit pour le cyclohexanone est supérieur à celui du système méthyléthylcétone.

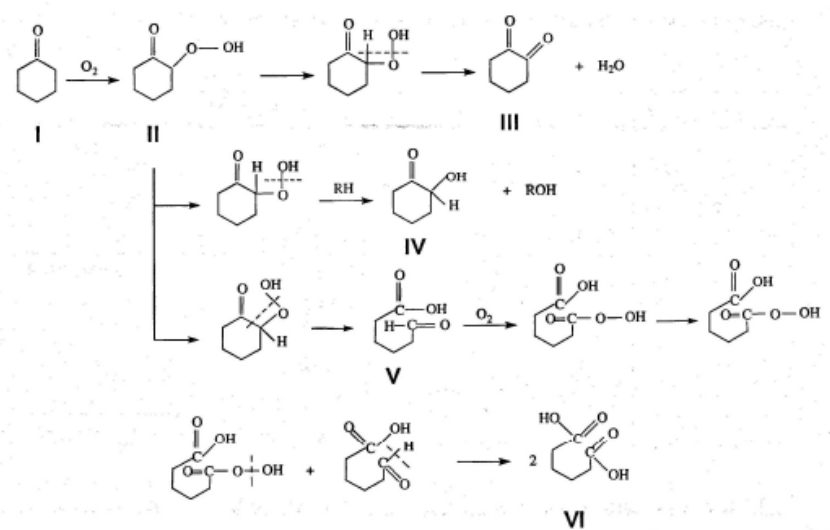


Figure C : Mécanisme probable d'oxydation de la cyclohexanone (Akubuiro, 1993).

## **Conclusions**

La revue bibliographique donne d'abondantes informations sur les matériaux de carbons actifs, les incidents thermiques associés et une vue d'ensemble de l'oxydation et les mécanismes d'inflammation avec les divers facteurs les influençant.

Les caractéristiques du charbon actif comme la composition chimique, la texture et la structure des carbones activés sont complexes et variées. Elles dépendent principalement de l'origine des matériaux utilisés ainsi que du mode d'activation employé. Pendant leur processus industriel de fabrication, les carbons chimiquement activés sont soumis à de plus basses températures que les carbons physiquement activés.

## ***Resumé en Français***

---

Les différents incidents thermiques dans des industries utilisant des charbons actifs ont été aussi évalués. La majorité des accidents a été associée aux composés organiques volatiles pendant leur adsorption ou à l'introduction de l'air dans le système de charbons actifs saturés en composés organiques volatiles. Les incendies ont été aussi observés pendant le transport de charbons actifs en raison de leur réactivité avec l'oxygène de l'air, ceci est principalement rencontré pour les charbons chimiquement activés et pour les charbons actifs récemment préparés.

Les mécanismes d'oxydation et d'inflammation des charbons actifs principalement par l'action de composés organiques volatiles et l'air ont été étudiés. Les groupements oxygénés de surface et la structure poreuse jouent un rôle important dans l'oxydation et les réactions d'inflammation avec des réactions de formation des complexes instables, et la libération de la chaleur et des produits d'oxydation. D'autre part, ce phénomène d'adsorption de composés organiques volatiles sur les charbons actifs dégagent de la chaleur en raison de leur phénomène d'adsorption. Concernant les différentes méthodes trouvées dans la littérature pour l'étude d'oxydation et les propriétés d'inflammation des charbons actifs, les résultats expérimentaux dépendent de la condition dans laquelle les essais ont été exécutés. Quoique l'American Society for Testing and Matériels ASTM D3466-76 soit les plus proches des températures prévalant en réalité, la déviation existait toujours et de là les expériences faites dans les conditions réelles d'application qui sont très difficiles à réaliser à l'échelle de laboratoire.

## **CHAPTER-3**

### **ETUDE EXPERIMENTALE**

Pour étudier les caractéristiques thermiques et les propriétés des charbons actifs, des procédures expérimentales ont été mise en oeuvre. Ce chapitre décrit les méthodes expérimentales pour la caractérisation des différentes propriétés des charbons actifs. La première partie décrit le choix des échantillons des charbons actifs utilisés pour l'étude avec les détails de fabrication et origine. La deuxième partie se concentre sur les différentes techniques de caractérisation avec l'instrumentation, la théorie, la méthodologie expérimentale et les procédures de calcul. La caractérisation des matériaux constitue en quatre parties principales. La première partie est sur l'étude d'analyse thermique pour déterminer l'oxydation et l'inflammation des échantillons des charbons actifs. Il est principalement abordé de l'utilisation de la thermogravimétrie couplée avec la calorimétrie différentielle (ATG - DSC).

La deuxième partie consiste en l'étude des propriétés de porosité par des mesures utilisant principalement l'adsorption de l'azote N<sub>2</sub> et des techniques de porosimétrie de mercure. La troisième partie se concentre sur la composition chimique des échantillons des charbons actifs et l'analyse de la teneur en cendre. La composition chimique est étudiée utilisant la titration de Boehm et les méthodes d'analyse élémentaires, tandis que l'analyse de teneur en cendre est étudiée par l'utilisation de méthode de American Society for Testing and Materials (ASTM) et par Microscopie Electronique à Balayage MEB-X. La partie finale de ce chapitre décrit les caractéristiques structurelles analysées utilisant la Microscopie Électronique à Transmission de Haute Résolution (METHR) et le Microscopie Électronique à Balayage (MEB).

L'objectif de cette étude est de mesurer les caractéristiques des échantillons de charbons actifs et ensuite analyser et étudier leur influence sur les propriétés d'oxydation et l'inflammation.

## ***Resumé en Français***

---

19 échantillons de charbons activés et non activés sont utilisés pour l'étude. Ils sont choisis selon l'origine des matériaux, le mode d'activation, la composition chimique et les caractéristiques poreuses. Les origines des matériaux sont la noix coco, le bois, le tourbe, le charbon, le Brai (Coal Tar Pitch) et de PAN(Polyacrylonitrile). Les échantillons sont commerciaux préparés en grandes quantités dans l'industrie ou préparés à petite échelle en laboratoire.

### **Les charbons activés physiquement**

Les échantillons des charbons activés physiquement utilisés pour cette étude ont été obtenus par carbonisation suite à la activation utilisant la vapeur à 800-1000 °C. La base polymère physiquement activé a été préparée en mélangeant le polyacrylonitrile PAN et le brai (Coal Tar Pitch) CTP, carbonisés à 520 °C pendant 2 heures et activés par la vapeur d'eau à 800 °C. Les numéros dans l'extension des noms indiquent la quantité de chaque constituant utilisé dans le mélange. Par exemple, l'échantillon CTP-PAN-3:1-a contient 75 % de CTP et 25 % de PAN dans le mélange et la lettre A indique que l'échantillon est activé.

Des échantillons carboniques activés imprégnés avec des métaux comme le cuivre et le chrome ont été aussi choisis pour cette étude. L'objectif est d'étudier l'influence du métal déposé sur les caractéristiques d'oxydation et l'inflammation. Les échantillons physiquement activés à base de noix de coco indiqués avec la lettre NC et le suffixe Cu et Cr représente des charbons actifs imprégnés.

### **Les charbons activés chimiquement**

L'activation chimique a été exécutée en utilisant une solution concentrée de H<sub>3</sub>PO<sub>4</sub>. Les variations de température pour l'activation chimique des échantillons carbonés sont entre 450 - 600 °C. Par exemple la température d'activation pour l'échantillon BC - 120 est environ 450 °C et pour l'échantillon de GF - 40 est du 600 °C.

### **Les échantillons carbonisés**

Les échantillons carbonisés bruts sont aussi choisis pour l'étude. Ces échantillons ne sont pas activés, mais ont été chauffés à 800-1000 °C dans un gaz inerte. La principale raison du choix de ces échantillons est de nous permettre de comparer les caractéristiques entre des

## *Resumé en Français*

---

Echantillons	Fournisseur	Matière première	Mode d'activation	Agent d'activation
NC-50	PICA	Noix de coco	Physique	Vapeur d'eau
NC-60	PICA	Noix de coco	Physique	Vapeur d'eau - 900 °C
NC-100	PICA	Noix de coco	Physique	Vapeur d'eau - 900 °C
RB-2	NORIT	Tourbe	Physique	Vapeur d'eau
BPL	CHEMVIRON	Charbon	Physique	Vapeur d'eau
GF-40	NORIT	Noyaux d'olive	Chimique	H <sub>3</sub> PO <sub>4</sub>
BC-120	PICA	Bois	Chimique	H <sub>3</sub> PO <sub>4</sub> - 450 °C
PICABIOL	PICA	Bois	Chimique	H <sub>3</sub> PO <sub>4</sub>
NC-70-Cu	PICA	Noix de coco	Physique	Vapeur d'eau
NC-70-CuCr	PICA	Noix de coco	Physique	Vapeur d'eau
CTP-A	LCSM Nancy	Brai de coke	Physique	Vapeur d'eau - 800 °C
CTP-PAN-3 :1-A	LCSM Nancy	Brai de coke et polyacrylonitrile	Physique	Vapeur d'eau - 800 °C
CTP-PAN-1 :1-A	LCSM Nancy	Brai de coke et polyacrylonitrile	Physique	Vapeur d'eau - 800 °C
PAN-A	LCSM Nancy	Polyacrylonitrile	Physique	Vapeur d'eau - 800 °C
PAN-C	LCSM Nancy	Polyacrylonitrile	Non-activé	-
CTP-PAN-3 :1-C	LCSM Nancy	Brai de coke et polyacrylonitrile	Non-activé	-
CTP-C	LCSM Nancy	Brai de coke	Non-activé	-
CTP-PAN-1 :1-C	LCSM Nancy	Brai de coke et polyacrylonitrile	Non-activé	-
Noix de coco carbonisé	PICA	Noix de coco	Non-activé	-

échantillons des charbons activés et non activés. Les échantillons choisis incluent des échantillons carbonisés avec l'extension 'C'.

Tableau A : Echantillons des charbons actifs choisi pour cette étude.

Les charbons actifs sélectionnés sont analysés pour obtenir leurs différentes caractéristiques physico-chimiques et structurales. La porosité des charbons actifs a été mesurée à partir des isothermes d'adsorption d'azote à la température de 77 K. La surface spécifique est déterminée par la méthode de BET, le volume de micropore par la méthode de t-plot et la DFT (Density Functional Theory) permet d'accéder aux distributions poreuses des charbons actifs.

La composition chimique des charbons est caractérisée en utilisant les techniques d'analyse élémentaires donnant la teneur en carbone, hydrogène, azote et le teneur en oxygène. En plus de ceux-ci, le teneur de cendre des carbones activés a été mesuré en utilisant la méthode American Society for Testing and Materials (ASTM), en effet la littérature montre qu'il ya une influence des cendres sur les propriétés d'oxydation et l'inflammation des charbons actifs. Finalement, la caractérisation structurale et nano-structurale a été étudiée en utilisant la Microscopie Électronique à Transmission de Haute résolution (METHR) et la Microscopie Électronique à Balayage (MEB) donnant les caractéristiques qualitative et quantitative des données structurales.

L'utilisation de la calorimétrie différentielle à balayage dans des conditions données produit des résultats qui sont représentatifs des propriétés intrinsèques de l'échantillon. L'inconvénient de cette technique est que les conditions réelles de fonctionnement de l'adsorber ne sont pas prises en compte ; les résultats obtenus ne sont donc pas forcément extrapolables et ils sont généralement surestimés [Suzin *et al.*, 1999]. L'ASTM (American Society for Testing and Materials, 1993) propose pour déterminer ces températures d'oxydation, de balayer un filtre (25 mm de diamètre et 25 – 75 mm de hauteur) par de l'air (vitesse de 50 cm.s<sup>-1</sup>) soumis à un programme de chauffe de 10 °C.min<sup>-1</sup> jusqu'à une température de 150 °C. Au delà, cette vitesse est réduite entre 2 et 3 °C.min<sup>-1</sup>. Toutefois, Suzin *et al.*, 1999 montrent qu'il est plutôt recommandé d'effectuer un suivi dynamique de l'évolution de la température avec les conditions opératoires de l'application.

## **Resumé en Français**

L'étude de l'oxydation et l'inflammation des charbons actifs ont été faite par calorimétrie différentielle à balayage couplée à un analyseur thermogravimétrique. Cette technique permet d'enregistrer deux types de mesures par le couplage d'un thermogravimètre et d'un calorimètre différentiel. Une unité de gestion permet d'acquérir les données suivantes :

- La masse de l'échantillon en fonction du temps et à une température donnée ;
- Le flux de chaleur dégagé ( $\Phi_C$ ) en fonction du temps et à une température donnée.

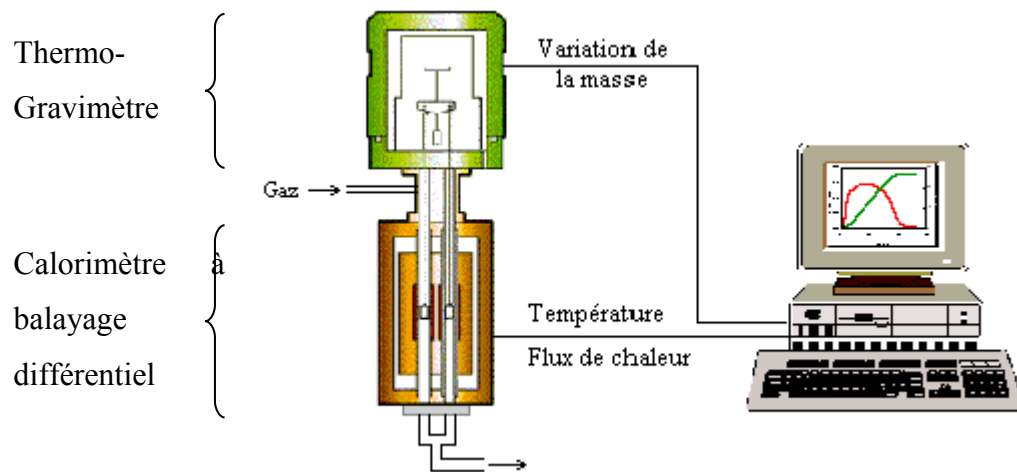


Figure.D : Schéma de l'appareil de mesure Thermogravimètre et Calorimètre à balayage différentiel

### **Thermogravimètre : la microbalance Setaram B111**

Le principe de fonctionnement de cette microbalance repose sur un mécanisme à fléau. La force nécessaire à l'équilibrage de la balance, référence et échantillon, est une transposition de la masse mesurée. Le fléau est asservi une position constante par le procédé d'équilibrage suivant :- un volet optique à fente solidaire du fléau occulte partiellement le faisceau d'une source lumineuse qui éclaire deux photocellules fixes. Le support de ce volet est muni de deux aimants permanents à haute stabilité dont les extrémités plongent dans quatre solénoïdes fixes.- un amplificateur reçoit le signal des photocellules, le courant de sortie de cet amplificateur circule dans les solénoïdes produisant sur les aimants une force qui maintient le fléau en position d'équilibre.La variation de masse est proportionnelle à la variation du courant lors de l'équilibrage électromagnétique.

### **Le calorimètre à balayage différentiel Setaram DSC111**

## ***Resumé en Français***

---

Désignée en anglais sous le terme Differential Scanning Calorimetry (DSC), la calorimétrie différentielle à balayage repose sur le principe de la calorimétrie à compensation de puissance. L'échantillon et la référence sont pourvus chacun d'éléments chauffants spécifiques. Le système comprend deux boucles de contrôle ; la première sert à programmer une augmentation de température de l'échantillon ou de la référence à une vitesse donnée et la seconde boucle permet d'ajuster la puissance d'entrée lorsqu'un déséquilibre thermique se produit entre l'échantillon et la référence.

### **Procédure Expérimentales**

#### *Préparation des échantillons*

Les échantillons sont d'abord écrasés et tamisés pour enlever l'influence de la taille de particules sur la réactivité des charbons actifs et maintenir l'uniformité des particules. Le diamètre moyen des particules est de 50 µm. Environ 3-5 mg de l'échantillon écrasé sont chargés dans le creuset du calorimétrie différentiel à balayage et le débit du gaz est maintenu autour de 1 L/h et avec une vitesse d'échauffement de 5 K.min<sup>-1</sup> [Suzin et al., 1999]. Le gaz utilisé pour l'essai d'oxydation contient 79 et 21 pourcentages d'hélium et d'oxygène respectivement. Le débit du gaz vecteur et le chauffage choisi ont été définis pour être dans les conditions optimums pour mesurer la température initiale d'oxydation (PIO) et la température d'inflammation instantanée (SIT) [Suzin et al., 1999].

#### *Programmation de température*

Le chauffage est programmé avec un signal de rampe donnant une vitesse d'augmentation de température. Le système est maintenu à une température constante utilisant une isotherme donnant un intervalle de temps stipulé. La détermination des paramètres de température d'oxydation et d'inflammation pour chaque échantillon réaliser avec la programmation de température suivante :

1. Une isotherme de 5 minutes à 30 °C est maintenue pour éliminer les perturbations au début du chauffage et donc stabiliser le signal.
2. Le système est alors chauffé de 20 °C à 105 °C avec une rampe à 5 C/min.
3. Ensuite une 2ème isotherme à 105 °C pendant 30 minutes, le but principal de cette isotherme est d'enlever l'humidité physisorbée dans les échantillons des charbons actifs [Suzin et al., 1999].
4. L'échantillon est alors chauffé de 105 °C à 650 °C avec la même rampe de température de 5 °C/min.

## ***Resumé en Français***

---

5. L'étape finale est le refroidissement de l'échantillon de 650 °C à 100 °C avec une vitesse de 10 C.min<sup>-1</sup>.

### *Corrections du signal*

Des expériences auxiliaires sont effectuées pour éliminer les biais incorporées dans le signal TG-DSC en raison des gradients de température, la convection et la flottabilité du gaz. Quand le creuset contenant l'échantillon est chauffé dans l'atmosphère gazeuse, il ya des changements de poids apparents avec l'augmentation de température et le changement de poids du gaz déplacé. L'échantillon semble alors prendre du poids durant le chauffage. Les courbes de correction sont nécessaires pour éliminer ces effets.

Des essais blancs sont effectués avec le creuset vide sous air et en atmosphère inerte. En raison de la haute sensibilité et les effets de flottabilité de l'équipement, les signal de variations de masse et de flux de chaleur sont normalement trouvés même pour les mesures de creuset vide. Pour éliminer ces biais, les signaux des expériences à blancs sont soustraits de l'expérimentation effectuée avec les échantillons. La courbe de chaleur d'oxydation est calculée à partir de l'Équation 3.11.

$$\Delta H(\text{oxidation}) = \left[ \left( \frac{\Phi_{\text{air}} - \Phi_{\text{blank/air}}}{ms} \right) - \left( \frac{\Phi_{\text{ref/He}} - \Phi_{\text{blank/He}}}{ms} \right) \right] \quad (\text{D})$$

Où,

ΔH (oxydation) = flux de chaleur/unité de masse de l'échantillon (mW/mg)

Φ L'air : Flux de chaleur de l'échantillon sous air (mW)

Φ Blanc/l'air : flux de chaleur du creuset vide sous air (mW)

Φ ref/He : flux de chaleur de l'échantillon sous hélium (mW)

Φ Blanc/Il : flux de chaleur du creuset vide sous hélium (mW)

Ms : Masse de l'échantillon de charbon actif (mg)

L'Équation D représente le flux de chaleur exprimé par unité de masse après la soustraction de tous les biais potentiels dans le système TG - DSC. Le flux de chaleur expérimental du blanc mesuré est soustrait de l'air et les expériences de référence pour corriger les biais aux mesures de creusets vides. Alors les expériences de référence sont soustraite des mesures dans l'air pour corriger les effets de flottabilité. L'expérience est répétée trois fois pour vérifier la répétitivité et le calcul du pourcentage d'erreur.

### **Thermogrammes TG-DSC**

La détermination des températures d'oxydation et d'inflammation des charbons actifs en utilisant des techniques d'analyse thermiques a été étudiée par Suzin *et al.*, [1999]. L'auteur indique deux régions d'intérêt pour les courbes de flux de chaleur associées au processus d'oxydation démarrant à relativement basse température et l'inflammation spontanée à température plus élevée. La région où les démarcages des réactions d'oxydation sont significatifs est dénommée température initiale d'oxydation (PIO). La région où le matériau s'enflamme d'une façon autonome est nommée température d'inflammation instantanée (SIT).

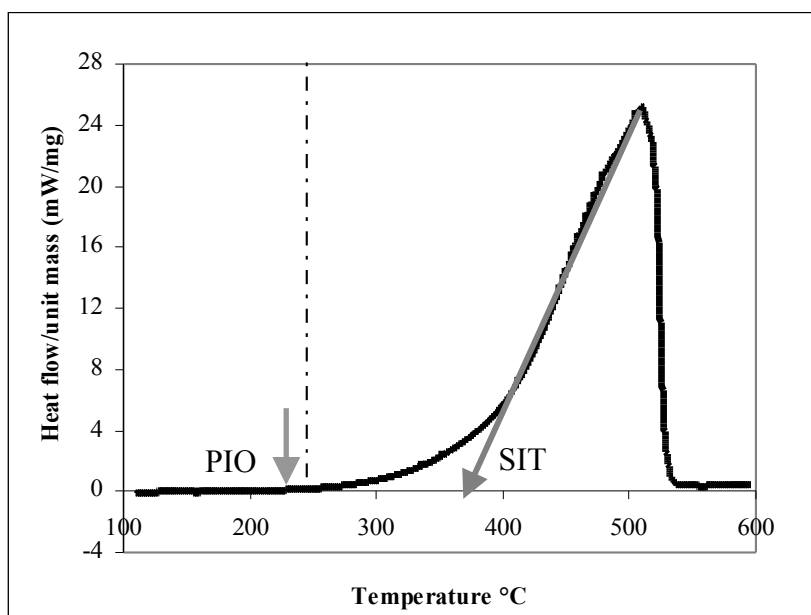


Figure : E Courbe be flux de chaleur pour un échantillon de charbon actif

Selon Suzin et al. [1999], la température d'inflammation instantanée peut être déduite de la température où la tangente au point d'inflexion croise la ligne de base de la courbe du flux de chaleur. La température d'inflammation instantanée définit la limite au-delà de laquelle la combustion de l'échantillon a lieu et mène à la consommation de la matrice de carbone observé sur la courbe de l'évolution de la masse. La température initiale d'oxydation représente le point au-delà duquel les réactions exothermiques deviennent significatives. Le processus d'oxydation à basse température est accompagné de l'oxydation partielle du carbone et les groupements oxygénés de surface. La température initiale d'oxydation a été extraite de la courbe de flux de chaleur nette en localisant le point initial de déviation mono tonique de la ligne de base.

### **Température d'oxydation et d'inflammation**

## **Resumé en Français**

---

La méthode d'évaluation de la température d'oxydation est basée sur celle de Suzin *et al.*, 1999, ils définissent la température initiale d'oxydation comme la température à partir de laquelle le flux de chaleur s'écarte de plus de 2 % de la moyenne des cinq points consécutifs. Lorsque ce niveau arbitraire est atteint, on considère que les réactions d'oxydation commencent à devenir significatives. L'évolution du flux de chaleur en fonction de la température est représentée sur la Figure F pour différents charbons actifs. La température d'inflammation est calculée à partir de la tangente avec la courbe de flux chaleur.

### **Etude cinétique**

Les paramètres cinétiques tant pour l'oxydation que des réactions de combustion ont été évalués à l'aide de l'équation d'Arrhenius appliquée aux courbes de DSC et de TG respectivement. Les thermogrammes de DSC et de TG de l'échantillon des charbons actifs, enregistrés pendant l'oxydation et la combustion des échantillons sont exprimés en termes d'énergie d'activation et le facteur de fréquence utilisant l'équation d'Arrhenius.

#### *Cinétique d'oxydation*

Le flux de chaleur par unité de masse de l'échantillon ( $\frac{\Phi}{m}$ ) est écrit sous forme de l'équation d'Arrhenius. Les paramètres cinétiques d'oxydation sont calculés entre les températures d'oxydation et d'inflammation des charbons actifs. Une réaction d'ordre zéro est assumée ici, c'est-à-dire que la réaction est indépendante de la concentration des réactifs. L'équation finale prend la forme suivante :

$$\frac{\Phi}{m} = Ae^{-\frac{AE}{RT}} \quad (\text{E})$$

$\frac{\Phi}{m}$  : Flux chaleur / unité de masse de charbon actif (mW.mg<sup>-1</sup>),

AE : énergie d'activation (kJ.mole<sup>-1</sup>),

A : facteur pre exponentiel (mW. mg<sup>-1</sup>),

T : Température de l'échantillon (K),

R : constante de gaz idéal (8.314 J. K<sup>-1</sup>. mol<sup>-1</sup>),

L'équation (F) est mise sous forme logarithmique et un graphique de la fonction logarithmique naturelle de la proportion du flux chaleur / unité de masse de charbon actif

## **Resumé en Français**

---

$\ln\left(\frac{\Phi}{m}\right)$  avec le temps contre l'inverse de température ( $1/T$ ) est fait comme indiqué dans la Figure G. Une ligne droite avec une pente ( $-AE/R$ ), donnant l'amplitude de l'énergie d'activation est obtenue. L'énergie d'activation a été calculée entre la température initiale d'oxydation et la température d'inflammation instantanée.

$$\ln\left(\frac{\Phi}{m}\right) = \ln(A) - \frac{AE}{RT} \quad (F)$$

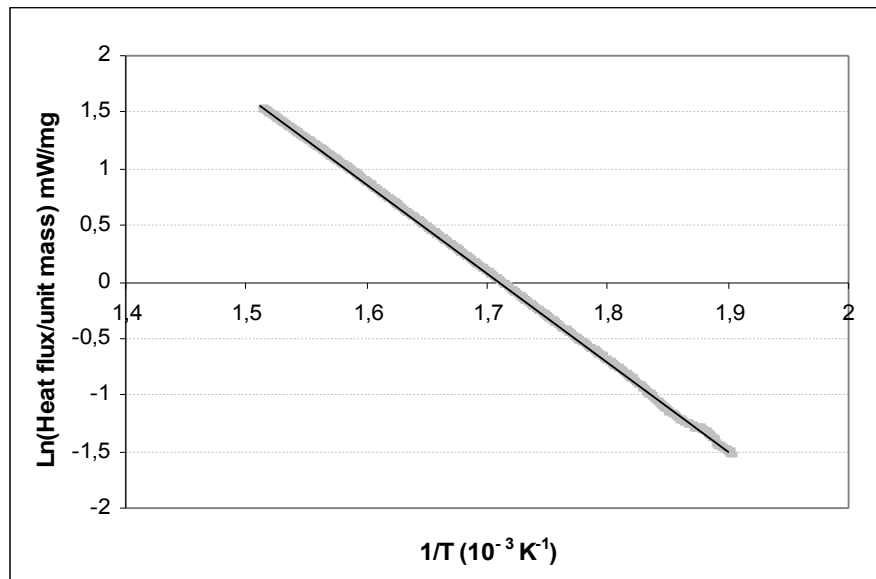


Figure : F Etude cinétique d'oxydation à partir flux de chaleur pour un échantillon de charbon actif

La déviation des données expérimentales de la ligne droite indique le degré d'inexactitude sur la supposition d'une réaction d'ordre zéro dans notre cas. Une bonne corrélation de régression de 0.99 est obtenue indiquant ici l'équation du modèle.

### *La Cinétique d'inflammation*

De la même manière, la perte de masse avec la température est écrite par l'équation d'Arrhenius pour calculer les paramètres cinétiques. La perte de masse des charbons actifs a lieu surtout après le démarrage de réactions d'inflammation. Dans la région de la température initiale d'oxydation, il n'y a pas de variation de masse significative pour pouvoir étudier la cinétique d'oxydation en utilisant la courbe de TG.

## *Resumé en Français*

---

$$\frac{dw}{dt} = A \exp\left(-\frac{Ea}{RT}\right)w \quad (G)$$

Dw/dt : masse de l'échantillon /température (mg. ° C<sup>-1</sup>),

Ea : énergie d'activation exprimée en (kJ.mole<sup>-1</sup>),

A : facteur pre-exponenetal (mW. ° C<sup>-1</sup>),

T : Température de l'échantillon (K).

L'équation (G) est mise sous forme logarithmique et un graphique de la fonction logarithmique naturelle de la variation de masse en fonction de la température. Ln (dw/dt) en fonction de 1/T est alors une ligne droite avec une pente (-Ea/R) comme indiqué dans la Figure H, donnant l'amplitude de l'énergie d'activation. La déviation des données expérimentales de la ligne droite indique le degré d'inexactitude de la supposition d'une réaction d'ordre un dans notre cas. Une bonne corrélation de régression de 0.99 est obtenue indiquant ici l'exactitude du modèle.

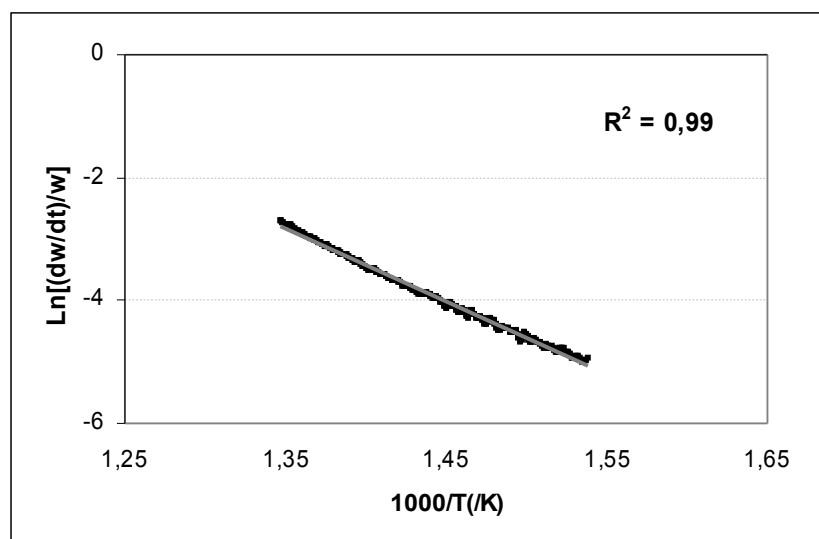


Figure :G Etude de cinétique d'oxydation à partir flux de chaleur pour un échantillon de charbon actif

### **ANALYSEUR ÉLÉMENTAIRE CHNS-O:**

L'analyseur élémentaire Thermo Finnigan Flash EA 1112 permet d'étudier la composition des matériaux, il est utilisé pour connaître leur composition en hydrogène, soufre, oxygène, carbone, et azote. Sur les charbons actifs il est utile principalement pour étudier leur teneur en carbone et oxygène.

## ***Resumé en Français***

---

Cet appareil donne un pourcentage de carbone, d'hydrogène, d'azote, de soufre et d'oxygène contenu dans des matériaux organiques, inorganiques et dans les polymères en fonction de la masse totale de l'échantillon. Il peut analyser des substances de différentes natures : solide, liquide et gazeuse. La technique utilisée par l'appareil est la combustion instantanée.

L'analyseur ne peut pas mesurer l'oxygène en même temps que les autres composants, ceci vient du fait que pour réaliser la combustion des échantillons de l'oxygène est utilisé, il y a donc une autre procédure pour en connaître sa teneur. Il faut donc effectuer deux passages d'un échantillon pour obtenir le pourcentage de tous ses composants.

Pour connaître le pourcentage d'hydrogène, d'azote, de carbone et de soufre, l'échantillon est placer en petite quantité (~1mg) dans une nacelle en étain (Sn) et est injecté dans un four à 950°C balayé par de l'hélium et une quantité optimale d'oxygène. Il s'en suit une combustion flash, chaque élément de l'échantillon donne un gaz de combustion différent, une réduction de certains d'entre eux se fait sur un tube de cuivre. Les gaz sont ensuite détectés par un catharomètre, il se compose d'un four a 65°C, d'une colonne chromatographique et d'un détecteur par différence de conductivité thermique, une seconde colonne sert de référence (gaz vecteur : He). Les pics obtenus pour chaque gaz donnent le pourcentage massique de chaque élément.

Le procédé de détection de l'oxygène est similaire et se fait sur une autre colonne chromatographique, l'échantillon est placé dans une nacelle en argent (Ag), il subit ensuite une pyrolyse dans un four a 1060°C sous atmosphère inerte (He). Plusieurs composés sont produits parmis lesquels des composés oxygénés (CO). La détection des gaz est faite en sortie de colonne et donne le pourcentage massique en oxygène de l'échantillon.

## **Conclusions**

Dans ce chapitre, les différentes techniques de caractérisation pour la mesure des propriétés texturale, chimique et la nanostructurale des échantillons charbons actifs a été étudié. Dans la première partie l'analyse thermique, et la calorimétrie différentielle à balayage sont utilisés pour l'étude de l'oxydation et de l'inflammation des charbons actifs. Généralement la méthode ASTM donne des températures d'oxydation et d'inflammation inférieures. Cependant la méthode American Society for Testing and Materials (ASTM) a tendance à se rapproches des conditions d'application. La calorimétrie différentielle à balayage semble être une méthode efficace en ce qui concerne l'analyse et la comparaison de grand nombre d'échantillons avec

## ***Resumé en Français***

---

les mêmes conditions expérimentales. L'autre avantage est l'exploitation de plusieurs paramètres comme le flux de chaleur, l'évolution de masse menant à la cinétique de réaction. Deux paramètres caractérisant l'oxydation et l'inflammation sont mesurés notamment la température initiale d'oxydation (PIO) et la température d'inflammation instantanée (SIT).

En ce qui concerne la caractérisation de porosité utilisant des techniques d'adsorption d'azote et porosimétrie à mercure, les paramètres diverses et les approches d'évaluation sont décrits avec les conditions de mesure. La composition chimique des charbons actifs est caractérisée utilisant les techniques d'analyse élémentaires donnant la composition en carbone, hydrogène, azote et oxygène. En plus, la teneur en cendre des charbons actifs a été mesuré utilisant la méthode de ASTM (American Society for Testing and Material) et des méthodes Microscopie Electronique à Balayage MEB-X. Finalement la caractérisation structurale et nanostructurale ont été réalisées par la Microscopie Électronique à Transmission de Haute résolution (METHR) et par Microscopie Électronique à Balayage (MEB).

**CHAPITRE – 4**  
**RESULTATS ET DISCUSSIONS**

Ce chapitre présent l'analyse et discussions sur les résultats obtenus selon les méthodes décrites dans le Chapitre 3. Il consiste en 4 sous parties. La première partie décrit les résultats expérimentaux obtenus incluant la caractérisation de la porosité des charbons actifs par techniques d'adsorption d'azote et de pénétration de mercure, suivie de l'analyse élémentaire et l'analyse de la teneur en cendres. Les résultats des propriétés structurales obtenues par Microscopie Électronique à balayage (MEB) et par Microscopie Électronique de Transmission à Haute Résolution (METHR) sont analysés. La 2ème partie décrit la réactivité d'oxydation et d'inflammation des charbons actifs déduite à partir des techniques de calorimétrie différentielle à balayage couplée avec la thermogravimétrie (TG-DSC).

Dans la 3ème partie de ce chapitre, une analyse qualitative est conduite pour éclairer la relation entre la texture, la nano structure et la composition chimique des charbons actifs et leur réactivité en présence d'oxygène et de composés organiques volatiles. Plus loin, la réactivité des charbons actifs est étudiée en changeant les conditions opératoires comme la concentration d'oxygène de balayage, le débit du gaz de balayage et la vitesse d'échauffement. Enfin, une étude statistique a été appliquée utilisant la Régression Linéaire Multiple (MLR) pour établir des relations quantitatives entre les réactivités des charbons actifs et leurs propriétés.

**PROPRIÉTÉS PHYSIQUES**

Les propriétés physiques des charbons actifs varient en fonction du mode d'activation utilisée, de la nature du matériau d'origine, et de plusieurs autres paramètres.

Les propriétés physiques importantes des charbons actifs sont la porosité et la surface spécifique. La surface spécifique est la surface de matériaux qui est disponible pour l'adsorption de matières chimiques, pour certains charbons actifs cette surface peut atteindre  $2000\text{m}^2/\text{g}$  de matériau. La méthode de préparation utilisée influe sur la taille des pores, on définit trois tailles de pores : les macropores, les mésopores et les micropores.

La taille des pores dépend de leur largeur, pour les pores en fente cela représente la distance entre les parois et pour les pores cylindriques il s'agit de leur diamètre. La largeur des

## ***Resumé en Français***

---

micropores est inférieure à 2nm, les mésopores ont une taille comprise entre 2nm et 50 nm et les macropores ont une largeur supérieure à 50nm. (*Bansal, Donnet Stoekli [13]*)

### **PROPRIÉTÉS CHIMIQUES**

La capacité d'adsorption des charbons actifs est déterminée par leur structure physique et poreuse. Mais les composés chimiques présents à leur surface influencent également cette capacité.

Les charbons actifs contiennent de petites quantités de matière minérale ainsi que des hétéro - atomes comme l'hydrogène et l'oxygène fixés chimiquement à leur surface. La présence d'hydrogène et surtout d'oxygène influence les propriétés adsorbantes des charbons. La présence de ces espèces est due au type de matériau d'origine et à la méthode d'activation utilisée.

La présence de ces groupements de surface, est liée à la structure des charbons actifs. Celle-ci est constituée d'un réseau de couches de carbone accrochées entre elles. Au bout de ces plans d'atomes de carbone, il y a des atomes insaturés. Ce sont les sites où les hétéro – atomes peuvent se fixer. Les plans de carbone contiennent également beaucoup de défauts, dislocations et discontinuités, ce qui aide à la présence de groupement en surface.

La nature des composés et la quantité d'oxygène sont influencées par la surface spécifique, la taille des particules, la teneur en cendre ainsi que le degré de carbonisation du charbon actif. Ces composés oxygénés peuvent également être formés par réaction avec d'autres gaz comme l'ozone, le dioxyde de carbone ainsi que par réaction avec des solutions comme l'acide nitrique.

Ces complexes oxygénés donnent des couples acides / base caractéristiques du carbone. Le caractère basique du carbone dû aux groupements oxygénés de surface est un problème pour beaucoup de chercheurs. Plusieurs études ont été réalisées sur le sujet. Les caractéristiques acides sont, par contre, clairement établies. (*Boehm [6]*)

A l'aide de méthodes spectroscopiques et de réactions chimiques, Boehm [6] définit quatre groupes d'oxydes acides. Il propose comme méthode de dosage de ces groupes acides une méthode acidimétriques utilisant des bases de plus en plus fortes :

1. hydrogénocarbonate de sodium –  $\text{NaHCO}_3$
2. carbonate de sodium –  $\text{Na}_2\text{CO}_3$
3. soude –  $\text{NaOH}$
4. ethanolate de sodium –  $\text{NaOC}_2\text{H}_5$

## ***Resumé en Français***

---

**Groupe 1 (GI)** : fonctions carboxyliques fortes dosées par les quatre bases

**Groupe 2 (GII)** : fonctions carboxyliques faibles et lactones dosé par toutes les bases sauf  $\text{NaHCO}_3$

**Groupe 3 (GIII)** : fonctions phénoliques dosées par  $\text{NaOH}$  et par  $\text{NaOC}_2\text{H}_5$

**Groupe 4 (GIV)** : fonctions carbonyles dosées par la base la plus forte  $\text{NaOC}_2\text{H}_5$ .

### **Composition chimique**

Il s'agit du pourcentage massique des éléments C, H, N, S et O dans l'échantillon. Il est remarquer que pour les charbons chimiquement activé, le rapport (O/C) : 40 % est très important par rapport aux charbons physiquement activé (2 – 13 %). Pour H/C, les échantillons présentent la même tendance que pour le ratio de (O/C). Tous les échantillons ne contiennent pas ou presque de soufre. L'azote est présent dans tous les échantillons à base de PAN et CTP.

## *Resumé en Français*

---

Echantillons	Matière première	C (%)	H (%)	N (%)	O (%)	O/C (%)	H/C (%)	N/C (%)
NC-50 <sup>(PA)</sup>	Noix de coco	93.8	0.5	0	1.6	1.7	0.5	0
NC-60 <sup>(PA)</sup>	Noix de coco	91.8	0.3	0.1	3.3	3.6	0.3	0.1
NC-100 <sup>(PA)</sup>	Noix de coco	91.1	0.5	0	3	3.3	0.6	0
RB-2 <sup>(PA)</sup>	Tourbe	88	0.3	0.2	5.2	5.9	0.3	0.2
BPL <sup>(PA)</sup>	Charbon	88	0.2	0.3	3.6	4.1	0.2	0.3
NC-70-Cu <sup>(PA)</sup>	Noix de coco	80	0.5	0.5	6.7	8.4	0.6	0.6
NC-70-CuCr <sup>(PA)</sup>	Noix de coco	73.2	2.6	0.7	9.1	12.4	3.6	1
CTP-A <sup>(PA)</sup>	Brai	92.7	0.8	0.7	1.6	1.7	0.9	0.8
CTP-PAN-3 :1-A <sup>(PA)</sup>	Brai de coke et polyacrylonitrile	85.7	1.1	4.8	2.7	3.15	1.3	5.6
CTP-PAN-1 :1-A <sup>(PA)</sup>	Brai de coke et polyacrylonitrile	84.3	1	8	6.2	7.3	1.2	9.3
PAN-A <sup>(PA)</sup>	Polyacrylonitrile	76.6	1.3	11.2	10.5	13.7	1.7	14.6
GF-40 <sup>(CA)</sup>	Noyaux d'olive	70.8	2	0.2	24.5	34.6	2.8	0.3
BC-120 <sup>(CA)</sup>	Bois	69.5	1.9	0.1	24.6	35.4	2.7	0.1
PICABIOL <sup>(CA)</sup>	Bois	68	1.8	0	27.6	40.6	2.6	0
PAN-C <sup>(C)</sup>	Polyacrylonitrile	77.6	0.9	16	4.9	6.3	1.2	20.6
CTP-PAN-3 :1-C <sup>(C)</sup>	Brai de coke et polyacrylonitrile	90.1	1.2	6.4	2.2	2.5	1.3	7.1
CTP-C <sup>(C)</sup>	Brai de coke	88.7	1.1	0.7	0.6	0.7	1.2	0.8
CTP-PAN-1 :1-C <sup>(C)</sup>	Brai de coke et polyacrylonitrile	82.7	0.9	11.1	2.7	3.3	1.1	13.4
Carbonized coconut shell-C <sup>(C)</sup>	Noix de coco	82.6	2.6	0.1	10.3	12.5	3.2	0.12

Tableau :B Composition chimique des charbons actifs

### **Méthode de Boehm**

Cette méthodes permet la mesure des concentrations des groupements oxygénées (GO) de surface : acides et basiques. Les concentrations en GO de surface son les plus élevées pour BC120 et GF40. Les principales raisons sont de mode de activation chimique pendant la

## *Resumé en Français*

---

fabrication de charbon actif. Ces résultats sont globalement concordants avec l'analyse élémentaire en tenant en compte l'erreur expérimentale < 25 %.

	GF-40	NC-60	NC-100	BC-120	BPL	RB-2
<b>Acidic complexes (mEq.L<sup>-1</sup>)</b>						
<b>GI</b>	0.20	0	0	0.65	0	0
<b>GII</b>	0.62	0.06	0.27	0.12	0.16	0.09
<b>GIII</b>	0.49	0.4	0.2	0.8	0.18	0.07
<b>GIV</b>	0.32	0.9	0.4	1.5	0	0
<b>Basic complexe (mEq.L<sup>-1</sup>)</b>						
	0.65	0.5	0.55	0.2	0.50	0.62

Tableau : C Groupements oxygénés de surface par méthode de Boehm

Echantillons	Matière première	Contenu de cendres (%)
NC-50 <sup>(PA)</sup>	Noix de coco	1.9
NC-60 <sup>(PA)</sup>	Noix de coco	1.65
NC-100 <sup>(PA)</sup>	Noix de coco	2.2
RB-2 <sup>(PA)</sup>	Tourbe	4.7
BPL <sup>(PA)</sup>	Charbon	4.5
GF-40 <sup>(CA)</sup>	Noyaux d'olive	0.4
BC-120 <sup>(CA)</sup>	Bois	0.3
Picabiol <sup>(CA)</sup>	Bois	0.3

Tableau : D Résultats de analyse quantitative des cendres de charbons actifs

On remarque que les charbons physiquement activés contiennent plus de cendres (2-5 %) que les charbons actifs chimiquement activé (0.3 %). L'analyse de la teneur en cendre et en particulier en élément inorganique montre que le % de potassium K est plus élevé (imprégnation KOH lors de l'activation) pour des charbons actifs à base de noix coco. Pour de base de tourbe et charbons il ya plus de présence de Al, Mg et Si (Alumine silicates).

Element	Coconut shell			Peat	Coal
% massique	NC-50	NC-60	NC-100	RB-2	BPL
K	22.7	15.5	10.60	4.60	1.40
Ca	5.60	3.70	0.50	2.80	1.30

## Resumé en Français

S	0.13	1.60	0	3.30	0.82
P	0.70	1.20	0.40	0.60	0.22
Al	0.30	0.10	3.70	1.40	8.80
Mg	1.80	2.50	0.30	1.03	0.30
Na	4.90	4.04	3.90	2.30	0.30
Fe	0.23	0.21	0.50	2.40	4.50

Tableau :E Résultats de analyse qualitatif des cendres de charbons actifs

L'appareil utilisé pour déterminer les caractéristiques de microporosité est l'analyseur ASAP 2010 produits par Micromeritics. Le principe de fonctionnement de cet analyseur est basé sur l'adsorption d'azote ( $N_2$ ) à 77,35 K, avec une mesure du volume d'azote adsorbé en fonction de la pression à l'intérieur du système. L'analyse d'isotherme d'adsorption fournit des renseignements sur la surface spécifique développée par l'adsorbant, le volume microporeux, et la taille des pores.

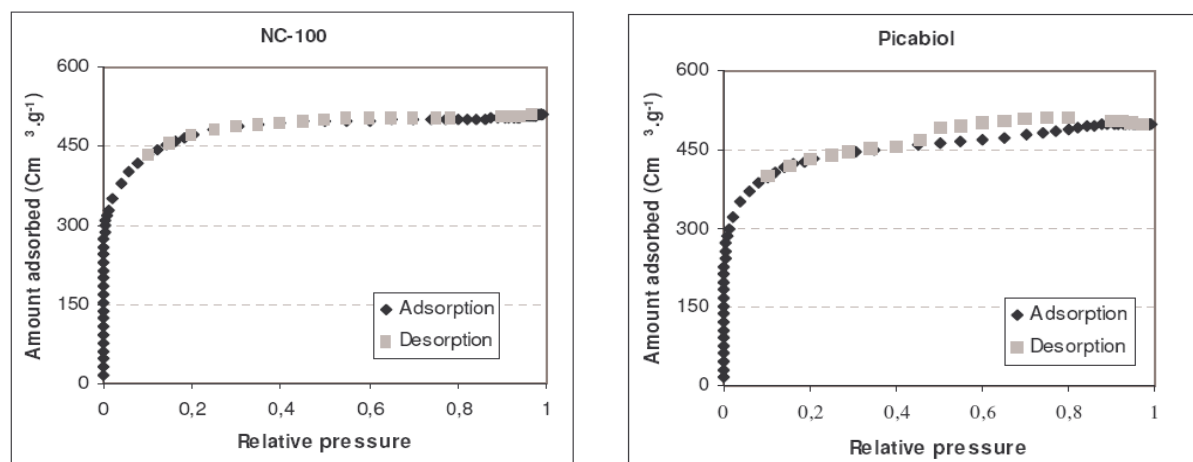


Figure : H Isothermes d'adsorption de  $N_2$  - 77 K pour les échantillons de NC-100 et Picabiol

### Surface Spécifique (SBET) des charbons actifs

On observe que les charbons chimiquement activés présentent une grande surface spécifique comprise entre 1500 et 2000  $m^2/g$ . Ceci est du à l'effet de acide phosphorique qui est ici l'agent d'activation chimique. L'acide phosphorique crée une structure poreuse importante suite à l'aromatisation de la structure squelettique du carbone. Les charbons physiquement activés eux présentent une surface spécifique presque constante entre 1000 et 1250  $m^2/g$  sauf

## **Resumé en Français**

pour NC-100 dont la surface spécifique est  $1800 \text{ m}^2/\text{g}$ . Pour le cas des charbons actifs physiquement activés à la base de noix coco, la surface spécifique augmente avec la durée d'activation (SBET : NC-100 > NC-60 > NC-50). Enfin les charbons actifs préparés au laboratoire à base de CTP et PAN possèdent une faible surface spécifique entre 100 -500  $\text{m}^2/\text{g}$ . Les échantillons carbonisés possèdent une faible surface spécifique.

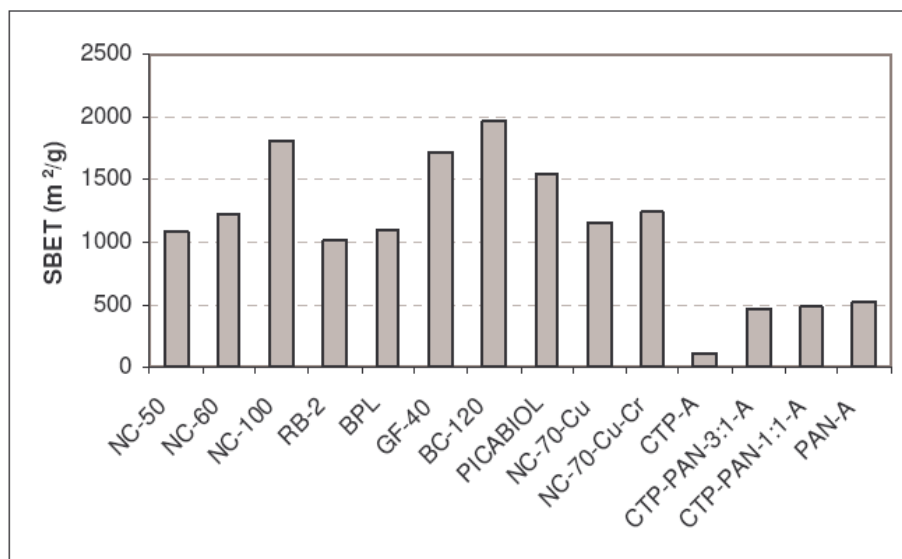
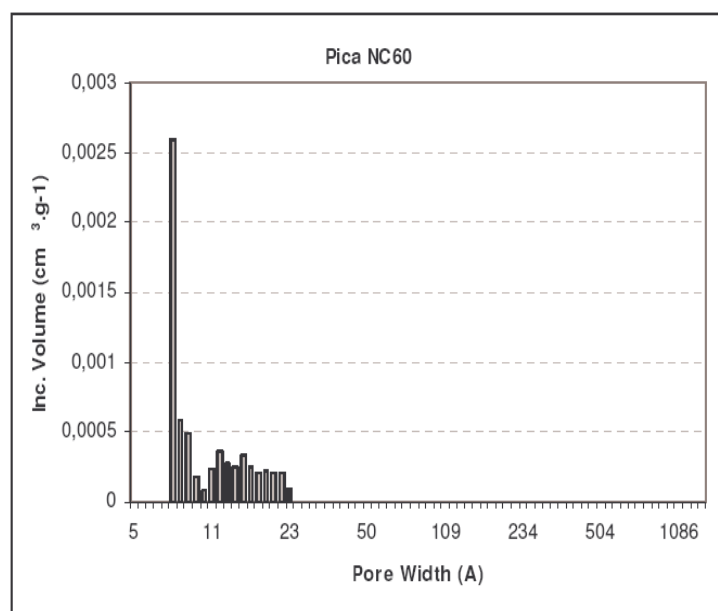


Figure : I Distribution de surface spécifique (SBET) des charbons actifs

### **Distribution en taille des pores – DFT (Density Functional Theory)**

La taille moyenne des micropores varie entre 0.90 et 1.40 nm. Les charbons actifs physiquement activés sont microporeux avec une distribution étroite [0.5 – 2.5 nm]. Par contre les charbons actifs chimiquement activés consistent des distributions plutôt mésoporeuses et macroporeuses.



## **Resumé en Français**

---

Figure : J Distribution de taille de pores - méthode de DFT

### **Volume des micropores < 2 nm**

Il n'ya pas de différence particulière au niveau des volume de micropores entre les différents types de charbons actifs. Leur valeur varient entre 0.2 et 0.35 cm<sup>3</sup>/g sauf pour CTP activé qui a une valeur de 0.4 cm<sup>3</sup>/g. Le volume de micropore ne suivent pas forcément les valeurs de surface spécifique de charbons actifs. C'est-à-dire que un charbon actif peut avoir un faible volume de micropore mais présenter une grande surface spécifique et inversement.

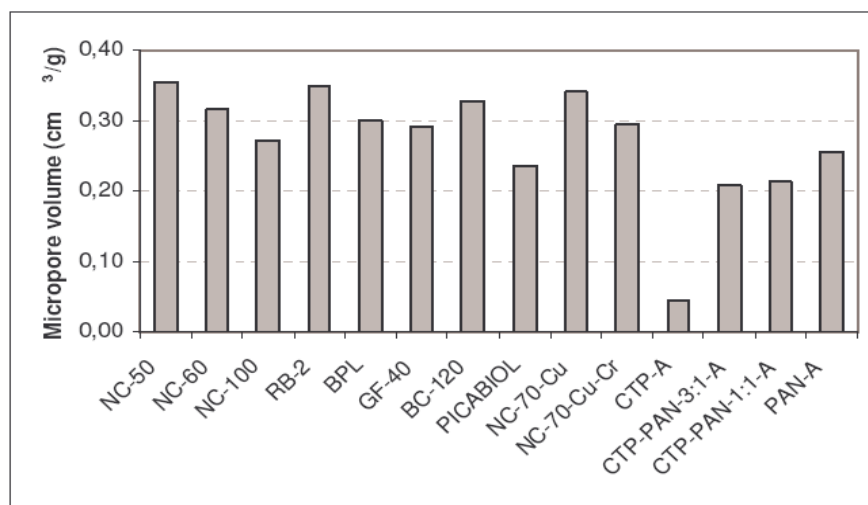


Figure : K Distribution de taille de pores - méthode de DFT

### **Volume des méso et macropores > 8 nm**

L'appareil monte en pression jusqu'à 30 000 psi (~2050.105 Pa) et cette augmentation est fractionnée en deux étapes. La première étape correspond au remplissage des macropores

## *Resumé en Français*

---

et du volume inter granulaire, la deuxième au remplissage des mésopores. Le volume mésoporeux est donc le volume de mercure introduit au cours de la deuxième montée en pression. Le volume poreux est donc le volume des pores supérieurs à 8 nm. Le volume mésoporeux est élevé pour les CA chimiquement activés. Un écart est observé pour

Echantillons	Matière première	Volume de meso et macro pore (cm <sup>3</sup> . g <sup>-1</sup> )
NC-50 <sup>(PA)</sup>	Noix de coco	1.20
NC-60 <sup>(PA)</sup>	Noix de coco	0.35
NC-100 <sup>(PA)</sup>	Noix de coco	0.47
RB-2 <sup>(PA)</sup>	Tourbe	0.34
BPL <sup>(PA)</sup>	Charbon	0.40
CTP-A <sup>(PA)</sup>	Brai de coke	0.07
CTP-PAN-3 :1-A <sup>(PA)</sup>	Brai de coke et polyacrylonitrile	0.25
CTP-PAN-1 :1-A <sup>(PA)</sup>	Brai de coke et polyacrylonitrile	0.27
PAN-A <sup>(PA)</sup>	Polyacrylonitrile	0.27
GF-40 <sup>(CA)</sup>	Olive stone	0.80
BC-120 <sup>(CA)</sup>	Bois	1.50
PICABIOL <sup>(CA)</sup>	Bois	1.34
NC-70-Cu <sup>(PA)</sup>	Noix de coco	0.33
NC-70-Cucr <sup>(PA)</sup>	Noix de coco	0.35

l'échantillon NC-50. Erreur expérimentale est de l'ordre de 5 %.

Tableau :F Résultats de volume des méso et macropores > 8 nm

## ***Resumé en Français***

---

### **Caractérisation Structurale**

Les résultats de caractérisation structurale montre les effets possibles des modes d'activation sur la nanostructure et la porosité des carbones résultants. L'activation physique consiste à 2 étapes notamment la carbonisation où les feuillets sont plus ou moins empilés. Dans le étape d'activation il ya de consommation des feuillets les plus courts et les plus distordus qui rendent les échantillons avec les feuillets plus longs, plus écartés et soudure de bords de feuillets (recombinaison des radicaux libres). On trouve le ‘grands’ pores plus ou moins allongés dans les échantillons physiquement activé.

L'activation chimique consiste à seulement 1 étape avec le processus d'aromatisation et réticulation (rôle de l'oxygène) des feuillets qui deviennent courts très distordus, très réticulés (L, N très petits, % feuillets ‘non empilés’ et de très grands). Les pores dans les échantillons activé chimiquement sont petits’ pores plus isométriques et il ya nombreux sites d’occupation des fonctions oxygénées.

## *Resumé en Français*

---

Echantillons	DFT méthode (nm)	HRTEM technique (nm)
NC-50 <sup>(PA)</sup>	1.35	0.38
NC-60 <sup>(PA)</sup>	0.97	0.40
NC-10 <sup>(PA)</sup>	1.11	0.39
RB-2 <sup>(PA)</sup>	0.92	0.42
BPL <sup>(PA)</sup>	0.93	0.38
CTP-A <sup>(PA)</sup>	1.30	0.38
CTP-PAN-1:1-A <sup>(PA)</sup>	1.11	0.39
PAN-A <sup>(PA)</sup>	1.15	0.39
GF-40 <sup>(CA)</sup>	1.15	0.40
BC-120 <sup>(CA)</sup>	1.12	0.39
Picabiol <sup>(CA)</sup>	1.38	0.41

Tableau :G Résultats de taille des micropores par DFT et par METHR

#### **Etude de réactivité des charbons actifs**

La mesure de la température initiale d'oxydation et de la température d'inflammation instantanée a été faite avec 19 échantillons de charbons de différentes origines de matériaux de base et leur mode d'activation. La température initiale d'oxydation des échantillons de charbons divers est comprise entre 150 et 350 °C tandis que leur température d'inflammation instantanée est entre 200 et 550 °C. Le modèle cinétique a été établi à partir du flux de chaleur et des courbes de perte de masse. La cinétique du processus d'oxydation a été déduite de la courbe du flux de chaleur en prenant une réaction d'ordre zéro, tandis que la réactivité d'inflammation a été déduite de la courbe de flux de chaleur avec un ordre 1 pour la réaction.

## *Resumé en Français*

---

## *Resumé en Français*

---

Echantillons	Mode d'activation	Matière première	PIO °C
NC-50	Physique	Noix de coco	220
NC-60	Physique	Noix de coco	203
NC-100	Physique	Noix de coco	240
BPL	Physique	Tourbe	253
RB-2	Physique	Charbon	260
CTP-A	Physique	Brai de coke	309
CTP-PAN-3:1-A	Physique	Brai de coke et polyacrylonitrile	264
CTP-PAN-1:1-A	Physique	Brai de coke et polyacrylonitrile	235
PAN-A	Physique	Polyacrylonitrile	225
GF-40	Chimique	Noyaux d'olive	183
BC-120	Chimique	Bois	178
Picabiol	Chimique	Bois	168
PAN-C	Non activé	Polyacrylonitrile	315
CTP-PAN-3:1-C	Non-activé	Brai de coke et polyacrylonitrile	267
CTP-C	Non-activé	Brai de coke	380
CTP-PAN-1:1-C	Non-activé	Brai de coke et polyacrylonitrile	307
Noix de coco carbonisé	Non-activé	Noix de coco	175
NC-70- Cu	Physique	Noix de coco	133
NC-70 -CuCr	Physique	Noix de coco	125

Tableau :H Température Initiale d'oxydation des charbons actifs

## *Resumé en Français*

---

Echantillons	Energie d'activation ( $E_a$ ) (kJ/mole)	Ln (A)	Gamme de température °C
NC-50 <sup>(PA)</sup>	71	14.6	227-400
NC-60 <sup>(PA)</sup>	65	13.4	188-400
NC-100 <sup>(PA)</sup>	75	13.6	271-480
BPL <sup>(PA)</sup>	104	17.2	408-520
RB-2 <sup>(PA)</sup>	85	14.6	322-516
CTP-A <sup>(PA)</sup>	136	21.8	397-517
CTP-PAN-3:1-A <sup>(PA)</sup>	118	19.3	358-520
CTP-PAN-1:1-A <sup>(PA)</sup>	79	13.4	332-485
PAN-A <sup>(PA)</sup>	74	12.8	281-475
GF-40 <sup>(CA)</sup>	49	9.7	170-400
BC-120 <sup>(CA)</sup>	46	8.7	208-400
Picabiol <sup>(CA)</sup>	33	6.6	160-380
PAN-C <sup>(C)</sup>	124	18.7	354-500
CTP-PAN-3:1-C <sup>(C)</sup>	202	31.5	421-550
CTP-C <sup>(C)</sup>	222	34.1	424-575
CTP-PAN-1:1-C <sup>(C)</sup>	141	22.5	426-575
Noix de coco carbonisé	45	10.2	219-400
NC-70-Cu <sup>(PA)</sup>	39	9.2	175-290
NC-70-CuCr <sup>(PA)</sup>	32	8.6	154-285

Tableau :I Energie d'activation de réactions d'oxydation

## *Resumé en Français*

---

Echantillons	Mode d'activation	Matière première	SIT °C
NC-50	Physique	Noix de coco	380
NC-60	Physique	Noix de coco	388
NC-100	Physique	Noix de coco	475
BPL	Physique	Tourbe	516
RB-2	Physique	Charbon	515
CTP-A	Physique	Brai de coke	544
CTP-PAN-3:1-A	Physique	Brai de coke et polyacrylonitrile	520
CTP-PAN-1:1-A	Physique	Brai de coke et polyacrylonitrile	498
PAN-A	Physique	Polyacrylonitrile	457
GF-40	Chimique	Noyaux d'olive	347
BC-120	Chimique	Bois	377
Picabiol	Chimique	Bois	367
PAN-C	Non-activé	Polyacrylonitrile	501
CTP-PAN-3:1-C	Non-activé	Brai de coke et polyacrylonitrile	546
CTP-C	Non-activé	Brai de coke	558
CTP-PAN-1:1-C	Non-activé	Brai de coke et polyacrylonitrile	540
Noix de coco carbonisé	Non-activé	Noix de coco	370
NC-70- Cu	Physique	Noix de coco	325
NC-70 -CuCr	Physique	Noix de coco	316

Tableau :J Température d'inflammation spontanée des charbons actifs

## *Resumé en Français*

---

Echantillons	Energie d'activation ( $E_a$ ) (kJ/mole)	Ln (A)	Gamme de température °C
NC-50	106	14.7	390-490
NC-60	106	14.4	390-495
NC-100	132	17.1	400-550
BPL	219	28.3	490-595
RB-2	205	27.1	490-570
CTP-A	299	21,8	495-595
CTP-PAN-3:1-A	233	19,3	480-595
CTP-PAN-1:1-A	204	13,4	450-580
PAN-A	138	12,8	460-590
GF-40	103	9,9	360-500
BC-120	104	8,7	430-520
Picabiol	104	6,6	422-497
PAN-C	164	18,8	354-500
CTP-PAN-3:1-C	237	31,5	421-550
CTP-C	302	34,1	424-575
CTP-PAN-1:1-C	216	22,5	426-575
Noix de coco carbonisé	89	10,2	219-400
NC-70-Cu	70	5.8	200- 375
NC-70-CuCr	62	4.3	195-365

Tableau :k Energie d'activation de réactions d'inflammation

## **INFLUENCE DES PARAMÈTRES OPÉRATOIRES SUR LA RÉACTIVITÉ**

Influence de la teneur en oxygène dans le gaz

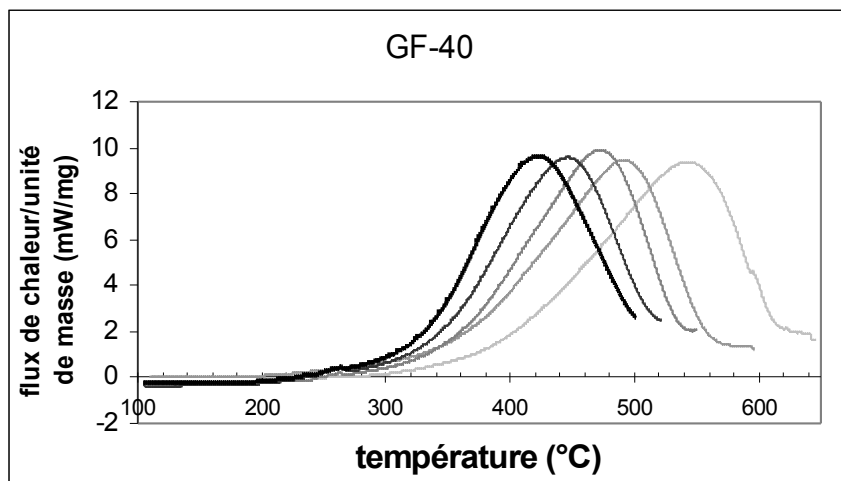
## **Resumé en Français**

---

Des oxydations ayant déjà été réalisés sous une atmosphère contenant 20% d'oxygène, le plan expérimental s'est limité à quatre autres pourcentages d'oxygène dans l'atmosphère : 10% d'oxygène pour 90% d'hélium (10/90), 40/60, 70/30 et 100% d'oxygène (100/0). On sélectionne 5 échantillons : PAN-A, GF-40, NC-60, Noix de coco et NC-70-Cu.

On obtient pour chaque échantillon les courbes de flux de chaleur par unité de masse en fonction de la température. Pour les échantillons NC-60, Noix de coco et NC-70-Cu (Annexe figures C, D, E pages 39, 40) la même évolution s'observe, l'amplitude du flux de chaleur augmente avec le pourcentage d'oxygène dans l'atmosphère et les échantillons débutent leur inflammation plus tôt ce qui conduit à une combustion complète et d'intensité très forte aux hautes teneurs en oxygène (figure F page 42). Pour l'échantillon GF-40 (figure A page 39) c'est différent, l'amplitude est presque constante, seule l'inflammation est avancée. Enfin il semble qu'il y ait un problème pour le PAN-A qui à 40% d'oxygène donne un pic.

**Figure 1 :** Exemple de courbes de flux de chaleur obtenues pour les différentes teneurs en



oxygène

Les courbes de perte de masse obtenues montrent une accélération avec l'augmentation du pourcentage d'oxygène. La vitesse d'inflammation de tous les charbons actifs est accélérée lorsque le concentration d'oxygène dans l'air augmente. Les courbes de la perte de masse débutent plus tôt lorsque le pourcentage d'oxygène est fort, on constate notamment pour le PAN-A (figure H page 43) qu'avec 10% d'oxygène la réaction n'est pas terminée.

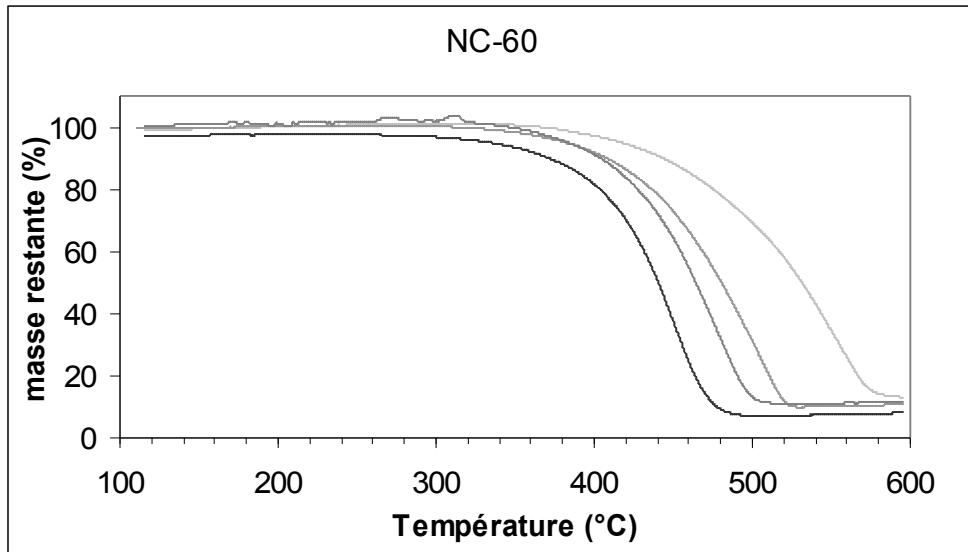


**Figure 2 :** Exemple de courbes obtenues pour le pourcentage de perte de masse avec les différentes teneurs en oxygène dans l'atmosphère

L'évolution du PIO (ANEXE 11 p 46) ne présente pas d'évolution pour les pourcentages d'oxygène supérieurs à 20%, sauf pour l'échantillon NC-70-Cu mais pour lequel il n'y a que trois points de mesures. Les échantillons GF-40 et PAN-A ont des valeur de PIO plus hautes pour 10% d'oxygène dans l'atmosphère. Une étude pourrait être faite pour déterminer plus précisément ce phénomène afin d'observer l'impact des faibles pourcentages d'oxygène dans l'air sur l'oxydation des charbons.

L'évolution du SIT est elle beaucoup plus intéressante à observer(ANNEXE 12 page 47). On constate avec les deux méthodes une baisse significative de la température de SIT avec l'augmentation du pourcentage d'oxygène dans l'atmosphère. L'inflammation des charbons actifs est donc fortement influencée par le pourcentage d'oxygène dans l'atmosphère.

L'évolution de l'énergie d'activation (ANNEXE 13 page 48) a tendance à diminuer avec l'augmentation du pourcentage d'oxygène, constatation faite pour les échantillons GF-40 et NC-70-Cu. On observe la même diminution d'énergie d'activation pour les autres échantillons mais la valeur obtenue pour 20% d'oxygène dans l'atmosphère est en décalage avec cette évolution. Ce problème nécessiterait de nouvelles manipulations afin de vérifier ces valeurs.

## **Resumé en Français**

L'influence de l'oxygène sur la vitesse de combustion du carbone est plus faible pour l'échantillon chimiquement activé (GF-40) que pour l'échantillon physiquement activé (NC-60) alors que les charbons chimiquement activés ont une résistance à l'oxydation moins bonne. L'explication est peut être due à la plus grande quantité d'oxygène présente dans le GF-40 qui aurait jouer un rôle lors de l'inflammation.

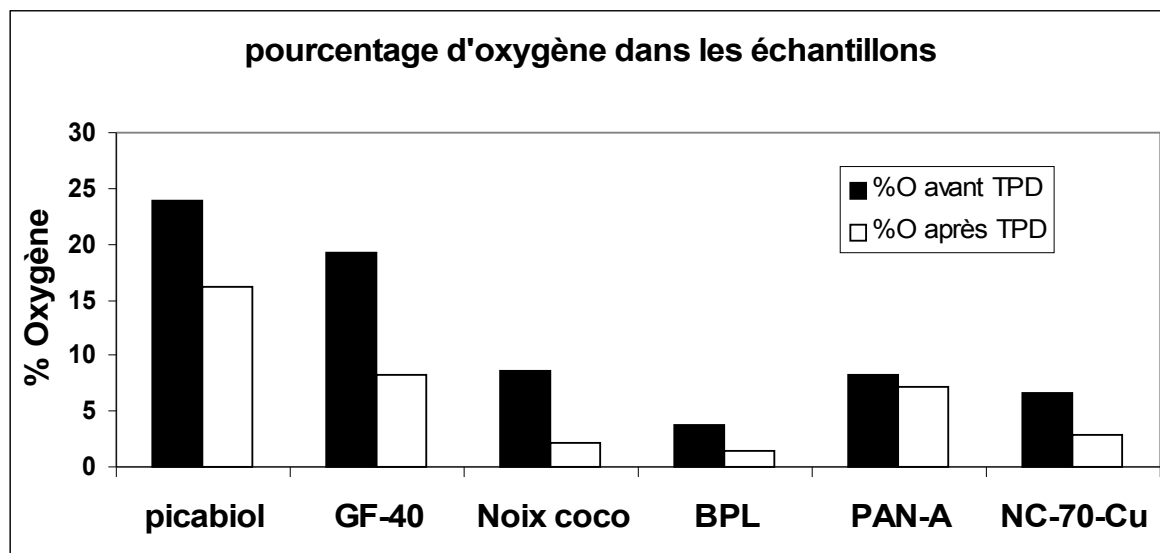
### **Résultats du TPD :**

#### **RÉSULTAT DE L'ANALYSE ÉLÉMENTAIRE :**

L'hydrogène et l'oxygène contenu dans les charbons nous donnent une idée des groupements fonctionnels de surface contenus dans les charbons actifs. On remarque également un plus grand pourcentage d'oxygène (de l'ordre de 5 fois plus) dans les charbons activés chimiquement que dans les charbons activés physiquement. Ces groupements de surface se sont formés pendant le processus d'activation chimique. Les charbons non activés, imprégnés et enrichis en azote contiennent plus d'oxygène que les physiquement activé mais moins que les charbons chimiquement activés. (*Annexe Tableau 5 page 38*)

Le soufre n'est présent dans aucun des charbons analysé et l'azote est présent seulement dans l'échantillon PAN-A qui est fabriqué à partir de fibre en contenant beaucoup.

Figure 3 : Pourcentage d'oxygène des charbons actifs avant et après TPD



On constate une très nette baisse du pourcentage d'oxygène dans tous les échantillons après avoir subi un traitement thermique. On a donc réussi avec cette méthode à évacuer une partie des groupes fonctionnels de surface présents sur les échantillons.

## *Resumé en Français*

---

### **INFLUENCE SUR LES PARAMÈTRES CARACTÉRISTIQUES :**

La méthode DSC a été utilisée ici pour mesurer les PIO, SIT et énergie d'activation. Les valeurs expérimentales sont comparées avec celles obtenues lors de précédentes manipulations réalisées par Thangavelu Jayabalan des mêmes charbons n'ayant pas subi de désorption.

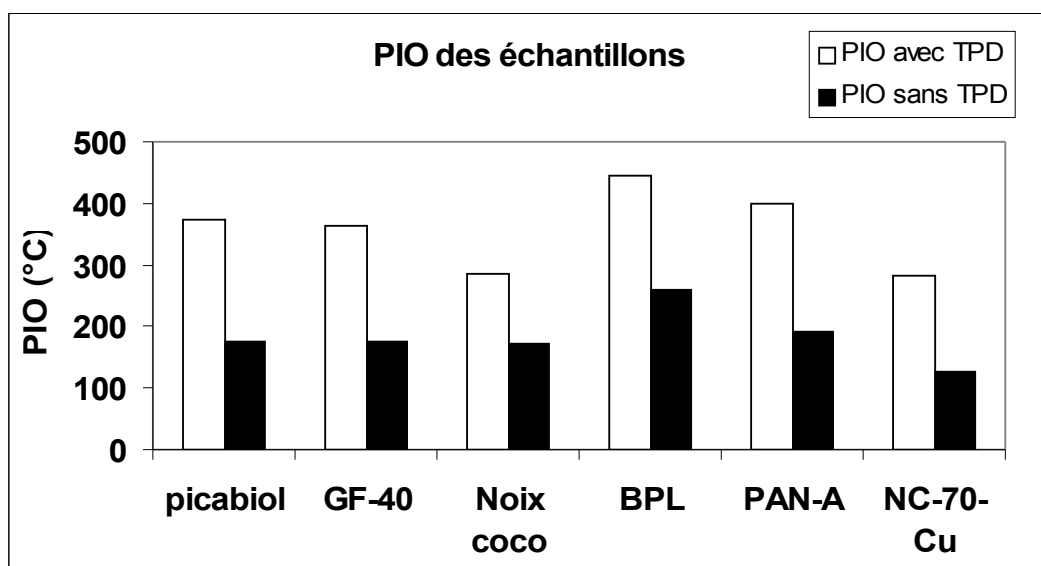
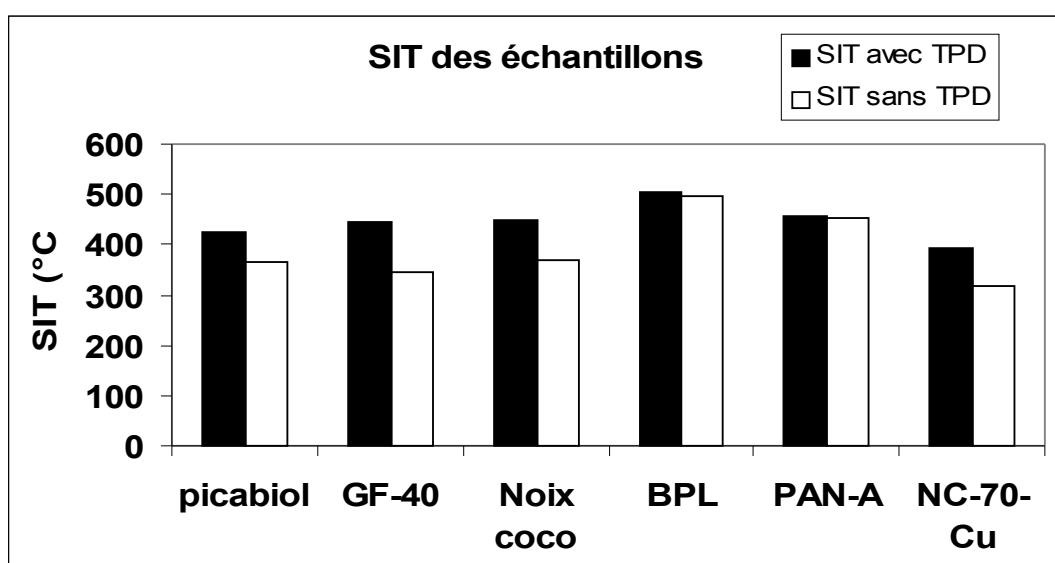


**Figure 4 : Température de PIO des charbons avant et après TPD**

L'évolution du PIO déterminé à partir des courbes DSC est très significative pour chacun des charbons étudiés, on constate une forte augmentation, de l'ordre du double, des températures de départ d'oxydation lorsqu'on applique un traitement aux échantillons. Des charbons ayant moins d'oxygène à leur surface commencent donc à s'oxyder moins vite et ce pour tout types de charbons. L'évolution du PIO pour les charbons chimiquement activés est plus marquée que pour les échantillons physiquement activés.



## **Resumé en Français**

**Figure 5 : Température de SIT des charbons actifs avant et après TPD**

La température de SIT augmente après traitement thermique, les groupements de surface influent sur l'inflammation. L'évolution est par contre beaucoup moins significative que pour le PIO voire pas du tout pour les échantillons physiquement activés et enrichis en azote.

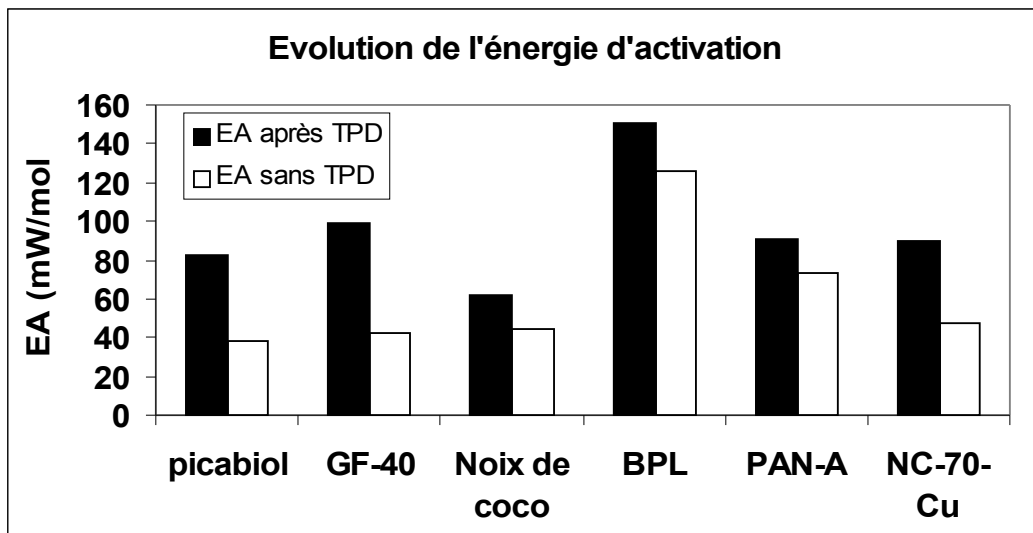


**Figure 6 : Energie d'activation des charbons actifs avant et après TPD**

On constate logiquement une augmentation de l'énergie d'activation lorsque l'échantillon a subit un traitement thermique. La teneur en oxygène du matériau a un effet sur la vitesse de combustion du charbon. Cet effet est plus important sur les matériaux activés chimiquement.

## **CONCLUSION**

L'influence de l'oxygène présent sur les charbons sous forme de fonctions de surface à pu être mise en évidence grâce aux analyses thermiques et aux analyses élémentaires réalisées. Ces essais ont débuté en évacuant les fonctions de surface des charbons et en vérifiant que la quantité d'oxygène présente sur le matériau diminuait significativement, ce qui est le cas. L'oxydation des charbons après évacuation des fonctions de surface a permis d'observer l'évolution des températures initiales d'oxydation et d'inflammation, ainsi que celle de l'énergie d'activation. L'observation des résultats montre qu'un traitement thermique permet d'obtenir une température de départ d'oxydation (PIO) deux fois plus élevée qu'avec des échantillons non traités. Un traitement thermique peut permettre d'augmenter la température de SIT, notamment dans le cas des charbons chimiquement activés. Pour les charbons

## ***Resumé en Français***

---

physiquement activés, on observe peu d'effet. L'énergie d'activation des charbons chimiquement activés et imprégné double après traitement, tandis que pour les autres échantillons, l'augmentation est entre 20% et 40%.

L'oxydation des charbons actifs sous plusieurs atmosphères contenant différents pourcentage d'oxygène à été réalisée afin de mettre en évidence l'influence de l'oxygène de l'air environnant sur leur oxydation et inflammation. L'évolution de l'énergie d'activation et des températures PIO et SIT a été observée. Le PIO ne varie pas de manière significative, lorsque le pourcentage d'oxygène est supérieur à 20% l'oxygène de l'air influence modérément la résistance à l'oxydation des charbons. En revanche, l'énergie d'activation et la température de SIT diminuent nettement avec l'augmentation de la concentration d'oxygène dans l'atmosphère, l'inflammation est donc plus rapide aux forts pourcentages d'oxygène.

D'autres essais permettraient d'étudier plus en détail l'influence de la méthode d'activation des charbons sur l'inflammation aux différents pourcentages d'oxygène dans l'atmosphère. Ces essais pourraient aider à comprendre pourquoi l'échantillon physiquement activé à brûlé plus facilement que l'échantillon physiquement activé.

## **ANALYSE DE LA RÉACTIVITÉ**

### **Influence de la teneur en oxygène des matériaux**

Les principaux résultats sont suivants :

1. Pour une faible teneur en oxygène pour un échantillon, la température Initiale d'oxydation (PIO) et température d'inflammation spontanée (SIT) sont plus élevée.
2. Les charbons actifs sont associés à des hétéro atomes, en particulier l'oxygène qui dépend de conditions d'activation et le precursor de charbon actifs.
3. Ces hétéro atomes ou composés de surfaces oxygénées réagissent avec l'oxygène de l'air pour donner CO, CO<sub>2</sub>, des complexes intermédiaires et dégage de la chaleur.
4. Exception pour 3 échantillons physiquement activés à la base de noix coco (NC-50, NC-60 et NC-100)
5. Ces échantillons à base de noix coco présentent une affinité accrue pour la chimisorption de l'oxygène.

Aussi en effet ces échantillons contiennent une proportion important en potassium (K) qui joue le rôle de catalyseur d'oxydation et de l'inflammation ce qui est représenté sur la figure suivante

## *Resumé en Français*

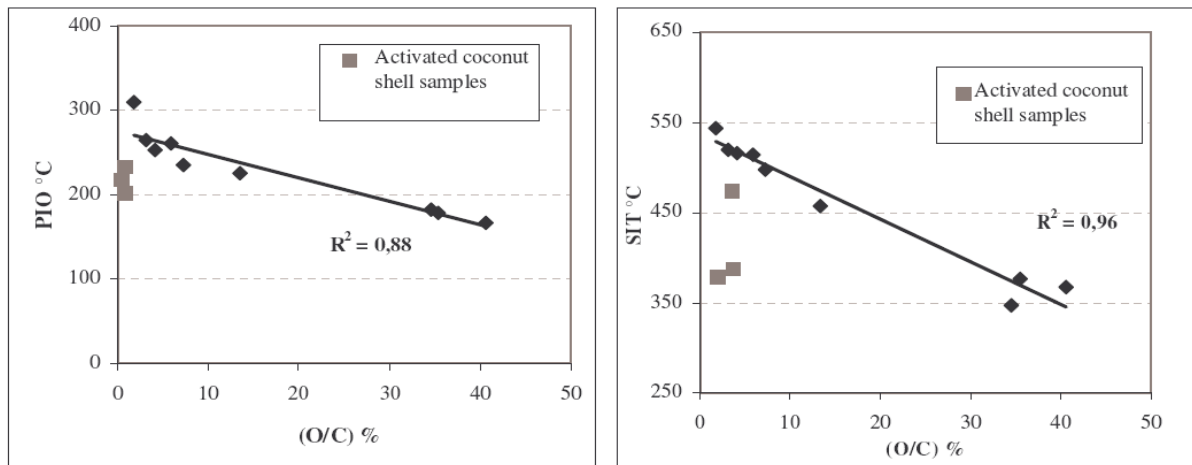


Figure : L Influence de la teneur en oxygène sur le PIO et SIT des charbons actifs.

### Influence de la teneur en azote

Les principaux résultats sont les suivants

1. Les échantillons enrichis en azote (mélanges CTP-PAN), pour des valeurs N/C > 1 % présentent une meilleure stabilité: PIO et SIT plus élevés.
2. Mais l'influence de N/C est faible par rapport O/C.

### Influence des métaux déposés sur charbon actif

On étudie l'influence des métaux sur le PIO et SIT. On compare les échantillons imprégnés avec le cuivre et le chrome et le non-imprégnées. On remarque que les échantillons imprégnés s'oxydent facilement que les échantillons non imprégnés. Les métaux jouent en même temps le rôle de catalyseur de l'oxydation et d'oxydant.

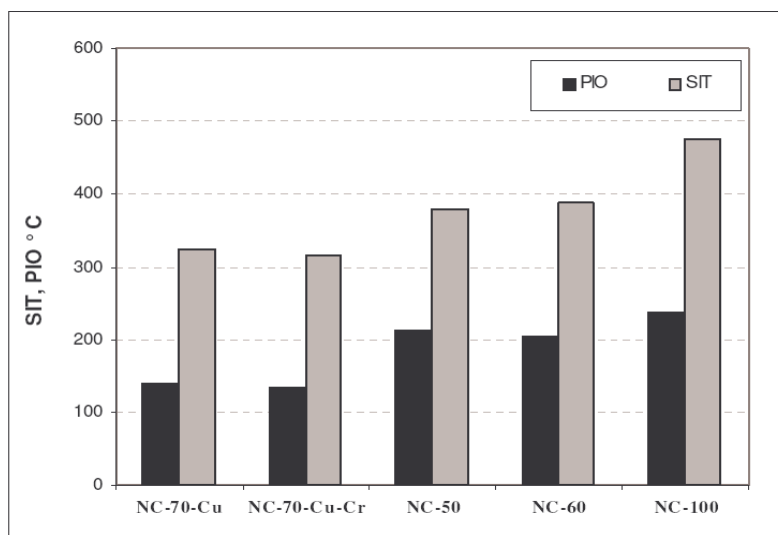


Figure : M Influence de imprégnation des métaux sur le PIO et SIT des charbons actifs

### Influence des propriétés texturales et structurales

## **Resumé en Français**

---

### *Texturales*

L'influence de la texture (SBET, Vmicro et Wmicro) n'est pas significative. Par contre quand le volume des pores (méso et macropores) augmente, on observe une faible tendance de diminution de PIO et SIT. Les méso et macro pores facilitent la diffusion de l'oxygène à l'intérieur des charbons actifs.

### *Etude structurale*

L'étude quantitative structurale sur les charbons permet de déterminer la longueur de feuillet graphitique. On observe que si la grandeur de feuillet augmente, l'énergie d'activation augmente. Cet à dire que la stabilité à l'oxydation monte. Quand la longueur augmente il y'a très peu d'oxygène dans le bordure et l'échantillons ne s'oxyde pas facilement.

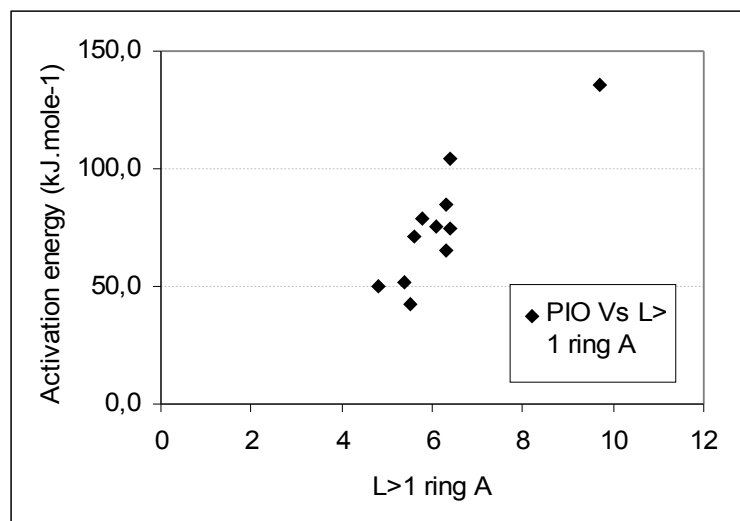
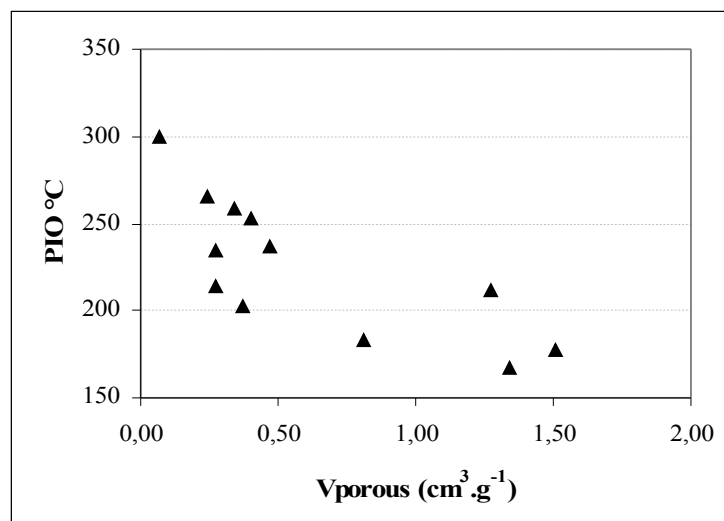


Figure : N Influence des propriétés texturales et structurales sur le PIO et SIT des charbons actifs

## ***Resumé en Français***

---

### **CORRÉLATIONS QUANTITATIVES PAR RÉGRESSION LINÉAIRE MULTIPLE**

L'analyse quantitative effectuée à partir des régressions linéaires multiples permet de distinguer les caractéristiques des matériaux les plus influents et d'évaluer leur poids sur les paramètres de réactivité. L'analyse quantitative des caractéristiques des matériaux confirme la composition chimique notamment le rapport oxygène sur carbone, en forme de groupements oxygénés de surface, et joue un rôle significatif dans le processus d'oxydation et d'inflammation. Le rapport oxygène sur carbone influence aussi bien la température initiale d'oxydation que la température d'inflammation instantanée, mais son influence est beaucoup plus ressentie pour la température initiale d'oxydation que pour la température d'inflammation instantanée. Les propriétés texturales (la surface spécifique, le volume poreux et la largeur du micropore) ne peuvent pas être validées comme des propriétés influentes. Cependant la dimension structurale nanométrique des unités de base  $L > 1$  aromatique joue un rôle important sur les mécanismes d'oxydation. Les feuillets courts contribuent au développement d'un nombre élevé de sites de réaction, accélérant ainsi le taux initial d'oxydation et réduisant la température initiale d'oxydation.

### **Influence de la nature du COV sur la réactivité**

Enfin, la présence de composés organiques volatiles adsorbés dans le matériau peut causer un début rapide des réactions d'oxydation. Pour les charbons actifs saturés avec des composés organiques volatiles particulièrement les cétones, la valeur de leur température initiale d'oxydation est réduite de 50 à 100°C. Les charbons actifs à base de noix de coco qui est plus facilement oxydable, à une température proche de 200 °C. Par ailleurs, les composés organiques volatiles et plus particulièrement les cétones s'oxydent à des températures beaucoup plus basses ; ainsi la méthylisobutylcétone adsorbés sur le charbon actif à base de noix de coco présente des températures d'oxydation inférieures à 120 °C. En revanche, les composés halogénés, hydrocarbonés, les alcools et les amines sont très peu réactifs. L'adsorption de cétones sur des charbons actifs à base de noix de coco apparaît donc fortement susceptible d'engendrer des problèmes d'inflammation du filtre.

<b>COV</b>	<b>Echantillons</b>	<b>PIO (°C)</b>	<b>PIO (°C) Sans COV</b>
<i>Cétone</i>	RB-2	153	260

## Resumé en Français

---

	BPL	125	253.2
	RB-2	137	260
Méthyléthylcétone	BPL	76	253.2

Tableau :L Influence de la nature du COV sur la réactivité

COV	Formule	PIO °C	T <sub>i</sub> COV (°C)
Méthylisobutylcétone	C <sub>6</sub> H <sub>12</sub> O	107	448
Méthyléthylcétone	C <sub>4</sub> H <sub>8</sub> O	118	404
Acétone	C <sub>3</sub> H <sub>6</sub> O	129	465
Tétrahydrofuran	C <sub>4</sub> H <sub>8</sub> O	136	321
Isobutylvinylether	C <sub>6</sub> H <sub>12</sub> O	136	311
Ethylacétate	CH <sub>3</sub> CH <sub>2</sub> OC(O)CH <sub>3</sub>	145	426
Isopropylether	(CH <sub>3</sub> ) <sub>2</sub> CHOCH(CH <sub>3</sub> ) <sub>2</sub>	156	238
Méthyléthyldioxalane	C <sub>9</sub> H <sub>18</sub> O <sub>2</sub>	158	387
Toluène	C <sub>7</sub> H <sub>8</sub>	> Tox (AC)	480
Cyclohexane	C <sub>6</sub> H <sub>12</sub>	> Tox (AC)	245
1,2 dichloroethane	C <sub>2</sub> H <sub>4</sub> Cl <sub>2</sub>	> Tox (AC)	413
Ethanol	<u>C<sub>2</sub>H<sub>6</sub>O</u>	> Tox (AC)	363
Chloroform	CHCl <sub>3</sub>	> Tox (AC)	249
Triéthylamine	C <sub>6</sub> H <sub>15</sub> N	> Tox (AC)	228
Hexane	<u>C<sub>6</sub>H<sub>14</sub></u>	> Tox (AC)	228

Tableau :M Influence de la nature du COV sur la réactivité

## CONCLUSIONS

- Les paramètres de réactivité des charbons actifs sont étudiés avec la mesure de point initial d'oxydation (PIO) et la température d'auto-inflammation (SIT).

## ***Resumé en Français***

---

- Le mise en évidence de l'influence des conditions opératoires (Conc d'O<sub>2</sub>, vitesse du gaz et vitesse d'échauffement) et des propriétés chimiques et structurales des charbons actifs a été montré.
- Les analyses qualitatives et quantitatives soulignent l'influence prépondérante de teneur en O/C et de la longueur des feuillets de graphène sur la réactivité des charbons actifs.
- Les modèles cinétiques simples des réactions d'oxydation et de combustion sont réussis avec des mesures d'énergies d'activation.
- Finalement la structure multi échelle des charbons actifs reste à l'heure actuelle encore mal comprise, qui montre limites des méthodes de caractérisation disponibles.

Les données mesurées précédemment ont permis une approche statistique dans le but de modéliser les énergies d'adsorption.

## **La Régression Linéaire Multiple (RLM)**

### **Aspects théoriques**

Une régression multivariable s'écrit sous la forme <sup>[27]</sup> :

$$y = f(x_i)$$

où      y : réponse ou variable expliquée ;

      x<sub>i</sub> : i<sup>ème</sup> variable explicative, i ∈ [0;k], ( k étant le nombre de variable explicatives).

La fonction f peut être sous diverses formes (exponentielle, logarithmique,..) mais pour des raisons de simplicité, nous utilisons la régression linéaire qui peut s'écrire dans ce cas :

$$y = \beta_0 + \sum_{i=1}^k \beta_i x_i + \varepsilon_r$$

où      β<sub>i</sub> : coefficient réel de la régression ;

      ε<sub>r</sub> : erreur de la régression.

Cette équation réelle est inconnue et est donc ajustée par une équation de la forme :

$$y = b_0 + \sum_{i=1}^k b_i \cdot x_i$$

où      b<sub>i</sub> : estimateurs des coefficients réels.

## ***Resumé en Français***

---

Afin de juger de la qualité de la régression nous avons sélectionné plusieurs paramètres. Ceux-ci sont : les coefficients de détermination  $r^2$  et  $r^2_{aj}$  et l'estimation de l'écart-type de

$$r^2 = \frac{\sum_{j=1}^n (\hat{y}_j - \bar{y})^2}{\sum_{j=1}^n (y_j - \hat{y}_j)^2} \quad r^2_{aj} = \frac{(n-1).r^2 - k}{n - k - 1}$$

l'erreur du modèle s.

Avec  $y_j$ : j-ème variable expliquée observée,  $j \in [1;n]$  ;

$\hat{y}$  : j-ème variable expliquée prédite ;

$\bar{y}$  : moyenne des  $\hat{y}_j$  ;

n : taille de l'échantillon ( $n-k-1$  :nombre de degrés de liberté).

$r^2$  représente la part de la variance de la réponse expliquée par le modèle de régression,  $r^2_{aj}$  est le coefficient de détermination  $r^2$  ajusté des degrés de liberté, l'intérêt étant de pouvoir comparer des modèles de tailles différentes.

L'écart-type de la régression s est calculé à partir de la formule :

$$s = \sqrt{\frac{\sum_{i=1}^n (y_i - \hat{y}_i)^2}{n - k - 1}}$$

Cette valeur est à comparer à l'écart-type des réponses observées y, pour analyser l'intérêt de la régression.

Afin de discriminer les variables explicatives permettant d'établir la meilleure régression, une méthode 'pas à pas' est appliquée. La procédure démarre par la sélection de la meilleure régression monovariable. La méthode consiste à introduire à chaque étape un prédicteur supplémentaire et à sélectionner la meilleure régression sur la base de la valeur de  $r^2_{aj}$ . Eventuellement, si un prédicteur devient non significatif, il est éliminé. L'algorithme s'arrête lorsqu'on ne peut plus ajouter de nouveau prédicteur significatif.

## **CONCLUSION ET PERSPECTIVES**

Les phénomènes d'auto-inflammation des charbons actifs sont le résultat de plusieurs processus complexes physiques et chimiques. Des tentatives ont été faites dans ce travail pour élucider la dépendance des propriétés des matériaux et des conditions opératoires qui

## ***Resumé en Français***

---

influencent la réactivité des charbons actifs. Une nouveauté dans ce travail est la quantification de l'influence de ces propriétés sur la réactivité d'oxydation et d'inflammation utilisant des corrélations statistiques. Les trois principales conclusions de cette étude : caractérisation des propriétés des charbons actifs, réactivité d'oxydation et d'inflammation suivie par les mécanismes et finalement l'influence quantitative des caractéristiques des matériaux sur sa réactivité et perspective de sécurité de processus.

### **Les propriétés de surface des charbons actifs**

Les résultats ont montré que le mode d'activation et le précurseur influencent principalement les propriétés des charbons actifs. L'activation chimique génère plus de mesopore aux carbones activés avec des surfaces spécifiques plus hautes, avec un grand nombre de groupements oxygénés de surface et une teneur en cendre négligeable. L'organisation structurale de ces carbones activés est fortement désordonnée et caractérisée par des feuillets graphitiques plus courts. D'autre part les carbones physiquement activés montrent des caractéristiques diversifiées en matière de stabilité comme les échantillons commerciaux et celle de laboratoire. En général les carbones physiquement activés possèdent des groupements oxygénés de surface en plus petite quantité et avec le teneur en cendre plus élevées. Les valeurs de la surface spécifique montre la variation par rapport les conditions d'activation et de précurseur d'échantillon. Les échantillons commerciaux possèdent des surfaces spécifiques plus élevées que les échantillons préparés dans le laboratoire. Les observations HRTEM montrent que les carbones physiquement activés sont bien organisés les couches graphitiques qui sont plus longues que pour les carbones chimiquement activés.

### **Études de réactivité**

L'étude de l'oxydation et de la réactivité de l'inflammation des charbons actifs en présence d'air ont été caractérisées par deux paramètres : La température initiale d'oxydation (PIO) et température d'inflammation instantanée (SIT). On a montré que ces valeurs varient avec les conditions appliquées (le débit du gaz de balayage, la vitesse d'échauffement, la composition d'oxygène dans le gaz de balayage). Le but était de faire des comparaisons quantitatives avec les échantillons divers et indiquer les propriétés influentes sur la réactivité des matériaux. L'étude cinétique a été faite pour différents régions d'oxydation et d'inflammation. Les valeurs de température initiale d'oxydation (PIO) et température d'inflammation instantanée (SIT) étaient légèrement plus hautes que celles trouvées par la méthode de ASTM (American

## ***Resumé en Français***

---

Society for Testing and Materials ASTM-D 3466-76. Cependant les résultats sont utilisés pour comprendre l'influence des propriétés sur la réactivité de charbon actif et pas pour mesurer les températures d'oxydation et d'inflammation en conditions de fonctionnement.

### **Influence de propriétés des matériaux et conditions opératoires sur la réactivité des charbons actifs**

L'influence des propriétés des matériaux et des conditions opératoires sur les paramètres de réactivité a été analysée qualitativement et quantitativement. L'analyse qualitative a donné les tendances générales concernant l'effet de la composition chimique et les caractéristiques de la porosité sur les paramètres de réactivité. Le rapport oxygène sur carbone a une influence plus grande sur les caractéristiques d'inflammation d'oxydation avec des exceptions concernant les charbons actifs à base de noix coco. Les caractéristiques de porosité comme la surface spécifique, le volume poreux et la largeur du micropore ont moins d'influence sur les paramètres de réactivité, au lieu de propriétés texturale le phénomène de réactivité des charbons actifs sont mieux expliquées avec l'aide des propriétés structurelles comme la longueur de feillet graphitique. Il a été trouvé que les charbons actifs qui sont stables ont un faible pourcentage de feuillets graphitiques non empilés et le nombre des feuillets empilés dans un USB sont grande qui limitent probablement l'accès à l'oxygène aux sites actifs. Les charbons actifs avec des couches graphitiques plus longues ont des températures d'oxydation et d'inflammation plus élevées.

Les composés organiques volatiles ont un impact fort sur la diminution des températures d'oxydation et d'inflammation des charbons actifs. Les températures d'oxydation et d'inflammation dépendent de la nature des composés organiques volatiles. Certaines types de composés organiques volatiles comme les cétones aromatiques sont plus réactifs que les amines, les hydrocarbures et les alcanes. Les composés organiques volatiles subissent des réactions d'oxydation sur la surface des charbons actifs libérant la chaleur exothermique amorçant les réactions d'inflammation et d'oxydation. Par certains charbons actifs comme la noix de coco activé physiquement présent avec les COV à une température initiale d'oxydation inférieure subissent des réactions d'oxydation bien avant l'oxydation des composés organiques volatiles.

La condition opératoire comme l'augmentation de la composition d'oxygène diminuent la température initiale d'oxydation et d'inflammation. La réactivité de carbones activés est

## ***Resumé en Français***

---

énormément réduite dans l'environnement avec très peu d'oxygène. Les carbones activés physiquement sont moins réactifs à la concentration d'oxygène de 21 % et leur réactivité chute brutalement à concentration d'oxygène pure (100 %) par rapport des charbons chimiquement activé à la même condition. Ce phénomène a été bien observé pour charbons à base de noix de coco. Cette observation indique que la réactivité des carbons actifs est spécifique aux conditions de fonctionnement.

L'augmentation de débit de gaz ne influence pas la réactivité des carbons actifs. Une augmentation du débit d'oxygène n'augmente pas la diffusion interne des molécules d'oxygène dans les micropores. Le chauffage du lit peut aussi être récompensé par la dissipation de chaleur par convection.

### **Perspectives**

Les résultats de ce travail peuvent être utilisés principalement dans les aspects de procédés et dans le processus de fabrication. Certaines propriétés peuvent être examinées pour augmenter la stabilité d'oxydation. Dans le point de vue de procédés précaution doit être mis pour certains matériaux pendant leur opération, transport et le stockage en raison de leur vulnérabilité pour d'oxydation et d'inflammation. Les résultats de ce travail peuvent être intégrés avec les modèles cinétiques simulant des unités industrielles. Le modèle de régression linéaire multiple a été essayé dans ce travail et cela peut être nouveau étendu au modèle de régression non linéaire en l'utilisant de la base de données. Finalement une profonde connaissance est exigée notamment pour la morphologie structurale des carbons actifs pour répondre aux leur ambiguïtés.



---

## APPENDIX

---

**APPENDIX-A:** Mineral analysis of ash content in the activated carbons using sem-X ray technique

**APPENDIX-B:** Adsorption and desorption isotherms of N<sub>2</sub> at 77 K for various activated carbons

**APPENDIX-C:** Calculation of specific surface area S<sub>BET</sub> from the plot of  $\frac{1}{V[P_0 / P - 1]}$  Vs  $\frac{P}{P_0}$

**APPENDIX-D:** Pore size distribution using DFT method

**APPENDIX-E:** t-Plots for micropore volume calculations

**APPENDIX-F:** Porosity characteristics obtained from N<sub>2</sub> at 77 K

**APPENDIX-G:** SEM micrographs of activated carbon samples

**APPENDIX-H:** HRTEM images of activated carbon samples

**APPENDIX-I:** DSC thermogram for a reference activated carbon sample

**APPENDIX-J:** PIO and SIT data measured before and after Temperature Programmed Desorption (TPD)

**APPENDIX-K:** PIO and SIT data at different oxygen concentrations of the ambient gas

**ANNEXE-L:** DSC curves measured with concentrations of oxygen at 10%, 21 %, 40 %, 70% & 100 %

**APPENDIX-M:** TG curves measured with concentrations of oxygen at 10%, 21 %, 40 %, 70% & 100 %

**APPENDIX-N:** PIO and SIT data for the flow rate of 1.2 L/hr and 2.4 L/hr

**APPENDIX-O:** PIO and SIT data for the heating rates 2, 5 and 8 K/min

**APPENDIX-P:** Analysis of residuals of the multiple linear regression equation relating the PIO with the predictor variables O/C ratio and L>1 ring

## APPENDIX-A

### MINERAL ANALYSIS OF ASH CONTENT OF THE ACTIVATED CARBONS USING SEM-X RAY TECHNIQUE

**Figure A-** :Graph showing elemental peaks for the mineral content of the NC-50

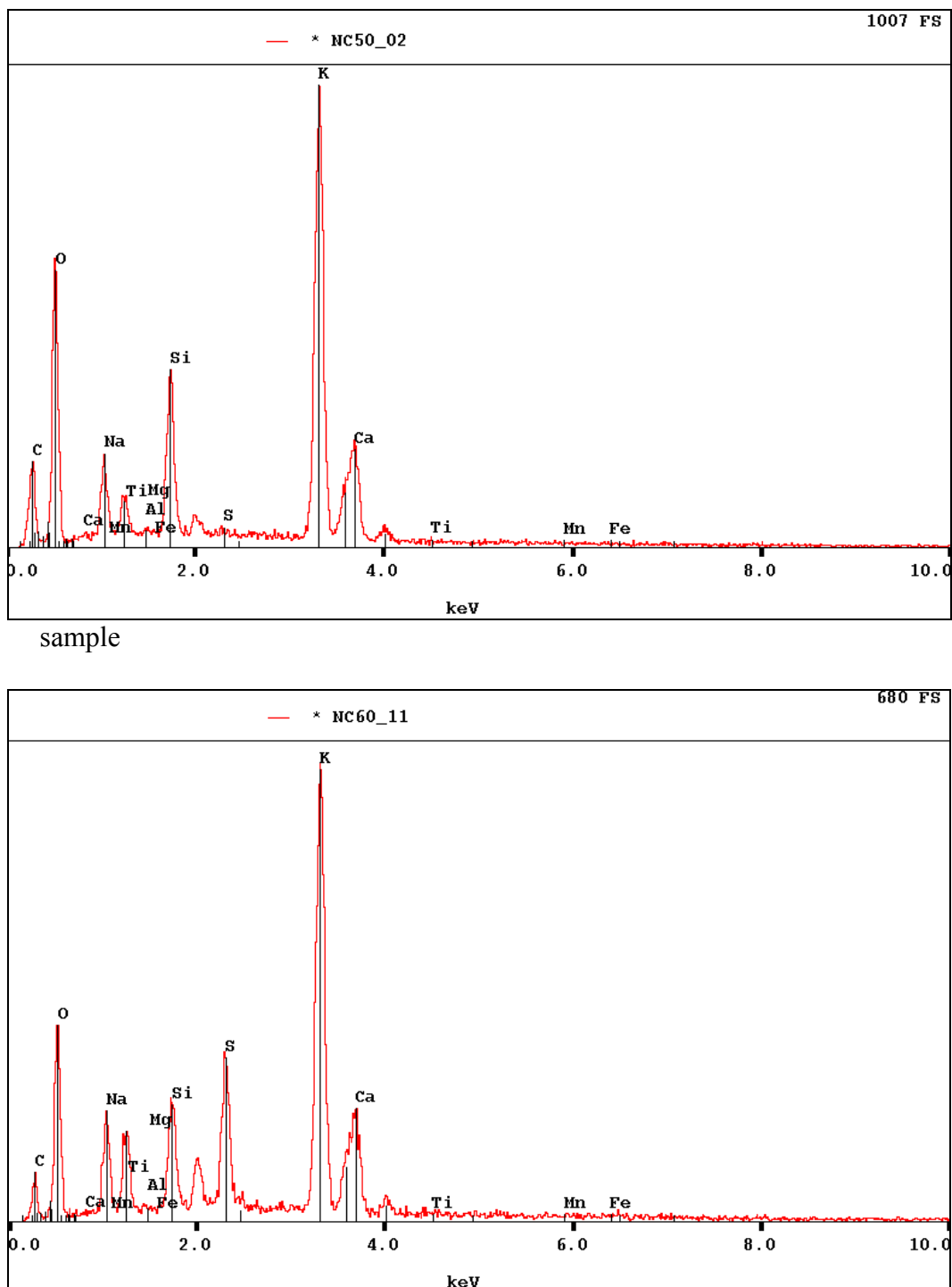


**Figure A-** :Graph showing elemental peaks for the mineral content of the NC-60 sample

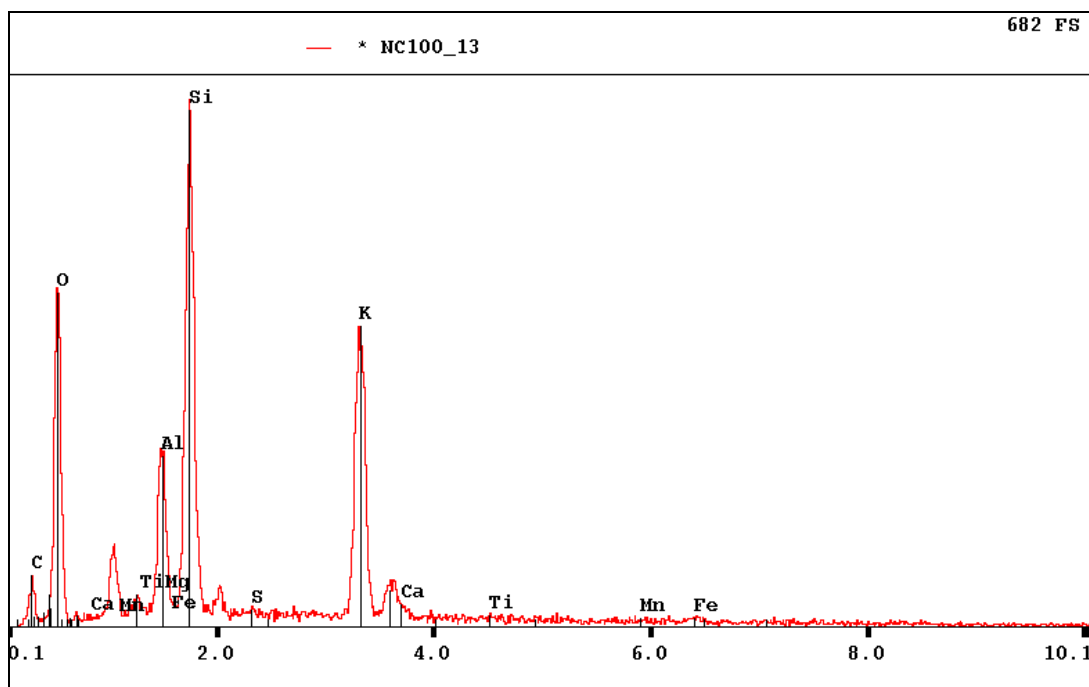


**Figure A- :** Graph showing elemental peaks for the mineral content of the NC-100 sample

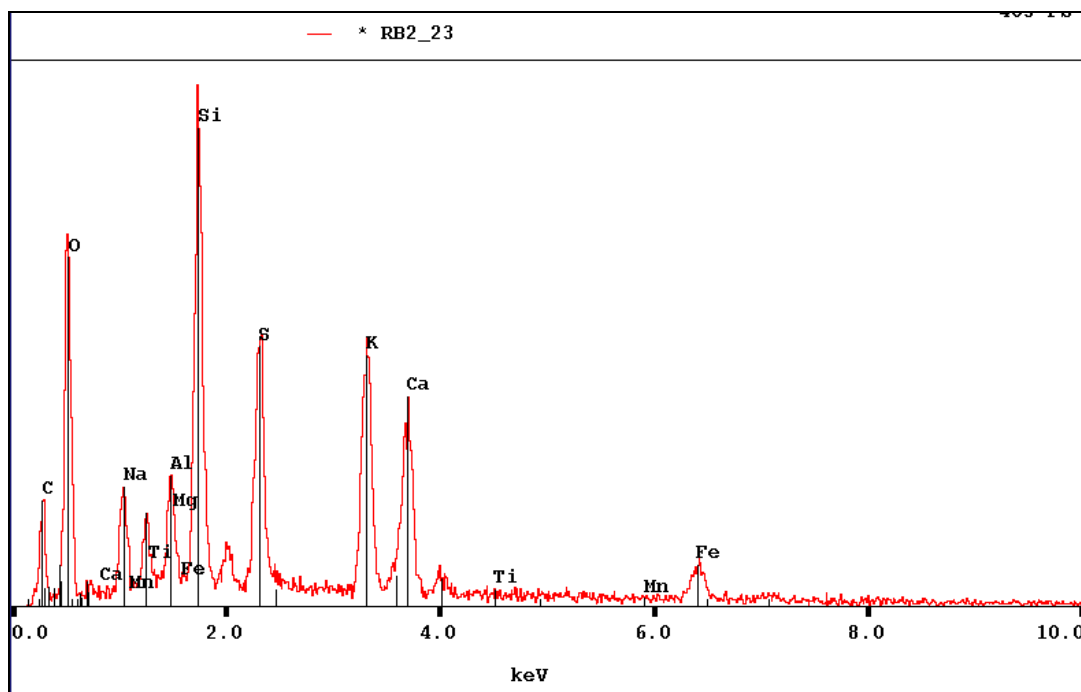


**Figure A- :** Graph showing elemental peaks for the mineral content of the RB-2 sample

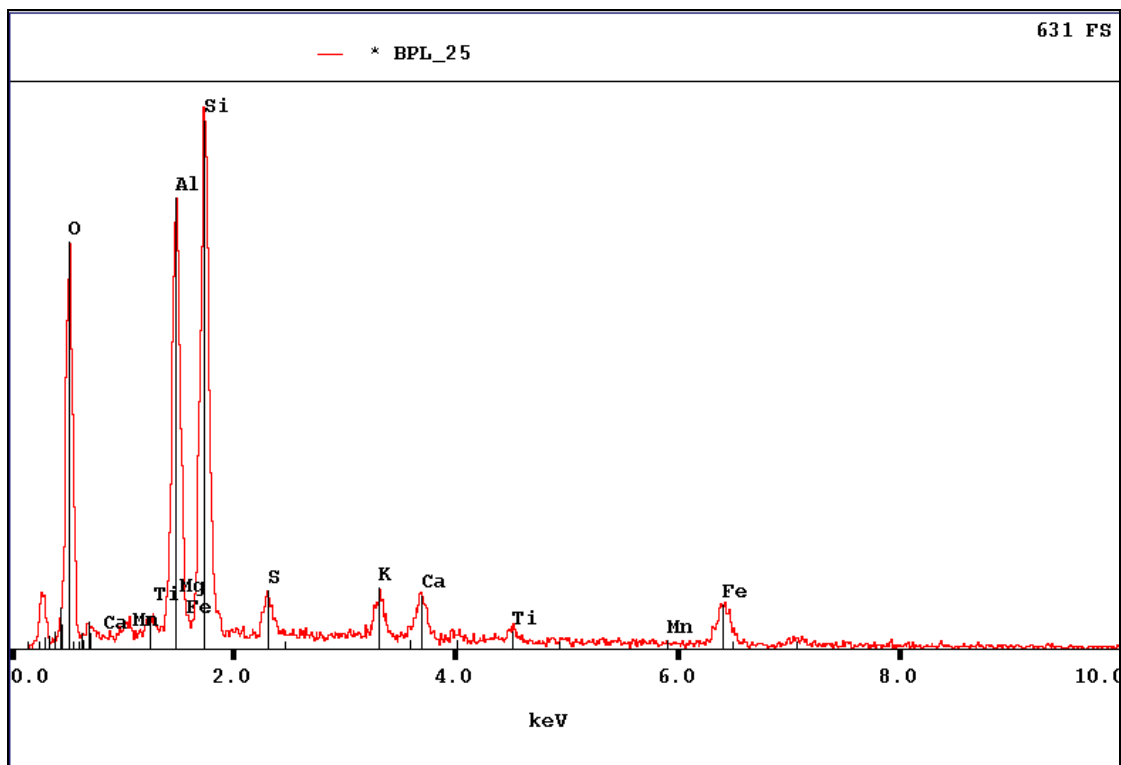
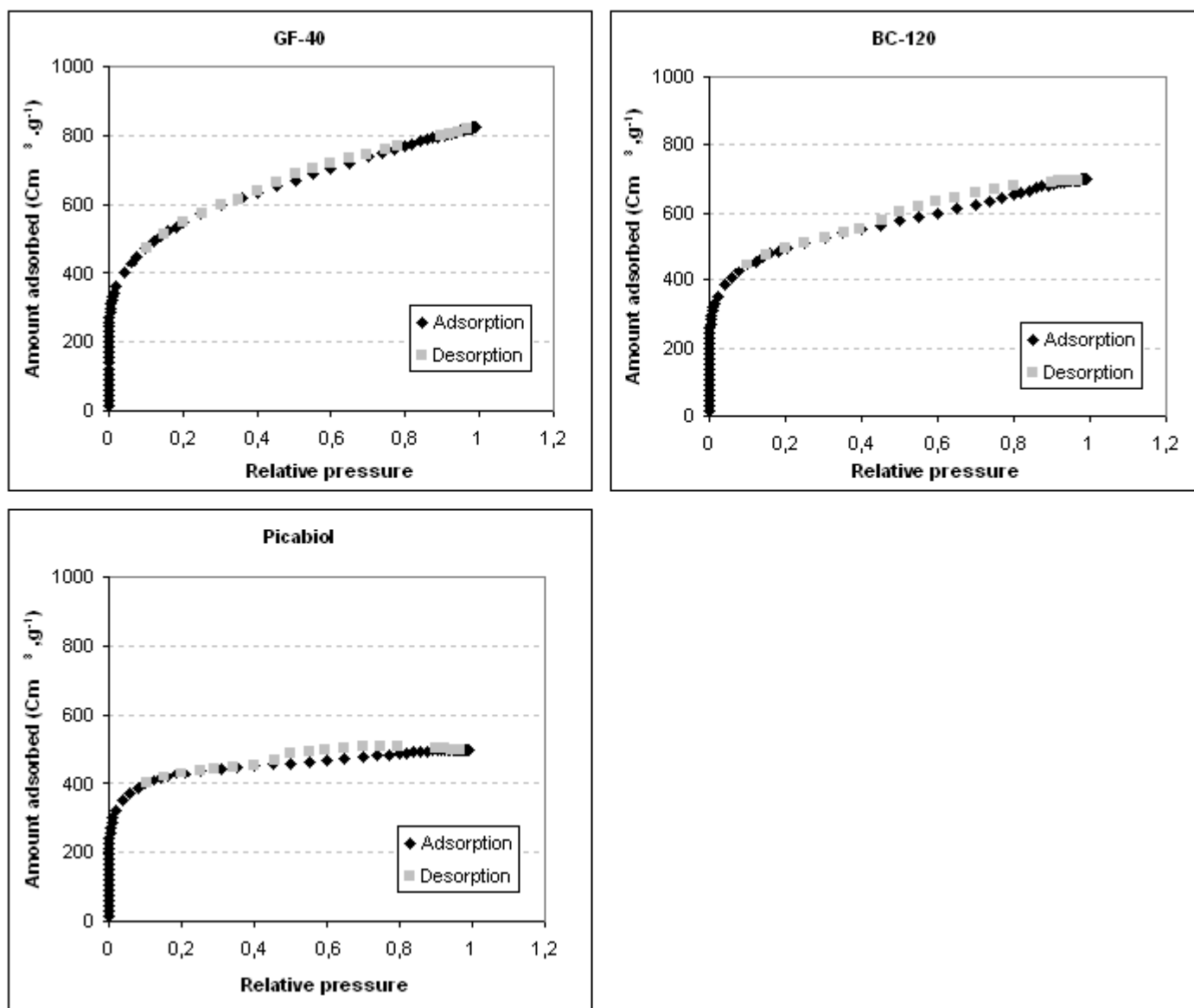


**Figure A-** : Graph showing elemental peaks for the mineral content of the RB-2 sample

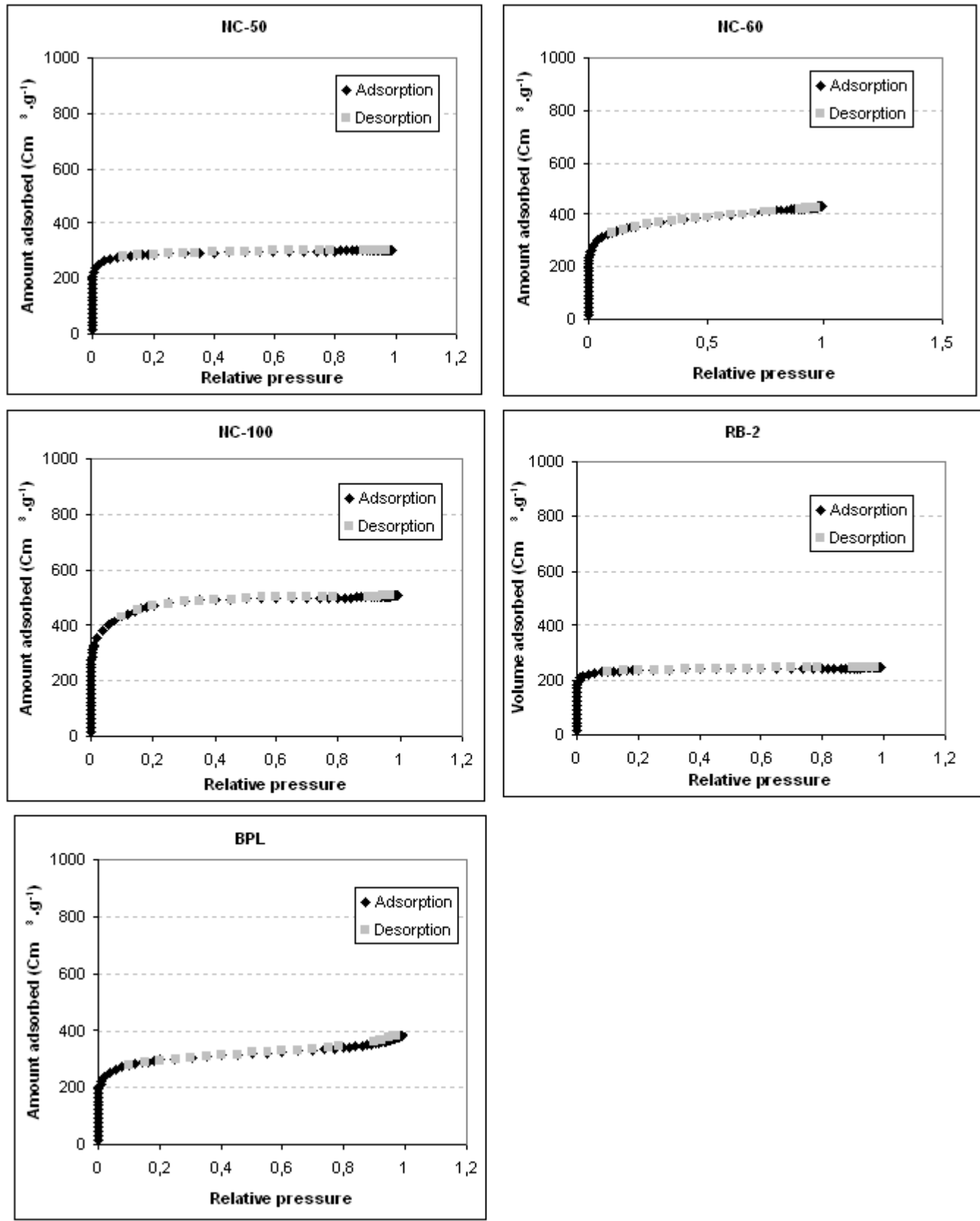
## APPENDIX-B

### ADSORPTION AND DESORPTION ISOTHERMS OF N<sub>2</sub> AT 77 K FOR VARIOUS ACTIVATED CARBONS

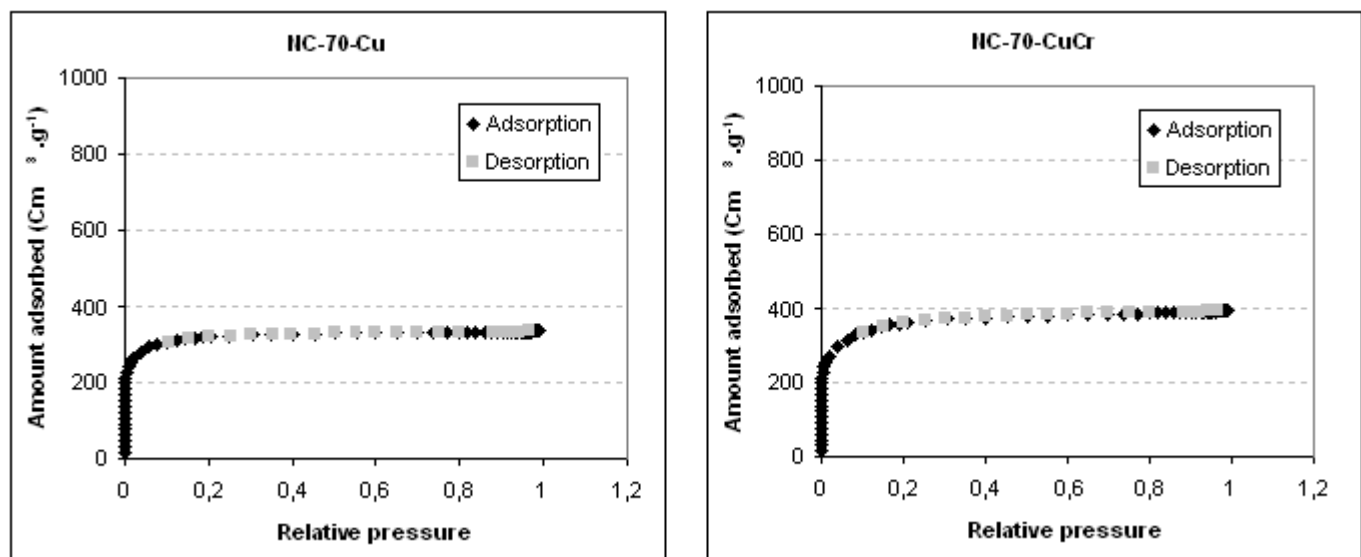
#### 1. CHEMICALLY ACTIVATED CARBONS



## 2. PHYSICALLY ACTIVATED CARBONS



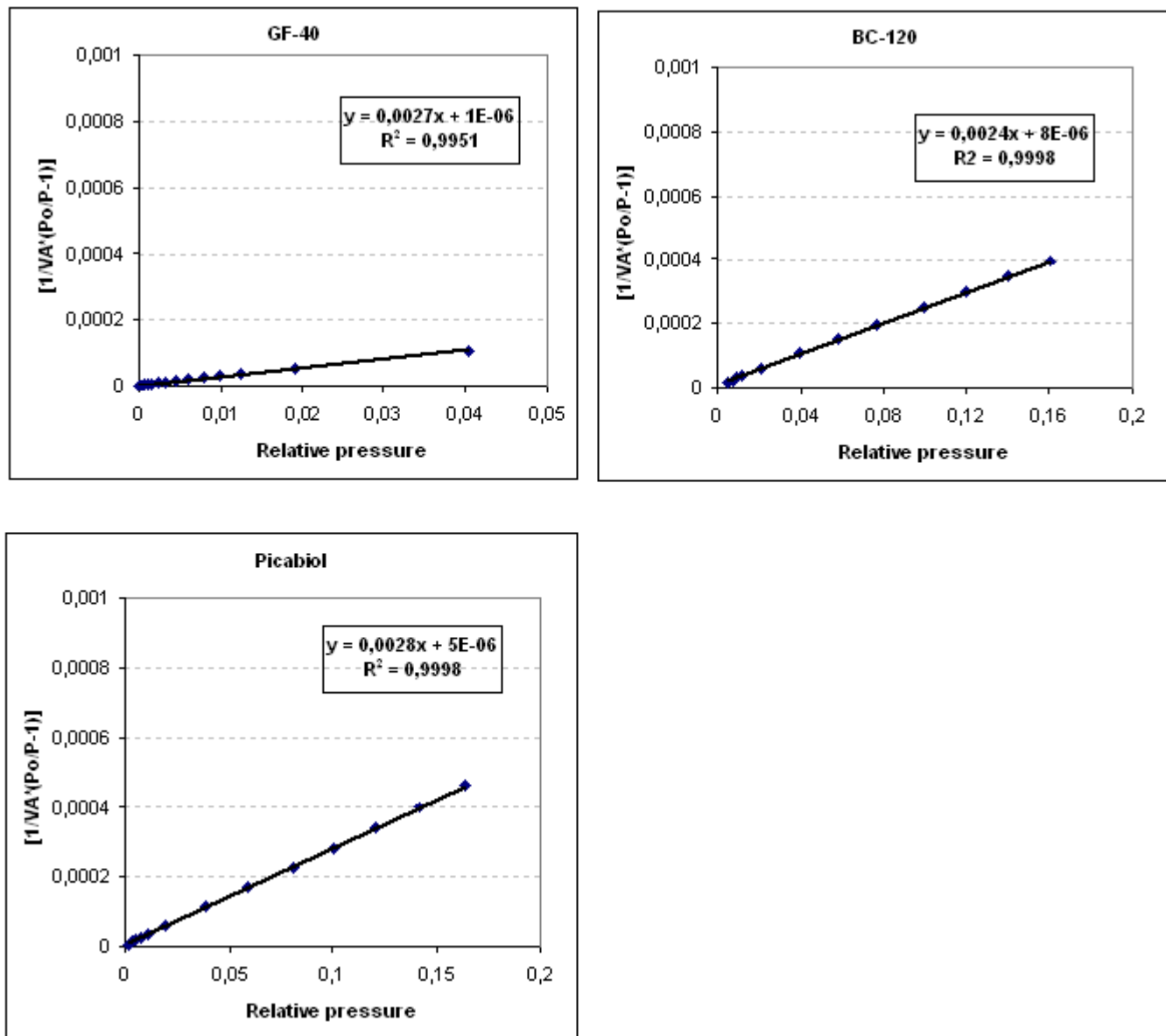
### 3. PHYSICALLY ACTIVATED METAL IMPREGNATED CARBONS



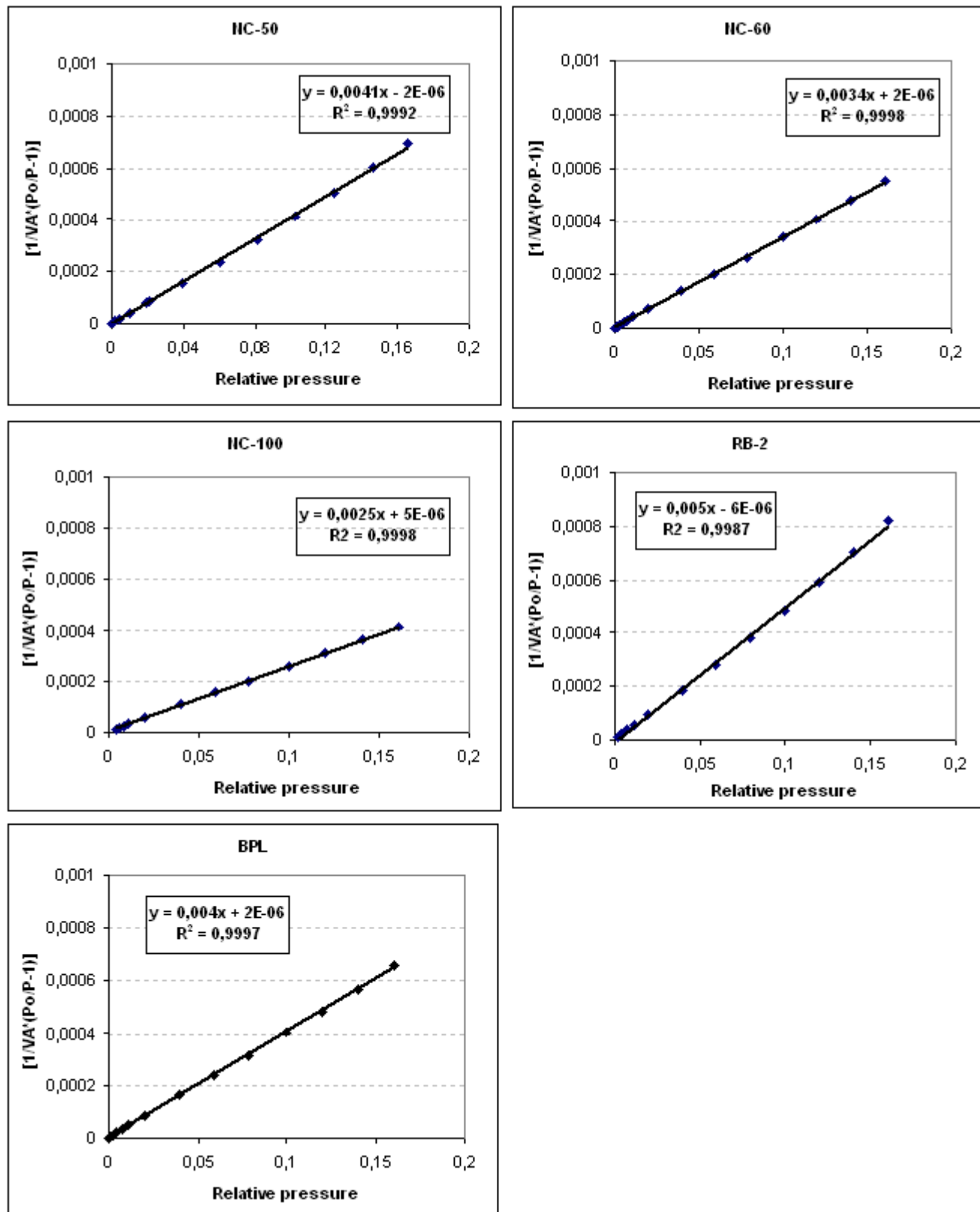
## APPENDIX-C

CALCULATION OF SPECIFIC SURFACE AREA  $S_{BET}$  FROM THE PLOT OF  $\frac{1}{V[P_0 / P - 1]} \text{ Vs } \frac{P}{P_0}$

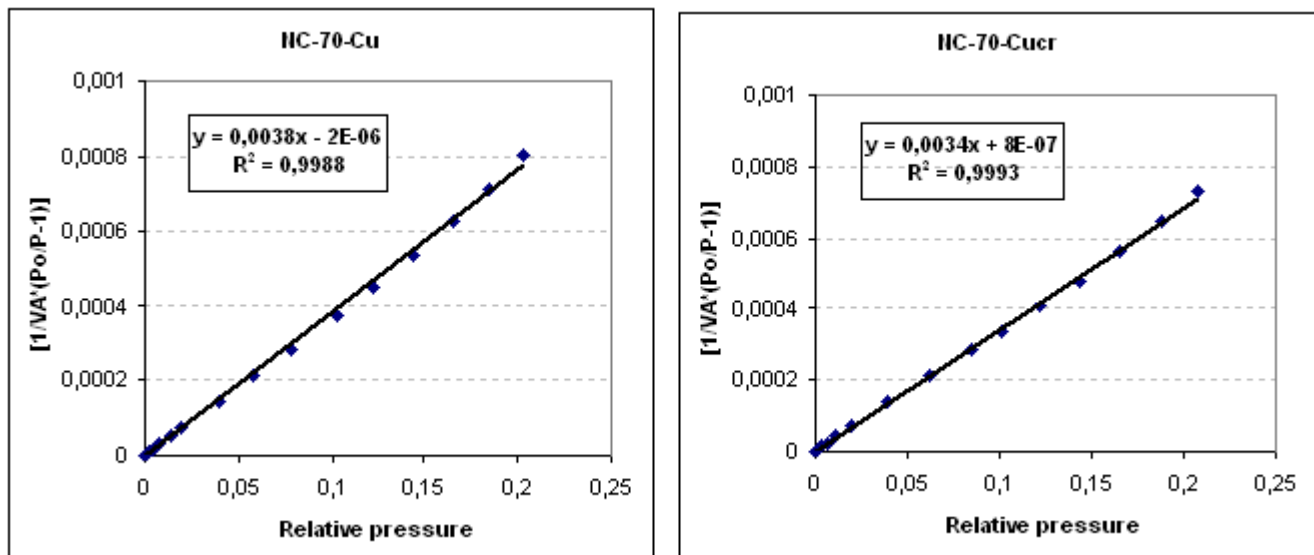
## **I. CHEMICALLY ACTIVATED CARBONS**



## 2. PHYSICALLY ACTIVATED CARBONS



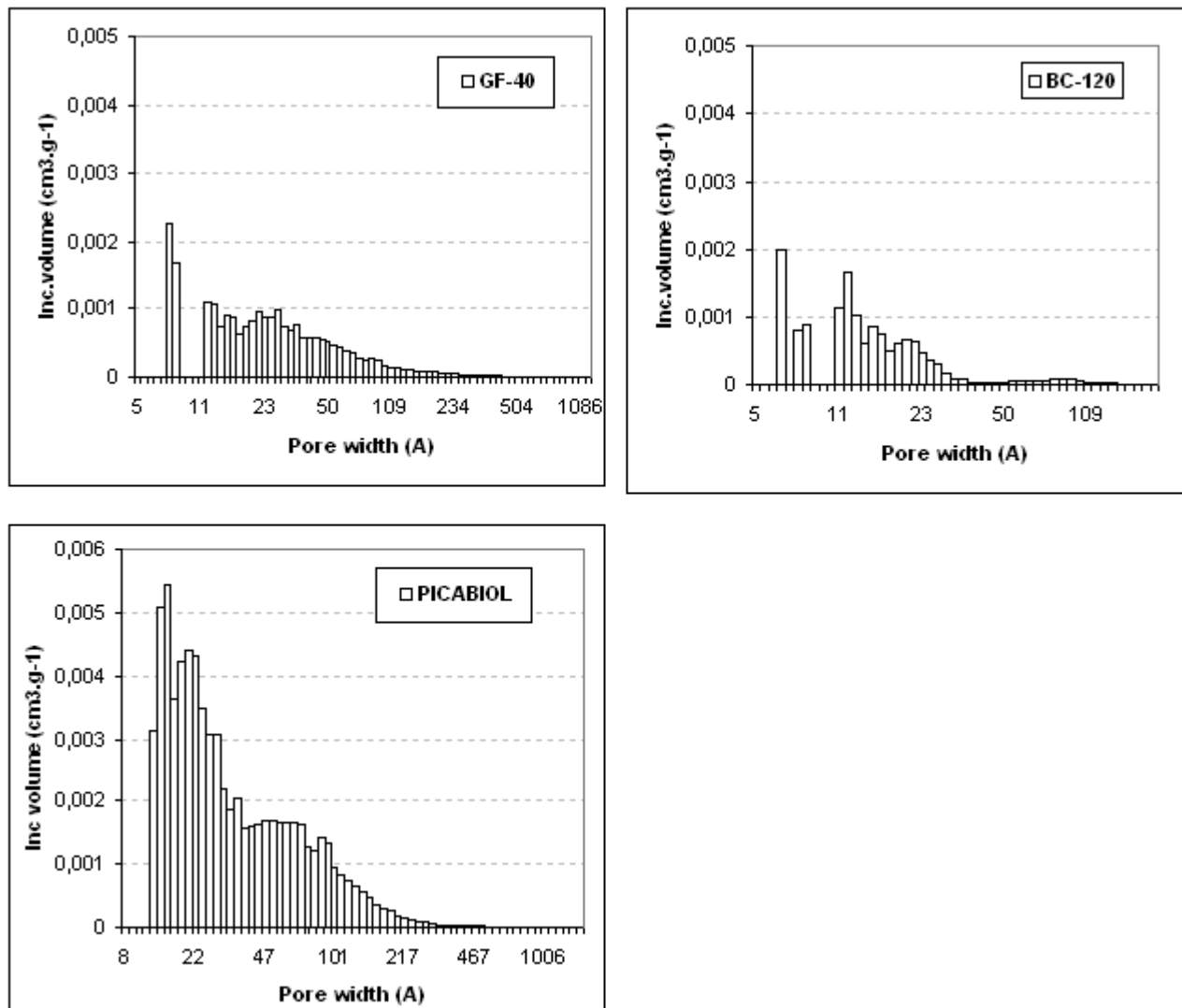
### 3. PHYSICALLY ACTIVATED METAL IMPREGNATED CARBONS



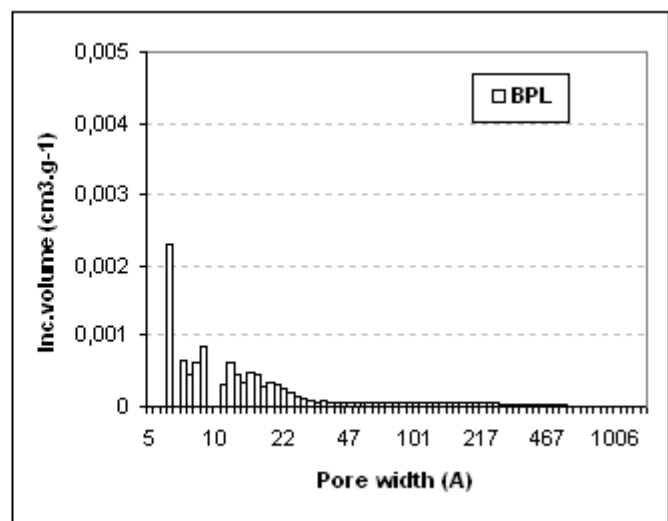
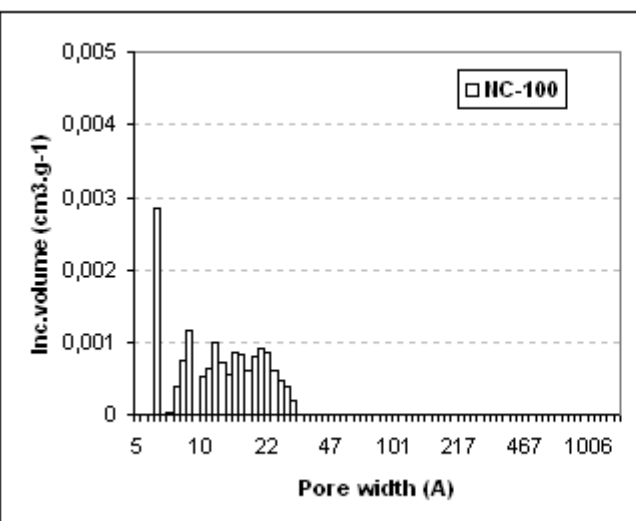
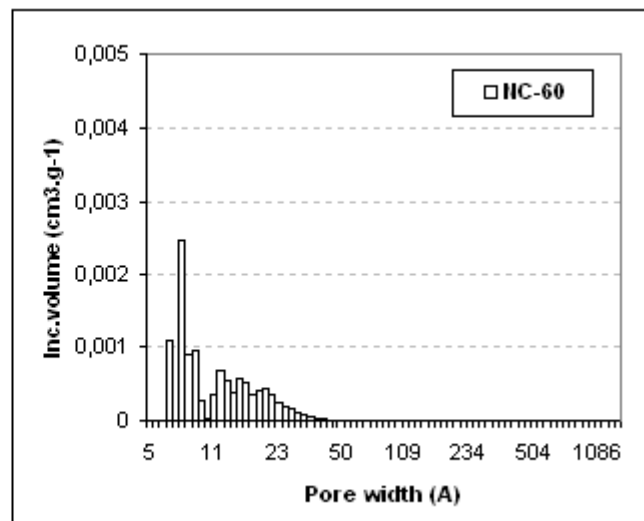
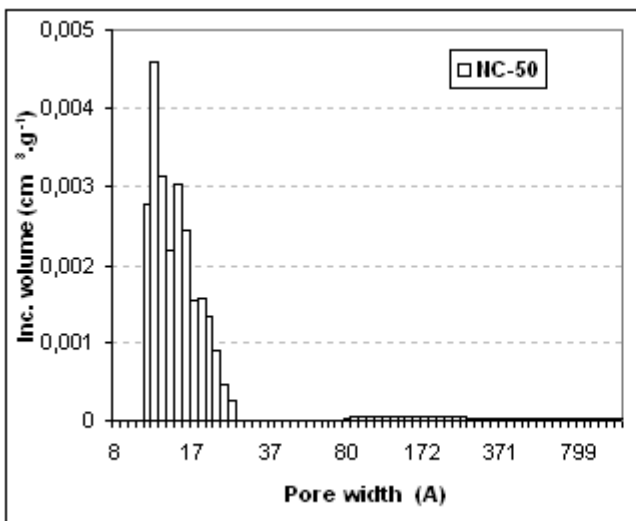
## APPENDIX-D

PORE SIZE DISTRIBUTION OF ACTIVATED CARBONS USING DFT METHOD

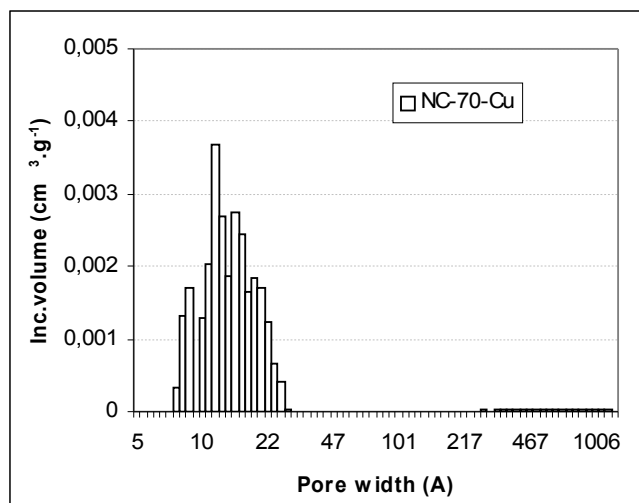
## ***1. CHEMICALLY ACTIVATED CARBONS***



## ***2. PHYSICALLY ACTIVATED CARBONS***



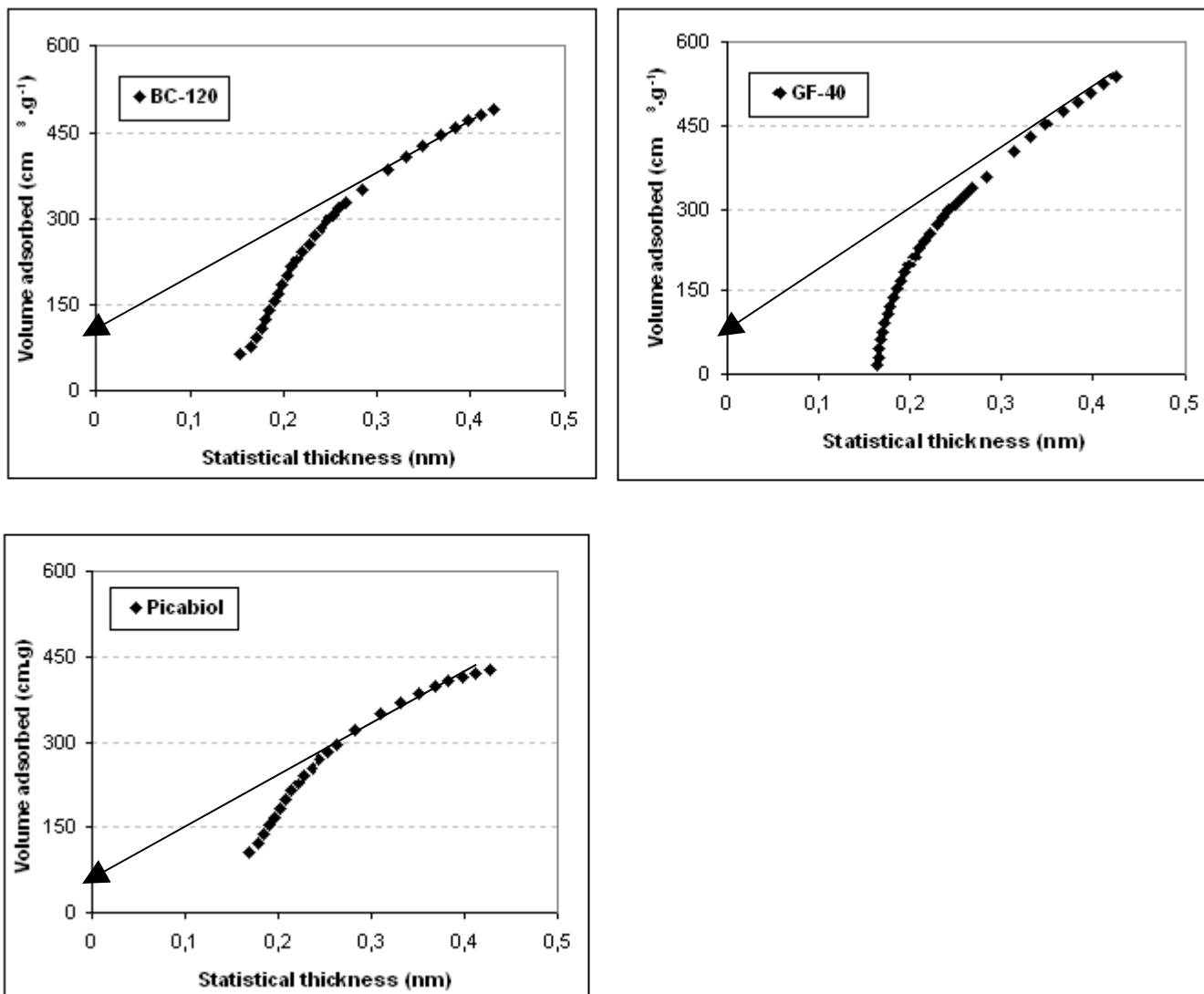
### 3. PHYSICALLY ACTIVATED IMPREGNATED CARBONS



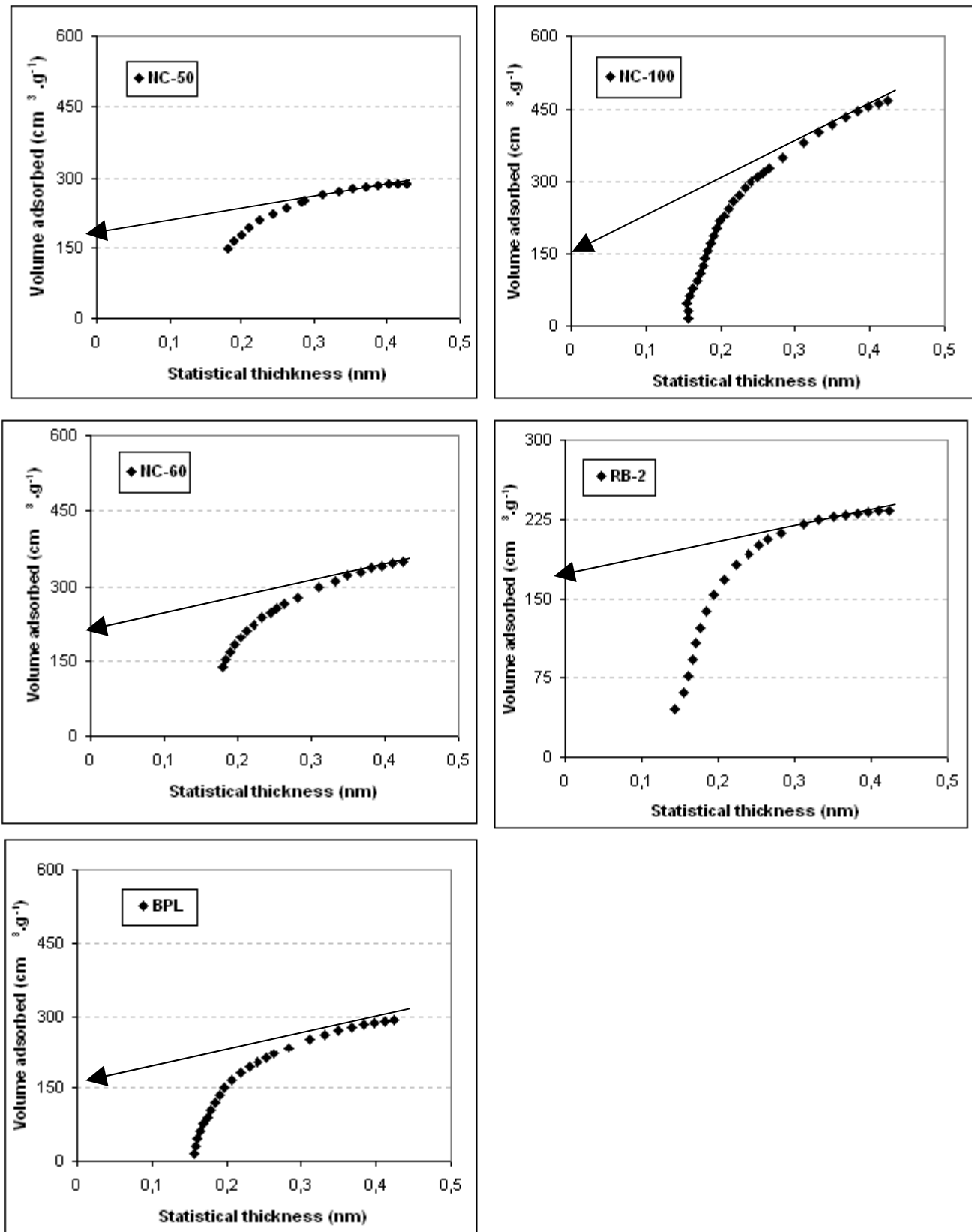
## **APPENDIX-E**

### **t-PLOTS OF THE ACTIVATED CARBONS FOR MICROPOROUS VOLUME CALCULATIONS**

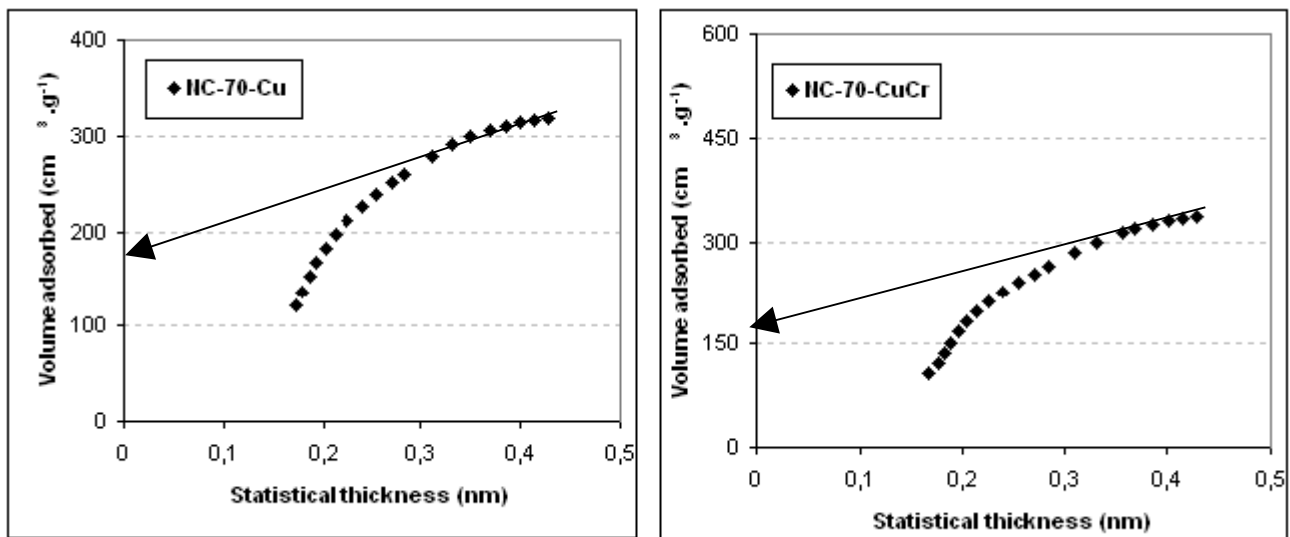
#### **1. CHEMICALLY ACTIVATED CARBONS**



**2. PHYSICALLY ACTIVATED CARBONS**



### 3. PHYSICALLY ACTIVATED IMPREGNATED CARBONS

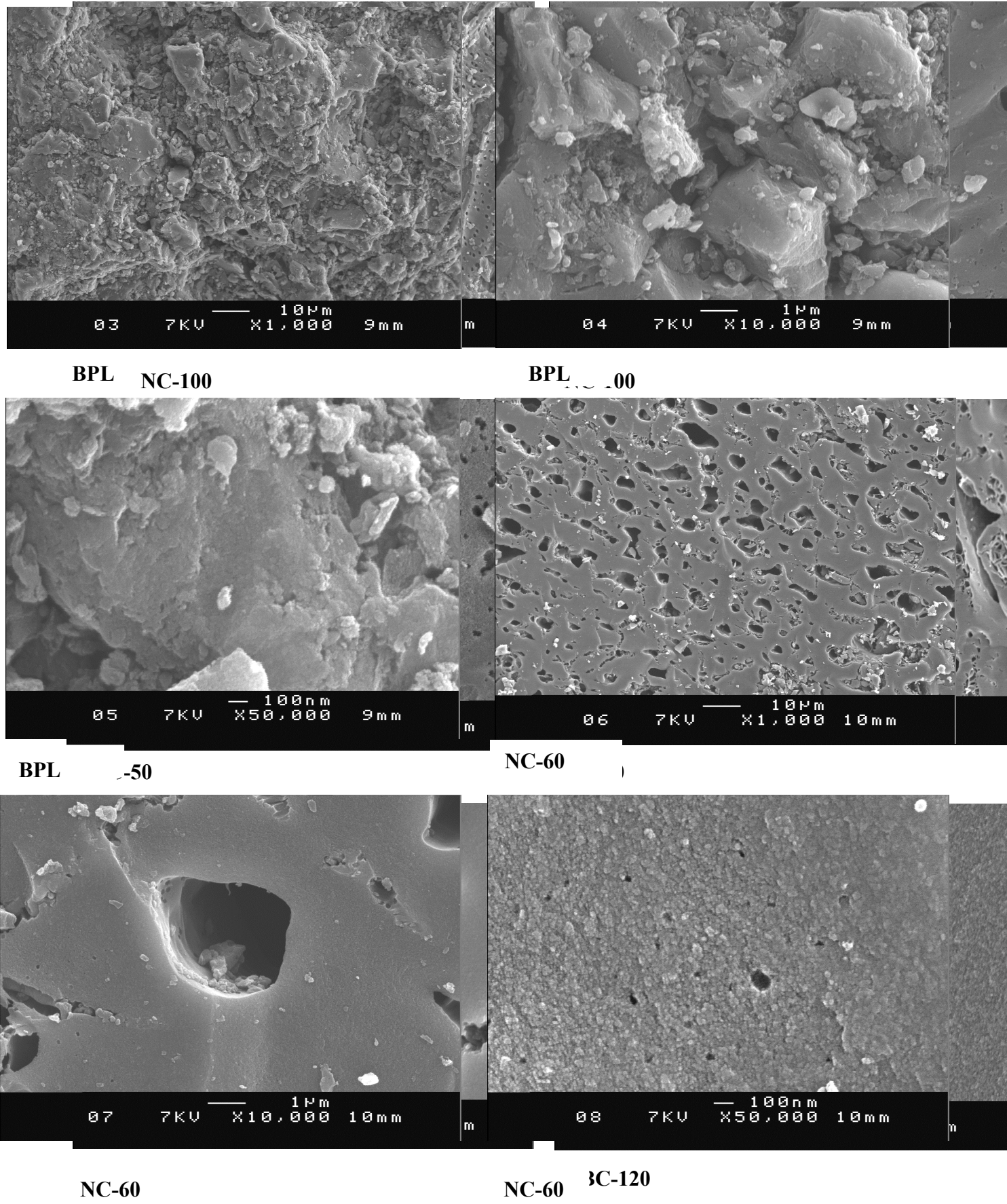


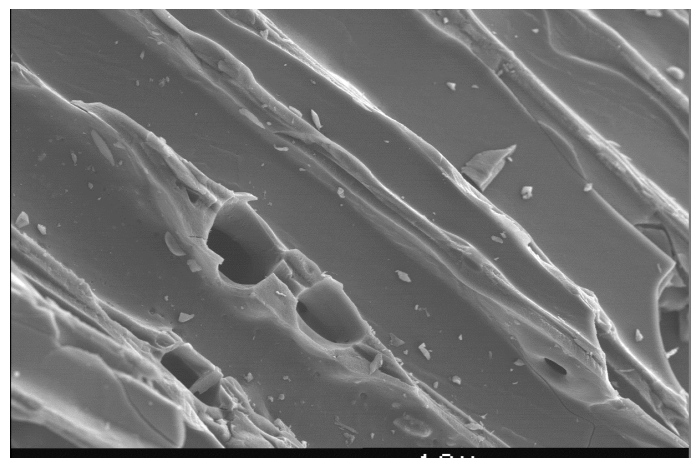
## APPENDIX-F

### *POROSITY CHARACTERISTICS OBTAINED FROM N<sub>2</sub> AT 77 K*

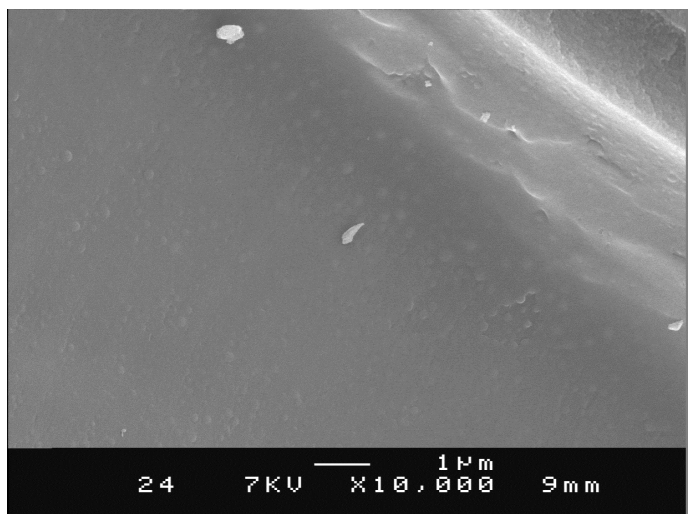
Sample	Precursor	Volume of micropores (cm <sup>-3</sup> . g <sup>-1</sup> )	Average width of micro pores DFT-method (nm)	Surface area (S <sub>BET</sub> ) (m <sup>2</sup> .g <sup>-1</sup> )
NC-50	<i>Coconut shell</i>	0.36	1.35	1078
NC-60	<i>Coconut shell</i>	0.32	0.97	1220
NC-100	<i>Coconut shell</i>	0.27	1.11	1803
RB-2	<i>Peat</i>	0.35	0.92	1012
BPL	<i>Coal</i>	0.30	0.93	1106
CTP-A	<i>Coal tar pitch</i>	0.04	1.30	102
CTP-PAN-3 :1-A	<i>Coal tar pitch and PAN fibre</i>	0.20	1.32	468
CTP-PAN-1 :1-A	<i>Coal tar pitch and PAN fibre</i>	0.21	1.11	482
PAN-A	<i>PAN fibre</i>	0.26	1.15	515
GF-40	<b>Olive stone</b>	<b>0.29</b>	<b>1.15</b>	<b>1718</b>
BC-120	<b>Wood</b>	<b>0.33</b>	<b>1.12</b>	<b>1975</b>
PICABIOL	<b>Wood</b>	<b>0.24</b>	<b>1.38</b>	<b>1534</b>
NC-70-Cu	Coconut shell	0.34	1.05	1458
NC-70-Cucr	Coconut shell	0.29	1.15	1239

**APPENDIX-G SEM MICROGRAPHS OF ACTIVATED CARBON SAMPLES**





23      7KV       $\times 1,000$       9mm



24      7KV       $\times 10,000$       9mm

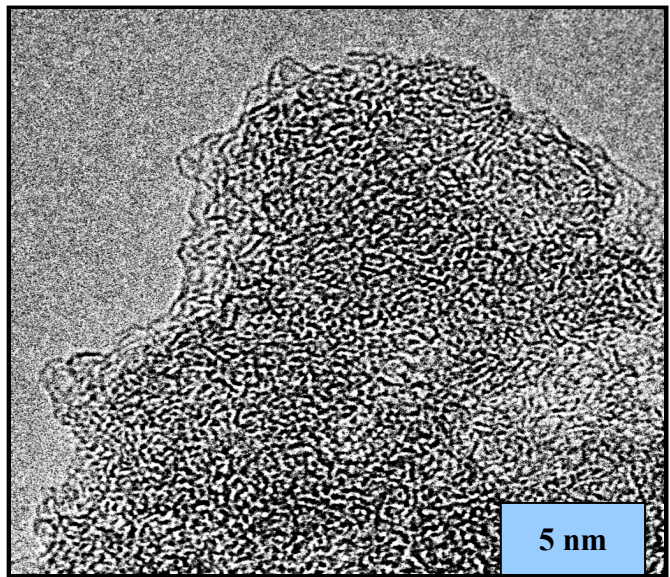
**RB-2**

**RB-2**

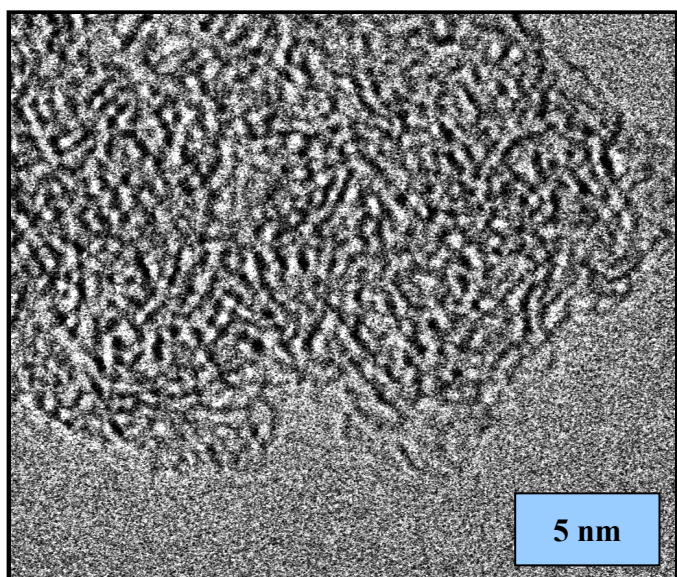
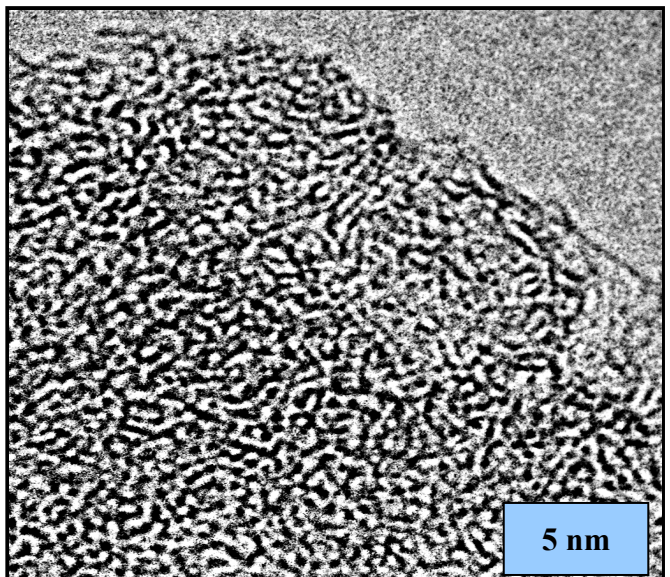
## **APPENDIX-H**

### **HRTEM IMAGES OF ACTIVATED CARBON SAMPLES**

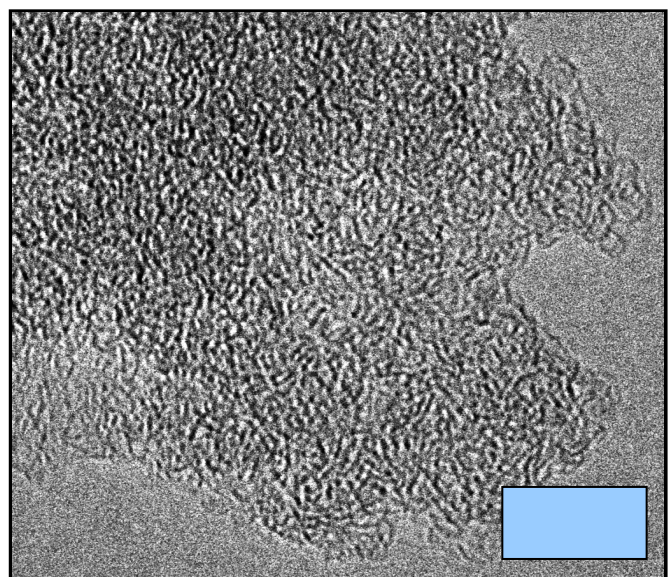
#### ***I. CHEMICALLY ACTIVATED CARBONS***

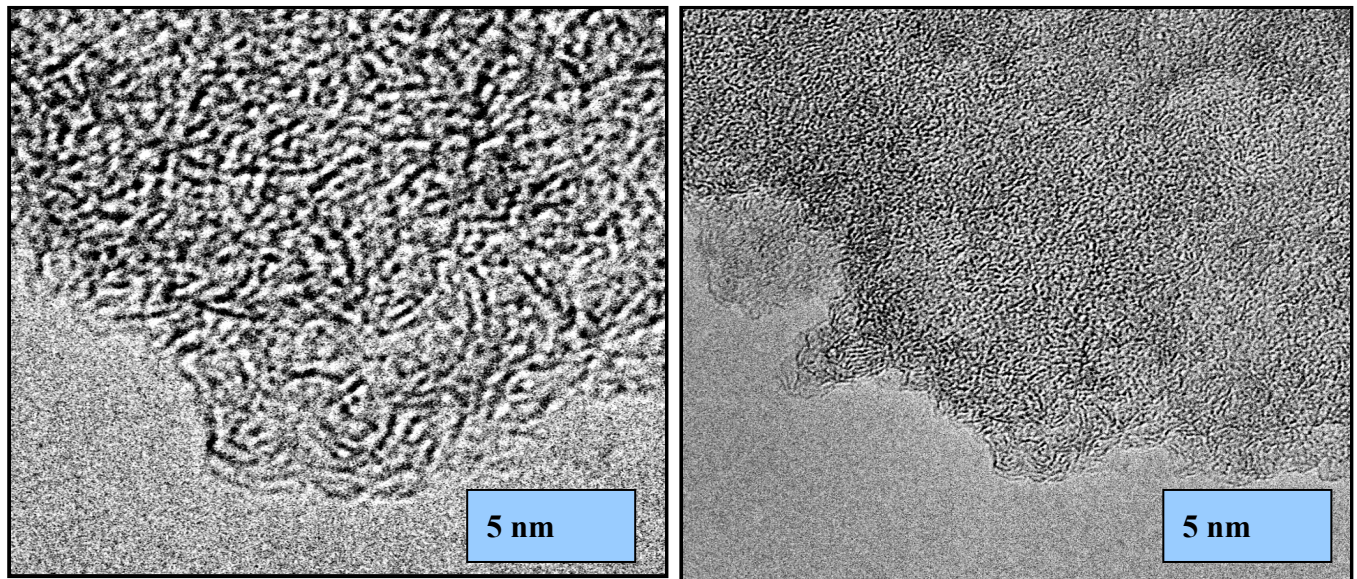


BC-120



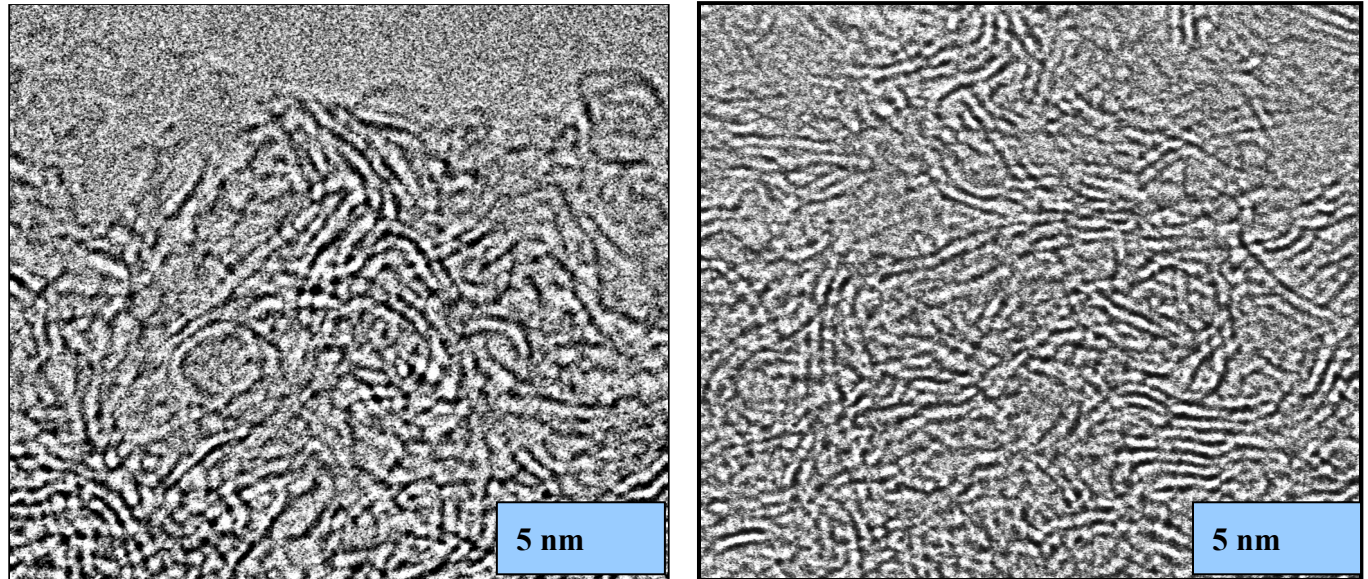
Picabiol



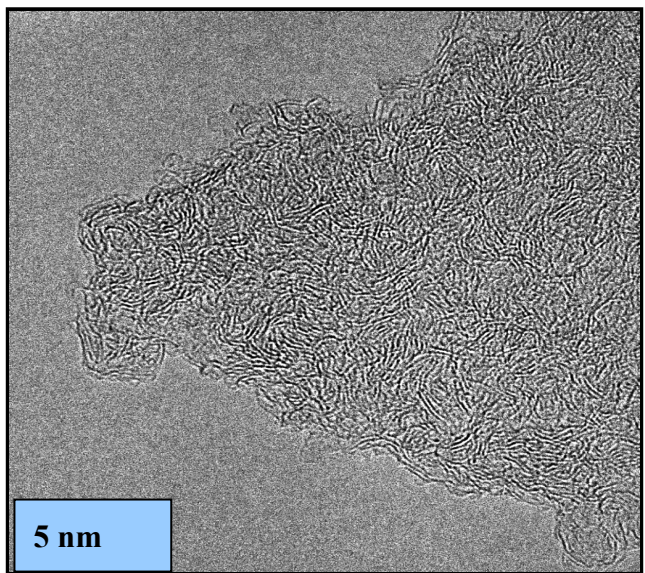
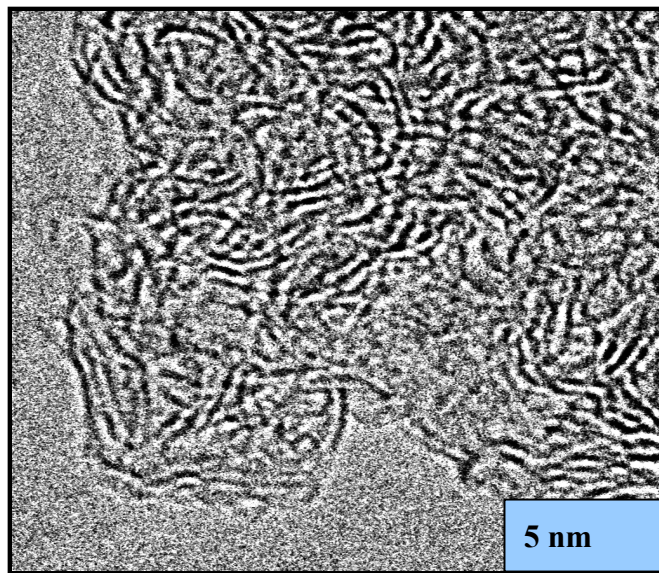


**GF-40**

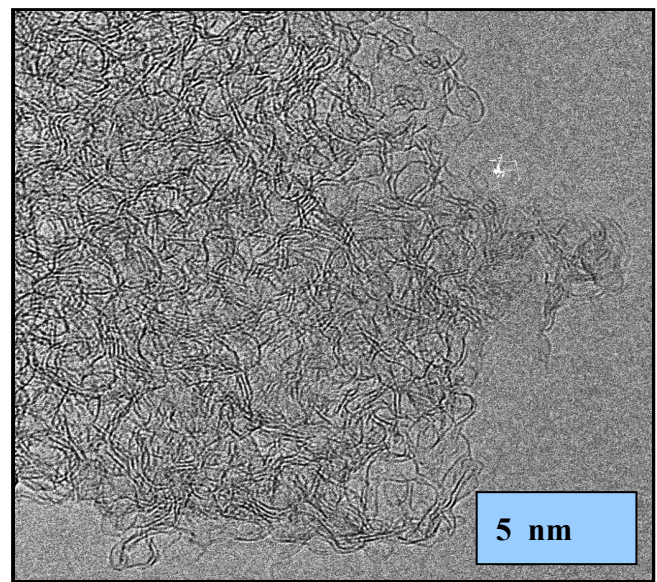
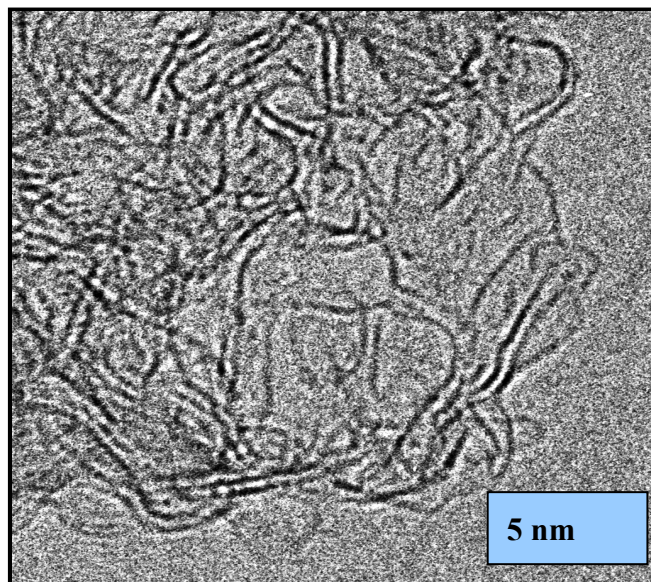
**2. PHYSICALLY ACTIVATED CARBONS**



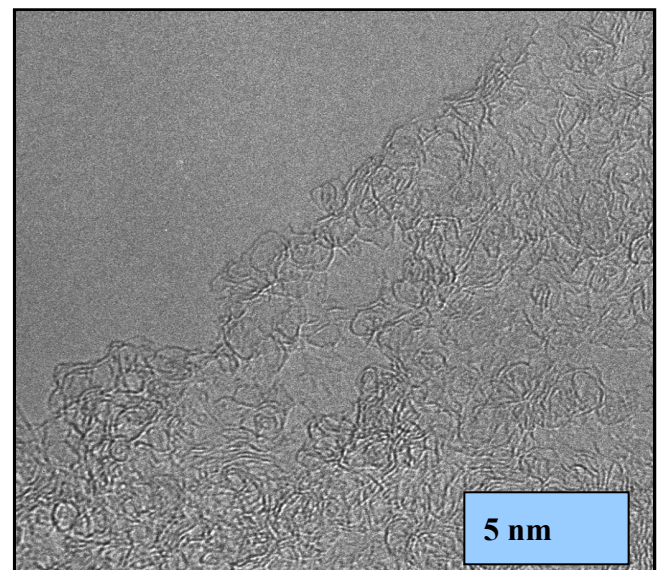
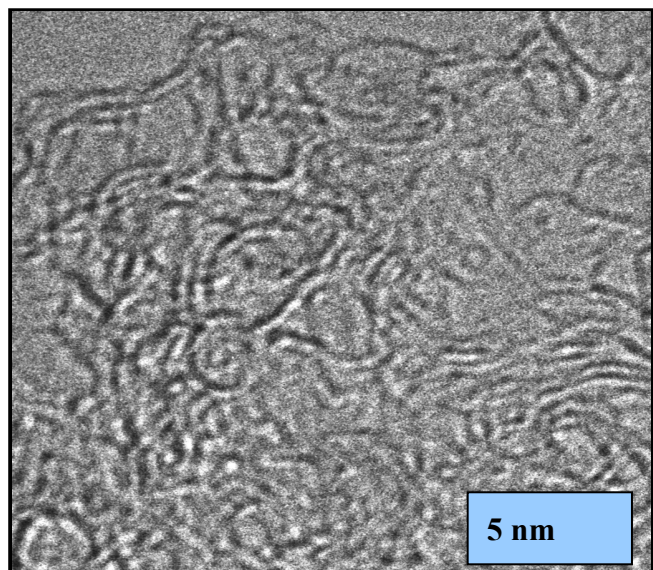
**NC-50**



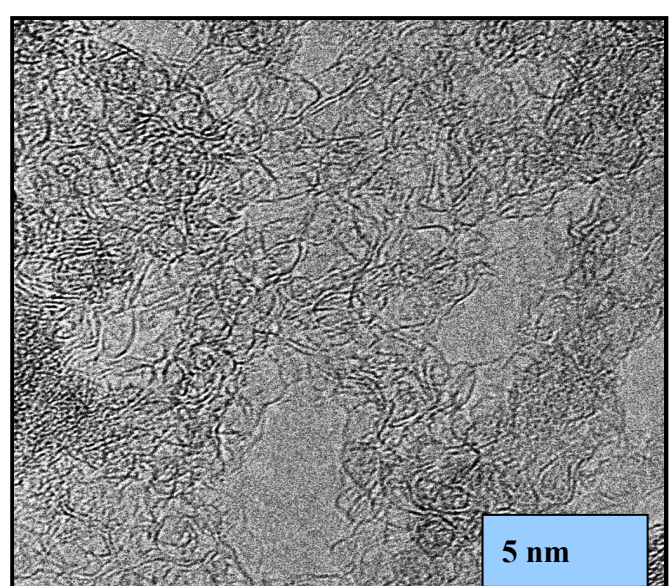
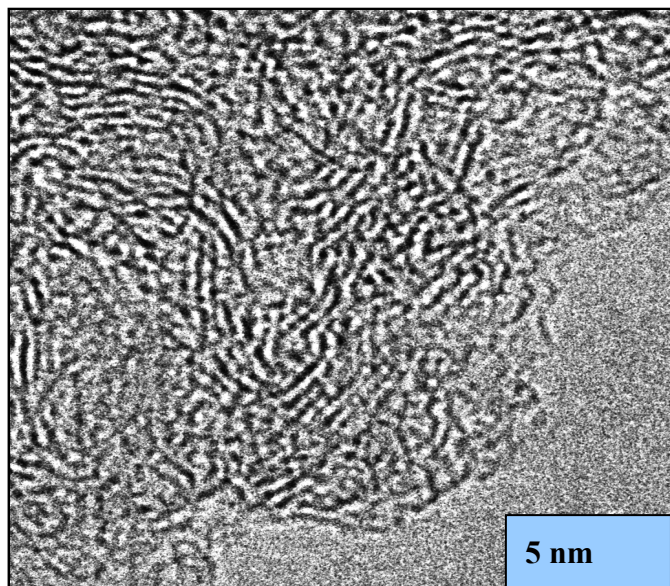
**NC-60**



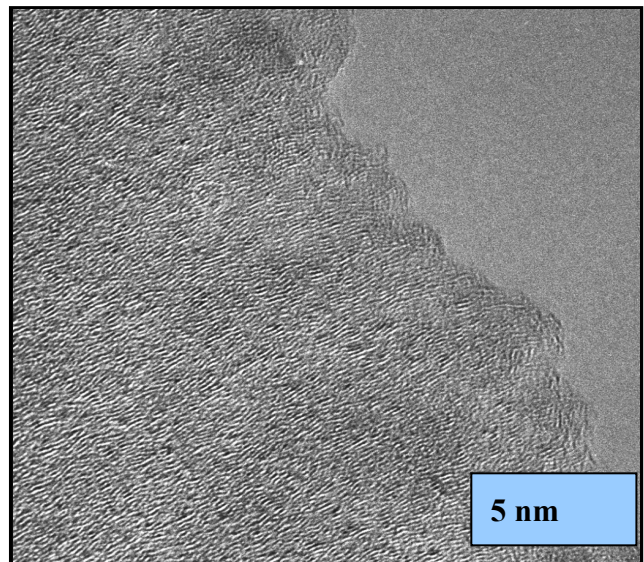
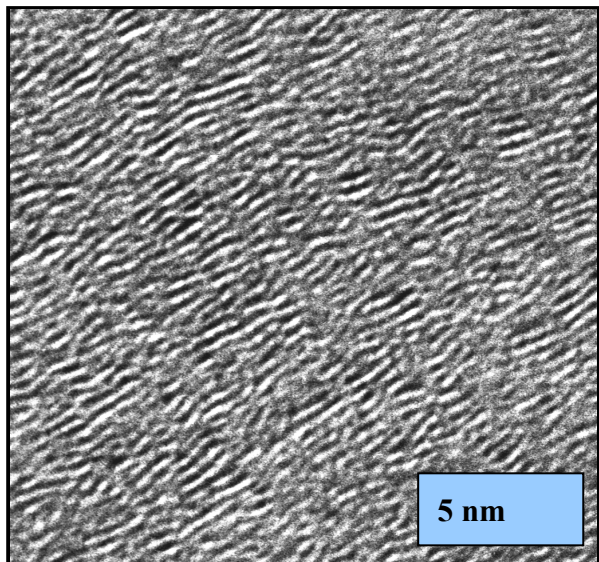
**NC-100**



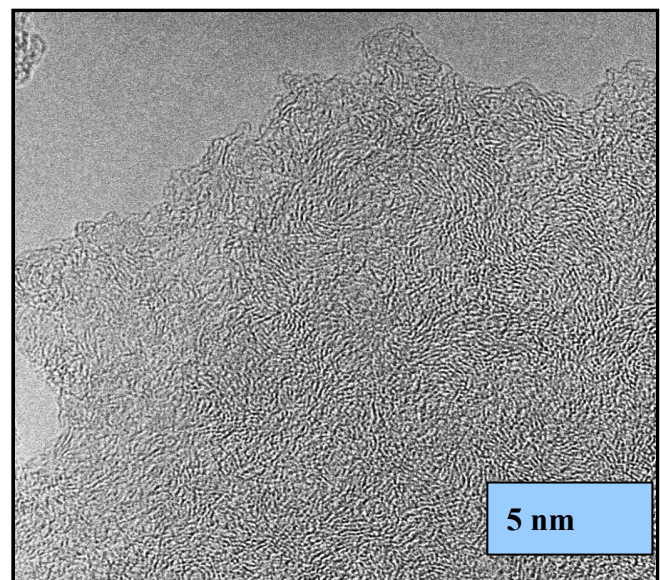
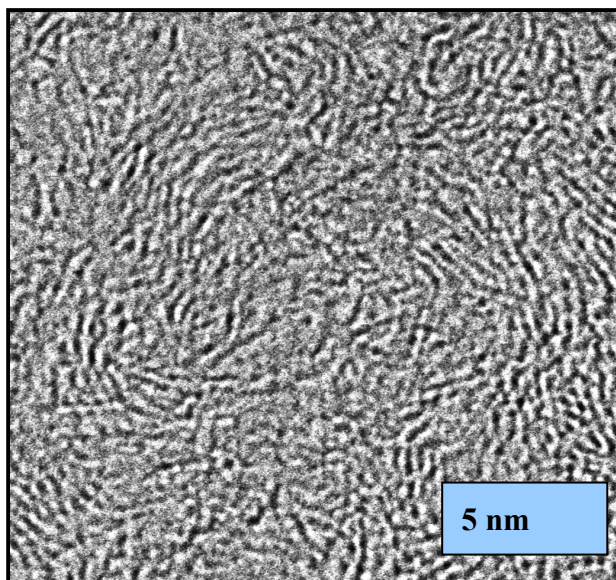
RB-2



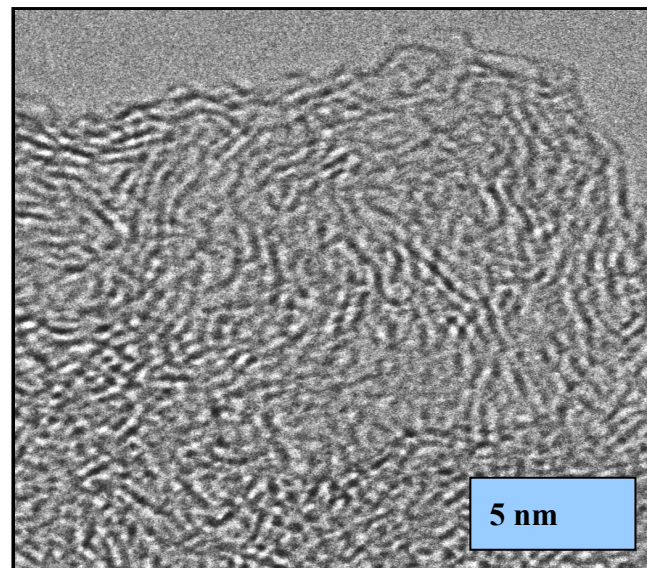
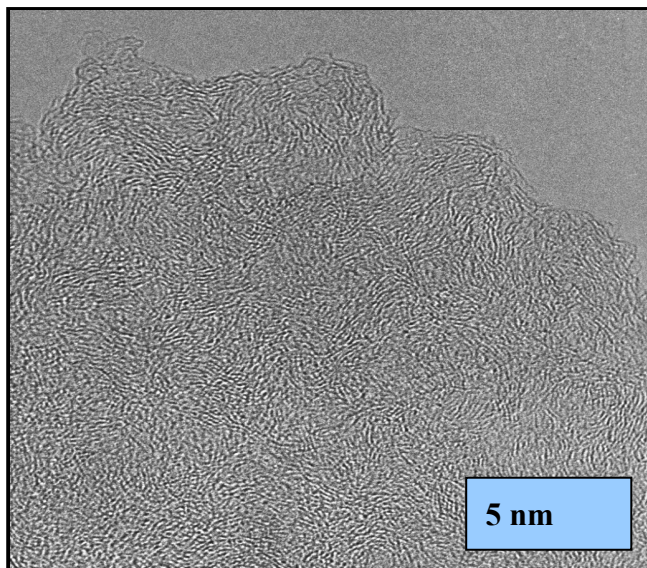
BPL



CTP-A

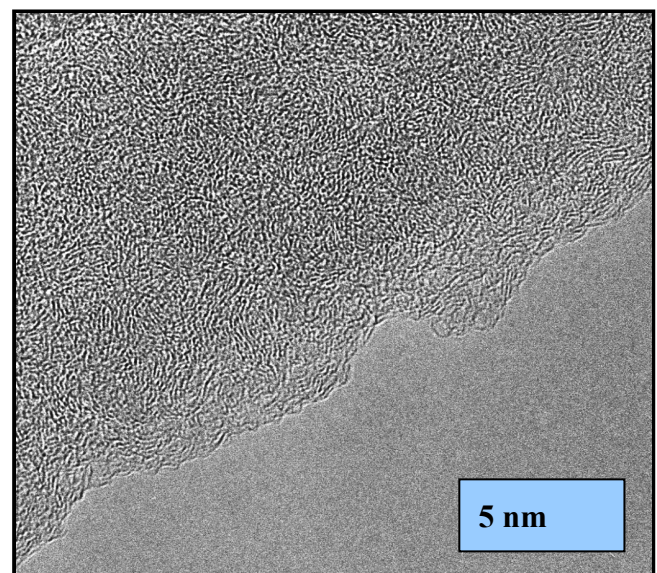
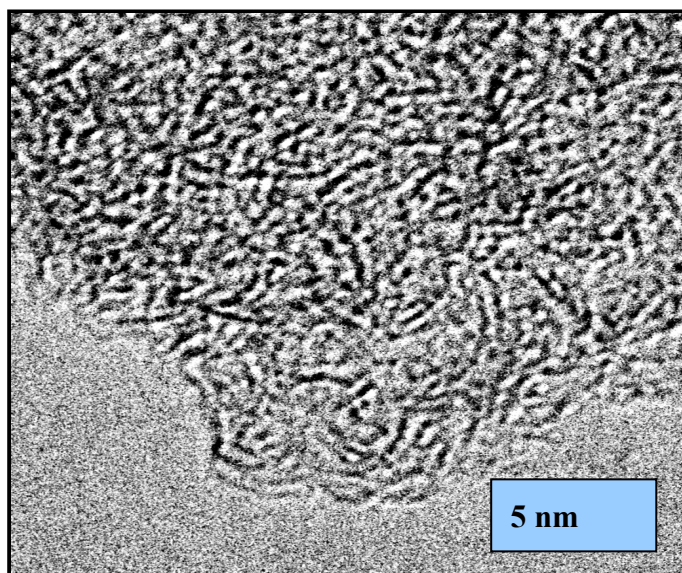


PAN-A

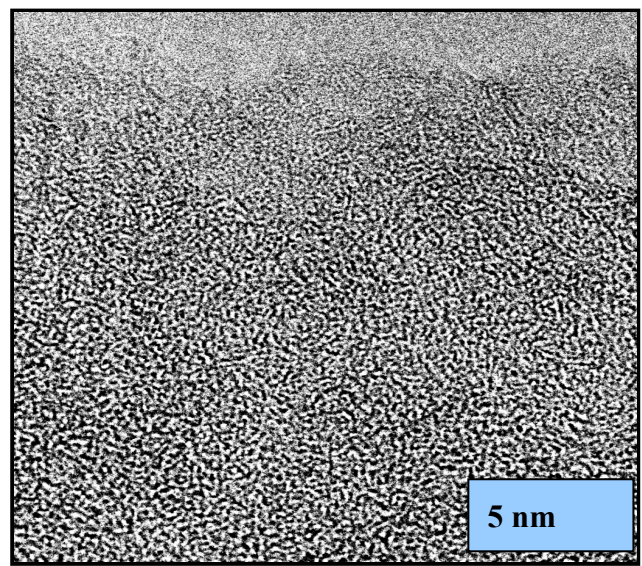
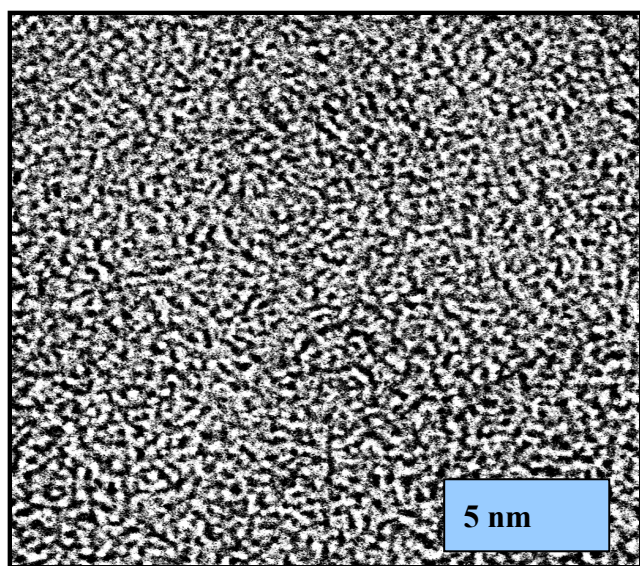


**CTP-PAN-1.1-A**

3. CARBONIZED SAMPLES



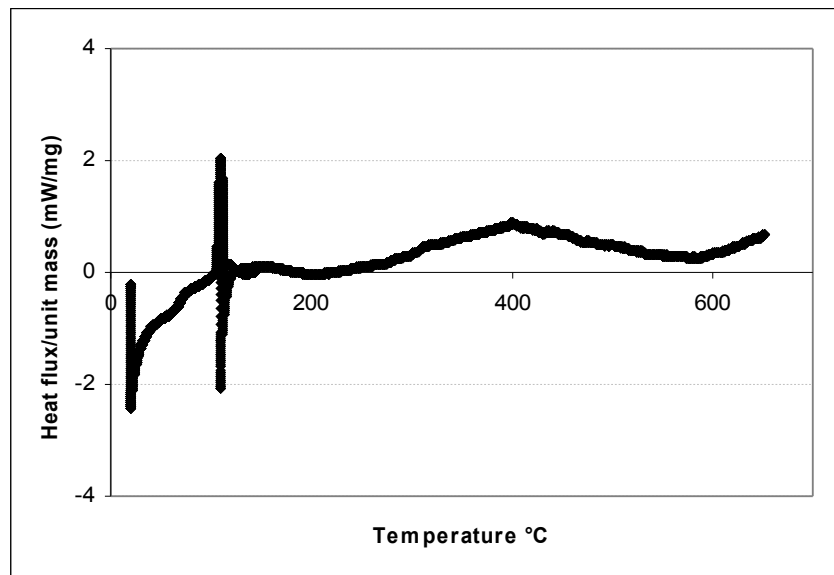
**PAN-C**



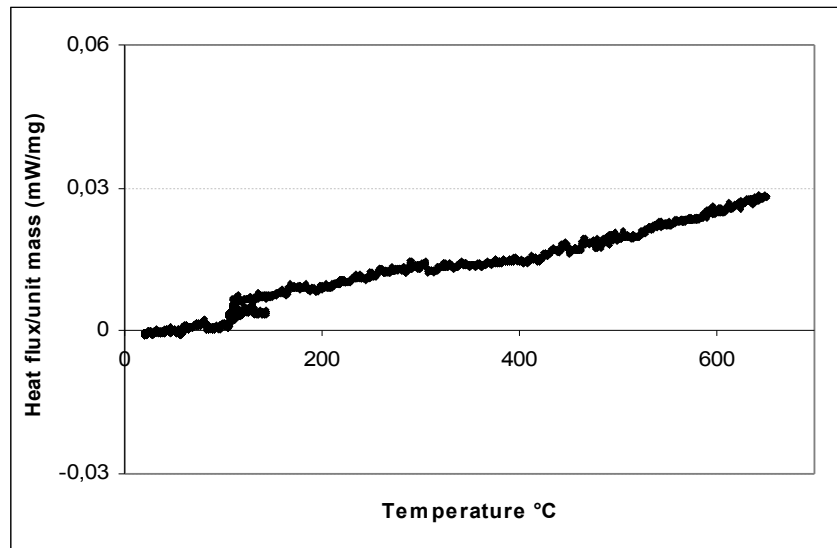
CARBONIZED COCONUT SHELL

## **APPENDIX-I**

### **1. DSC THERMOGRAM FOR THE REFERENCE EXPERIMENT OF AN ACTIVATED CARBON SAMPLE USING TG-DSC**



### **2. DSC THERMOGRAM FOR THE REFERENCE EXPERIMENT OF AN ACTIVATED CARBON SAMPLE USING TG-DSC**



## **APPENDIX-J**

THE PIO AND SIT VALUES OF THE ACTIVATED CARBONS BEFORE AND AFTER TEMPERATURE PROGRAMMED DESORPTION (TPD)

Sample	Before TPD		After TPD	
	SIT °C	PIO °C	SIT °C	PIO °C
<i>NC-60</i>	444	200	468	268
<i>NC-100</i>	475	240	475	307
<i>BPL</i>	516	253	516	346
<i>GF-40</i>	347	170	425	212
<i>BC-120</i>	377	183	428	234
<i>Picabiol</i>	367	167	421	240
<i>PAN-A</i>	457	225	457	302
<i>Coconut shell-C</i>	370	175	449	234

ANNEXE-K

**THE PIO AND SIT VALUES FOR THE ACTIVATED CARBONS AT DIFFERENT OXYGEN CONCENTRATIONS OF  
THE AMBIENT GAS**

**1. 10 % OXYGEN**

Sample	PIO °C	SIT °C
<i>GF-40</i>	246,70	380
<i>NC-60</i>	274,00	420
<i>Coconut shell-C</i>	220,00	380
<i>PAN-A</i>	270,00	475

**2. 21 % OXYGEN**

Sample	PIO °C	SIT °C
<i>GF-40</i>	183	347,5
<i>NC-60</i>	203,00	388,75
<i>Coconut shell-C</i>	175,00	370
<i>PAN-A</i>	225	457

**3. 40 % OXYGEN**

Sample	PIO °C	SIT °C
<i>GF-40</i>	180,00	340
<i>NC-60</i>	184,00	378
<i>Coconut shell-C</i>	162,00	362
<i>PAN-A</i>	217,00	442

#### 4. 70 % OXYGEN

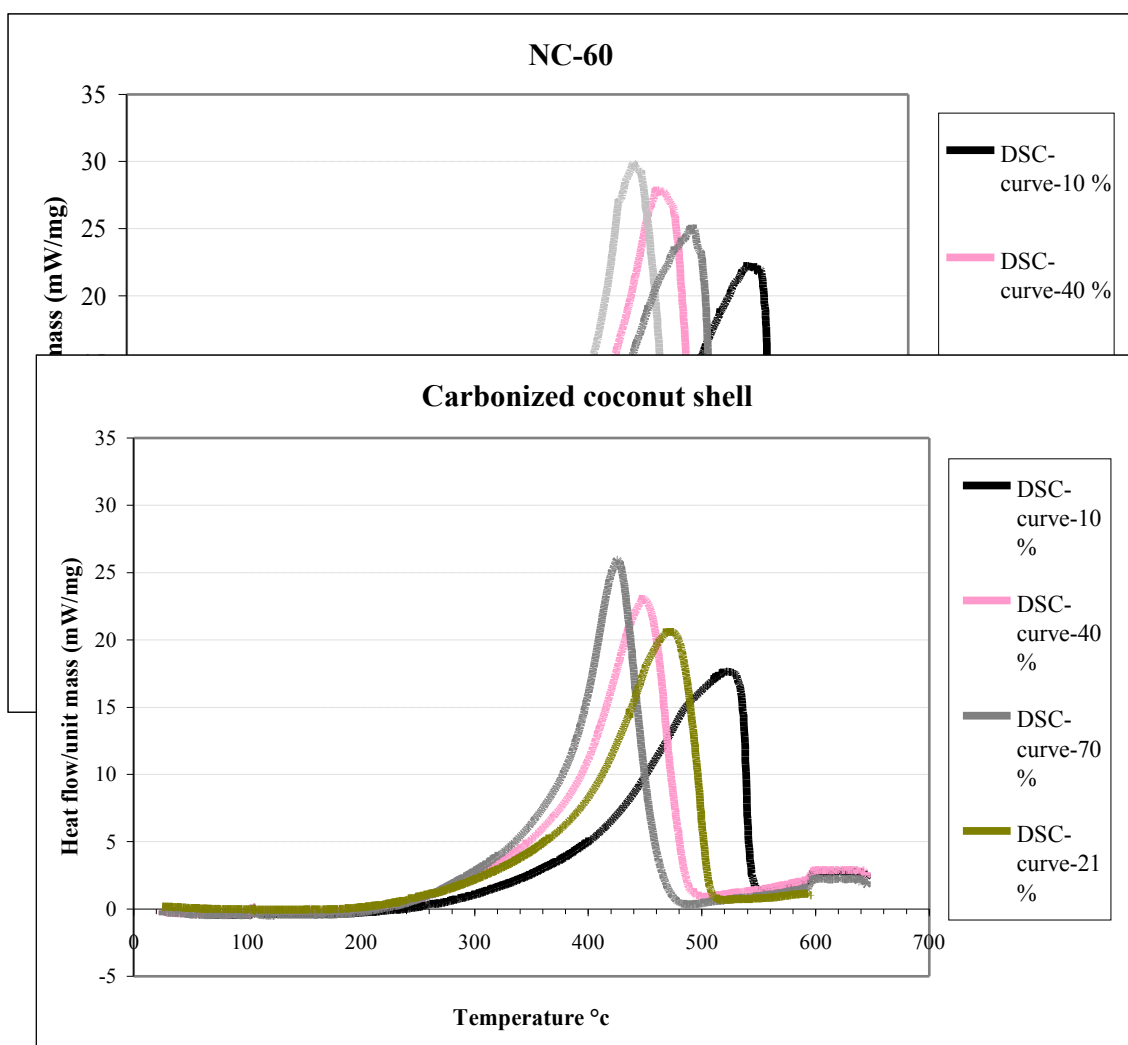
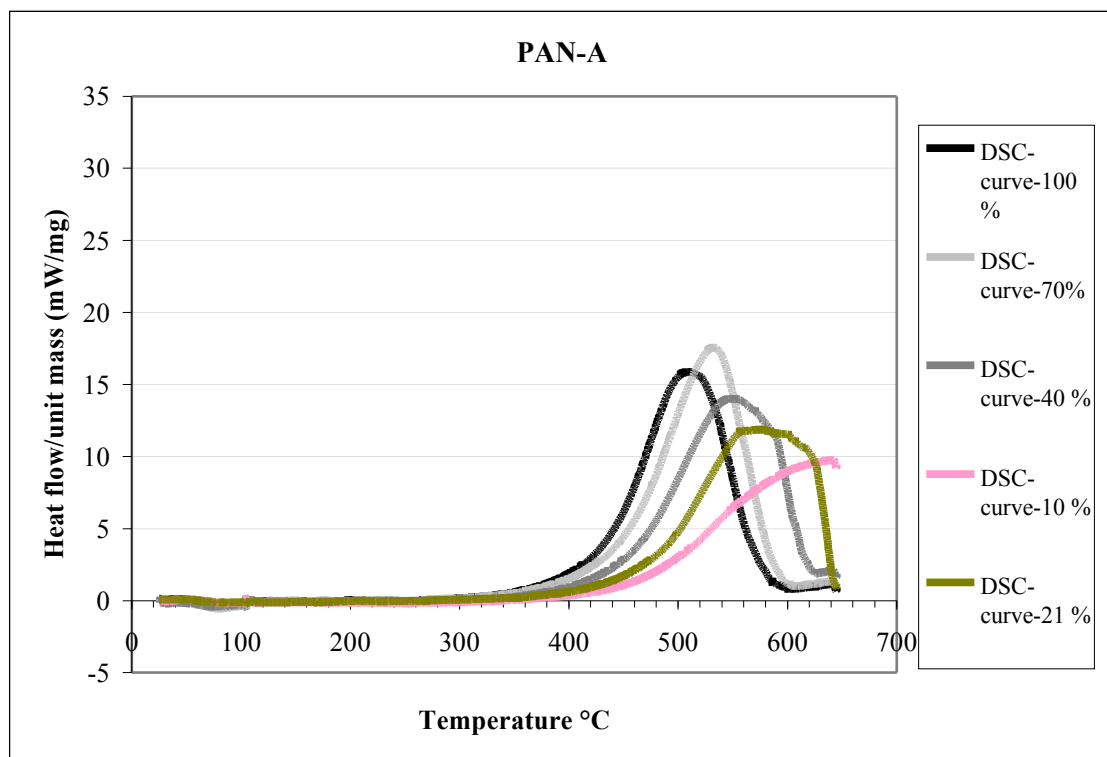
Sample	PIO	SIT
<i>GF-40</i>	182,00	320
<i>NC-60</i>	168	365
<i>Coconut shell-C</i>	155	360
<i>PAN-A</i>	205,00	436

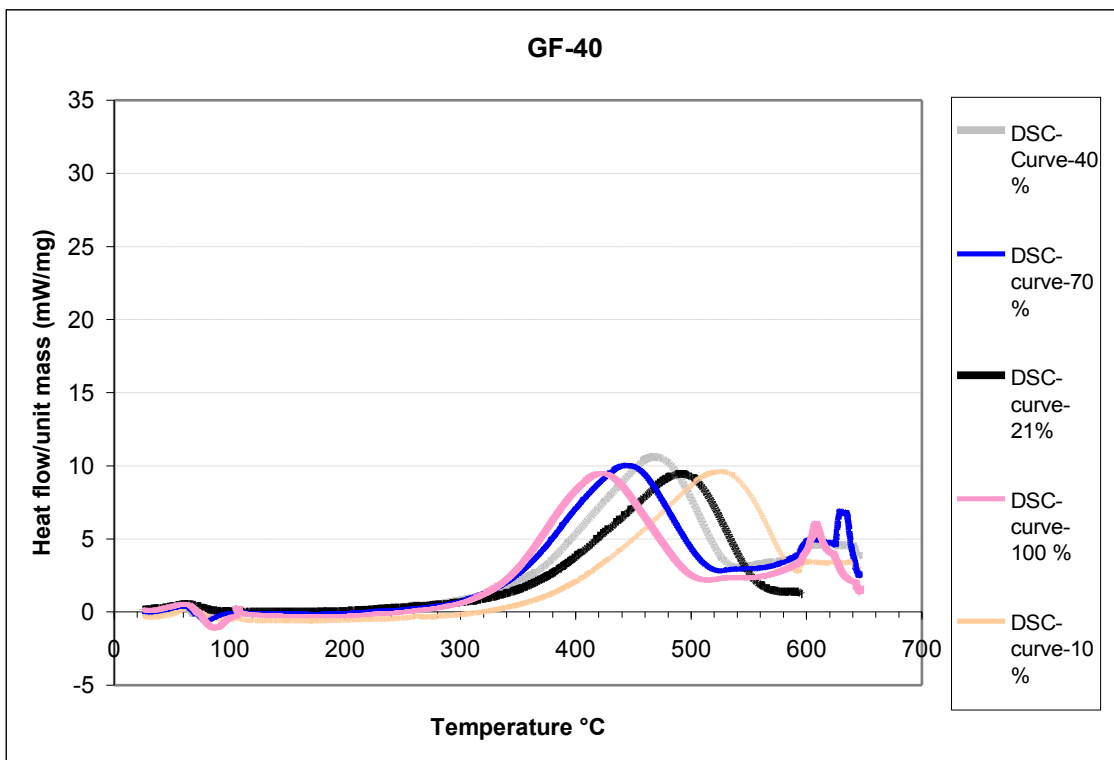
#### 5. 100 % OXYGEN

Sample	PIO	SIT
<i>GF-40</i>	183	320
<i>PAN-A</i>	198,00	420

#### ANNEXE-L

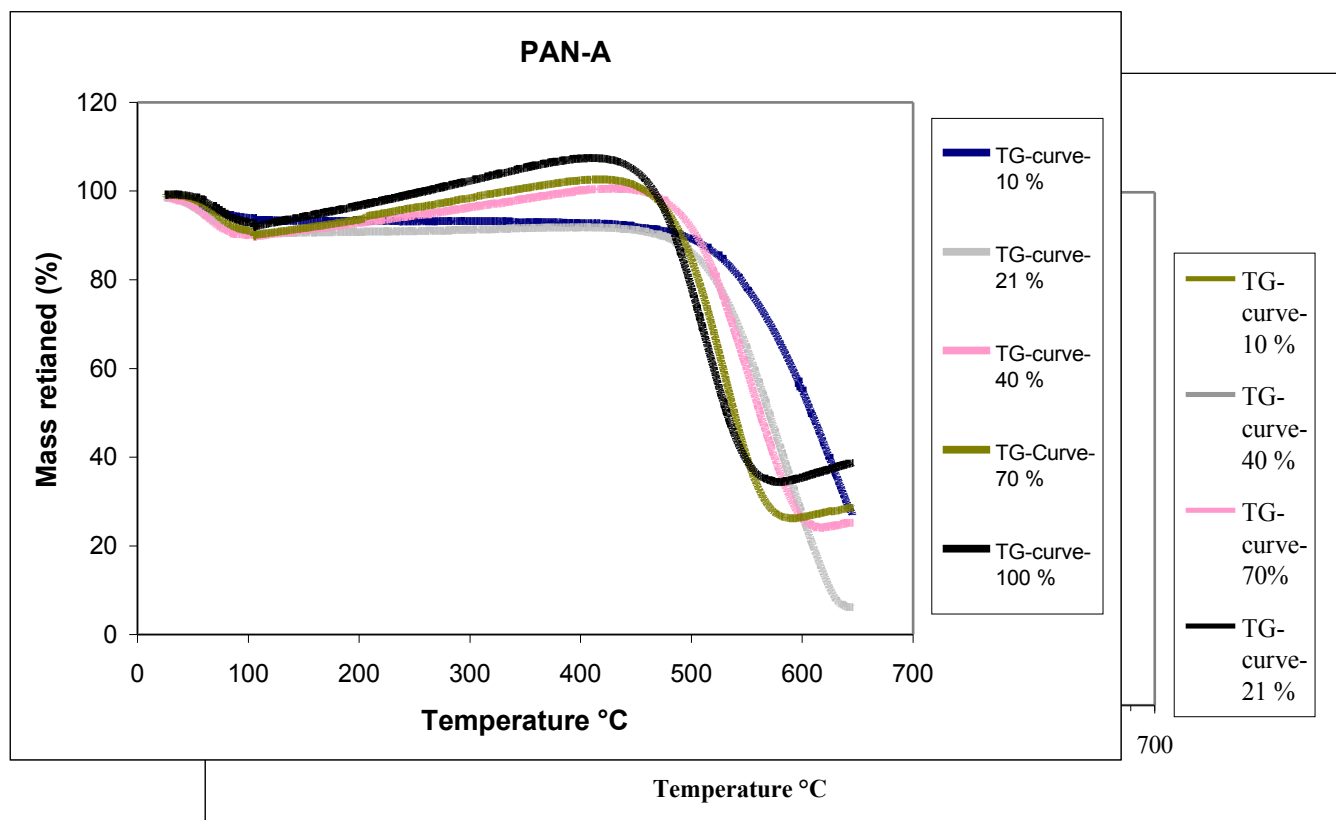
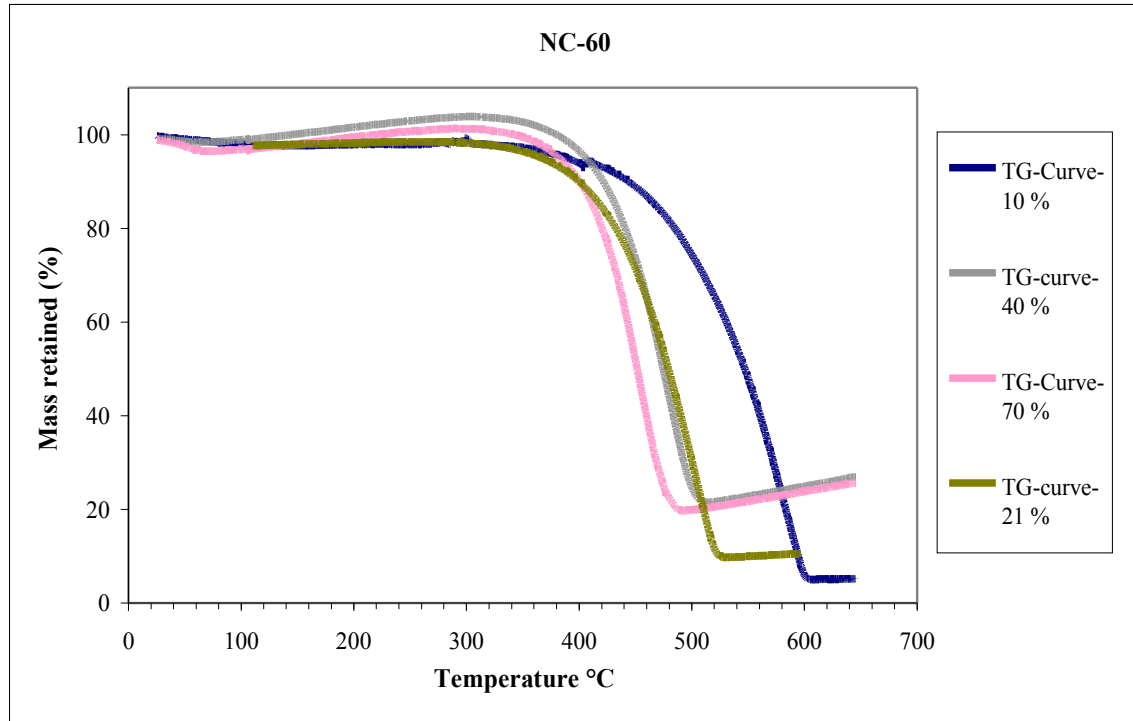
**DSC CURVES OF THE CARBON SAMPLES FOR THE CONCENTRATION OF OXYGEN AT 10%, 21 %, 40 %,  
70% & 100 %**

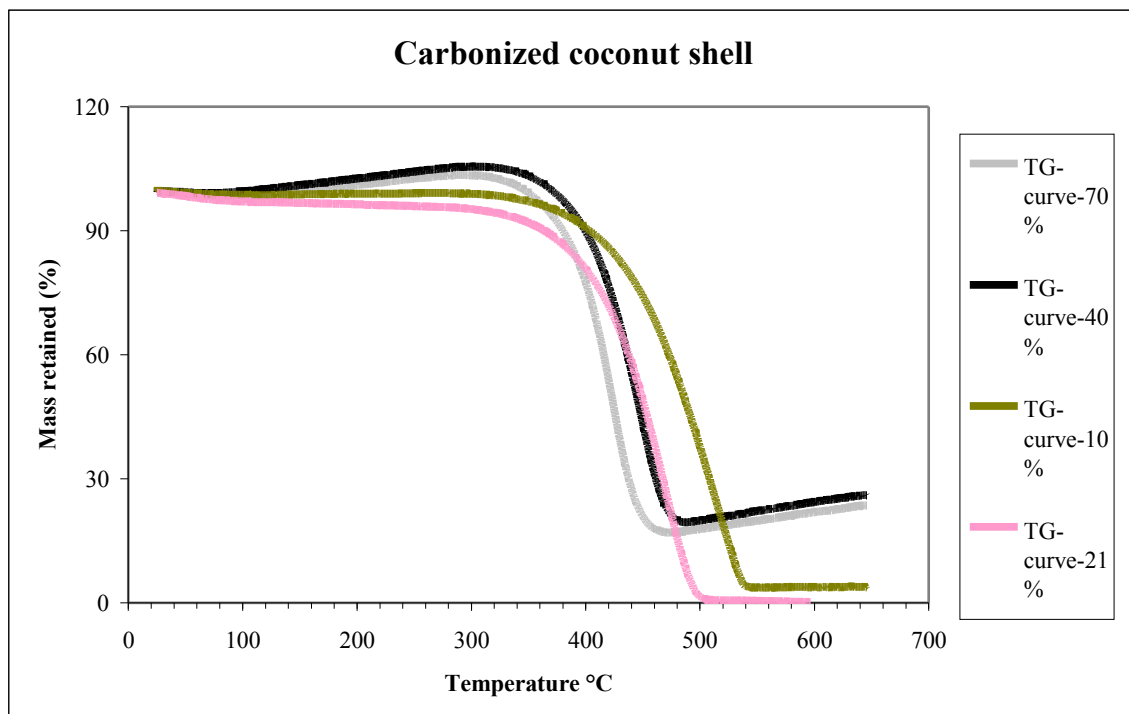




## ANNEXE-M

**TG CURVES OF THE CARBON SAMPLES FOR THE CONCENTRATION OF OXYGEN AT 10%, 21 %, 40 %, 70% & 100 %**





#### APPENDIX-N

**PIO AND SIT VALUES OF THE ACTIVATED CARBON SAMPLES FOR THE FLOW RATE OF 1.2 L/hr AND 2.4 L/hr**

Sample	Flow rate 1,2 L/hr		Flow rate 2,4 L/hr	
	PIO °C	SIT °C	PIO °C	SIT °C
<b>GF-40-40 %</b>	<b>180</b>	<b>340</b>	<b>164</b>	<b>335</b>
<b>GF-40-70%</b>	<b>182</b>	<b>320</b>	<b>160</b>	<b>321</b>
<b>NC-100-40%</b>	<b>194</b>	<b>475</b>	<b>163</b>	<b>446</b>
<b>NC-100-70%</b>	<b>178</b>	<b>450</b>	<b>151</b>	<b>429</b>
<b>GF-40-5%</b>	<b>260</b>	<b>399</b>	<b>223</b>	<b>383</b>

## APPENDIX-O

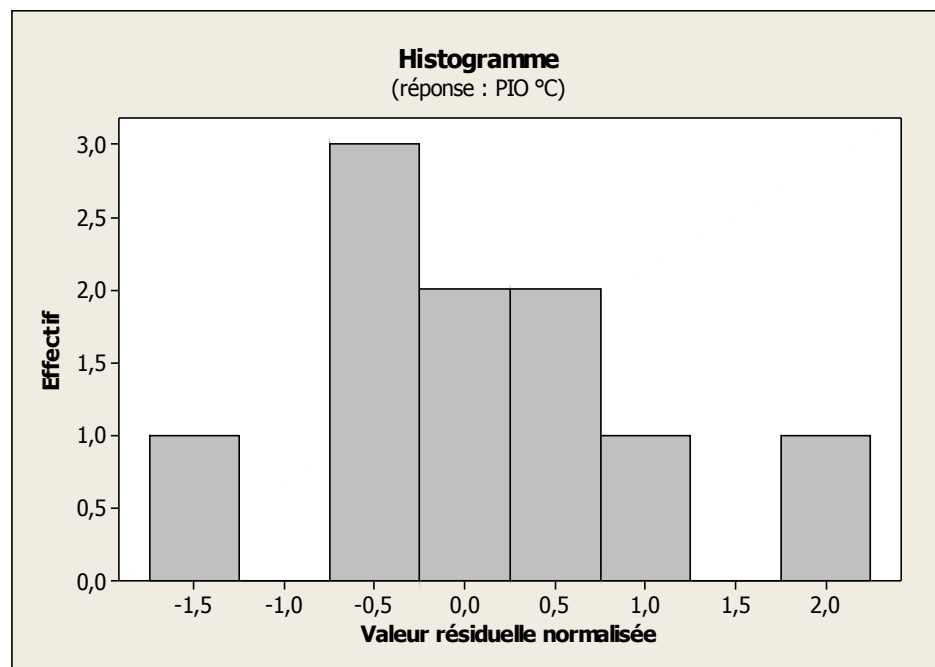
**PIO AND SIT VALUES OF THE ACTIVATED CARBON SAMPLES FOR THE HEATING RATE 2, 5 AND 8 K/min**

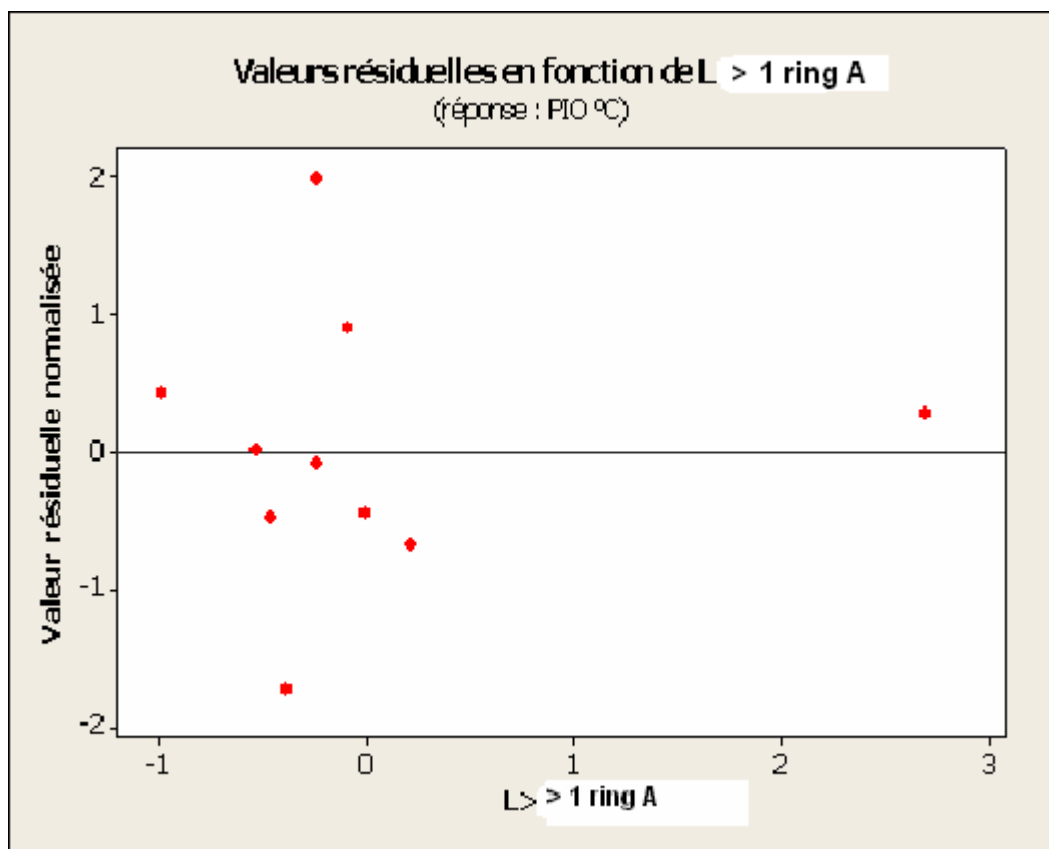
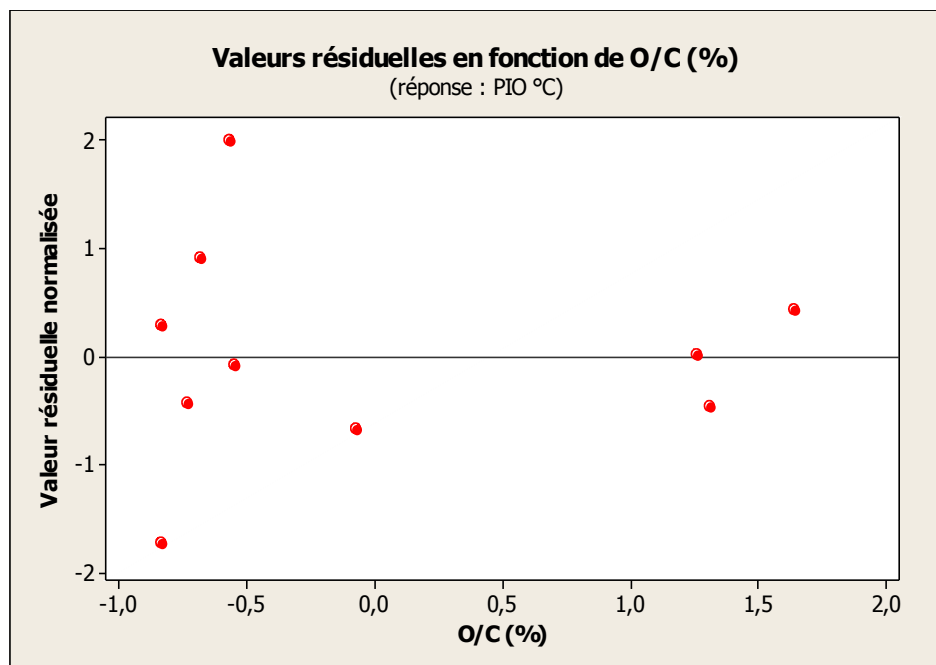
Sample	Heating rate (K/min)	PIO °C	SIT °C
BC-120	2	188	370
	5	178	378
	8	156	380
GF-40	2	201	335
	5	183	343

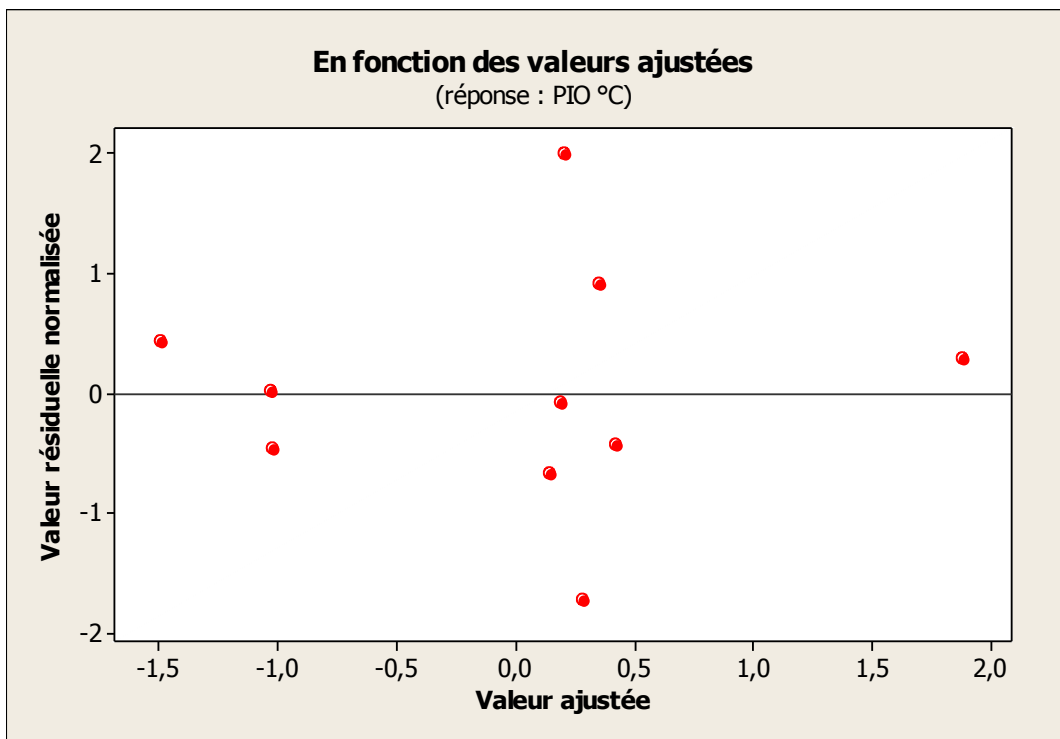
	8	160	345
<b>BPL</b>	2	268	497
	5	224	510
	8	213	512

#### APPENDIX-P

ANALYSIS OF RESIDUALS FOR THE MULTIPLE LINEAR REGRESSION EQUATION WITH THE RESPONSE VARIABLE **PIO** AND THE PREDICTOR VARIABLES **O/C RATIO** AND **L>1 RING**







### Résumé: Etude de l'oxydation de matériaux carbonés

Ce travail s'intéresse à l'oxydation des charbons actifs utilisés industriellement pour leurs capacités d'adsorption des polluants présents dans l'air. L'objectif est d'accéder à une meilleure connaissance des mécanismes physiques et réactionnels impliqués lors de l'oxydation de ces matériaux carbonés. Les lits de charbon actif sont actuellement très répandus dans la pratique industrielle. Cependant de nombreux incidents liés à l'inflammation spontanée des containers en service ou au repos ont été reportés. Ces inflammations accidentelles résultent de phénomènes mal contrôlés, liés à l'introduction d'air dans le système ou à l'accumulation locale de chaleur produite par des réactions exothermiques. La prévention des accidents d'inflammation nécessite une meilleure compréhension des mécanismes initiant l'oxydation.

Le but de ce travail est de développer des modèles cinétiques capables de prédire la vitesse d'oxydation des matériaux en fonction de leurs propriétés et paramètres opératoires. La réactivité du charbon actif est mesurée par des analyses (ATG-DSC) sous atmosphère oxygénée sous différentes conditions de températures.

Les résultats d'ATG-DSC ont clairement mis en évidence que l'oxydation du matériau était initiée à basse température et qu'elle pouvait être caractérisée par la mesure du Point d'Oxydation Initiale (PIO). Il y a une transition de l'oxydation basse température à l'oxydation haute température qui est accompagnée d'une augmentation rapide du flux de chaleur et d'une diminution de la masse de l'échantillon. L'auto inflammation du matériau est caractérisée par la mesure de paramètres comme les énergies d'activation et SIT (self ignition). Le type d'activation du charbon actifs, leur teneur en oxygène et leur propriété poreuse ont une influence sur l'oxydation. Des outils statistiques comme la Régression Linéaire Multiple (RLM) permettent de quantifier l'influence des propriétés significatives.

### **Abstract: Oxidation of carbon materials**

Activated carbons widely used as adsorbents in air treatments are prone to oxidation and self heating due to external heating, exothermic chemical reactions, and adsorption reactions

The aim of this work is to establish a quantitative relationship between the intrinsic properties of activated carbons and their reactivity leading to oxidation and ignition. The correlation is established by analysing a large number of activated carbons samples having diversified origin and characteristics. Carbon samples were characterized for their physical and chemical properties. Their oxidation and ignition reactivity in air were studied using Thermogravimetry (TG) and Differential Scanning Calorimetry (DSC). The Point of Initial Oxidation (PIO) representing the beginning of the oxidation reactions and the Spontaneous Ignition Temperature (SIT) where the bed combustion takes place in a self sustaining manner [were experimentally determined. In addition, activation energy (Ea) was calculated from the TG curves indicating the weight loss of the combustion reactions.

In a first approach, oxidation and ignition behaviours described by the PIO, SIT, and Ea values versus intrinsic properties of the activated carbon were examined. Global qualitative trends were underlined. In a second step, a more rigorous analysis was realised and quantitative statistical correlations between oxidation and ignition properties and intrinsic characteristics of the porous carbonaceous materials were investigated using multiple linear regression (MLR). Results indicated that the properties of the activated carbons had a significant influence. The surface oxygenated groups and the metal impregnates increased the reactivity of the material whereas the nitrogen content stabilized the reactivity of the samples. The porosity characteristics like the specific surface area, pore volume also contributed to the increase in the reactivity of the material.

**Mot clés :** Charbons actifs, Oxydation et inflammation, Sécurité du procédé, caractérisation du matériau.